Adaptation of avian-origin influenza virus to the horse

Julien André Roger AMAT

Submitted in fulfilment of the requirements for the degree of
Doctor of Philosophy in Virology

School of Veterinary Medicine
College of Medical, Veterinary & Life Sciences
Oilthigh Glaschu – University of Glasgow

May 2022

ABSTRACT

The mechanisms and consequences of evolution on viral fitness following interspecies transmission and long-term adaptation are poorly understood. Influenza A viruses (IAVs) circulate among wild birds and have been linked to the emergence of viruses of humans, pigs, dogs, and horses. Since the mid 1950s, equine influenza viruses (EIVs) have emerged in Europe (H7N7, in 1956), America (H3N8, in 1963) and Asia (H3N8, in 1989). All EIVs are thought to have originated in birds, and only the H3N8 EIV lineage that emerged in 1963 circulates today.

I used EIVs to study changes in viral fitness following host shifts. To this end, I compared the *in vitro* and *ex vivo* infection phenotypes of A/equine/Lexington/1/1966 (EIV/66), a representative of the extinct H7N7 EIV lineage; A/equine/Jilin/1/1989 (EIV/89), also extinct; and two viruses of the currently circulating H3N8 EIV lineage: A/equine/Uruguay/1/1963 (EIV/63) and its descendant A/equine/Ohio/1/2003 (EIV/2003). I also studied A/ruddy shelduck/Mongolia/963v/2009 (AIV/2009), an avian influenza virus phylogenetically related to EIV/89.

The results obtained showed that while each virus displayed a unique infection phenotype, EIV/2003 exhibited the highest overall fitness, consistent with the long-term circulation of this lineage among horses. Traits associated with increased fitness included enhanced viral replication, efficient cell-to-cell spread in cells and tissues, and resistance to interferon. Notably, transcriptomics revealed important differences among EIVs in terms of intracellular pathways affecting host immunity, inflammation, and cellular transcription.

This study showed that within-host fitness is determined by the interplay between virus-host interactions and evolution. In turn, within-host fitness will likely impact long-term adaptation of IAV to mammals.

TABLE OF CONTENTS

FIGURES

TABLES

Publications based on research project

Long-term adaptation following influenza A virus host shifts results in increased within-host viral fitness due to higher replication rates, broader dissemination within the respiratory epithelium and reduced tissue damage. **Julien A.R. Amat**, Veronica Patton, Caroline Chauché, Daniel M. Goldfarb, Joanna Crispell, Quan Gu, Alice M. Coburn, Gaelle Gonzalez, Daniel Mair, Lily Tong, Luis Martinez-Sobrido, John F. Marshall, Francesco Marchesi, Pablo R. Murcia PLoS Pathog., (2021), 17(12): e1010174. https://doi.org/10.1371/journal.ppat.1010174

Contributed to, but not included in this thesis

Human Rhinovirus Infection Blocks Severe Acute Respiratory Syndrome Coronavirus 2 Replication Within the Respiratory Epithelium: Implications for COVID-19 Epidemiology. Kieran Dee, Daniel M. Goldfarb, Joanne Haney, **Julien A.R. Amat**, Vanessa Herder, Meredith Stewart, Agnieszka M. Szemiel, Marc Baguelin, Pablo R. Murcia, The Journal of Infectious Diseases, (2021), Volume 224, Issue 1, Pages 31–38, https://doi.org/10.1093/infdis/jiab147

Severe Acute Respiratory Syndrome Coronavirus 2 Serosurveillance in a Patient Population Reveals Differences in Virus Exposure and Antibody-Mediated Immunity According to Host Demography and Healthcare Setting. Ellen C. Hughes*, **Julien A.R. Amat***, Joanne Haney, Yasmin A. Parr, Nicola Logan, Norah Palmateer, Sema Nickbakhsh, Antonia Ho, Peter Cherepanov, Annachiara Rosa, Andrew McAuley, Alice Broos, Imogen Herbert, Ursula Arthur, Agnieszka M. Szemiel, Chloe Roustan, Elizabeth Dickson, Rory N. Gunson, Mafalda Viana, Brian J .Willett, Pablo R. Murcia, The Journal of Infectious Diseases, (2021), Volume 223, Issue 6, Pages 971–980, https://doi.org/10.1093/infdis/jiaa788

Absence of adaptive evolution is the main barrier against influenza emergence in horses in Asia despite frequent virus interspecies transmission from wild birds. Henan Zhu, Batchuluun Damdinjav, Gaelle Gonzalez, Livia V. Patrono, Humberto Ramirez-Mendoza, **Julien A.R. Amat**, Joanna Crispell, Yasmin A. Parr, Toni-ann Hammond, Enkhtuvshin Shiilegdamba, Y. H. Connie Leung, Malik Peiris, John F. Marshall, Joseph Hughes, Martin Gilbert, Pablo R. Murcia, PLoS Pathog., (2019), 15(2): e1007531. https://doi.org/10.1371/journal.ppat.1007531

Acknowledgements

Part of the work presented in this thesis has been carried in collaboration with members of the Murcia laboratory or external colleagues:

- RNA libraries preparation and samples sequencing were done by Lily Tong, Daniel Mair, and Ana Da Silva Filipe (CVR Genomics).
- Equine tracheal tissues were kindly provided by Fernando Montesso (Animal Health Trust, Newmarket UK). Equine trachea collection was done by Pablo Murcia, while equine explant preparation was assisted by Ilaria Piras, Joanne Haney, and Daniel Goldfarb.
- Chapter 4: Tissue processing was done by Lynn Stevenson, Lynn Oxford and Frazer Bell (diagnostic laboratory, Glasgow UK), while immunostaining was done by Veronica Patton.
- Chapter 4: Development of the image analyses programme was done in collaboration with Daniel Goldfarb, and data collection assisted by Veronica Patton.

As for my personal acknowledgments

I would like to express my gratitude to Pablo Murcia first for giving me the opportunity to join his laboratory, but also to have been an excellent mentor in and out of the lab. These four years of PhD have been a real pleasure and I felt they allowed me to grow both scientifically and personally.

Additionally, I would like to thank my other supervisor Francesco Marchesi who has been extremely supportive throughout my PhD, including during the COVID-19 time.

Finally, I would like to thank the Vet School for funding, and the administrative staff (Marie and Peter especially) for always being nice with me and answering my sometimes-annoying e-mails.

Obviously, my PhD journey would not have been memorable without amazing friends and colleagues, and I would like to give a big thanks to Jo, Kieran, Andreu, Yasmin, Ellen, Caroline, and Nico to be always here to answer questions and help if needed. But also, the Palmarini's gang (Meredith, Rute, Vanessa, and Mariana) as well as the lunch team (Daniel, Will and Chris)!

J'aimerai aussi remercier ceux qui sont restés/retournés en France à savoir mes parents, mon frère qui ont toujours eu à cœur ma réussite, mais aussi Alex & Kadou pour avoir qui ont toujours su, et qui continueront d'être là pour moi.

Declaration

I, Julien André Roger Amat, hereby certify that, except where explicit reference is made to the contribution of others, this thesis is the result of my own work and has not been submitted for any other degree at the University of Glasgow or any other institution. Some of the work has been published in appropriate journals, as indicated in page 9. I acknowledge that the work undertaken for the completion of this PhD thesis was supported by the Georgina Gardner Endowment (Grant number 145813-01), the John Crawford endowment (Grant number 123939-01) and the Veterinary Fund Small Grant Scheme of the University of Glasgow, awarded to Pablo R. Murcia and Julien A.R. Amat.

Date: 3rd of May 2022

Signature:

Printed name: Julien André Roger Amat

Abbreviations

Aim2	-	Absent in melanoma 2 protein
AIV	-	Avian influenza virus
AIV/2009	-	A/ruddy shelduck/Mongolia/963v/2009
AP-1	-	Activator protein 1
ASC	-	Apoptosis-associated speck-like protein containing a carboxy-terminal CARD
ATP	-	Adenosine triphosphate
BALT	-	Bronchus-associated lymphoid tissue
BGH	-	Bovine growth hormone
Bp	-	Base pair
BRALT	-	Bronchiole-associated lymphoid tissue
BSA	-	Bovine Albumin Fraction V
CARD	-	Caspase activation and recruitment domain
CC3	-	Cleaved caspase 3
CDS	-	Coding sequence
CI	-	Confidence interval
Cm	-	Centimetre
Cm^2	-	Squared centimetre
CMV	-	Human cytomegalovirus
CO_2	-	Carbon dioxide
CPE	-	Cytopathic effect
CpG	-	CG dinucleotide
CPM	-	Counts per million
CPSF30	-	Cellular polyadenylation-specific factor 30
CRM1	-	Chromosomal Maintenance 1
cRNA	-	Complementary RNA
DAMP	-	Danger-associated molecular pattern
DE-ISG	-	Differently expressed ISG
DEG	-	Differentially expressed gene
DF1	-	Chicken embryonic fibroblasts
DMEM	-	Dulbecco's modified Eagle's medium
DNA	-	Deoxyribonucleic acid
DPBS	-	Dulbecco's Phosphate Buffered Saline
dsRNA	-	Double-stranded RNA
E.Derm	-	Equine Dermal fibroblasts
EID	-	Equine influenza disease
EIV	-	Equine influenza virus
EIV/2003	-	A/equine/Ohio/1/2003
EIV/63	-	A/equine/Uruguay/1/1963
EIV/66	-	A/equine/Lexington/1/1966

EIV/89 - A/equine/Jilin/1/1989

EPS15 - Epidermal growth factor receptor substrate 15

ER - Rough endoplasmic reticulum

ESCRT - Endosomal sorting complex required for transport

FBS - Fetal Bovine Serum

FC-1 - Florida clade 1

FC-2 - Florida clade 2

FCHO - F-BAR domain only protein

GAS - gamma interferon activation site

GC - Guanine cytosine

GLM - Generalized linear mixed-effect

GO - Gene ontology

GSDMD - Gasdermin D

H_2O - Water

HA - Haemagglutinin

HEK293T - Human Embryonic Kidney cells

Hpi - Hours post infection

IAV - Influenza A virus

IFIT - IFN induced proteins with tetratricopeptide repeats protein

IFITM - IFN-induced transmembrane protein

IFN - Interferon

IFNAR - IFN α and β receptor

Ig - Immunoglobulin

IKK - Inhibitor of nuclear factor kappa-B kinase

IL - Interleukin

IRAK - Interleukin-1 receptor- associated kinase

IRD - NCBI Influenza Resource Database

IRF - Interferon regulatory factor

ISG - IFN-stimulated gene

ISGF3 - IFN-stimulated factor 3

ISRE - IFN-stimulated response element

Jak1 - Janus kinase

LB - Luria broth

LGP2 - Laboratory of genetics and physiology 2

log_2 FC - Log_2 Fold change

LTALT - Laryngo-tracheal associated lymphoid tissue

M1 - Matrix 1 protein

M2 - Matrix 2 protein

M^2 - Squared meter

MALT - Mucosa-associated lymphoid tissue

MAPK - p38 mitogen-activated protein kinase

MAVS	-	Mitochondrial antiviral-signalling protein
MDA5	-	Melanoma differentiation-associated protein 5
MDCK	-	Madin-Darby canine kidney cells
Min	-	Minute
mL	-	Millilitre
MOI	-	Multiplicity of infection
mRNA	-	Messenger RNA
MTOC	-	Microtubule-organising center
MX	-	Myxovirus resistance
MyD88	-	Myeloid differentiation primary response 88
NA	-	Neuraminidase
NAP1	-	NAK-associated protein 1
NCBI	-	National Center for Biotechnology Information
NEMO	-	Inhibitor of nuclear factor kappa-B kinase subunit gamma
NEP	-	Nuclear export protein
NeuGcα2,3Gal	-	α2,3 N-glycolylneuraminic acid
NF-κB	-	Nuclear factor kappa-light-chain-enhancer of activated B cells
Ng	-	Nanogram
NGS	-	Normal Goat Serum
NK cells	-	Natural killer cells
NLRP3	-	NOD-like pyrin domain-containing 3
Nm	-	Nanometre
NP	-	Nucleoprotein
NS1	-	Non-structural protein 1
O:E	-	Observed/expected
OAS	-	2'-5'-oligoadenylate synthases
ºC	-	Degree Celsius
PA	-	Polymerase acidic protein
PAMP	-	Pathogen-associated molecular pattern
PB1	-	Polymerase basic protein 1
PB2	-	Polymerase basic protein 2
PC	-	Principal component
PFU	-	Plaque-forming unit
PI(4,5P_2)	-	Phosphatidylinositol 4,5-biphosphate
PKC	-	Protein kinase C
Pol II	-	RNA polymerase II
Poly(A)	-	Polyadenylated
Poly(I:C)	-	Polyinosinic:polycytidylic acid
Pre-mRNA	-	mRNA precursor
PRR	-	Pathogen recognition receptor

RG - Reverse genetic
RIG-I - Retinoic acid-inducible gene I
RIP1 - Kinases receptor interacting protein
RLR - RIG-like receptors
RNA - Ribonucleic Acid
RNAse L - Ribonuclease L
RNF135 - Ring finger protein 135
RSAD2 - Radical S-adenosyl methionine domain containing 2
SA - Sialic acid
SD - Standard deviation
SEM - Standard error to the mean
ssRNA - Single stranded RNA
STAT - Signal transducer and activator of transcription
TAB2 - Mitogen-activated protein kinase kinase kinase 7-interacting protein 2
TAK1 - Mitogen-activated protein kinase kinase kinase 7
TBK1 - TANK binding kinase 1
$TCID_{50}$ - Median tissue culture infectious dose
TLR - Toll-like receptor
TM - Melting temperature
TPCK - Tosylsulfonyl Phenylalanyl Chloromethyl Ketone
TRAF - TNF receptor-associated factor
TRIF - TIR-domain-containing adapter-inducing interferon-β
TRIM - Tripartite motif family
Tyk2 - Tyrosine kinase 2
uIFN - Universal IFN
UK - United Kingdom
USA - United States of America
UTR - Untranslated region
VO_2max - Maximal aerobic capacity
vRNA - Viral genomic RNA
vRNP - Viral ribonucleoprotein
µL - Microlitre
µm - Micrometre
$µm^2$ - Squared micrometre

À la mémoire de ma mère,

Chapter 1: Introduction

1.1 General introduction

Pathogens and their hosts have co-evolved for millions of years, and their relationship has been extensively studied. Questioning the cause and the origins of our maladies found its origin in ancient Greece when Hippocrates (c. 460—c. 370 BC) introduced the humoral theory for the first time in *Corpus Hippocraticum*. This idea was based on the equilibrium of four different "humors" i) blood, ii) phlegm, iii) yellow, and iv) black bile, all contained within the human body. Sickness was presented as the result of unbalanced humors, usually caused by polluted air, referred to as miasma by Hippocrates. This theory remained a dogma in medicine for several centuries.

However, in 1847 Ignaz Semmelweis, a Hungarian physician, observed a 50% decrease of "childbed fever" cases (nowadays known as postpartum infections) when newborns were delivered by midwives rather than obstetricians (Semmelweis 1861). As doctors were involved in post-mortem examinations and midwives were not, Semmelweis postulated that infections were due to a transferable cause, referred to as "cadaverous particles". These observations led to the premise of the germ theory, although the aetiologic agent of such infections remained unknown. It was only a few years later that the work led by Louis Pasteur (Pasteur 1878) and Robert Koch (Koch 1884) popularised and formalised the germ theory, marking the fall of humoral theory and establishing a direct link between pathologies and pathogens. The newly formulated paradigm was originally limited exclusively to bacteria due to technological limitations, which did not allow identification and observation of other transmissible pathogens such as viruses. It was only at the end of the 19th century that Martinus Beijerinck, repeating the work of Dmitri Ivanovsky, mentioned for the first time the presence of a *contagium vivum fluidum* (translating as contagious living fluid), which later became known as a virus (Beijerinck 1898). The presence of a virus as a transmissible infectious agent was confirmed in 1935 when Wendell Stanley crystallised the causal agent of tobacco mosaic disease, tobacco mosaic virus (Stanley 1935). In the past century, we have witnessed the isolation and characterisation of a myriad of viruses including but not limited to the influenza A virus (IAV) in pigs (Shope 1931), and in humans (Dochez et al. 1933; Smith et al. 1933), both causing influenza disease in their respective host. However, it was only in 1955 that the aetiologic agent of "fowl plague", a domestic fowl infection associated with high mortality and first described in 1878, was linked to IAV (Perroncito 1878; Schäfer 1955). A year after this discovery, in 1956, horses experienced an

emerging respiratory disease, which was later attributed to IAV (Sovinova et al. 1958; Espmark et al. 1956).

1.2 Influenza A virus

IAVs are enveloped viruses containing an 8-segmented, negative-sense (also refers as antisense) and single-stranded RNA (ssRNA) genome. IAV is classified as part of the *Orthomyxoviridae* family, which groups the *Alphainfluenzavirus* (Influenza A virus), *Betainfluenzavirus* (Influenza B virus), *Gammainfluenzavirus* (Influenza C virus), and *Deltainfluenzavirus* (Influenza D virus), as well as *Isavirus*, *Quaranjavirus*, and *Thogotovirus* genera (ICTV 2011). Due to a ssRNA genome, and associated with the lack of proofreading activity of the viral RNA polymerase (Steinhauer et al. 1992), IAV possesses a propensity of genetic mutation accumulation acquired during viral replication estimated to be 300-times higher than DNA (deoxyribonucleic acid) viruses (Drake 1993; Duffy et al. 2008), which pushed the scientific community to establish a viral subtypes classification. The IAV subclassification was originally defined serologically, while subtype nomenclature was based on two surface glycoproteins, neuraminidase (NA) and haemagglutinin (HA), both embedded in the viral membrane, and as of today, 11 different NA (N1—11), and 18 HA (H1—18) have been identified (Centers for Disease Control and prevention 2022).

1.2.1 Ecology

As described, the multitude of IAVs subtypes contribute to a unique and complex ecological landscape summarised in Figure 1-1. IAV is a zoonotic pathogen infecting humans and a wide range of animals, from mammalian (porcine (Van Epps 2006), equine (Espmark et al. 1956; Sovinova et al. 1958; Waddell et al. 1963; Scholtens and Steele 1964; Guo et al 1992), and canine (Zhu et al. 2015; Voorhees et al. 2018)) to avian hosts (Perroncito 1878). The extensive list of susceptible species highlighted in Figure 1-1 is most likely a simplistic view of the real complexity of IAV ecological landscape, as some species might not have been sampled yet.

Wild waterfowl populations (especially *Anseriformes*, and *Charadriiformes*) are considered to be the main reservoir of IAV. Birds contribute to the worldwide spread of the pathogen due to long-distance migratory movements (Easterday et al. 1968; Lycett et al. 2016). However, some of the IAV subtypes remain specific to certain host and species, for example, H13 and H16 have been isolated mainly in *Charadriiformes* (more precisely gulls; (Hinshaw

et al. 1982; Fouchier et al. 2005)), while H17 and H18 have been only found in bats so far (Tong et al. 2012; Tong et al. 2013). This specificity highlights a potential limit of the *in vitro* system in place based mainly on Madin-Darby canine kidney cells (MDCK) to study IAV. However, despite the apparent heterogeneity of IAVs, all viral subtypes share a similar structure and composition (see section 1.3.3).

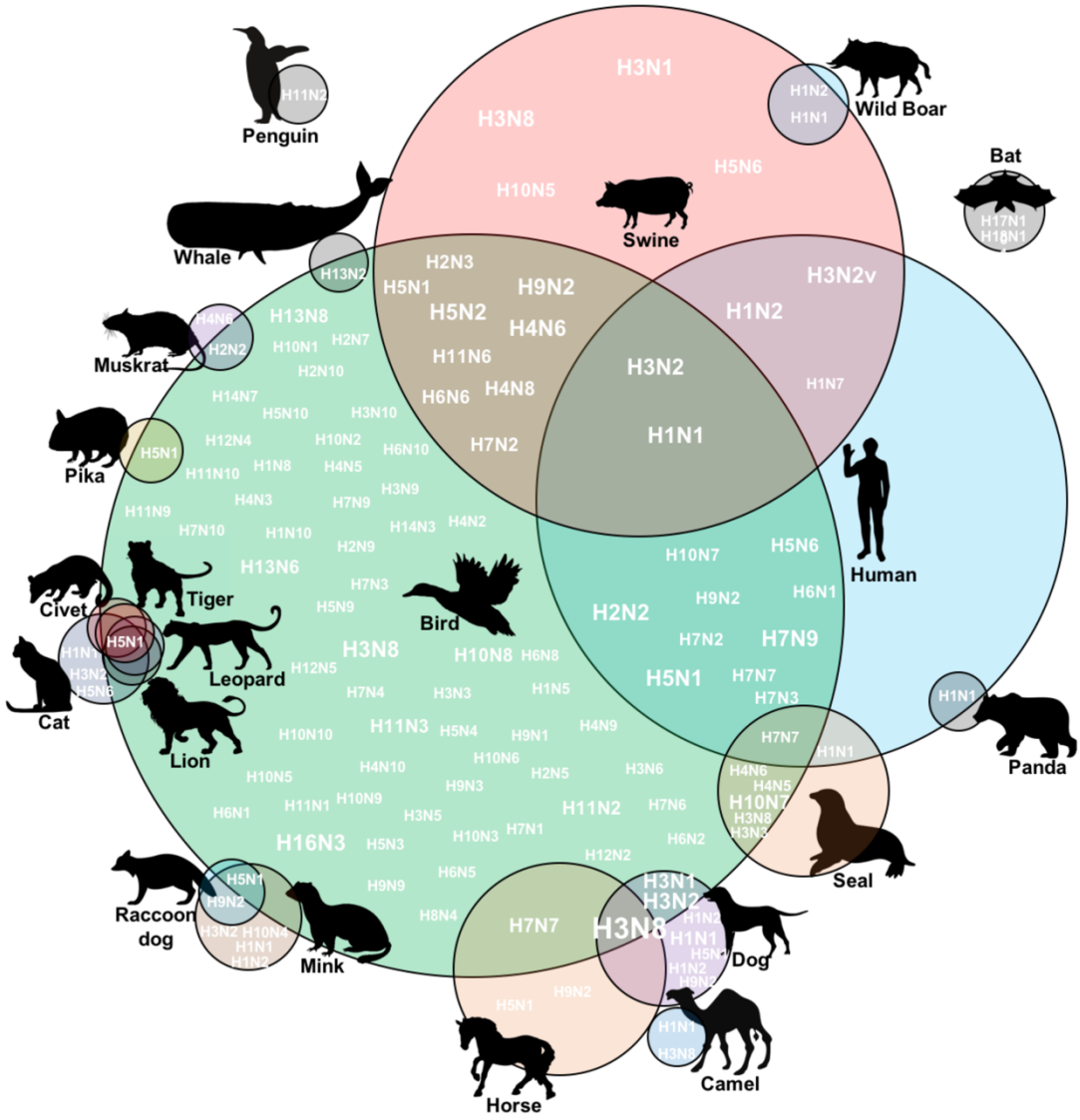

Figure 1-1: In-Flu-Venn-Za, an artistic representation of IAV distribution among susceptible hosts. Data used to generate this artwork were collected form the NCBI Influenza Virus Resource database, and strictly complete genome sequences (containing the 8 segments) were used. The scale of circles representing each susceptible host identified is arbitrary but reflects the number of sequences contained, and their overlaps reflects the number of shared subtypes. Black silhouettes were added next to circles and represent the corresponding species.

Concurrently to their suspected role of viral reservoir, birds represent the main source of interspecies transmission, which can lead to single and isolated event (dead-end host), or to emergence of new endemic lineage. As an example, the first zoonotic infection of H5N1 avian influenza virus (H5N1 AIV) in human was reported in Hong Kong in May 1997, while additional cases were recorded in November and December of the same year (Chan 2002). These introduction events caused a total of 18 human influenza infection, 6 of which were fatal (Chan 2002). Since 1997, the total number of H5N1 infections and deaths in humans is 862 and 455, respectively (World Health Organization 2016).

This example contrasts with the interspecies transmission initiated by an H3N8 AIV infecting horses in 1963 (Waddell et al. 1963; Scholtens and Steele 1964). This event led to an outbreak of influenza disease in horses, and the establishment of an endemic H3N8 equine influenza virus (EIV) lineage which is still circulating nowadays (see section 1.3.1.1).

1.2.2 Transmission routes

Mammalian IAVs replicate in epithelial cells of the respiratory tract and are transmitted via aerosols and droplets. Interestingly, AIVs preferentially replicate in epithelial cells of the digestive tract and transmit between individuals via an orofaecal route (Webster et al. 1978). The observed tropism of AIV leads to the production of virion-rich faeces, which represent an important source of water contamination, likely at the origin of zoonotic hotspots in watery areas along wild bird migratory routes (Webster et al. 1978; Cavailler et al. 2010; Bouwstra et al. 2017).

Webster et al. (1978) showed that A/duck/Memphis/546/74 (and others AIVs subtypes) were able to infect both the respiratory and digestive tracts of experimentally inoculated ducks, despite the low pH found in the gizzard (range 2.9—4.4). Such results remained exclusive to AIV as mammalian IAV (human H3N2 and swine H1N1 viruses) did not generate a productive infection in the digestive tract of ducks while they did in respiratory tract. This study suggests than in addition to a diversified cellular tropism, AIVs resist lower pH better than mammalian IAVs.

1.2.3 Financial impact of influenza disease

Influenza represents a major human public health and an important economic concern due to its seasonality, its pandemic potential, and the associated costs. The average annual cost of seasonal human influenza infections to the United States has been estimated to be 11.2 billion (6.3—25.3 billion United States dollars) (Putri et al. 2018). However, the important

cost of human influenza infections to human society is reinforced by animal influenza impacting various industries.

IAV infections were responsible for important losses in poultry and pork meat production. Combined, the two industries generated approximatively 34 million tons of meat in 1961, and accounted for 48% of the global world meat production (Food and Agriculture Organization of the United Nations 2022). This phenomenon has been accentuated more recently as in 2018, they were responsible of nearly 250 million tons of meat production, which represented 71% of total world production (Food and Agriculture Organization of the United Nations 2022). However, as birds and pigs rarely suffer of lethal infections, the economic losses were associated with an extended time needed to reach slaughter weight as a result of apathy and anorexia caused by infection. The cost of swine influenza has been estimated to be nearly 65 million British pounds per annum in the United Kingdom (UK).

Interestingly, the equine industry has been massively impacted by IAV infections, not because of its important role in the meat production (estimated to 559,000 tons in 1961, and 792,000 tons in 2018), but on the indirect economical loss generated by horse racing and related activities (Food and Agriculture Organization of the United Nations 2022).

The Australian 2007 equine influenza disease (EID) outbreak (see section 1.3.1.3) was responsible for an estimated economic burden of 263 million Australian dollars, covering the different governmental assistance packages, and an additional 97.7 million Australian dollars dedicated to the emergency response (Smyth et al. 2011).

The 2019 EI outbreak in the UK led to a racetrack national shutdown that impacted 228 horse premises and 23 horse racing events over a period of 6 days and generated a shortfall estimated to be a 1.5 million British pound cut to horse racing. Nevertheless, the total cost associated with the outbreak remains currently unknown.

As EID can significantly affect the economy of a country, it is also important to highlight that in other areas of the world where people still rely on equids for transportation or milk production, the economic burden, and the consequences of EID are even more detrimental.

1.3 Equine influenza virus (EIV)

1.3.1 EIV history

1.3.1.1 EIV history : the origins

Equine disease outbreaks compatible with EID (see section 1.4.1) have been documented since 1299, and suggest that EIVs circulated for several centuries (reviewed by Morens and Taubenberger 2010). However, in 1956, the aetiologic agent of EID was first isolated in Prague (former republic of Czechoslovakia; Sovinova et al. 1958). The virus belonged to the H7N7 EIV subtype and was initially referred to as equine-1 influenza. Recent phylogenetic inferences based on a host-specific local clock model converged to an estimated date of H7N7 EIV emergence between 1830 and 1870 (Worobey et al. 2014). Such estimations are in line with an important EIV outbreak recorded in 1872 and referred to as the 1872 western hemispheric equine panzootic in the literature (Morens and Taubenberger 2010; Kheraj 2018). The 1830—1870 IAV introduction led to the establishment of an endemic H7N7 EIV lineage that circulated worldwide in equine populations before a sudden and unknown extinction. EIV H7N7 was last isolated in 1977 but serological studies in unvaccinated horses suggest that it might have circulated at least until 1994 (Madić et al. 1996).

The H7N7 interspecies transmission recorded in 1956 did not remain unique, as in 1963, a second outbreak of avian-origin influenza was reported in Florida and referred to as equine-2 influenza (Waddell et al. 1963; Scholtens and Steele 1964). This time, the subtype associated with this infection was H3N8 EIV, and the interspecies transmission is believed to have been caused by the transportation of Argentinian horses presenting clinical signs in line with EID (Waddell et al. 1963; Scholtens and Steele 1964). Argentinian authorities did not report any positive horses at the time, however, Uruguayan (Castro et al. 2019) and Brazilian (Favaro et al. 2018) governmental agencies did, suggesting a most likely South American outbreak prior to the North American outbreak. The hypothesis of a viral circulation in southern america anterior to 1963 was in line with phylogenetic inferences which estimated the EIV H3N8 most recent common ancestor to have emerged between 1943 and 1962 (Murcia et al. 2011). The H3N8 avian-origin influenza interspecies transmission event led to the establishment of an endemic H3N8 EIV lineage, which has since circulated uninterruptedly and has been the cause of many more EI outbreaks around the world. In addition, phylogenetic analyses highlighted the important frequency of the H3N8 intrasubtype

(homosubtypic) reassortment event, which most likely enhanced virulence, while the heterosubtypic reassortment (between co-circulating H7N7 and H3N8 EIV lineages) exclusively generated H7N7 viruses harbouring H3N8 internal genes (apart from M; Murcia et al. 2011). The potential extinction of EIV H7N7 subtype is often debated as it could be the consequence of heterosubtypic reassortment events leading to a decrease of within-host viral fitness (*e.g.* viral entry, viral replication efficiency, virus transmissibility) most likely favouring EIV H3N8 circulation, or alternatively, linked to a subclinical circulation of EIV H7N7 in equine population. As of today, the question remains open, and additional investigations are required to answer it.

1.3.1.2 Major H3N8 EI outbreaks from 1960s to 1980s

H3N8 EIV caused several outbreaks in the United States between its first characterisation in 1963 and the 1980s and has been since considered endemic (Cullinane and Newton 2013). However, the transcontinental nature of EIV pandemic was highlighted by the emergence and characterisation of EIV in Europe (Switzerland) in 1965 (Paccaud et al. 1966), in Asia in 1971 (Japan; Kawaoka et al. 1989)), and in Africa (Algeria; Kawaoka et al. 1989)) in 1972. The 1980s marked an increase of H3N8 outbreak reports. In December 1986, South African authorities reported for the first time in their history an H3N8 EI outbreak seemingly as a consequence of the importation of infected horses from Kentucky, United States of America (USA). South African government decided to quickly respond by cancelling all race meetings and restricting animal movements. The following week, a national vaccination campaign started, and mitigation measures remained in place for several weeks. Although surrounding countries experimented EI outbreaks in the following months (May in Lesotho, August in Namibia) South African authorities declared the country EI-free in September 1987. The South African EI outbreak shed light on the limitation of importation rules in place at that time and led to establishment of stricter importation guidelines. From March 1987, importation of horses in South Africa requires a mandatory vaccination at least 30 days and not more that 60 days before despatch and included a compulsory vaccination of South African equids (Guthrie et al. 1999).

Three years later in 1989, Europe reported an EI outbreak involving H3N8 Suffolk/89 EIV (Binns et al. 1993). Phylogenetic analyses highlighted that Suffolk/89 HA was more closely related to Kentucky/86 and Kentucky/87 than Fontainebleau/79 or even Miami/63, crediting the hypothesis of a single lineage of equine H3N8 circulating worldwide (Binns et al. 1993). As competition horses travel internationally more than any other domestic animals because

of racing events, the worldwide equine population is considered as a single geographical pool of susceptible animals rather than isolated individual groups.

The same year, northeast China experienced an H3N8 EIV emergence involving Jilin/89 (Guo et al. 1992). Jilin/89 outbreak highlighted a more recent and new interspecies transmission event originated form circulating AIV. Guo et al. (1992) found that at least 4 out of 8 segments of Jilin/89 were recently derived from avian sources. EIV Jilin/89 was responsible of nearly 20% mortality in infected horses, while morbidity was estimated to 48% (Guo et al. 1992). Fortunately, the virus did not persist in the equine population, and stopped circulating soon after its emergence (Webster and Thomas 1993).

1.3.1.3 The 2007 Australian EI outbreak

Although horses were imported regularly since the 18th century to Australia (Department of the Environment and Arts 2004), it was only in the 1970s than animal transport by air raised new concerns regarding infectious disease importation. In order to prevent EI outbreaks from occurring, Australia and New Zealand put in place strict quarantine measures including a mandatory 35 days of isolation of any imported animal (21 days pre-export and 14 days post-arrival), and up-to-date vaccination. The proactive measures in place in these countries were sufficient to grant them the EI-free status, which was later confirmed by a serological study (Christley et al. 2001). However, in August 2007 an H3N8 EIV introduction was reported in Australia for the first time resulting from the importation of vaccinated but subclinically infected horses from Japan (Watson et al. 2011). Due to the EI-free status of the country, Australian authorities believed that quarantine measures were sufficient to prevent EI spread and did not promote a vaccination campaign, thus the entire Australian horse population was naïve (with the exception of imported animals for which vaccination was mandatory, and animals to be exported if required by the country of destination). The 2007 Australian EI outbreak resulted in 70,000 individual infection (Sack et al. 2019) and, as a result, the country implemented extremely restrictive policies involving the prohibition of animal movements within the country, the quarantine of infected farms (over 10,000), and an emergency vaccination campaign (over 150,000 horses; Watson et al. 2011). The national movement restrictions were crucial to contain the epidemic dispersal initially, while the vaccination campaign actively accelerated the disease fade out phase (Cowled et al. 2009). However, the relative impact of the two measures remains to be determined (Cowled et al. 2009). Both actions contributed to precipitate the end of the outbreak, which was declared over in December 2007 (Watson et al. 2011).

The Australian episode highlights the importance but also the limit of vaccination campaigns as vaccinated animals can still be subclinically infected and cause local outbreaks. This point will be discussed further in section 1.4.2.

1.3.1.4 Major H3N8 EIV outbreaks from 2010s to date

In the past ten years, along with the reduction of sequencing costs, and the democratisation of aerial transportation of horses, EI outbreaks events became more frequent. Although in the past decades most of the interspecies transmission events seemed to happen in developed countries (North America, Europe, and South Africa) they did not remain exclusive to them. Recently, African (Algeria 2011, Senegal 2019), South American (Argentina 2012; 2018, Brazil 2012; 2015, Chile 2012, Uruguay 2012; 2018), and Asian countries (China 2010; 2011; 2012; 2017; 2020, Mongolia 2010; 2011, Kazakhstan 2012) experienced reports of EIV outbreaks affecting horses, as well as donkeys and mules (reviewed by Oladunni et al. 2021).

1.3.2 H3N8 EIV phylogeny and nomenclature

The abundance of H3N8 EIV outbreaks since its first emergence in 1963, and the monophyletic relationship linking them led to the establishment of various lineages and sublineages. Therefore, all the H3N8 EIVs circulating before Johannesburg/86 were indexed in the pre-divergent H3N8 EIV lineage. After 1986, isolated H3N8 EIVs were categorised within the Eurasian or the American lineage, reflecting mainly the location of isolation. Finally, H3N8 EIV isolated in the late 2000s and referred as American lineage were subdivided into the Florida clade 1 (FC-1), and Florida clade 2 (FC-2) which represent the currently circulating sublineages. A summary of such organisation is given in Figure 1-2, however it did not include H7N7 EIVs or H3N8 EIV originated from the Chinese 1989 outbreak as these viruses were not associated to the EIV/63 outbreak and represent alternative phylogenies.

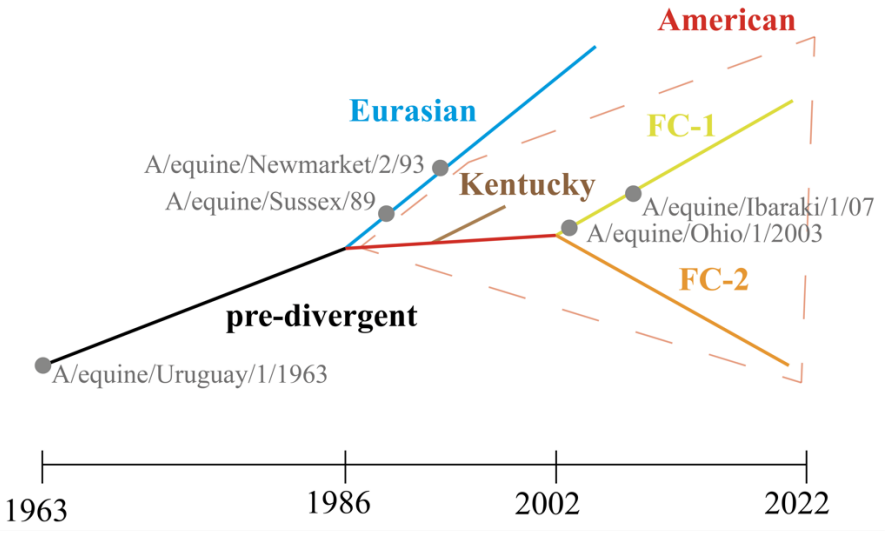

Figure 1-2: Schematic of H3N8 EIV phylogeny and nomenclature. Pre-divergent, Eurasian, and American H3N8 EIV lineages are shown in black, cyan and red, respectively. Additionally, the American lineage was subdivided into Kentucky, Florida clade 1 (FC-1) and Florida clade 2 (FC-2) sublineages, and depict in brown, green and orange, respectively. A selection of viruses were represented with grey circles. Adapted from Oladunni et al. (2021).

1.3.3 Viral organisation

Historically, influenza virions were described in textbooks as spherical particles with a diameter ranging from 80 to 120 nanometre (nm). However, in 1949 influenza A viruses were reported as filamentous particles in clinical isolates (Chu et al. 1949). Influenza virions should be described as a heterologous viral population including spherical, but also bacilli (95 nm in diameter and up to 250 nm in length) and filamentous shaped particles reaching up to several micrometres in length (Figure 1-3 A; Mosley and Wyckoff 1946; Calder et al. 2010). It has been observed that filamentous virions are more abundant in clinical isolates than in lab-grown preparations where spherical particles are more common, suggesting that the filamentous phenotype conferred an evolutionary advantage *in vivo*, no longer needed in a more artificial system (Seladi-Schulman et al. 2013). However, the biological reasons and the genetic determinants underpinning such morphology are not fully characterised.

Within IAV virions there are 8 viral genomic segments helically wrapped with high affinity and without sequence specificity around viral nucleoproteins (NP; Eisfeld et al. 2015). Additionally, there are associated at their distal end with a trimeric RNA polymerase complex made of polymerase basic protein 1 and 2 (PB1, PB2), and the polymerase acidic protein (PA) forming the viral ribonucleoprotein complex (vRNP; Figure 1-3 B; Pflug et al. 2014). The internal organisation of influenza A viral particles showed vRNPs in a 7+1

arrangement surrounded by an endoskeleton made of matrix 1 protein (M1) aggregation and located beneath the viral membrane (Noda et al. 2006). Besides the viral protein shell described, there is another structural protein, matrix 2 protein (M2), found less frequently than M1, which ensures a contact point between M1 and the viral membrane where both proteins are embedded (M1 and M2 protein functions are further described in section 1.3.3.2; Pinto et al. 1992). Furthermore, IAV is classified as an enveloped virus as it displays a surrounding phospholipid bilayer from the hijacked cell membrane (see section 1.3.4.3; Shaw et al. 2008).

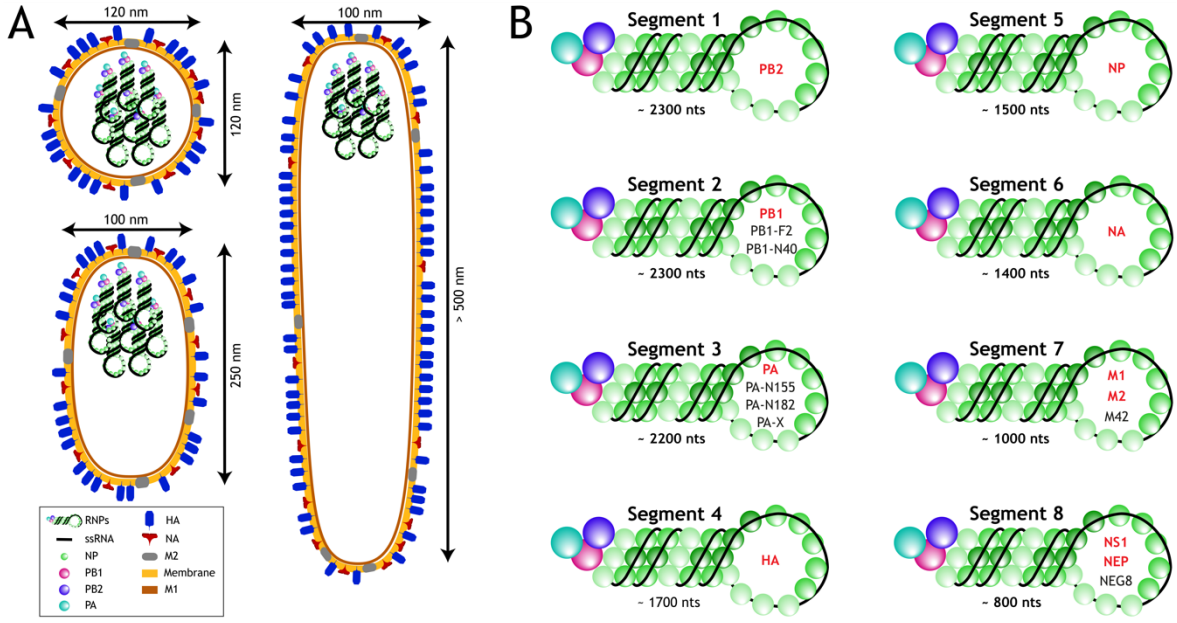

Figure 1-3: Influenza A morphology and viral composition. (A) Schematic representation of IAV pleiomorphic particles showing the location and organisation of vRNPs in each of the different viral shapes. Protein composition of virion is showed in the left bottomed legend. **(B)** Schematic structural organisation of of vRNPs. The main viral proteins encoded by each vRNP are given in the globular head in red and black for main and accessory proteins, respectively. Additionally, the length of genomic sequence for each vRNP is given underneath as nucleotides (nts). Adapted from **Pinto (2019).**

1.3.3.1 Genome organisation and coding strategy

The EIV genome is made of antisense ssRNA and accounts for approximately 13 kilobases divided into eight individual segments. Influenza virus encodes up to 17 proteins and developed various strategies to optimize their coding potential (Dubois et al. 2014). This potential is increased using alternative splicing (first highlighted by the discovery of influenza encoded 9th protein (nuclear export protein; NEP; Lamb et al. 1978)), ribosomal

frameshift (disclosed by PA-X protein identification; Jagger et al. 2012), and the use of different initiating translation sites (as characterisation of PB1-F2 (Chen et al. 2001) and PB1-N40 (Wise et al. 2009) proteins revealed). Influenza-encoded proteins are usually segregated into two groups, referred as main and alternative.

1.3.3.2 Main proteins

The main influenza proteins can be considered those that are essential to infectious virion formation. Canonical translation leads to expression of PB2, PB1 and PA from segments 1, 2 and 3, respectively, the surface glycoproteins (HA and NA from segment 4 and 6), NP from segment 5, M1 and non-structural protein 1 (NS1) from segments 7 and 8, respectively. NP proteins are found tightly associated with influenza RNA genomic segments and form the vRNPs, a structural conformation essential to nuclear import and transcriptional activity. Associated with the distal end of vRNPs is found the heterotrimeric RNA-dependent RNA polymerase complex promoting the viral genomic RNA (vRNA) expression through cap-snatching (PB2 binding to the mRNA precursor (pre-mRNA) 5′-end, and PA cleaving it; Blass et al. 1982), and elongation (PB1; Biswas and Nayak 1994).

The surface glycoprotein HA mediates viral binding to the cellular receptor (Rogers and Paulson 1983), and is involved in viral entry (reviewed by Rossman and Lamb 2011) and budding, two important stages of the viral replication cycle (see section 1.3.4.1 and 1.3.4.2). The second surface protein, NA, possesses a sialidase activity and facilitates mucus cleavage, an essential step to expose host cellular receptors to viral particles (Matrosovich et al. 2004; Rossman and Lamb 2011). In addition, NA is responsible for the release of newly synthesised virions. Both HA and NA are the main targets of the neutralising antibody (Rossman and Lamb 2011).

The matrix protein (M1) mediates the interaction between vRNPs and the surface glycoproteins. This characteristic gives to the protein a role in genome nuclear export and virus assembly.

The NS1 protein is the main viral antagonist of the host innate immune response (Egorov et al. 1998; García-Sastre et al. 1998). NS1 acts on many viral replication steps to counteract the broad host response to infection and is often associated with a strong inhibition of type I interferon (IFN) response, participating to viral replication and viral spread maximisation (reviewed by Hale et al. 2008). Interestingly, NS1 depleted EIV, was not associated with clinical manifestations in infected horses (Quinlivan et al. 2005).

In addition to the proteins generated from canonical translation, there are two genomic products obtained from canonical translation and subsequent mRNA splicing and also categorised as influenza main proteins. These proteins are involved in viral particle uncoating (M2; (reviewd by Helenius 1992), and nuclear export of vRNPs (NEP) and are coded by segment 7 and 8, respectively (O'Neill et al. 1998).

1.3.3.3 Accessory proteins

Other proteins encoded by IAVs are the result of various coding strategies and are referred to as accessory proteins as they are not essential to virion formation. Some of them are produced from unspliced viral mRNAs translation such as PB1-F2 (alternative initiation site) or PA-X (ribosomal frameshift) and are associated with IFN antagonism and pro-apoptotic activities, or host transcriptional shutoff, respectively (Chen et al. 2001; Jagger et al. 2012; Varga et al. 2012; Feng et al. 2016). Finally other viral accessory proteins are generated via either alternative initiation sites (PB1-N40; Wise et al. 2009, PA-N155, PA-N182; Muramoto et al. 2013), or mRNA splicing and leaky scanning (M42), while NEG8 was only identified in *in silico* prediction (Clifford et al. 2009; Wise et al. 2012). Most of these proteins are associated with undefined functions, with the exception of M42 which possesses a similar function to M2 (Wise et al. 2012).

1.3.4 Replication cycle

Viral replication relies on completion of three important steps: virus entry, virus intracellular replication cycle, and virus release. Unsuccessful completion of at least one phase leads to virus replication failure and to abortive infection. However, before its initiation, viral particles must find their way through the respiratory protective layer made of Muc5b and Muc5ac mucins (Rousseau et al. 2007). The respiratory mucus represents the first line of defense against IAV as it contains a cocktail of antimicrobial molecules (*e.g.* defensins, lysozyme, immunoglobulin A (IgA)), immunomodulatory molecules (*e.g.* cytokines) in addition to the 1—10 micrometre (μm) thick gel-like mucus layer (Figure 1-4 a-f; Yang et al. 2014). As the extracellular mucosal environment is rich in sialic acids (SAs; Yang et al. 2014), the balance of HA/NA proteins on the viral surface is critical to allow an efficient mucus penetration and cellular attachment (Vahey and Fletcher 2019). Protein imbalance in favour of HA will result in a reduced penetration pace (due to numerous intra-mucus HA-SA interactions) and the mucociliary clearance of entrapped particles to the pharynx where they will be swallowed before reaching the cellular surface (Cohen et al. 2013). In contrast,

an excess of NA at the viral surface will results in a quick mucus penetration pace, but the excessive NA catalytic activity might not allow a long-lasting interaction between cellular expressed SA and HA, essential to initiate the virus entry step (Yang et al. 2014).

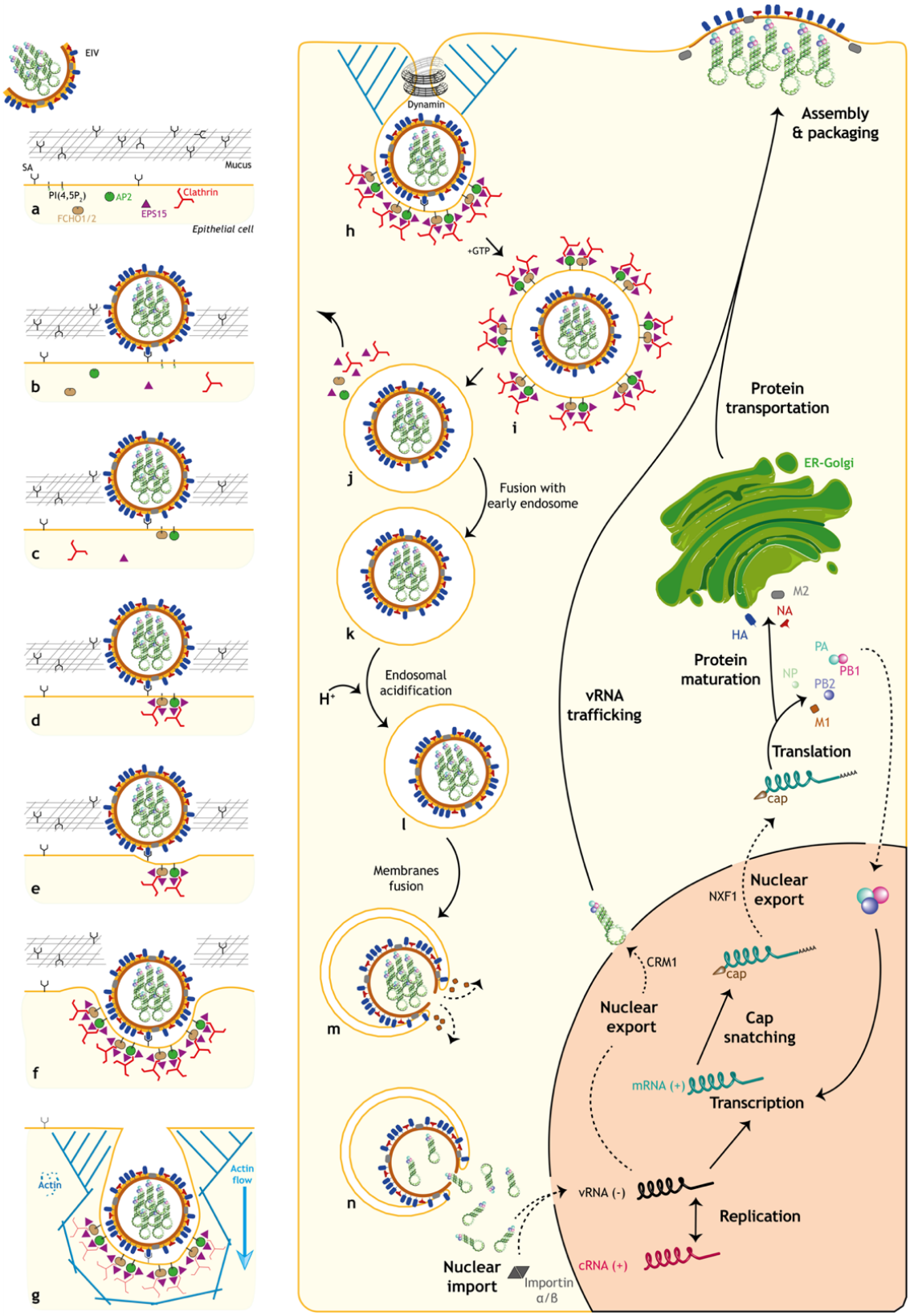

Figure 1-4: Influenza virus replication cycle. (A—B) Influenza A vial particles travel through the mucus and bind to sialic acid receptors. **(C—E)** Sialic acid bindings induce the recruitment of FCHO1 and FCHO2 as well as clathrin and EPS15 to form the clathrin coat, which initiates the clathrin-mediated endocytic pathway. **(F—G)** Under the influence of clathrin accumulation and actin polymerisation, the plasma membrane is curved. **(H)** Following dynamin action, the curved plasma membrane is cleaved, and endocytosis vesicle formed. **(I—N)** Using the endosomal maturation pathway, the viral particle is undergoing conformational changes leading to membranes fusion, and particle uncoating. The following steps lead to the replication, transcription, and translation of viral protein used to form the nascent progeny, budding at the plasma membrane. Adapted from Pinto (2019).

1.3.4.1 Viral entry

As mentioned, HA binding to the surface of host epithelial cells via SA groups initiates infection (Figure 1-4 b). However, several modified forms of SA exist and EIV HA preferentially binds to α2,3 N-glycolylneuraminic acid (NeuGcα2,3Gal), while for example human HA binds to α2,6 N-glycolylneuraminic acid (Suzuki et al. 2000). Distribution of SA is variable depending on the host but also on the tissue investigated and has been identified as the major determinant of viral tropism given its ability to dictate the infection outcome (Suzuki et al. 2000; Wasik et al. 2017). After viral particles bind to a susceptible cell surface, the virus is internalised following a default clathrin-mediated endocytosis (Figure 1-4 d—h), or on rare occasions via a caveolae-dependent route (highlighted in MDCK cells; Nunes-Correia et al. 2004).

Clathrin-mediated endocytosis is the main cellular endocytic pathway and relies on a complex protein-protein interaction constraining the plasma membrane, forcing it to bend and to create a coated vesicle which will later fuse with endosomes (Bitsikas et al. 2014). In more detail, the recruitment of primary initiator proteins (adaptor protein 2; Cocucci et al. 2012; or F-BAR domain only protein 1 (FCHO1) and FCHO2; Henne et al. 2010) initiates the process of clathrin coat formation (Figure 1-4 c). Both proteins are attached to phosphatidylinositol 4,5-biphosphate PI(4,5P_2), an important constituent of the plasma membrane. However, the initial phases of clathrin coat construction are not fully elucidated yet (Umasankar et al. 2012; Brach et al. 2014; Ma et al. 2015). Following adaptor protein 2 and FCHO1/FCHO2 recruitment, clathrin, epidermal growth factor receptor substrate 15 (EPS15), epidermal growth factor receptor substrate 15-like 1, intersectins 1, and intersectins 2 proteins are recruited and bind to the initiator proteins and form the clathrin scaffold complex (Figure 1-4 d; Kaksonen and Roux 2018). The presence of clathrin polymers in the scaffolding complex induces a smooth and increasing curvature of the plasma membrane

due to clathrin lattice structures (Figure 1-4 e; Heuser and Evans 1980). In addition to the clathrin coat, the actin cytoskeleton contributes to plasma membrane bending (Gottlieb et al. 1993; Lamaze et al. 1997). Although actin polymerisation is likely to play an important role, the underpinning mechanism is not fully elucidated (Figure 1-4 f-g; Collins et al. 2011). Finally, the scission step represents the last part of the clathrin-mediated endocytosis and is catalysed by the GTPase dynamin, which forms a helical structure around the neck of the clathrin-coated pseudo-vesicle and breaks it (Figure 1-4 h—i). However, the mode of action underpinning the dynamin-mediated constriction is still debated (Antonny et al. 2016). Quickly following the vesicle internalisation, the clathrin coat disassembles (Figure 1-4 j), and the newly formed vesicle fuses with the endosome (Figure 1-4 k).

Interestingly, in inhibited clathrin-mediated and caveolae-mediated endocytic pathways, influenza virus remained infectious revealing the existence of a dynamin-dependent endocytic pathway (Sieczkarski and Whittaker 2002). It was only recently that micropinocytosis uptake was identified as a clathrin and caveolae independent but a dynamin-dependant internalisation and was associated with filamentous particle entry (de Vries et al. 2011; Rossman et al. 2012). Following internalisation, viral particles travel towards the nucleus via an endosomal transport (Figure 1-4 k—n). It is only when the early endosome becomes a late endosome (associated with a drop in pH by endosomal acidification; Figure 1-4 l) that HA changes conformation and exposes a 14 amino acid-long peptide known as the fusion peptide, responsible for the fusion between the viral and endosomal membranes (Figure 1-4 m; Stegmann 2000). Membrane fusion results in the release of viral genomic segments into the cytosol close to the cell nucleus (Figure 1-4 n). Concomitantly to viral particle uncoating supported by the M2 proton channel activity, vRNPs are imported within the nucleus through nuclear pores complexes mediated by the nuclear localisation sequences motifs displayed by NP sequence and the importin-dependent nuclear import pathways as they are too voluminous to be passively imported (O'Neill et al. 1995).

1.3.4.2 Viral replication and transcription

Viral replication relies on the production of three RNA types: the positive sense viral mRNAs, the negative sense vRNAs, and the positive sense complementary RNAs (cRNA). Each of these RNAs have a special function, the mRNA is used to synthetise influenza proteins, the vRNAs is used as a genomic template to quickly produce the cRNAs which will be used as a replication intermediate to generate full length negative sense vRNA and

associated with newly synthesised PB1, PB2, PA, and NP proteins to form the vRNPs intended for progeny virions formation.

As influenza viral RNA polymerase cannot synthesise and methylate cap structures (essential to RNA processing and preventing mRNA degradation; (Vlugt et al. 2018; Galloway and Cowling 2019), viral transcription requires the succession of key steps referred to as cap snatching leading to the addition of a cap on the 5′ terminus of the newly generated mRNA. Quickly, the vRNP via its PB2 protein binds (via its cap-binding domain) to host RNA polymerase II (Pol II) and approaches the host pre-mRNA (5′-capped; Vlugt et al. 2018). Once the vRNP-Pol II complex is formed and the host pre-mRNA is close enough, PA cleaves the host pre-mRNA 10 to 14 nucleotides downstream of the cap (Plotch et al. 1981; Vlugt et al. 2018; te Velthuis and Oymans 2018). Following preinitiation steps, the nascent viral mRNA is then subject to elongation (PB1) until a termination characterised by a stuttering of the RNA polymerase on a sequence of uridine, leading to the addition of a polyadenylated (poly(A)) tail at the 3′-end (Poon et al. 1999; te Velthuis and Oymans 2018). The vRNA, now capped and poly(A)-tailed (also referred as viral pre-mRNA) can be exported through the nuclear pore complex to the cytosol mediated by the nuclear export factor 1 (NXF1 and translated by the host cytoplasmic translational machinery as any cellular mRNA (York and Fodor 2013). The first proteins to be synthesised following infection are NP and NS1, while M1, M2, HA, NA, and NEP are expressed later. The difference in protein production kinetics observed is most likely due to the important role played by NP and NS1 and is reinforced by the higher abundance of these two proteins (Skehel 1972; Skehel 1973). However, the mechanism in favour of NP and NS1 translation to the detriment of late genes remains unknown. The newly shaped surface embedded proteins (HA, NA, M2) are sent to the rough endoplasmic reticulum (ER) and the Golgi apparatus to complete their maturation following post-translational modifications (*i.e.* HA and NA glycosylation), and before being directed to the apical plasma membrane region rich in lipid rafts (Scheiffele et al. 1999; Schmitt and Lamb 2005). The viral proteins participate in virion assembly and egress processes and are sent either to the cell surface or back to the nucleus where they also play a role in vRNA transcription and replication (PB1, PB2, PA), or vRNP formation and export (NP, M1). The mechanism underpinning vRNP nuclear export differs from vRNA as they rely on the action of a cellular β-importin (Chromosomal Maintenance 1, (CRM1))-dependent pathway involving the interaction of RanGTP cofactor with the NEP N-terminal nuclear export signal (NES). Inhibition of the CRM1 pathway as well as the use of anti-NEP antibodies were shown to specifically block vRNP export (O'Neill et al. 1998;

Watanabe et al. 2001). Furthermore, NEP is found at the plasma membrane where it is involved in virion budding (Gorai et al. 2012). Finally, the multiple intracellular functions of NS1 are described in a dedicated section 1.7.1.3.

1.3.4.3 Virion assembly, packaging, and viral budding

Newly generated proteins are targeted to the apical plasma membrane, where virion assembly and budding take place involving different pathways. As mentioned, HA and NA surface proteins are glycosylated during their maturation in the Golgi apparatus and are sent to the apical plasma membrane via secretory vesicles, while M1 reaches the cellular surface following the exocytic pathway. HA and NA proteins are specifically exported to lipid raft rich areas also called viral "budozone" (Schmitt and Lamb 2005). Such areas are important for efficient viral budding as it was demonstrated that a mutation in the HA transmembrane domain was sufficient to disrupt its lipid raft association and significantly impair viral replication. However, another study found that depletion of cholesterol, an important component of the lipid raft, was associated with an increase of released viral particles concomitantly to a reduction of virus stability (Barman and Nayak 2007). These conflicting results suggest that "budzones" might be important for virus stability and not essential for budding. Originally Chen et al. (2007) demonstrated that HA and NA, in the absence of M1 and M2, represent the minimum requirements to initiate budding vesicle formation in a virus-like particle model. The introduction of M1 protein was found to produce virus-like particles morphologically closer to IAV particles most likely due to its interaction with HA and NA cytoplasmic tails and transmembrane domains (Ali et al. 2000; Chlanda et al. 2015). Finally, following their CRM1-dependent nuclear export, vRNPs, adjacent to the microtubule-organising center (MTOC), traffic to the plasma membrane using a Rab11 and microtubule-dependent vesicular transport mediated by PB2 interaction (Bruce et al. 2010). The proteins now aggregated nearby the apical plasma membrane initiate virus packaging. Packaging represents the step in which vRNP bundles are included in virions and is concomitant to viral budding. Originally, it was believed that the packaging mechanism relied on a random process influenced by stochastic segment interactions and leading to formation of virion that do not necessarily contain the 8 different segments (Enami et al. 1991). However, more recent results have shown that the genome packaging process is the result of a specific interaction between the terminal non-coding and coding regions of vRNPs, leading to the incorporation of one copy of each segment into each viral particle and arranged in 7 segments surrounding a central segment organisation (Noda et al. 2006; Liang et al.

2008; Fournier et al. 2012; Bolte et al. 2019). Anchoring of vRNPs to the plasma membrane is mediated by M1 proteins, which bind to NP and to HA cytoplasmic tails (Noton et al. 2007). Synchronously to vRNP docking, the aggregation of influenza proteins at the plasma membrane (HA, NA, M1, and M2) induces a curvature of the plasma membranes which initiates the viral budding stage (Chen et al. 2007). For a long time, the mechanism underpinning it was attributed to the presence of a YRKL amino acid motif in M1 protein, considered as a late domain and known to interact with the host endosomal sorting complex required for transport (ESCRT) machinery (Hui et al. 2006). However, due to a lack of reproducibility, the work of Hui et al. has since been retracted , and the involvement of NP has been suggested, but the underpinning mechanism remains unanswered (Rossman et al. 2010). In addition to the roles of M1 and M2 in budding initiation, the two proteins have been found to participate in vesicle elongation contributing to filamentous viral particle generation (Roberts et al. 1998). Furthermore, the ability given to M1 to influence filamentous particle formation has been attributed to a structural change of M1 helical turn which increase the stabilisation of the budding complex (Calder et al. 2010). *De facto*, M1 is often consider as the main determinant of influenza virion morphology.

Finally, the lipid bilayers scission step marks the completion of the viral replication cycle, and the release of virion progeny from the infected cell. The completion of viral budding has been recently linked to the action of M2 protein (Rossman et al. 2010). Surprisingly, M2 mimics the function of host ESCRT-III protein complex (~20 proteins involved) and leads to virion detachment from infected cells. The M2 cytoplasmic tail contains a 17 amino acid amphipathic helix and is responsible for the plasma membrane curvature and inducing budding and detachment of the nascent particle (Rossman et al. 2010). Rossman and colleagues (2010), found that viruses lacking M2 protein (ΔM2) were still able to produce nascent particles, however, they remain attached to the cell surface and exhibit a beads-on-a-string morphology. This result demonstrated the involvement of M2 in the membrane scission process and the necessity of it to produce nicely shaped and infectious viral particles.

1.4 Equine influenza disease

1.4.1 Clinical manifestations

Equine influenza virus is a highly contagious pathogen, and the aetiologic agent of EID. In horse, EIV is responsible for respiratory tract infections and is characterised by clinical signs ranging from mild to severe including but not limited to pyrexia (39.1ºC—41.7ºC; often

biphasic), rhinitis, pharyngitis, tussis, and fatigue (Myers and Wilson 2006; Muranaka et al. 2012). The onset of clinical signs is typically 1—5 days, and animals remain infected for up to a week. Infections by H3N8 EIV however are usually more severe than H7N7 EIV, and post-mortem examination of infected animals highlighted a clear change of lesion distribution within the respiratory tract of horses (Rose 1966). In H7N7 EIV experimentally infected ponies, pathological changes were confined to the bronchioles, while in H3N8 EIV naturally infected foals, lesions were also present in the alveoli (Rose 1966). In both scenarios, chest auscultation usually reveals an inspiratory and expiratory bronchovesicular wheeze in line with increased breathing difficulties (Myers and Wilson 2006). Interestingly, it has been noted that naïve individuals shed more virus for a longer period than previously exposed horses (Myers and Wilson 2006). Infected individuals contribute to pathogen transmission via the production of aerosols and fomites generated during coughing episodes. Most of the infection will resolve without additional complications, but severe cases could progress to pneumonia, mainly due to concomitant or secondary bacterial infections (*i.e. Staphylococcus aureus*, *Streptococcus pneumoniae*, or *Haemophilus influenzae*; Morris et al. 2017; Sack et al. 2019), especially in foals (Patterson-Kane et al. 2008; Elton and Bryant 2011). However, it has been reported that severity of clinical signs is often associated with H3N8 EIV, the exposure dose, the horse immunological status (previous exposure, and/or vaccination), and the viral strain exposed to (Rose 1966; Myers and Wilson 2006; Elton and Bryant 2011). Interestingly, during the EI outbreak in Northeast China (EIV/89 Jilin) the clinical features associated with infection included enteritis in addition to the classically observed pneumonia (Myers and Wilson 2006).

Furthermore, and in some rare cases, myalgia, myositis or myocarditis could be associated with infection, impacting animal movements and athletic horse performance (Rose 1966; Myers and Wilson 2006). These signs represent a significant economic burden as they lead to an extended resting period and could last several weeks before a return to full training capacities.

1.4.2 Measure to prevent and reduce disease burden

The main prophylaxis to EIV infection, to reduce clinical signs of EID, and to restrict viral shedding is vaccination. However, several technologies were used to produced vaccines as shown by inactivated whole virus vaccine such as the bivalent vaccine (South Africa/4/2003 (H3N8); Newmarket/2/93 (H3N8)) licenced by Merck under the name Equilis® Prequenza-TE, or the modified live EIV vaccine (Kentucky/91 (H3N8)) commercialised by Merck

under the appellation Flu Avert®. Additionally, there are bivalent (Ohio/03 (H3N8); Richmond/1/07 (H3N8)) recombinant virus vector vaccine such as Proteqflu-TE® manufactured by Boehringer Ingelheim (Oladunni et al. 2021). Although the vaccine composition appears to be outdated, a recent study showed that a vaccine containing South Africa/4/2003 remained effective and neutralised A/equine/Tipperary/1/2019 and A/equine/Essex/1/2019 two viruses from the FC-1 lineage and isolated during the 2019 British EI outbreak (Nemoto et al. 2021). Nevertheless, vaccine composition should be constantly monitored as a single amino acid change in the HA has been reported to significantly impaired vaccine efficacy (Yamanaka et al. 2015).

EI vaccination is classically done by intramuscular injection (Equilis® Prequenza-TE, Proteqflu-TE®) but can also be realised through intranasal administration (Flu Avert®) (Oladunni et al. 2021). EI vaccination is mandatory in several countries especially during animal movement such as for breeding or international competitions (Terrestrial Animal Health Code). Vaccination confers a protective individual immunity that quickly wanes (6 months after first-time injection) and requires successive doses as well as an annual booster dose administration to maintain its to protective level. Young foals (under the age of 4 months) are exempt from vaccination due to interference between vaccine antigens and the remaining colostral antibodies, potentially explaining the increased mortality observed in this group (Van Maanen et al. 1992). However, the multitude and conflicting vaccination guidelines given by the vaccine manufacturers, the *Fédération Équestre Internationale* (Fédération Equestre Internationale 2022), the British Horseracing Authority (British Horse Association 2022), and the World Health Organisation for Animal Health (World Organisation for Animal Health (OIE) 2019), to promote efficient vaccination create a general confusion among equine health professionals most likely explaining the bad practices observed. A recent British study investigated veterinary practitioners' awareness and compliance with vaccine manufacturers datasheets and shown a failure to follow the recommended EI vaccination schedule. Although 90% of the practitioners vaccinated foals around 5 months as recommended by all vaccine manufacturers, only 35% and 10% stuck to these guidelines regarding the second (4—6 weeks) and third (5 months) vaccination time intervals, respectively (Wilson et al. 2021). Interestingly, it was noted that >99% of veterinary surgeons were aware and followed booster dose (12 months) guidelines. However, clinicians raised the issue of an important vaccine hesitancy from horses owner mainly driven by the feeling of unnecessary need (77%) and previous or anticipated adverse drug reaction (56.7%, or 47.1%, respectively; Wilson et al. 2021). Such studies are essential to

understand better the caveats of the current vaccination campaigns and to improve awareness of both professionals and horse owners. Given the current size of the British equine population, and the vaccine sales in the country, it has been estimated that around 30% of the British horses are vaccinated (Wilson et al. 2021).

Complementary measures to vaccination exist and rely on the isolation of infected animals and travel bans, two measures that aim to reduce the intra- and inter- herd propagation of infection, limiting *de facto* the outbreak to local clusters only. Both preventive measures when combined are sufficient to limit the propagation of EI as demonstrated during the 1986 South African (Guthrie et al. 1999) and 2007 Australian (Cowled et al. 2009) EI outbreaks.

1.5 The equine respiratory tract

As mentioned, EIV represents a respiratory pathogen of the horse and understanding the equine respiratory tract anatomy and histology is essential to fully comprehend the changes induced by infection.

The respiratory tract oversees ventilation, a succession of unconscious, involuntary, and automatic movements allowing exchange of gases between the organism and its surrounding environment, essential to host homeostasis. This complex mechanism rests on two main events, the inhalation, and the exhalation stages.

1.5.1 Role of the respiratory tract

The main role of the respiratory tract is to assure a constant supply of oxygen to the organism. Additionally, the respiratory tract plays an important role by humidifying, warming up, and filtering the inhaled air (Davis et al. 2002; Davis et al. 2006). Subfreezing air intake was linked to abnormal cooling and desiccation of the lower respiratory surfaces, leading to adverse effects such as immediate exercise-induced bronchoconstriction and late phase airway obstruction (Davis et al. 2006). The uninterrupted intake of air is necessary to generate energy which guarantees a good cellular function to the animal. Once inhaled, the oxygen which is conditioned (warmed, filtered and humidified within the nasal turbinates), is transported into the blood, and then disseminates to the whole organism. The absorbed oxygen will catalyse a multiple oxidoreduction reaction (known as Krebs cycle), which will generate as an end product a combination of adenosine triphosphate (ATP), carbon dioxide (CO_2), and water (H_2O). ATP molecules are used as the main source of energy by the

organism, while the CO_2 and H_2O represent waste and will be evacuated from the organism. The waste disposal process is handled by the second stage of the ventilation, the exhalation.

1.5.2 Anatomy of the respiratory tract

The respiratory tract is usually described following a craniocaudal orientation and represents a succession of organs from the nasal cavity to the alveoli sacs. However, this extensive system is often subdivided into upper and lower respiratory tracts, located in the head and the neck or within the chest of the animal, respectively.

1.5.2.1 The upper respiratory tract

As its designation suggests, the upper respiratory tract includes the cranial organs involved in the respiration process. Breathed in air is taken from the environment into the nasal or the oral cavities. In most mammals the connection between the oral and the nasal cavities happen in a funnel shaped organ called pharynx. However, it is interesting to note that horses and rodents represent the only mammalian species considered as obligate nasal breathers (Holcombe et al. 2007; Jekl 2021). In non-pathological conditions the equine soft palate contacts the epiglottis, transforming the mouth into an airtight cavity (Barone 1984; Cheetham 2019). Abnormal positioning of the epiglottis and soft palate, also known as dorsal displacement of the soft palate, is a pathological condition affecting 10 to 20 % of poorly performing horses in which larynx is obstructed, leading to a reduction of air intake. (Parente et al. 2002; Lane et al. 2006; Cercone et al. 2019).

Following passage through the pharynx, air is directed to the larynx before entering the trachea. The larynx regulates the airflow inhaled by the animal during exercise while the trachea addresses inhaled air to the lungs. In horses, the larynx maximal inspiratory cross-sectional area at the level of *rima glottidis* ranges from 88 cm^2 during resting period to 301.7 cm^2 during canter (Lafortuna et al. 2003). The intense stretching of soft tissue indicates that horses have enormous aerobic capabilities outperforming other mammals of similar body mass (*i.e.* equine maximal aerobic capacity (VO_2max) = 150 millilitre per minute per kilogram (mL/min/kg), while steer, an animal of similar body mass reached a VO_2max = 60 mL/min/kg). Such respiratory capacities qualify horses as an athletic species (Lafortuna et al. 2003).

1.5.2.2 The lower respiratory tract

The lower respiratory tract is constituted of the trachea, bronchi and lungs and occupy most of the thoracic cavity. The trachea is a cylindrical 70—80 centimetre (cm) long organ in adult horses and it is held permanently open (in non-pathological conditions) by a succession of 48 to 60 c-shaped incomplete hyaline cartilage rings open dorsally (Cheetham 2019). The trachea height varies from 4 cm to 3 cm following a craniocaudal axis (Carstens et al. 2009). The gap between the cartilage ends is covered by the smooth trachealis muscle which can marginally alter the tracheal height during ventilatory contraction. Interestingly, it does not appear that equine trachea dimensions are related to animal body mass, while differences have been observed between breeds (Carstens et al. 2009). The trachea bifurcates into two primary bronchi, which will then form the two individual lungs. Each lung is surrounded by a protective layer made of serous membranes (the pleurae) which prevents tissue frictions created by the volumetric changes resulting of inhalation and exhalation. The right lung is more voluminous than the left and contains an extra lobe, referred as the intermediate lobe (also known as accessory), in addition to the apical and diaphragmatic lobes (also known as cranial and caudal lobes, respectively) present in both lungs (Budras et al. 2012). The primary bronchi are divided into bronchioles and terminal bronchioles while going deeper into the lung. The lower respiratory tract containing the primary bronchi, bronchioles, and terminal bronchioles is often referred as the conducting zone, and contrast with the transitional and respiratory zone of the respiratory tract where gaseous exchange takes place (Figure 1-5). The transitional and respiratory zones contain the respiratory bronchioles, the alveolar ducts, and the alveolar sacs. The gradual stratification of the lower respiratory tract allows an exponential increase of the tissue surface, which associated with hyper vascularisation, contributes to maximise the gas exchange efficiency between the animal and the environment. Johnson et al. (2014) estimated the horse lung surface area to 629.9 m^2 (interquartile range (IQR) = 452.6—936.7 m^2).

1.5.3 Histology of the respiratory tract

The equine respiratory tract is made of several histological layers (*i.e.* mucosal, submucosal, cartilaginous and muscular). In addition to the different layers constituting the respiratory tract, there is a heterogeneous tissue composition reflecting the various functions of the different parts of the respiratory tract.

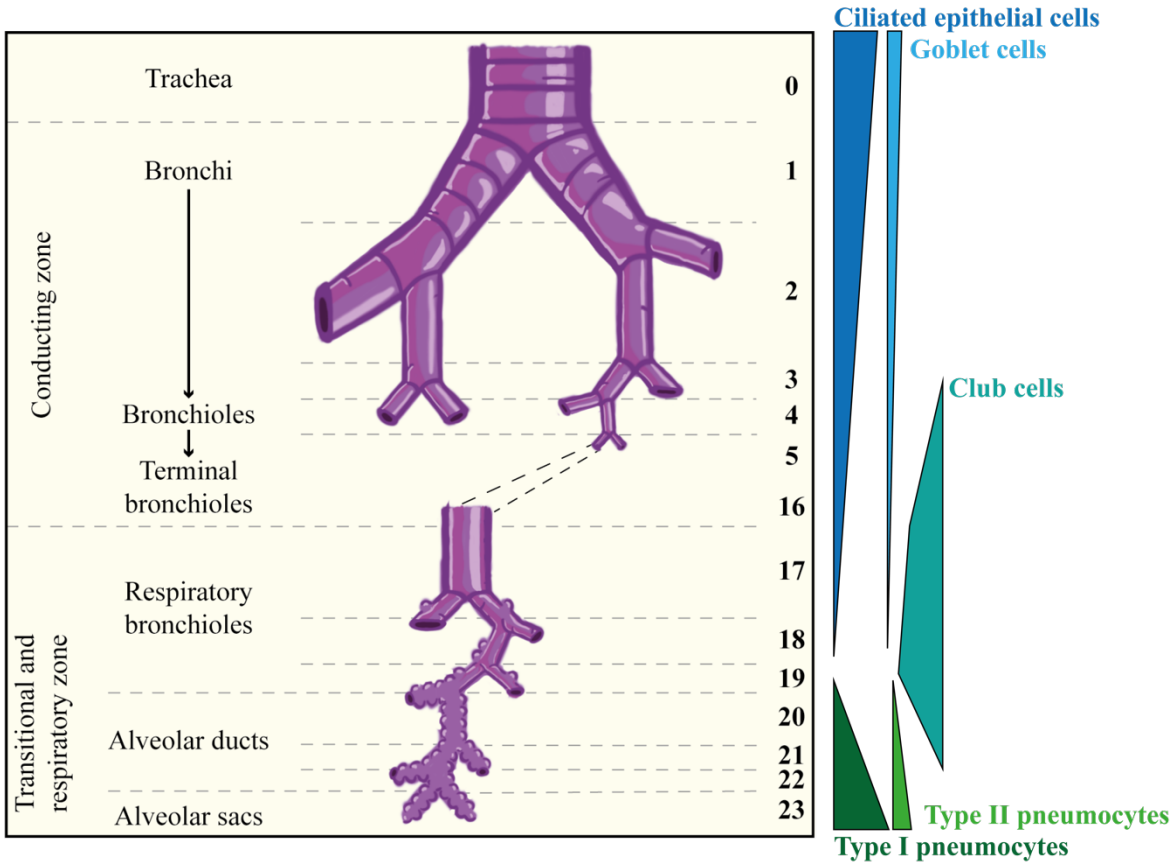

Figure 1-5: Schematic representation of the equine lower respiratory tract organisation and composition. Numbers on the right display the order of bifurcation, ranging from 0 (single tube) to 23. On the right a schematic diagram represents the relative proportion of cell types within the different tissues of the equine lower respiratory tract. Adapted from West and Luks (2016) with help from Jeremy Amat.

1.5.3.1 Mucosa

The mucosa is constituted of ciliated pseudostratified columnar epithelium in which goblet cells are embedded and rest on the lamina propria (Navarro et al. 2017). The goblet cells assure synthesis and secretion of mucins (glycoproteins) which partially constitute the mucus (Ma et al. 2018) and, in co-operation with synchronous cilia movements, allow clearance of pathogens and debris at a pace of 1.6 ± 0.24 cm/min in the horse (Nelson and Hampe 1983). The co-operation between cilia movements from the epithelial cells and the presence of mucus on the cellular apical surface is usually referred as the mucociliary elevator in the literature. The respiratory epithelium morphology evolves along the respiratory tract from a pseudostratified to a cuboidal morphology in the most caudal part (Mair et al. 1987). The change in morphology is associated with a loss of cilia on the apical surface of epithelial cells (Mair et al. 1987). Additionally, the abundance of goblet cells

decreases along the respiratory tract, while club cells increase in number, and type I and type II pneumocytes appear in the alveoli (Figure 1-5).

Such variation in mucosa cellular composition highlights different tissue functions. As mentioned, in the conducting zone of the respiratory tract, the ciliated and the goblet cells perform an effective filtration of air. Additionally, the ciliated epithelial cells constitute a physical barrier between the environment and the organism, while the lamina propria made of connective tissue provides support and nutrition to the epithelium. The lamina propria is important in local mucosal immunity as it contains B and T lymphocytes, natural killer cells (NK cells), dendritic cells, and macrophages. Finally, the lamina propria contains elastic fibres and blood vessels, which are essential to accommodate the change of tracheal diameter during breathing and warming up inhaled air, respectively.

In the transitional and respiratory zone of the respiratory tract, Club cells (also known as bronchiolar exocrine cells) replace the goblet cells and assure the protection of the respiratory mucosa via abundant mucopolysaccharide secretions. In addition, Club cells contribute to the degradation of mucus produced in the upper respiratory tract, as well as in the defence against toxins by producing cytochrome P450 enzymes. Club cells also represent regional progenitor cells of the epithelium in response to pathogen-induced damage and contribute to the airway epithelial lining fluid by producing surfactant proteins (Zheng et al. 2017). Finally, in the most caudal part of the respiratory tract, the respiratory epithelium is made almost entirely of type I and type II pneumocytes. While the type I pneumocytes are thin flattened cells and represent 95% of the alveoli surface area, the type II pneumocytes are cuboidal cells and cover less than 5% of the alveoli area. The type I pneumocytes, as suggested by the large surface covered, are responsible for gas exchange between alveoli and capillaries, while the type II pneumocytes secrete the pulmonary surfactant, preventing the alveoli from collapsing by reducing surface tension. Taken all together, this heterogeneous cell composition of the respiratory mucosa allows various functions that are dynamic and evolve along the respiratory tract. However, the mucosa layer is complemented by additional layers such as the submucosa.

1.5.3.2 Submucosa

The submucosa contains elastic fibres and seromucous tubular glands that communicate with the respiratory tract lumen. Those tubular glands provide, in association with the goblet cells, the mucus lining the upper respiratory tract epithelium and participate in pathogen clearance and air moisturising. As horses commonly suffer from respiratory diseases associated with

excess secretions in the airway lumen, Widdicombe and Pecson (2002) demonstrated that this feature is most likely the consequence of mucus-producing cells hyperplasia and vascular transudation rather than abnormal mucous glands number. Additionally, the submucosa, which is made of connective tissue, contains patches of lymphoid tissue known as mucosa-associated lymphoid tissue (MALT). MALTs are functionally close to lymphoid follicles found in the lymphatic nodes and contain B and T lymphocytes as well as macrophages and plasma cells. MALTs are responsible for systemic immunity by sensing antigens that travelled through the mucosa undetected. Based on their location within the respiratory tract, they are named differently; laryngo-tracheal associated lymphoid tissue (LTALT) in the trachea, bronchus-associated lymphoid tissue (BALT) in the bronchus, and bronchiole-associated lymphoid tissue (BRALT) in the bronchioles (Mair et al. 1987). Interestingly, Mair et al. (1987) observed larger LTALT patches in the horse than in other mammals, and a quasi-absence of BALT in equine bronchi. The reduced BALT patches were counterbalanced by the extended presence of BRALT tissue in the deeper sections of the equine respiratory tract. However, the structural and functional similarities with Peyer's patches observed suggested a crosstalk between the respiratory and digestive mucosal immunity.

Underneath the submucosal layer is found another histological layer, the cartilaginous and muscular layer.

1.5.3.3 Cartilaginous and muscular

Both, the cartilaginous and muscular layer prevent the collapse of the respiratory tract. The cartilaginous layer is only present in the trachea and bronchi of the horse. A series of c-shape hyalin cartilage structures are found in the trachea and maintain it open (see section 1.5.2). The bronchi do not exhibit open cartilaginous rings but plate-like structures. However, it is important to note that in the rest of the respiratory tract, cartilaginous structures are replaced by smooth muscle. In the bronchioles and terminal bronchioles, the smooth muscle cells and the surfactant protein secreted by club cells maintain the respiratory tract architecture.

1.6 Host defence against influenza A virus

The structural organisation of the epithelium, including the apical cilia and the mucus layer containing decoy sialic acid are essential for successful viral clearance. However, EIVs can, overcome these physical limitations and bind to sialic acids decorating the surface of cells. In these specific scenarios, the virus is able to enter the cell and replicate as described in

section 1.3.4. However, host cells evolved and acquired several mechanisms to interfere with and impair viral replication. These mechanisms rely on an early and efficient detection of viral pathogens and include the danger-associated molecular patterns (DAMPs) and pathogen-associated molecular patterns (PAMPs). However, for a long time DAMPs were exclusively restricted to a theoretical model hypothesised by Matzinger (1994) and required the identification a decade later of High Mobility Group Box 1 and uric acid crystals as immune activators to be accepted (Shi et al. 2003). Both DAMPs, and PAMPs are recognised by pathogen recognition receptors (PRRs) and initiate a complex cascade of protein-protein interactions leading to efficient antiviral activity.

1.6.1 Detection of IAV

To maximise detection efficiency, host cells have evolved and acquired complementary sensors known as PRRs. These sensors are represented by three distinct classes: the Toll-like receptors (TLRs), the NOD-like pyrin domain-containing 3 (NLRP3; Sabbah et al. 2009), and cytosolic retinoic acid-inducible gene I (RIG-I)-like receptors (RLRs).

1.6.1.1 The Toll-like receptors

The TLRs are proteins found embedded in the host plasma membrane (TLR1, TLR2, TLR4, TLR5, TLR6, and TLR10), and in endosomal membrane (TLR3, TLR7, TLR8, and TLR9). These locations allow detection of viral nucleic acids present in the extracellular environment or produced by uncoating and degradation of viral particles during endocytosis. Their different associations (homomeric or heteromeric) contribute to the wide range of microbial ligands recognised, however, most of the TLRs (with the exception of TLR3) rely on myeloid differentiation primary response 88 (MyD88) recruitment to initiate a downstream signalling cascade.

During IAV infection, the virus is detected by endosomal embedded TLRs, especially TLR3 and TLR7 detecting double-stranded RNA (dsRNA), and ssRNA, respectively (Diebold et al. 2004; Lund et al. 2004; Botos et al. 2011; Iwasaki and Pillai 2014).

TLR3 is widely expressed in intestinal epithelial and immune cells including myeloid dendritic cells, macrophages, and mast cells (Bugge et al. 2017). However, TLR3 are exclusively found in the endosomal membrane of myeloid dendritic cells, while they were expressed in both cellular and endosomal membranes of macrophages and mast cells (Matsumoto et al. 2003). In acidic conditions (Leonard et al. 2008), viral dsRNA binds to TLR3 N-terminal ectodomain (Botos et al. 2009), inducing TLR3 dimerisation and

recruitment of the TIR-domain-containing adapter-inducing interferon-β (TRIF) (Yamamoto et al. 2003; Botos et al. 2011). This step initiates the MyD88-independent signalling pathway (Figure 1-6) which involves the sequential interaction with TNF receptor-associated factor 3 (TRAF3), TANK binding kinase 1 (TBK1), inhibitor of nuclear factor kappa-B kinase subunit epsilon (IKKε), and NAK-associated protein 1 (NAP1; Oganesyan et al. 2006). Alternatively, the signalling pathway can lead to recruitment of TNF receptor-associated factor 6 (TRAF6), kinases receptor interacting protein (RIP1), mitogen-activated protein kinase kinase kinase 7 (TAK1), mitogen-activated protein kinase kinase kinase 7-interacting protein 2 (TAB2), p38 mitogen-activated protein kinases (MAPKs), and inhibitor of nuclear factor kappa B kinase regulatory subunit alpha (IKK-α), subunit beta (IKK-β), and subunit gamma (NEMO; Figure 1-6; Häcker and Karin 2006). Ultimately, the signalling pathway induces dimerisation and the translocation of interferon regulatory factor 3 (IRF3), as well as the translocation of nuclear factor kappa-light-chain-enhancer of activated B cells (NF-κB), and activator protein 1 (AP-1), three transcription factors mediating the production of type I IFNs, proinflammatory cytokines and chemokines, respectively (Figure 1-6). Additionally, the NEMO-IKKα-IKKβ complex participates in the negative regulation of Iκβ, an inhibitor of NF-κB translocation (Figure 1-6; Zheng et al. 2020; Chen et al. 2021).

TLR7 is expressed in few cell types including human plasmacytoid dendritic (Takagi et al. 2016), and B cells (Barr et al. 2007), but also to lower levels in non-immune cells (*i.e.* hepatocytes, epithelial cells; Schaefer et al. 2004; Lee et al. 2006; Tengroth et al. 2014). To prevent TLR7 recognition of self-genomic information, the receptor locates exclusively in endosomal membranes (Petes et al. 2017). As mentioned previously, TLR7 activation leads to IFN production via a MyD88-dependent pathway (Figure 1-6). Following ssRNA sensing and binding (concomitantly to guanosine binding), TLR7s dimerise and recruit MyD88 adaptor protein (Zhang et al. 2016). This step initiates a succession of protein recruitments including the formation of the interleukin-1 receptor- associated kinase 4 (IRAK4) and IRAK1 complex, activating in turn TRAF6 catalysing the formation of the TAK1-TAB2 complex as previously described (Figure 1-6). The TAK1-TAB2 complex is responsible for the nuclear translocation of NF-κB and AP-1 transcription factors preceding the production of pro inflammatory cytokines.

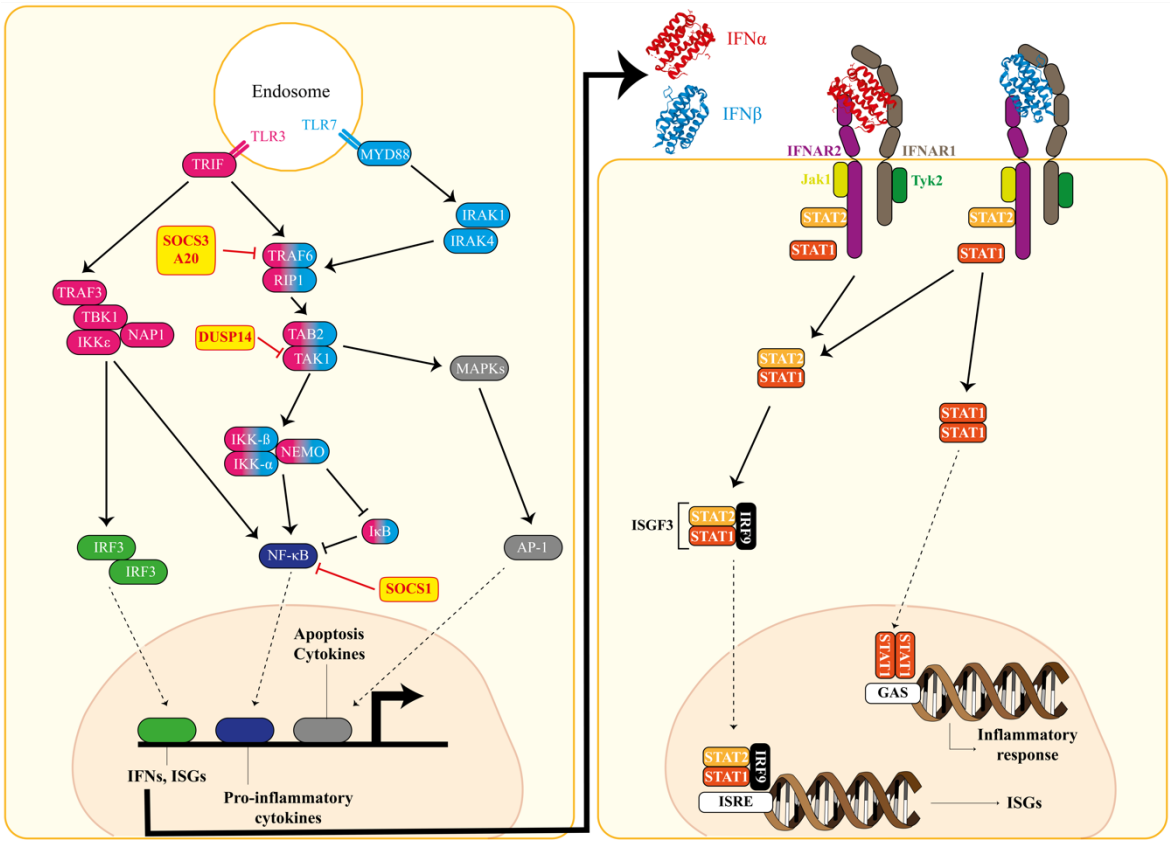

Figure 1-6: Schematic representation of IFN production and Jak-STAT pathways. In the left panel, pathway stimulation originated from TLR3 receptors is shown in magenta, while TLR7-related pathway is shown in blue. Transcription factors IRF3, NF-κB and AP-1 are shown in green, dark blue, and grey, respectively. Yellow boxes are used to display well characterised proteins blocking the IFN production pathway. In the right panel, 3D structures of IFNα and IFNβ are shown in red and blue, respectively. Both proteins are binding to IFNAR1 and IFNAR2 receptors (in brown and violet) and initiate the Jak-STAT pathway. They include the successive recruitment of Jak1, Tyk2, STAT1, STAT2, and IRF9 proteins displayed in yellow, green, dark orange, orange, and black, respectively. Protein complexes are then translocated to the nucleus where they recognise either ISRE or GAS sequences, leading to ISGs production and inflammatory response, respectively.

1.6.1.2 The NOD-like pyrin domain-containing 3

As described, TLR activation leads to production of IFN and IFN stimulated genes (ISGs) activation, including the release of pro-interleukin-1β (IL-1β) and pro-IL18 cytokine precursors. NLRP3 expressed by myeloid cells (monocytes, DCs, neutrophiles, and macrophages), and bronchial epithelial cells can form a multiprotein inflammasome complex. NLRP3 inflammasome complex formation is initiated by M2 protein acting as a viroporin in multiple intracellular compartments, including the trans-Golgi-network, during its trafficking to the plasma membrane (Ichinohe et al. 2010). Following the inflammatory

signal given by M2 proton export, NLRP3 associates with apoptosis-associated speck-like protein containing carboxy-terminal CARD (ASC) and caspase-1 proteins to form the inflammasome (Spel and Martinon 2021). The latter is cleaving pro-IL-1β and pro-IL18 precursors into IL-1β and IL-18 active cytokines leading to pyroptosis, a proinflammatory form of cellular death mediated by gasdermin D (GSDMD; (Shi et al. 2015; Opdenbosch and Lamkanfi 2019).

The exact mechanism by which IAV activates the inflammasome is unclear but remains essential as highlighted by genetically modified mice lacking NLRP3, ASC, or caspase-1. These mice show a decreased inflammatory cytokines in the lungs associated with an increased mortality and viral clearance defects (Allen et al. 2009; Thomas et al. 2009). These activated inflammatory cytokines recruit monocytes and neutrophils into the lungs and participate in the control and regulation of infection and tissue pathogenesis, respectively.

1.6.1.3 The RIG-I-like receptors

In addition to the previously described PRRs, the cytosolic RLRs are probably the most studied, and regroup RIG-I (also known as DDX58), melanoma differentiation-associated protein 5 (MDA5), and laboratory of genetics and physiology 2 (LGP2) (Hornung et al. 2006). RIG-I and MDA5 are expressed in all cell types and are most often studied in innate immune and mucosal epithelial cells. Both RIG-I and MDA5 are categorised as ATP-dependent DExD/H box RNA helicases (Fullam and Schröder 2013) and are structurally similar. They contain, from the C-terminal to the N-terminal ends, one C-terminal regulatory domain, two helicase domains, and two caspase activation and recruitment domains (CARD), but recognise different types of RNAs (Yoneyama et al. 2004). RIG-I senses short 5′-triphosphated dsRNA (Hornung et al. 2006; Pichlmair et al. 2006), while MDA5 binds preferentially to longer dsRNA, not necessarily 5′-triphosphated such as polyinosinic:polycytidylic acid (poly(I:C)) (Kato et al. 2006; Kato et al. 2008). The inactive proteins show interaction between their own CARD and helicase domains, while activation induces an ATP-dependent conformational change exposing the CARD domains to other interactors (Kowalinski et al. 2011). The series of steps required for RIG-I and MDA5 activation have been described by Kolakofsky et al. (2012). Briefly, RIG-I CARD domains are phosphorylated by protein kinase C α and β (PKC-α/β) and choline kinase β at the N and C terminal regions, respectively, while MDA5 CARD domains are phosphorylated by RIO Kinase 3 and other unknown kinases. Following phosphorylation steps, the E3 ubiquitin ligase tripartite motif-containing protein 25 (TRIM25) and the ring finger protein 135

(RNF135, also known as RIPLET) polyubiquitinate (K63-linked polyubiquitination) the C and N terminal CARD domain of RIG-I, respectively. MDA5 polyubiquitination mediators remain unidentified as studies led to conflicting results. However, TRIM65 has been recently found to be an essential mediator of MDA5 activation by K63-linked polyubiquitination (Lang et al. 2017). Activated RIG-I or activated MDA5 form oligomeric complexes that interact with the mitochondrial antiviral-signalling protein (MAVS) found embedded in the outer membrane of mitochondria, peroxisome, and the rough endoplasmic reticulum (ER; Kawai et al. 2005; Seth et al. 2005). Following activation by either RIG-I or MDA5, mediated by RLR-CARD/MAVS-CARD interaction, mitochondrial MAVS proteins (Seth et al. 2005) (also known as IPS-1 (Kawai et al. 2005), CARDIF (Meylan et al. 2005), and VISA (Xu et al. 2005) in the literature) aggregate and bind TRAF family members (TRAF2, TRAF3, TRAF5, and TRAF6) proteins (S. Liu et al. 2013) via a proline-rich region (PRR), initiating a succession of protein-protein interactions leading to the synthesis of IFN and stimulation of ISGs induced by translocation of IRF3, and NF-κB as previously described (Seth et al. 2005). Despite their clear mechanistic differences, RIG-I and MDA5 proteins share a relatively recent common origin when compared to other DExD/H box helicase proteins (*i.e.* LGP2, DICER; (Brisse and Ly 2019). MDA5 orthologues are found in most vertebrates, while RIG-I orthologues are found in mammals, ducks (Barber et al. 2010), and fish (Poynter et al. 2015).

The third and last RLR, LGP2, although structurally close to RIG-I and MDA5, lacks CARD domains, essential requirements for MAVS interaction and activation (Lenoir et al. 2021). Since its discovery, LGP2 has since been identified as an immune regulator, however conclusions from mouse studies were often disparate (Venkataraman et al. 2007; Satoh et al. 2010), but suggest that high levels of LGP2 expression, in response to viral infection, acts as a negative control of antiviral signalling pathway, preventing detrimental effects of overstimulation (Komuro and Horvath 2006; Parisien et al. 2018).

During IAV infection, viral detection and subsequent IFN production in respiratory epithelial cells are mainly dependent on RIG-I, while MDA5-dependent sensing and IFN production occur in limited host species, such as chickens, which are RIG-I deficient (Karpala et al. 2011; Liniger et al. 2012).

1.6.2 Influenza PAMPs

PAMPs are generated during the whole viral life cycle, and studies indicate that they were driven mainly, but not exclusively, by viral RNA synthesis in airway epithelial cells and

monocyte-derived DCs as vRNPs alone were not sufficient to initiate a strong IFN response (Österlund et al. 2012; Crotta et al. 2013). In fact, Killip et al. (2014) demonstrated that IRF3 phosphorylation (as a proxy for IFN induction) was not reduced following small interfering RNA treatment, highlighting the role of RNA synthesis in IRF3 activation and IFN production, even in the absence of viral protein production. Additionally, they highlighted that 5,6-dichloro-1-β-D-ribofuranosyl-benzimidazole treatment (inhibiting vRNA nuclear export) was associated with a reduction of IRF3 activation and IFN production. Furthermore, IFN induction in IAV infected cells correlates with the accumulation of vRNA and is completely abrogated by virus inactivation following heat or ultraviolet treatment (Österlund et al. 2012; Crotta et al. 2013). However, the above studies have been limited to a small number of IAV strains and might not represent the full repertoire of PAMPs recognised by RIG-I during IAV infection.

1.6.3 Interferons and IFN-stimulated genes production

Originally, IFN, a secreted cytokine with antiviral attributes was discovered in 1957 by Isaacs and Lindenmann. Following this discovery, IFN was extensively studied and led to the identification of several IFN encoding genes, and IFN classes subdividing the IFN molecules in three distinct types (IFN type I, IFN type II, and IFN type III). Isaacs and Lindenmann identified IFN belongs to the type I IFN and exist in several distinct forms (α, β, δ, ε, κ, τ, and ω), encoded by multigenic families (*i.e.* 13 genes and 3 genes coding for IFN-α and IFN-β , respectively; nicely reviewed by Randall and Goodbourn 2008). For practicality, I will refer to the type I IFN molecules as IFN-α and IFN-β. Type I IFN is recognised by the IFN α and β receptor (IFNAR) surface receptors (Figure 1-6). IFNAR receptors (IFNAR1, and IFNAR2) are both embedded in plasma membrane and their cytosolic tails are associated with a Tyrosine kinase 2 (Tyk2), and a Janus kinase 1 (Jak1), respectively (Figure 1-6; Precious et al. 2005; Tang et al. 2007). Additionally, IFNAR2 is attached tightly by the cytoplasmic tail to the signal transducer and activator of transcription 2 (STAT2) and more loosely to STAT1 (Figure 1-6). During IFNAR activation by type I IFN ligands, a conformational change induces the phosphorylation of IFNAR1 by Tyr2, and STAT1 by Jak1, leading to the heterodimerisation of STAT1 and 2, and subsequently the recruitment of the Interferon regulator factor 9 (IRF9) (Krishnan et al. 1996). Activated STAT1/STAT2 associated with IRF9 form the IFN-stimulated factor 3 (ISGF3) complex which recognises and binds to the genomic IFN-stimulated response element (ISRE) sequence (AGTTTCNNTTTCNC) within the nucleus (Figure 1-6; Tang et al. 2007). Such

recognition initiates the transcription of hundreds of ISGs acting as antiviral factors that block viral replication and further virus spread. However, STAT1 could also form homodimers leading to their translocation to the nucleus and binding to gamma interferon activation site (GAS; TTNCNNNAA), inducing a massive transcription of cytokines and chemokines (Figure 1-6; Li et al. 1996). Similarly, STAT1/STAT2 complex lacking IRF9 recruitment can lead to GAS sequence recognition and inflammatory response exacerbation. Like type I IFN, type II IFN, especially IFN-γ, is critical to both the innate and adaptive immunity. IFN-γ is recognised by IFN gamma receptor 1 (IFNGR1) which mediates the phosphorylation and activation of Jak1 and Jak2, leading to STAT1 homodimerisation. As described previously, the STAT1-STAT1 complex is responsible for the production of cytokines and chemokines, giving to IFN-γ the ability to act as an activator of macrophages and stimulator of NK and neutrophil cells activation (Decker et al. 1997).

To complete the picture, type III IFNs are also important in the early stimulation of ISG induced by viral infection (Kotenko et al. 2003). Type III IFN includes the IFN-λ1 (also known as IL-29), IFN-λ2 (also known as IL-28A), IFN-λ3 (also known as IL-28B) and IFN-λ4 all binding to the IFN-λR1 receptors mainly expressed in epithelial cells (Broggi et al. 2017). IL-10Rβ constitutes the second IFN-λ receptor and in opposition to IFN-λR1, IL-10Rβ is more broadly expressed in mammalian tissues (Sheppard et al. 2003). Thus, type III IFNs are thought to act as a mucosal barrier. IFN-λ receptor complex induces ISG expression similarly to type I IFN involving the formation of ISGF3 complex (Zhou et al. 2007). However, recent studies suggest that, in addition to Jak1 receptor activation, Jak2 also mediates type III IFN signalling (Broggi et al. 2017). Type I and type III IFN signalling display different kinetics as type III IFN induces a delayed, modest, but sustained ISG expression, while type I IFN is more rapid and efficient to stimulate brief ISG expression (Pervolaraki et al. 2018; Stanifer et al. 2020). These results might suggest that both IFN types might act in concert, leading to a quick and intense ISG expression (also associated with cytokine and chemokine production) attributed to a type I IFN response, while during the same time type III IFN is slowly inducing ISG expression, assuring the stability of the response over time without the immunopathology associated with type I IFN response. However, experimental confirmation is difficult as ISG are cell type dependent, and metanalysis difficult to generate as IFN input and timeframe of response are often different among published works (Stanifer et al. 2020).

As earlier described, the IFN response to viral infection is multifactorial, complex and requires a tightly control to prevent detrimental effects of long and exacerbated responses.

Therefore, shortly after IFN exposure, cell enter an IFN-desensitised state that can last several days (Larner et al. 1986). This state is established in cells by multiple mechanisms, either intrinsic or mediated by the actions of ISG such as the suppressor of cytokine signalling (SOCS) proteins, induced early in the IFN response to infection. These proteins inhibit JAK-STAT signalling by binding to either the IFN receptor or the JAK proteins. Receptor endocytosis and turnover play also an important role in reducing the level of JAK-STAT signalling. In addition, STAT activity can be modulated by members of the family of protein inhibitors of activated STAT (PIAS), however the precise mechanisms by which these proteins inhibit IFN signalling is still to be elucidated (reviewed by Schneider et al. 2014).

1.6.4 Interferon-stimulated genes

As extensively described in the previous sections, EIV sensing by host cells leads to increased expression of ISG, which associated with IFN, cytokine, and chemokine production contributes to the host response to infection. As every single stage of the virus life cycle is a potential target for ISGs intervention, they act on multiple steps of the replication to minimise viral escape. Of these ISGs, several have been extensively studied and identified as important influenza restriction factors.

1.6.4.1 Myxovirus resistance (Mxs)

The IFN-induced GTP-binding proteins are also known as Mxs include the Mx1 and Mx2 proteins. They were the first ISG proteins found to restrict IAV replication and are induced by type I and type II IFNs (Haller et al. 1980; Haller 1981). Mutations in the murine *Mx1* gene were correlated to an increased susceptibility of BALB/c and CBA/J mice to influenza (Staeheli et al. 1988). Murine Mx2 in opposition to Mx1 nuclear localisation, is cytosolic and is also considered an ISG, however, no antiviral activity against influenza has been identified so far. Studies on *MxA* gene (the human orthologue of the murine *Mx1* gene) have suggested that its oligomerisation forms a ring-like structure that binds to NP and prevents vRNPs nuclear import, aborting viral replication (Turan et al. 2004). Furthermore, a recent study investigating the host specificity of Mx1 antiviral function found that human and equine MxA/Mx1 proteins exhibit antiviral potential against non-human and non-equine IAV, respectively. In fact, EIV resistance to equine Mx1 inhibition has been linked to the presence of a histidine at position 52 in NP. The H52N mutation in NP was sufficient to induce a potent viral inhibition, while an N52H mutation in avian IAV NP has been shown

to be protective (Urooj et al. 2019). However, influenza inhibition by Mx1 is also thought to be the consequence of the disruption of NP-PB2 interaction, which results in a less efficient vRNP assembly and subsequent polymerase activity.

1.6.4.2 Interferon-induced proteins with tetratricopeptide repeats (IFITs)

IFN-induced proteins with tetratricopeptide repeat protein orthologues have been identified in mammals, birds, fish, and amphibians. This protein family is composed of four members named IFIT1 (also known as ISG56), IFIT2 (also known as ISG54), IFIT3 (also known as ISG60), and IFIT5 (also known as ISG58). In *Equus caballus*, IFIT proteins are encoded by genes localised on chromosome 1. Most cell types do not express IFIT proteins under basal conditions, with the exception of some myeloid cell subsets (Daffis et al. 2007). However, *ifit* gene promoters possess two or more ISRE motifs generally located within 200 base pair (bp) upstream of the transcriptional starting site, inducing a rapid and important levels of IFIT expression in most of the cells following viral sensing (Sarkar and Sen 2004; Y. Liu et al. 2013). IFIT proteins inhibit viral replication by either binding to eukaryotic initiator factor 3 (eIF3), interfering with the translational process, or binding to 5′-triphosphated vRNA sequences.

1.6.4.3 Interferon induced transmembrane (IFITMs)

IFN-induced transmembrane proteins (IFITMs) are a protein family including IFITM1, IFITM2, IFITM3, IFITM5 and IFITM10, and the first three are known to have antiviral functions against influenza (Brass et al. 2009; Huang et al. 2011; Feeley et al. 2011). While IFITM1 localises to the plasma and early endosomes membranes, IFITM2 and 3 are preferentially found in late endosomes and lysosomes (Mudhasani et al. 2013). IFITMs inhibit viruses that are internalised via the endosomal pathways (clathrin and caveolin mediated; see section 1.3.4.1), suggesting a potential block of viral fusion during the endosomal journey. However, even though the potential event underpinning IFITM restriction seems to be related to HA fusion activity, the exact mechanism by which this takes place has not yet been fully elucidated (Brass et al. 2009; Feeley et al. 2011).

1.6.4.4 2'-5'-Oligoadenylate synthetase (OAS)

The 2′-5′-oligoadenylate synthases (OAS) act in concert with ribonuclease L (RNase L) leading to degradation of cytosolic vRNA (reviewed by Silverman 2007). OAS is activated by dsRNA binding which converts ATP into 2′-5′-oligoadenylate and in turn activates RNase

L. Activated RNase L is responsible for cleavage of viral and cellular RNA, aborting the viral infection. Moreover, RNase L cleaved products have been shown to trigger RIG-I activation, which enhance IFN secretion (Malathi et al. 2007; Chakrabarti et al. 2011).

1.6.4.5 Tripartite motif proteins (TRIMs)

The TRIM family of proteins is composed of more than 60 members and exhibits a wide range of activities including E3 ubiquitin ligase activity, SUMOylation and ISGylation. Among them is found TRIM25, responsible for ubiquitination and activation of RIG-I as previously described (see section 1.6.3).

1.6.4.6 Interferon-stimulated gene 15 (ISG15)

INF-stimulated gene 15 (ISG15) is a 15 kilodalton (kDa) protein first identified in 1979, and is one of the most overexpressed ISGs (Farrell et al. 1979). However, despite reports describing ISG15 functions and interactors *in vitro*, its role *in vivo* remains unclear (Bogunovic et al. 2012). ISG15 is secreted from immune cells (neutrophils, monocytes, lymphocytes) and enhances the production of type I IFN (Bogunovic et al. 2013). Recent studies have shown that the ISGylation of both host and viral proteins and the non-covalent binding of ISG15 to host proteins can disrupt viral replication and act as an antiviral (reviewed by Perng and Lenschow 2018). For example, ISGylation of viral NS1 at distinct sites disrupts its interaction with several binding partners, limiting its ability to disrupt the host antiviral response (see section 1.7.1.3), which in turn impaired viral replication (Tang et al. 2010). Additionally, ISGylation of host proteins such as the tumor susceptibility gene 101 (TSG101) leads to a reduction of viral egress efficiency, and a limitation of viral infection. However, such ISGylation can easily be reverted following the action of deISGylases such as USP18 (reviewed by Perng and Lenschow 2018).

1.6.4.7 Radical S-adenosyl methionine domain containing 2 (RSAD2/Viperin)

Viperin (also known as RSAD2) is encoded by the *rsad2* gene and is a well-known and broad antiviral effector. RSAD2 can be induced by at least two different pathways, the JAK-STAT signalling pathway and by IRF3 activation. Due to its ER and ER-derived lipid droplets location, viperin is involved in the inhibition of influenza virus budding. IAV virus release inhibition has been linked to the capacity of viperin to alter plasma membrane fluidity and lipid rafts formation by interacting with farnesyl diphosphate synthase, an enzyme involved in isoprenoid biosynthesis (Wang et al. 2007).

1.6.5 Other immune players

As demonstrated previously, the innate immune response plays an important role in controlling virus replication, however, host clearance and recovery from infection requires the adaptive immune response (van der Sandt et al. 2012). The chemokine production stimulated during IAV infection initiates a rapid recruitment of monocytes and neutrophils to the site of infection. The recruitment of immune cells is complemented by the activation of NK cells and guarantees an efficient clearance of viral and dead cells. The stimulated immune cells have the capacity to transport antigens from the site of infection to the draining lymph nodes where they encounter antigen presenting cells (*e.g.* dendritic cells). The activation of effector T cells is a crucial step for the induction of adaptive immune responses by the presentation of viral antigens to naïve and memory B and T lymphocytes (reviewed by Iwasaki and Pillai 2014).

The B lymphocytes are the first components of the adaptive immune system to be in contact with viral antigens. Once activated, they differentiate into plasmocytes, in charge of antibody production. In the lung, plasmocytes generate mainly IgG and IgM, whereas in the upper respiratory tract IgA is the predominant antibody (reviewed by Waffarn and Baumgarth 2011; Iwasaki and Pillai 2014). Most IAV proteins are recognised by these different antibodies, however, the avidity and efficiency of binding are depending on the targeted protein. The preferred targets of neutralising antibodies are the viral surface glycoproteins HA and NA. Seroconversion usually happens after six to seven days post-exposure and antibody titres increase during the first month (Waffarn and Baumgarth 2011).

The T lymphocytes are responsible for eliminating infected cells by expressing FAS ligand or TNF-related apoptosis-inducing ligand (TRAIL), initiating the extrinsic apoptotic pathways and engaging the cells in a programmed cell death. Additionally, T cells are responsible for the production of proinflammatory cytokines (van der Sandt et al. 2012).

1.7 Viral evolution

Following influenza infection, a race begins between the host immune system and the virus. Eventually, most viral infection will be successfully controlled by the host immune response. However, IAVs have evolved various strategies to control the early step of this response, notably by blocking the type I IFN system, in order to facilitate its own replication and transmission and thus maintain its position in the current ecological landscape.

1.7.1 Escape strategies

As described in section 1.6, host cells have several and sometimes redundant strategies to minimise and quickly clear viral infection. However, EIV has developed countermeasures to avoid host restriction factors and to keep the ability to infect, replicate and spread efficiently in equine cells. Due to genomic constraints only a limited number of viral proteins are encoded, and viral genomic content must be optimised (see section 1.3.3, and 1.3.3.1).

1.7.1.1 Antigenic drift

As mentioned before, Steinhauer et al. (1992) highlighted the poor fidelity of RNA virus polymerase (including IAV) during viral replication and linked it to the lack of proofreading activity. This feature allows a more frequent apparition of point mutations during viral replication and induces a genomic plasticity which under selection pressures lead to a directed viral evolution. This mechanism of viral adaptation has been coined as antigenic drift and, coupled to the fast viral generation time, is responsible for rapid viral adaptation. However, all viral segments do not appear to accumulate mutations at the same rate as seen in HA, NA and PA, identified as the most mutated influenza segments (Murcia et al. 2011).

1.7.1.2 Antigenic shift

Complementary to antigenic drift, EIV also relies on a more drastic mechanism to quickly evolve. Due to the segmented nature of the genome, reassortment of entire viral segments can happen in cells co-infected with more than one EIVs and this has been referred as antigenic shift. Such dramatic change allows the emergence of novel viruses and facilitates the crossing of species barriers. Mechanisms have been extensively studied in HA and NA proteins, allowing them to quickly evolve and escape from neutralising antibodies, but antigenic shift has also been responsible for shaping evolution of other viral proteins.

1.7.1.3 Viral responses to host restriction factors: IAV NS1

NS1 is the main IAV blocker of IFN induction, for which it has evolved multiple mechanisms (nicely reviewed by Hale et al. 2008). Activation and translocation of transcription factors such as IRF3, NF-κB and AP-1 (see section 1.6.3) have been shown to be inhibited by NS1, leading to decreased IFN-β expression (Talon et al. 2000; Wang et al. 2000; Ludwig et al. 2002). Direct interactions between NS1 and RIG-I have been described and impact the subsequent canonical pathway (see section 1.6.1.3; reviewed by Krug 2015).

Additionally, NS1 interacts with TRIM25 (Koliopoulos et al. 2018) and RNF135 (Rajsbaum et al. 2012) proteins, which are responsible for RIG-I polyubiquitination.
NS1 is also known to bind to dsRNA, preventing RLR recognition (Hatada and Fukuda 1992). In addition to limiting RIG-I activation, the dsRNA-binding function of NS1 has also suggested to impair the function of ISGs which have been shown to have direct antiviral functions against IAV, such as the OAS and RNase L (Min and Krug 2006).
Finally, NS1 protein from early H3N8 EIVs showed a general inhibitory effect on cellular gene expression leading to a host protein shut-off mediated by cellular polyadenylation-specific factor 30 (CPSF30; Chauché et al. 2018).

1.7.1.4 Viral response to host restriction factors: IAV HA

As described in section 1.7.1.2, the surface glycoproteins possess an increased propensity to mutation accumulation, which under selection pressures led to a directed viral evolution. Antigenic drift has been linked to immune evasion.

Chapter 2: Aims

2.1 Aims

The overall objective of this study was to determine the impact of evolution on virus adaptation to a new host species. Using equine influenza virus as a model system, the specific aims of this study were:

I. To characterise the *in vitro* and *ex vivo* phenotype of infection of evolutionarily distinct EIVs of the currently circulating H3N8 lineage
II. To characterise the *in vitro* phenotype of infection of A/equine/Jilin/1/1989 and a phylogenetically related H3N8 avian influenza virus.
III. To generate a reverse genetics system to study the *in vitro* phenotype of infection of H7N7 EIVs.
IV. To characterise the *in vitro* phenotype of infection of A/equine/Lexington//1/1966 (H7N7).

Chapter 3: Materials and Methods

3.1 Bacterial transformation and plasmid preparation

3.1.1 Ampicillin stock solution

One gram of ampicillin sodium salt (Sigma-Aldrich, UK) was dissolved in 10 mL of H_2O and filtered using 0.22 µm filters before it was aliquoted (1 mL) and stored at -20ºC.

3.1.2 Competent cells transformation

MAX Efficiency® Stbl2™ chemically competent *E. coli* cells (ThermoFisher Scientific, UK) were transformed following the manufacturer's protocol. Briefly, competent cells were thawed on wet ice before they were gently mixed, and 100 microlitres (µL) distributed in Eppendorf tubes. Between 1 and 10 nanogram (ng) of stock plasmid was added to the aliquoted MAX Efficiency® Stbl2™ chemically competent cells and mixed by gentle pipette tip movements. Once mixing was completed, the tubes were incubated 30 min on ice. Following incubation, mixtures of DNA-competent cells were subjected to heat-shock treatment (42ºC) for 25 seconds before they were incubated on ice for 2 min. Then 900 µL of room temperature S.O.C. medium (Invitrogen, UK) was added, and Samples were incubated at 30ºC for 1 hour with shaking (225 revolutions per minute). Additional tube containing pUC19 plasmid DNA was processed as a positive control, allowing calculation of transformation efficiency if needed. A volume of 10 µL and 20 µL of the transformed competent cells were streaked onto two Petri dishes (Thermo Scientific, UK) containing Luria broth (LB) agar (E&O Laboratories limited, UK) supplemented with ampicillin (100 µg/mL) before they were incubated overnight at 37ºC. Colonies from transformed competent cells were individually selected and incubated with 5 mL of LB media supplemented with ampicillin (100 µg/mL) before they were incubated overnight at 37ºC. Following incubation, 2 mL of this overnight culture was sampled and incubated a further day with 48 mL of LB media supplemented with ampicillin (100 µg/mL).

3.1.3 Plasmid purification

Bacterial cultures containing the plasmid were purified using the Qiagen plasmid Midi Kit (Qiagen, UK) according to the manufacturer's protocol. Briefly, bacterial cultures were pelleted by centrifugation at 6,000*g* and 4ºC for 15 min. Bacteria were then resuspended in 4 mL of resuspension buffer (P1; supplemented with RNAse A, and LyseBlue reagents) until

no cell clumps remained. The resuspended cells were treated with 4 mL of lysis buffer (P2), mixed vigorously, and then incubated at room temperature for exactly 5 min. A volume of 4 mL of chilled neutralisation buffer (P3) was added to samples and tubes thoroughly mixed before an incubation of 15 min. The solution was then centrifugated at 20,000*g*, 4ºC for 30 min and in the meantime, QIAGEN-tip 100 columns were prepared by the addition of 4 mL of equilibration buffer (QBT). After centrifugation, the supernatant was loaded into the QIAGEN-tip 100 column. After the solution passed entirely through the column, a further 4 mL of washing buffer (QC) was loaded into it, and this step was repeated twice. Finally, 5 mL of elution buffer (QF) was loaded into the column. Eluted solution containing DNA was then precipitated by adding 3.5 mL of room temperature isopropanol (Honeywell, UK) followed by a vigorous mix and centrifugation at 15,000*g*, 4ºC for 30 min. The pellet (DNA) was washed by using 2 mL of room temperature 70% ethanol followed by a centrifuge step of 15,000*g* for 30 min. Finally, the DNA pellet was air-dried and resuspended in 15—50 uL of ultra-pure H_2O, before being stored at -20ºC until future use.

3.1.4 Plasmid quantification

Concentration and quality of the purified DNA plasmid were quantified by using a Nanodrop Spectrophotometer 2000 (Thermo Scientific, UK). Briefly, concentration was recorded as µg/µL, while plasmid purity and protein contamination were assessed using the ratio of measured spectrophotometric absorbance at 260 nm and 230 nm, and 260 nm and 280 nm, respectively.

3.1.5 Plasmid sequencing

The sequence accuracy of plasmids obtained were confirmed by Sanger sequencing (Source Biosciences) and compared to the publicly available sequences from National Center for Biotechnology Information (NCBI) Database.

3.1.6 DNA oligos

DNA oligos used in plasmid sequencing experiment were manually designed from A/equine/Jilin/1/1989(H3N8) (EIV/89) publicly available viral sequence and the empty pDP2002 expression plasmid using Geneious v9.1.7. Primers were designed to contain between 17 and 25 nucleotides, as well as a 40—60% guanine cytosine (GC) content, and to reach full coverage. Furthermore, three additional DNA oligos (Influenza universal primers)

were used as previously described (Hoffmann et al. 2001). An extended list of DNA oligos used in this study is shown in Table 3-1. DNA oligos were high performance liquid chromatography purified (Sigma-Aldrich, UK) and resuspended in H_2O to obtain a final concentration of 100 nanomolar.

Table 0-1:DNA oligos composition details

DNA Oligo name	Length	GC (%)	Sequence (5′-3′)	TM (ºC)
pDP2002_Primer1Fw	22	50.0%	AAAATGCCGACTCGGAGCGAAA	63.4
pDP2002_Primer2Fw	22	50.0%	AAATCGACGCTCAAGTCAGAGG	60.7
pDP2002_Primer3Fw	22	54.5%	TGGCCCCAGTGCTGCAATGATA	64.6
pDP2002_Primer4Fw	23	52.2%	ACGTTCTTCGGGGCGAAAACTCT	64.8
pDP2002_Primer5Fw	20	50.0%	TTTGACTCACGGGGATTTCC	57.8
pDP2002_Primer6Rev	21	52.4%	TTTTTGGGGACAGGTGTCCGT	62.1
Seg1_50Fw	21	52.4%	GAGATCTAATGTCGCAGTCCC	58.0
Seg1_719Rev	20	45.0%	ACCTCAATGTACACACTGCT	56.8
Seg1_946Fw	22	45.5%	GCTGTGGATATATGCAAAGCAG	57.8
Seg1_1689Fw	22	45.5%	CAGAAATTGGGAGACTGTGAAG	57.0
Seg2_320Fw	19	57.9%	CCCACCCAGGGATCTTTGA	58.6
Seg2_644Rev	23	43.5%	CCCTATTGTTCTTTGTGTGACCA	58.9
Seg2_845Fw	23	43.5%	GAGGGAATGAGAAGAAGGCTAAA	57.9
Seg2_1625Fw	23	43.5%	GATAAACAATGACCTTGGACCAG	57.4
Seg3_151Fw	23	43.5%	GAAGTCTGCTTCATGTATTCGGA	58.6
Seg3_682Rev	18	55.6%	GGAGACTTTGGTCGGCAA	57.2
Seg3_973Fw	22	40.9%	TGGAAAGAGCCCAACATTATCA	57.7
Seg3_1715Fw	22	45.5%	ATGTGAGAACTAACGGAACCTC	57.8
Seg4_104Fw	19	52.6%	TACAGCAACACTGTGCCTG	58.0
Seg4_686Rev	21	52.4%	TGTGACTCTTCCTGAGGCTTG	59.7
Seg4_886Fw	21	47.6%	CAGATGCACCTATTGACACCT	57.7
Seg5_703Fw	22	45.5%	GAGAGAATGTGCAACATCCTCA	58.4
Seg5_842Rev	18	55.6%	AGGATGAGTGCAGACCGT	57.9
Seg6_641Fw	18	55.6%	AGGGGTGCCTACTGATGT	57.1
Seg6_897Rev	22	45.5%	TGTCTCTACATACGCATTCCAC	58.0

Seg7_233Fw	17	58.8%	AGTGAGCGAGGACTGCA	57.7
Seg7_899Rev	25	40.0%	CCCTCTTTTCAAACCGTATTTAAGG	58.4
Seg8_45Fw	23	43.5%	CAACCTCGTTTCAGGTAGATTGT	58.7
Seg8_840Rev	25	40.0%	CCTTATCTCACTCTCAACTTCAAGT	58.3
Uni12_PCR	17	58.8%	CAGGGAGCAAAAGCAGG	55.4
Uni12G_PCR	17	64.7%	CAGGGAGCGAAAGCAGG	57.6
Uni13_PCR	25	44.0%	CGGTCTCGTATTAGTAGAAACAAGG	59.0

TM : Melting temperature

3.2 Design of a reverse genetics plasmid set to rescue A/equine/Lexington/1/66 (H7N7)

The strategy used to design the 8 individual plasmids is described in Figure 6-1 A, but briefly, the publicly available sequences of EIV/66 segments were used to construct the DNA insert sequences. As the viral sequences of the 5′ and 3′ untranslated regions (UTRs) were unavailable, they were inferred based on the consensus found in the multiple alignment (MUSCLE; Edgar 2004) of all complete and full length H7N7 EIV genomes available (n=12). Both UTRs were associated with *BsmBI* restriction site sequences (5′-GAGACG-3′) on their distal ends. The detail of plasmids composition is given in Table 3-2. The eight DNA insert sequences designed were synthesised, cloned in the pDP-2002 expression plasmid, and quality controlled (Genewiz, USA). All the EIV/66 plasmid sequences are available in Appendix 2.

Table 0-2: A/equine/Lexington/1/1966(H7N7) plasmids composition details

Accession ID	5′-UTR	3′-UTR	Segment	Vector
CY039398.1	5′-AGCGAAAGCAGGTCAAATATATTCAAT-3′	5′-TGTAAAACTGTTCAAAAACGACCTTGTTTCTACT-3′	1	pDP-2002
CY039397.1	5′-AGCGAAAGCAGGCAAACCATTTGA-3′	5′-GAAAAAATGCCTTGTTTCTACT-3′	2	pDP-2002

CY039396.1	5′-AGCGAAAGCAGGTACTAATTCAAA-3′	5′-TTTTGGCAATGCTACAATTTGCTGTCCATACTGTCCAAAAAAGTACCTTGTTTCTACT-3′	3	pDP-2002
CY039391.1	5′-AGCAAAAGCAGGGGATACATA-3′	5′-GTTTGAAAAAACACCCTTGTTTCTACT-3′	4	pDP-2002
CY039394.1	5′-AGCAAAAGCAGGGTAGATAATCACTCACTGAGTGACATCAAAATC-3′	5′-AGAAAAATACCCTTGTTTCTACT-3′	5	pDP-2002
CY039393.1	5′-AGCAAAAGCAGGGGGATTTTAAA-3′	5′-AATGAAAAAAACCCTTGTTTCTACT-3′	6	pDP-2002
CY039392.1	5′-AGCAAAAGCAGGTAGATGTTGAAAG-3′	5′-AAAACTACCTTGTTTCTACT-3′	7	pDP-2002
CY039395.1	5′-AGCAAAAGCAGGGTGACAAAAACATA-3′	5′-TGATAAAAAACACCCTTGTTTCTACT-3′	8	pDP-2002

3.3 Cell culture

3.3.1 Cell maintenance

Sterile standard tissue culture conditions were maintained in all experiments. MDCK (ATCC CCL-34) and human embryonic kidney cells (HEK293T, ATCC CRL-11268) were grown at 37ºC, 5% CO_2 in Dulbecco's modified Eagle's medium (DMEM) high glucose, GlutaMax and pyruvate supplemented (ThermoFisher Scientific, UK), 10% of fetal bovine serum (FBS; Gibco Life Technologies, UK). For simplicity, the aforementioned media will be referred to as maintenance media, in the following sections . Equine Dermal fibroblasts (E.Derm, NBL-6; ATCC CCL-57) were grown at 37ºC, 5% CO_2 in DMEM high glucose, GlutaMax and pyruvate supplemented with 15% FBS, and 1% non-essential amino acids (Gibco, Life Technologies, UK).

3.3.2 Subculture

Cells were routinely amplified in flasks and passaged once confluency reached 90% to 100%. The protocol to passage cells consisted of washing the cell monolayer with Dulbecco's phosphate buffered saline (DPBS; Gibco, Life Technologies, UK) following a 5 min incubation at room temperature with TrypLE™ Express Enzyme (Gibco, Life Technologies, UK) for HEK293T, and E.Derm cells. MDCK cells were incubated at 37ºC, 5% CO_2 for 20 min. Once detached, cells were diluted (1/3 for E.Derm, 1/10 for MDCK and HEK293T cells) in maintenance media and transferred to new culture flasks. MDCK and HEK293T cells were passaged up to 40 times before a new batch of cells was used, while E.Derm were passaged no more than 12 times.

3.3.3 Long-term storage

For long-term storage, cells were harvested and centrifugated at 200*g* for 5 min before being resuspended into a solution of 10% dimethyl sulfoxide (ThermoFisher Scientific, UK) diluted in FBS. The cell suspension was then distributed in 1 mL aliquots in 2 mL cryogenic tubes (Alphalaboratories, UK). Tubes were stored at -80ºC using a freezing container (Mr. Frosty™; ThermoFisher Scientific, UK) filled with methanol (Fisher chemical, UK) to gentle cool down the cryotubes. Following a 24 hours incubation at -80ºC, the frozen cryotubes were transferred to liquid nitrogen for long term storage.

3.4 Equine tracheal explant culture

3.4.1 Explant preparation and maintenance

Horse tracheas were aseptically collected upon euthanasia of Welsh Mountain ponies performed at the Animal Health Trust (Newmarket, UK), and transported in medium consisting of 50% DMEM high glucose, GlutaMax and pyruvate, 50% Roswell Park Memorial Institute (RPMI) 1640 medium (Gibco, Life Technologies, UK) supplemented with penicillin-streptomycin (penicillin, 100 units/mL; streptomycin, 100 µg/mL; Gibco, Life Technologies, UK) and fungizone (2.5 µg/mL, Gibco, Life Technologies, UK). The culture medium was replaced 5 times over a period of 6 hours. Following tissue transportation and washing steps, the trachea was surgically cleaned by removing excess connective tissue surrounding the cartilage and distal ends. A longitudinal section was

performed all along the trachea posterior wall. The opened-up trachea was then dissected into 0.5 to 1 cm^2 pieces and physically separated from the underlying cartilage structures. Such isolated tracheal epithelium was then placed facing upwards onto a sterile section of filter paper that was in turn placed onto agarose plugs allowing support to the tracheal explants. The whole system was contained in a 6-well plate filled with culture medium. Medium reached by capillarity through the filter paper the basal portion of the explants, as described previously (Nunes et al. 2010), mimicking the air interface found in the respiratory tract of living animals. Explants were maintained at 37ºC, 5% CO_2 for up to 7 days.

3.4.2 Explant infection

Equine tracheal explants were infected with either 200 or 10,000 plaque-forming units (PFU) for each studied virus and used for image analysis or viral replication kinetics and RNA sequencing experiments, respectively. In both cases a mock-infected control was processed concomitantly to the experimental infections. Virus was diluted in a solution of DMEM high glucose, GlutaMax and pyruvate supplemented with 0.3% bovine albumin fraction V (BSA; Gibco Life Technologies, UK), and 1 µg/mL of tosylsulfonyl phenylalanyl chloromethyl ketone (TPCK) treated trypsin (Sigma-Aldrich, UK). Diluted inocula (5 µL) was deposited on tracheal explants, and were incubated at 37ºC, 5% CO_2, for the time needed to conduct the experiment.

3.4.3 Explant long-term storage

Equine tracheal explants were kept in 1 mL of sterile DPBS and stored at -80ºC, 1 mL of 70% ethanol solution and stored at room temperature, or 1 mL of TRIzol reagent (ThermoFisher Scientific, UK) and stored at -80ºC depending on their use in virus growth kinetics, immunohistochemistry, or RNA sequencing experiments, respectively.

3.5 Virus

3.5.1 Isolates and reverse genetics viruses

Experiments in this study were performed using mainly RG generated EIVs, but also included one virus isolate. The information (name, accession number, nature, and abbreviation) of viruses used in the study are summarised in Table 3-3. The isolation information, and passage history of A/ruddy shelduck/Mongolia/963v/2009 (H3N8) isolate

(AIV/2009) were unknown. AIV/2009 viral stocks were generated by infecting MDCK cells at a multiplicity of infection (MOI) of 0.01. Briefly, MDCK cells were washed with DPBS while viral isolate was diluted in a solution of DMEM high glucose, GlutaMax and pyruvate supplemented with 0.3% BSA, and 1 µg/mL TPCK treated trypsin, as previously described (Martínez-Sobrido and García-Sastre 2010). Following those steps, diluted virus was added on MDCK cells (volume sufficient to prevent cells to dry-out), and incubated at 37ºC, 5% CO_2 until cytopathic effects (CPE) were observable. Once CPE reached 80% cell death, supernatant was collected and centrifugated to eliminate cellular debris (200*g*, 5 min), before it was aliquoted and stored at -80ºC until further use.

Table 0-3: Viruses and brief description of the viruses used in this study

Virus	Taxonomy ID	Virus origin	Subtype	Abbreviation
A/equine/Uruguay/1/1963	387234	RG*	H3N8	EIV/63
A/equine/Lexington/1/1966	475494	RG*	H7N7	EIV/66
A/equine/Jilin/1/1989	385585	RG*	H3N8	EIV/89
A/equine/Ohio/1/2003	336799	RG*	H3N8	EIV/2003
A/ruddy shelduck/Mongolia/963v/2009	1316888	Isolate	H3N8	AIV/2009

*Reverse genetics

3.5.2 Virus rescue

Viruses (A/equine/Uruguay/1/1963 [EIV/63], EIV/66, EIV89, A/equine/Ohio/1/2003 [EIV/2003]) were rescued using an eight-plasmid RG system as previously described (Hoffmann et al. 2000). Briefly, viral cDNA (corresponding to the CDS flanked by 5′ and 3′ UTRs) of each of the eight influenza segments were inserted between a 225 bp long polymerase I promoter sequence and a 33 bp long murine terminator sequence. These sequences are flanked by the Pol II promoter from human cytomegalovirus (CMV), and the polyadenylation signal from bovine growth hormone (BGH). The 8 plasmids (corresponding to segment 1 to 8) were transfected (2.5µg of plasmid DNA in total) in a co-culture of MDCK/HEK293T cells (1:2) using TransIT-LT1 reagent (Cambridge Bioscience, UK) diluted in Opti-Minimum Essential Medium (Life Technologies, UK), according to

manufacturer protocol. The day after transfection, culture medium was replaced by DMEM high glucose, GlutaMax and pyruvate supplemented with 0.3% BSA and 1 µg/mL TPCK treated trypsin. Supernatant was collected 2 to 3 days following transfection as CPE reached 80% cell death, with the exception of EIV/66 for which CPE took 3 to 4 days to appear. Collected supernatants were centrifugated to eliminate cellular debris (200*g*, 5 min), before storage at -80ºC until further use. These tubes were labelled as P_0 and correspond to virus passage 0.

3.5.3 Generation of viral stocks

Following virus titration (as described in 3.5.7) P_0 virus was used to infect MDCK cells at a MOI of 0.01. Briefly, MDCK cells were washed with DPBS while virus was diluted in a solution of DMEM high glucose, GlutaMax and pyruvate supplemented with 0.3% BSA, and 1 µg/mL TPCK treated trypsin. Following those steps, diluted virus was added on MDCK cells (volume sufficient to prevent cells to dry-out), and incubated at 37ºC, 5% CO_2 until CPE were observable. Once CPE reached 80% cell death, supernatant was collected and centrifugated to eliminate cellular debris (200*g*, 5 min), before it was aliquoted and stored at -80ºC until further use. These tubes were labelled as P_1, and the exact same process was repeated to generate P_2 viral stocks. For experimental infection, a minimum of two viral stocks of each virus were rescued and grown independently. The RG viruses used in the study were never passaged more than P_2.

3.5.4 Viral growth curves in MDCK

Confluent monolayers of MDCK cells in a 12-well plate were infected at MOI 0.001 and 0.1 (based on viral titre calculated in MDCK cells as described in 3.5.7). Viral stocks were diluted in DMEM high glucose, GlutaMax and pyruvate supplemented with 0.3% BSA, and 1 µg/mL TPCK treated trypsin and added to the freshly DPBS-washed cell monolayer (200 µL). At this steps 200 µL of unused inocula was collected and used for back titration (essential to confirm the use of comparable infectious doses). The infected cells and controls were incubated 1 hour at 37ºC, 5% CO_2, and rocked every 15 min to prevent desiccation. Following incubation, cells were washed with DPBS, and wells filled with 2,200 µL of DMEM high glucose, GlutaMax and pyruvate supplemented with 0.3% BSA, and 1 µg/mL TPCK treated trypsin medium. At this stages 200 µL of supernatant was collected which corresponded to 0 hours post infection (hpi). MDCK cells were then incubated at 37ºC, 5% CO_2 until next timepoint (8; 12; 24; 48; 72; 96 hpi) collection. Importantly, the volume of

collected medium for each individual time point was compensated by the addition of 200 µL of DMEM high glucose, GlutaMax and pyruvate supplemented with 0.3% BSA medium, and 1 µg/mL TPCK treated trypsin medium. Titrations were done in technical and experimental triplicates, using at least two independent rescued viral stocks.

3.5.5 Viral growth curves in E.Derm

Confluent monolayers of E.Derm cells in a 12-well plate was infected at MOI 0.001 based on viral titre calculated in E.Derm cells. Viral stock was diluted in DMEM high glucose, GlutaMax and pyruvate supplemented with 0.3% BSA and added to the freshly DPBS-washed cell monolayer (200 µL). At this steps 200 µL of unused inocula was collected and used for back titration. Infected and control E.Derm cells were incubated 1 hour at 37ºC, 5% CO_2, and rocked every 15 min to prevent desiccation. Following incubation, E.Derm cells were washed with room temperature DPBS, and wells filled with 2,200 µL of DMEM high glucose, GlutaMax and pyruvate supplemented with 0.3% BSA medium. At this stages 200 µL of supernatant was collected, which corresponded to 0 hpi. Plates were then incubated at 37ºC, 5% CO_2 until next timepoint (8; 12; 24; 48; 72; 96 hpi) collection. Importantly, the volume of collected medium for each individual time point was compensated by the addition of 200 µL of DMEM high glucose, GlutaMax and pyruvate supplemented with 0.3% BSA medium. Titrations were done in technical and experimental triplicates, using at least two independent rescued viral stocks.

3.5.6 Viral plaque morphology

Viral plaque morphology was determined by plaque assays in MDCK cells. Briefly, MDCK cells were seeded in a 6-well plate and confluent MDCK cells monolayers were infected using 200, 20, and 2 PFU from serially diluted viral stocks of the different viruses. Following a DPBS wash, diluted inocula (200 µL) were added to the MCDK cells and the plate incubated for 1 hour at 37ºC, 5% CO_2. After incubation, MDCK cells were washed with DPBS once, and a mixture of 1:1 sterile 2.4% Avicel (diluted in H_20 and autoclaved; Avicel RC/CL, Microcrystalline cellulose & Sodium carboxymethylcellulose1, Sigma-Aldrich, UK), and 2X Temin's Modified Eagle Medium (2X MEM; Gibco; Life Technologies, UK), supplemented with 0.3% BSA and 1 µg/mL TPCK treated trypsin added (2 mL). MDCK cells were incubated for 48 hours at 37ºC, 5% CO_2, before they were fixed in 4% freshly made formaldehyde solution (Fisher chemical, UK). Following fixation, MDCK cells were stained using Coomassie blue staining solution (45% Methanol, 10% glacial acetic acid

(VWR international, UK), 0.1% Coomassie Brilliant Blue R-250 (Sigma-Aldrich, UK), and H_2O), and incubated for 10 min. Once plates were completely dry, they were scanned (Epson Perfection 3200 photo), and diameters measured using ImageJ software (v2.0.0-rc-56/1.52g). At least 40 plaques were counted in each condition (with the exception of EIV/66, which did not form plaques) and were obtained from experimental triplicates.

3.5.7 Virus titration by median tissue culture infectious dose ($TCID_{50}$)

Viral stocks and replication kinetics titres were determined in both cell lines (MDCK and E.Derm) by median tissue culture infectious dose ($TCID_{50}$) and given as $TCID_{50}$/mL. Briefly, E.Derm cells were seeded and infected the day after when confluency was around 70%. E.Derm cells were washed in DPBS while in the meantime virus was diluted following a 10-fold serial dilution (from neat to 10^{-7}). Once diluted in DMEM high glucose, GlutaMax and pyruvate, 0.3% BSA, virus dilutions were used to infected E.Derm cells (100 µL), and incubated for 72 hours at 37ºC, 5% CO_2. The presence of CPE was scored manually (binary output) in each of the wells, and the results obtained were converted in viral titres using the Spearman and Kärber algorithm (Hierholzer and Killington 1996). All the titrations were done in four technical replicates to allow an accurate viral titre calculation. Comparison between $TCID_{50}$-obtained titres and plaque assay obtained titres were conducted and gave no statistical difference.

Of note, titrations in MDCK cells did not require cells seeding in advance as they are more resistant than E.Derm cells and were added directly to the diluted virus wells. Additionally, the infectious medium of MDCK, but not E.Derm cells, contained 1 µg/mL of TPCK treated trypsin in addition to DMEM high glucose, GlutaMax and pyruvate supplemented with 0.3% BSA medium.

3.6 Immunostaining

3.6.1 Flow cytometry

Flow cytometry was used to determine the proportion of infected E.Derm cells for transcriptomic experiments. Briefly, at 4 and 24 hpi, E.Derm cells were washed in DPBS before they were resuspended with trypsin-EDTA (Gibco; Life Technologies, UK) and fixed in 4% freshly made formalin solution (Sigma-Aldrich, UK). E.Derm cells were transferred

to 96-well plate and centrifugated (500*g*, 4ºC, 5 min). E.Derm cells were permeabilised with 100 µL of 1% TritonX-100 (Sigma-Aldrich, UK) and incubated for 10 min on ice. Following permeabilisation, cells were centrifugated (500*g*, 4ºC, 5 min) and blocked with 100 µL of 10% normal goat serum (NGS; ThermoFisher Scientific, UK) and incubated on ice for 1 hour. Following incubation, E.Derm cells were immunostained with the addition of 100 µL of a mouse anti influenza (NP subtype A, clone EVS238, European Veterinary Labs) primary antibody, diluted (1/750; so final volume was 200 µL and dilution 1/1500) in blocking solution, and incubated on ice for 2 hours. After incubation, E.Derm cells were washed twice in DPBS and centrifugated (500*g*, 4ºC, 5 min), before 100 µL of secondary antibody was added (rabbit anti-mouse IgG conjugated with Alexa Fluor 488 (1/2000; ThermoFisher Scientific, UK)) and incubated 1 hour on ice. After incubation, E.Derm cells were washed twice in DPBS and centrifugated (500*g*, 4ºC, 5 min), before a final resuspension in 200 µL of DPBS. Stained cells were subjected to flow cytometry analysis (Guava flow cytometer; Merck, UK), and the percentage of infected cells calculated using FlowJo v10.3 software. The gating strategy used to identify viable and infected E.Derm cells populations is shown in Appendix 3. Infections reaching 50% ± 5% infected cells at 4 hpi and their corresponding dilution at 24 hpi were RNA-extracted. Experiments were carried out three times independently.

3.6.2 Histological staining and immunostaining

Equine tracheal explants were fixed in 10% buffered formalin solution, and then handed to the histology lab for processing and staining with haematoxylin and eosin. Blank sections were also obtained and immunostained (Table 3-4 for antibody details) by Veronica Patton. Briefly, blank sections were first treated with a solution of 10% hydrogen peroxide supplemented with 0.05% Tween 20 (Scientific Laboratory Supplies, UK) to prevent endogenous peroxidase activity. NP-stained sections were incubated with 1% TritonX-100 solution, while cleaved caspase-3 (CC3), Ki67 and MX1 stained section were pressure-cooked (Menarini Diagnostic, UK) in pH 6.0 citrate buffered solution. Following pre-treatment, sections were blocked (10% NGS supplemented with 0.005% Tween 20) and incubated with their corresponding primary antibody (Table 3-4 for the dilutions used). Mouse EnVision/HRP (Dako, Agilent, UK) or Rabbit EnVision/HRP (Dako, Agilent, UK) were used as secondary antibodies, and Liquid DAB (3.3'-Diaminobenzidine) + Substrate Chromogen System (Dako, Agilent, UK) as chromogen. Sections were counterstained with Mayer's haematoxylin, dehydrated in ascending alcohol series and xylene, and coverslipped.

Three images per section per timepoint for each staining were acquired by Veronica Patton at 40x magnification with an Olympus BX51 microscope.

Table 0-4: List of antibodies used in the study and their details

Antibody	Species	Specificity	Supplier	Reference	Dilution
Anti Influenza NP	Rabbit	Polyclonal	European Veterinary labs	EVS238	1/400
Anti-Cleaved Caspase 3	Rabbit	Monoclonal	Cell Signalling	D175	1/400
Anti-MX1	Mouse	Monoclonal	Georg Kochs*	Clone M143	1/200
Anti-Ki67	Mouse	Monoclonal	Dako	MIB-1	1/150

*Provided by

3.7 RNA sequencing

3.7.1 Sample preparation and RNA sequencing

Total RNA from infected E.Derm cells, or infected equine tracheal explants was extracted using TRIzol reagent and further purified according to the manufacturer's protocol using RNeasy mini-spin columns (Qiagen, UK). Sample RNA concentration was measured with a Qubit Fluorimeter (Life Technologies, UK) and the RNA integrity was determined using an Agilent 4200 TapeStation (Agilent, USA). A quantity of 500 ng of total RNA from each sample were used to prepare libraries for sequencing, using an Illumina TruSeq Stranded mRNA HT kit (Illumina, USA), according to the manufacturer's instructions. Briefly, polyadenylated RNA molecules were captured, followed by fragmentation. RNA fragments were reverse transcribed and converted to dsDNA, end repaired, A-tailed, ligated to indexed adaptors and PCR amplified. Libraries were pooled in equimolar concentrations and sequenced in an Illumina NextSeq 500 sequencer using a high output cartridge, generating single reads with a length of 75 bp. The steps including the libraries preparation and the sequencing of samples were done by Lily Tong, Daniel Mair, and Ana Da Silva Filipe from CVR Genomics.

3.8 In silico analysis

3.8.1 Transcriptome analyses

The quality of raw RNA sequencing reads was assessed using FastQC (Andrews 2010). Reads with a Phred quality score < 30, and sequencing adaptors were removed using Trim Galore (v. 0.6.5; https://www.bioinformatics.babraham.ac.uk/projects/trim_galore/). High quality reads were mapped to the horse genome (Equus caballus, accession number GCA_000002305.1) using TopHat2 (Kim et al. 2013) and Bowtie2 (Langmead and Salzberg 2012). The different bioinformatic tools available to quantify gene expression were benchmarked and showed an increased number of differentially expressed genes (DEGs) following the use of Cuffdiff2 or EdgeR (DESeq2, and TSPM (two-stage Poisson model) giving a significantly lower number of DEGs; Rajkumar et al. 2011). To estimate the impact of algorithm selection on RNAseq data, IFN-treated E.Derm cells were analysed with both methods (Cuffdiff2 and EdgeR). The use of EdgeR (Appendix 1 A) showed a slight increase of DEGs number. Additionally, DEGs highlighted in both methods showed similar regulation intensities (Appendix 1 B). All subsequent analyses were therefore conducted using the EdgeR pipeline. The number of aligned reads were counted using HTseq (Anders et al. 2015) and normalised to counts per million (CPM). A list DEGs compared to mock-infected samples was generated using EdgeR (Robinson et al. 2009). Genes with Benjamini-Hochberg corrected p-values ≤ 0.05 were considered significant, and an additive expression threshold of $|\log_2 \text{Fold change}| \geq 1$ applied. The code used in this section is available in Appendix 5.

3.8.2 Gene Ontology enrichment

Gene Ontology terms (GO terms) enrichment was investigated using the Database for Annotation, Visualisation and Integrated Discovery (DAVID; (Huang et al. 2007). DEGs lists were separated in two distinct datasets based on the gene regulation observed (down, and upregulation) and in turn input into DAVID webtool. Results were exported as column separated values files from the website and merged using dplyr v1.0.7 R-package (https://github.com/tidyverse/dplyr/) before a significance threshold (p-value ≤ 0.001) was applied. Additionally, a selection of significantly enriched GO terms was performed and focused on GO terms in relation with immune and/or inflammation responses. Such

subsetting relied on the presence of the following terms in the GO name: ‘interferon’, ‘IFN’, ‘cytokine’, ‘virus’, ‘viral’, ‘ISG’, ‘inflam’ and ‘immun’, and was not case sensitive.

3.8.3 Image analyses

Respiratory epithelium areas from the infected equine tracheal explant microphotographs were extracted from the surrounding tissues by Veronica Patton using a manual contouring method before the length and area were measured. Extracted images were colour deconvoluted to separate brown (DAB) from blue (nuclei) channels (Landini et al. 2021), and default automatic thresholding was used to identify areas of positive signal. Binarisation of the DAB vector allowed quantification of positive pixels, which were then converted into area of positive stain for each of the studied cellular markers. For nuclear stains, the image calculator was used to determine the localization of the positive pixels and overlap with DAPI-positive pixels used to numerate the number of stained nuclei. Measurements were normalised to epithelial length, or nuclei count. All image analyses were done using ImageJ software (v2.0.0-rc-56/1.52g).

3.8.4 Phylogeny

Complete, and publicly available H3N8 EIV sequences (n = 136) were downloaded from the NCBI Influenza Resource Database (IRD; Bao et al. 2008) with associated metadata (isolation date, country), and are summarised in Appendix 6. Nucleotide alignments of the main CDS were generated for each segment using MUSCLE (Edgar 2004). RAxML was used to infer the phylogenetic tree for each segment using the GAMMA model and 1000 bootstrap replicates (Stamatakis 2014). Trees were edited using FigTree v1.4.4 software (https://github.com/rambaut/figtree/releases).

3.8.5 Genomic content analysis

The frequencies of adenine (A), cytosine (C), guanine (G), and thymine (T) as well as dinucleotides, in each of the publicly available H3N8 EIV CDS (n = 136) were quantified using the SSE v1.4 software (Simmonds 2012). CG dinucleotide (CpG) were converted to observed/expected (O:E) ratio using the formula :

$$CpG\ (O{:}E)\ ratio = \frac{f(CpG)}{f(C) \times f(G)}$$

In which f(CpG) represents the frequency of CpG observed, while f(C) and f(G) represent frequencies of Cytosine and Guanine, respectively. GC content and CpG O:E ratio correlation with virus sampling date were investigated using Pearson correlation test. Significance levels used were * < 0.05; ** < 0.01; *** < 0.001.

3.8.6 Statistical analysis

Statistical analyses, data curation, and data preparation were carried out using R studio v3.5.1 software. The statistical tests used along this study vary from generalized linear mixed-effects models (GLM models) using the lme4 package (Bates et al. 2015) to Student's t-test, depending on the homoscedasticity and variance of the analysed data. Statistical test and significance levels used in each of the analysis are provided in figure captions to avoid confusion. Similarly, the number of replicates and nature of calculated error bars (standard deviation (SD), standard error to the mean (SEM), or 95% confidence interval (95% CI)) are included in figure captions.

3.8.7 Data visualisation

Graphs found in this manuscript were generated using the R packages ggplot2 (Wickham 2011) and VennDiagram (Chen and Boutros 2011). Error bars were calculated based on the mean value, and the standard deviation (SD), standard error to the mean (SEM), or 95% confidence interval (95% CI) of the studied variable by using Rmisc (v 1.5) package (https://cran.r-project.org/package=Rmisc). Linear regression when applicable was estimated and drawn by using the geom_smooth function associated with the 'loess' method, and the formula 'y ~ x' of ggplot2 package.

3.9 Ethics statement.

Animal work was approved by the Ethics Committee of the School of Veterinary Medicine of the University of Glasgow (ethics approval R25A/12). As no regulated procedures were carried out on animals a Home Office license was not required.

Chapter 4: Equine influenza long-term adaptation

4.1 Introduction

The main reservoir of IAV is wild birds and transmission of avian-origin IAV to mammals has been reported on several occasions affecting, but not limited to, humans, pigs, dogs, and horses. Viral dissemination within a susceptible population is closely related to contact rates, but spatial distribution and density of individuals are also key factors to amplify and propagate the initial and isolated interspecies transmission event. In addition to ecological barriers, establishment of endemic lineages relies on intracellular virus replication, and virus-host co-evolution history has led cells and organisms to develop countermeasures to avoid infection, to reduce viral load (*i.e.* number of viral particles in an organism), and to improve pathogen clearance. The developed mechanisms aim to reduce infection cost and to limit virus-induced damage to the host. The first cellular barrier to infection is the presence/absence of receptors for virus binding and entry. As mentioned in the introduction (see section 1.3.4.1), modified sialic acids are the main receptors for IAVs, such as NeuGcα2,3Gal, a cellular receptor abundantly present at the surface of susceptible mammalian cells.

However, as IAV, like all viruses, relies entirely on the host cell machinery to complete its replication cycle and expand in number. To do so, the virus requires a finely tuned molecular interaction with its host and offers a myriad of cellular countermeasures to limit infection. A key intrinsic host antiviral defence against infection resides in the type I IFN response induced following IAV detection by PRRs. Furthermore, it has been demonstrated that exacerbation of the type I IFN response resulted in an increased immunopathology in infected tissues, enhancing the clinical signs of EI (Wattrang et al. 2003).

As most of interspecies transmission events result in dead-end infections (*i.e.* infection without onward transmission), only a few result in the establishment of novel lineages that become endemic. The mechanism underpinning the fate of interspecies transmission events remain unclear, and seem to be the results of a favourable series of concerted events which act on multiple cellular and ecological factors. Additionally, I hypothesise that host type I IFN response is a key underpinning mechanism, and its exacerbation leads to an increased immunopathology which I think is evolutionarily driven and decreases with time. To address the evolution of viral within-host fitness (*i.e.* replication kinetics, cell-to-cell spread, IFN sensitivity), I studied phenotypic and genomic content evolution of EIV from 1963 to 2003. Additionally, I used two monophyletically-related EIV isolated in 1963 (EIV/63) and 2003 (EIV/2003) in a series of *in vitro* and *ex vivo* experimental infections and assessed the

infection phenotypes of both viruses using classical virology techniques coupled to transcriptomics. Finally, I explored the extent of damage attributed to either EIV/63 or EIV/2003 infection at the natural site of infection by using equine tracheal explants, immunostaining of histological sections, and image analysis.

4.2 Results

4.2.1 Genomic content and phylogenetic relationship

As mentioned in section 1.3.1.1, H3N8 EIV was first isolated from infected horses in 1963 and has since uninterruptedly circulated in equine population. I analysed (Figure 4-1) the phylogenetic relationship among the totality (n=66) of fully-sequenced and publicly available H3N8 EIV genomes from 1963 to 2003. I observed (Figure 4-1) a monophyletic relationship linking EIV/2003 to EIV/63 which was supported across the 8 genomic segments investigated.

Additionally, I noticed in Segment 4 (HA) and Segment 6 (NA) cladograms that inter-taxa distances are more important (~10-fold) than in other phylogenetic trees (Segment 1 (PB2), Segment 2 (PB1), Segment 3 (PA), Segment 5 (NP), Segment 7 (M) ,and Segment 8 (NS)). This result suggests that H3N8 EIV segment 4 (HA) and segment 6 (NA) are preferentially accumulating mutations.

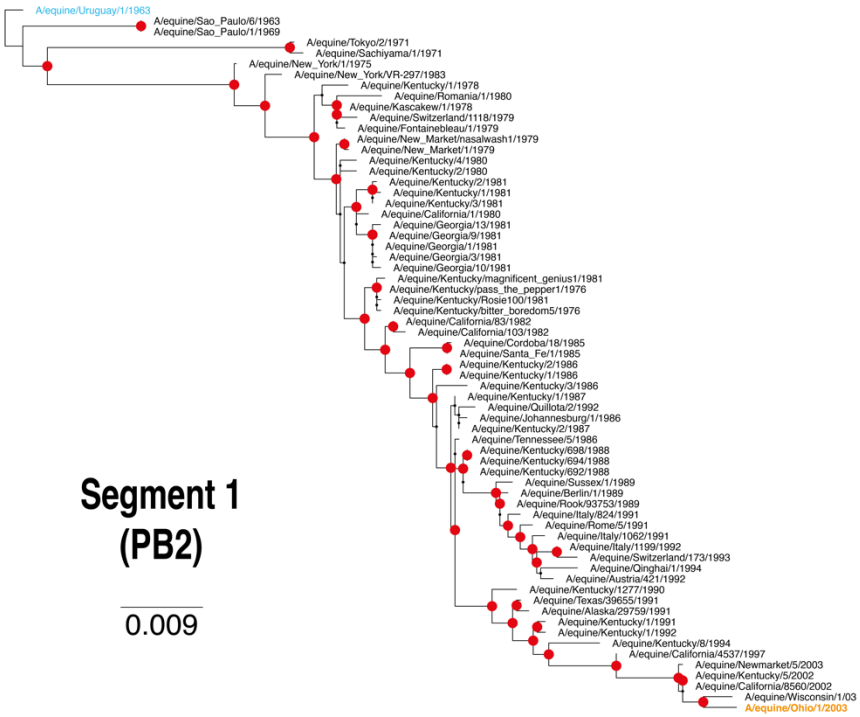

Segment 1 (PB2)

0.009

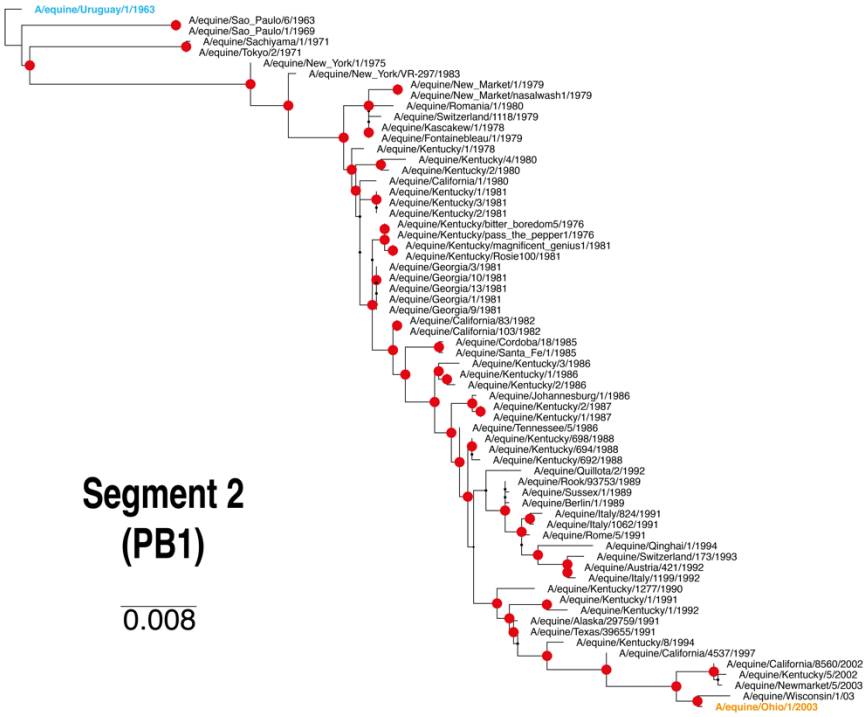

Segment 2 (PB1)

0.008

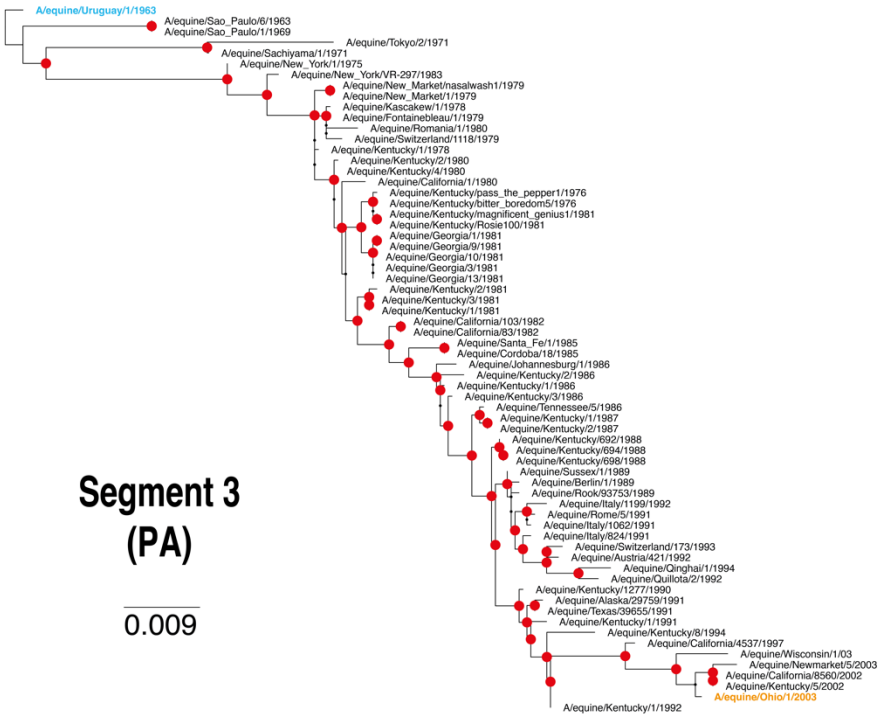
A/equine/Uruguay/1/1963
A/equine/Sao_Paulo/6/1963
A/equine/Sao_Paulo/1/1969
A/equine/Tokyo/2/1971
A/equine/Sachiyama/1/1971
A/equine/New_York/1/1975
A/equine/New_York/VR-297/1983
A/equine/New_Market/nasalwash1/1979
A/equine/New_Market/1/1979
A/equine/Kascakew/1/1978
A/equine/Fontainebleau/1/1979
A/equine/Romania/1/1980
A/equine/Switzerland/1118/1979
A/equine/Kentucky/1/1978
A/equine/Kentucky/2/1980
A/equine/Kentucky/4/1980
A/equine/California/1/1980
A/equine/Kentucky/pass_the_pepper1/1976
A/equine/Kentucky/bitter_boredom5/1976
A/equine/Kentucky/magnificent_genius1/1981
A/equine/Kentucky/Rosie100/1981
A/equine/Georgia/1/1981
A/equine/Georgia/9/1981
A/equine/Georgia/10/1981
A/equine/Georgia/3/1981
A/equine/Georgia/13/1981
A/equine/Kentucky/2/1981
A/equine/Kentucky/3/1981
A/equine/Kentucky/1/1981
A/equine/California/103/1982
A/equine/California/83/1982
A/equine/Santa_Fe/1/1985
A/equine/Cordoba/18/1985
A/equine/Johannesburg/1/1986
A/equine/Kentucky/2/1986
A/equine/Kentucky/1/1986
A/equine/Kentucky/3/1986
A/equine/Tennessee/5/1986
A/equine/Kentucky/1/1987
A/equine/Kentucky/2/1987
A/equine/Kentucky/692/1988
A/equine/Kentucky/694/1988
A/equine/Kentucky/698/1988
A/equine/Sussex/1/1989
A/equine/Berlin/1/1989
A/equine/Rook/93753/1989
A/equine/Italy/1199/1992
A/equine/Rome/5/1991
A/equine/Italy/1062/1991
A/equine/Italy/824/1991
A/equine/Switzerland/173/1993
A/equine/Austria/421/1992
A/equine/Qinghai/1/1994
A/equine/Quillota/2/1992
A/equine/Kentucky/1277/1990
A/equine/Alaska/29759/1991
A/equine/Texas/39655/1991
A/equine/Kentucky/1/1991
A/equine/Kentucky/8/1994
A/equine/California/4537/1997
A/equine/Wisconsin/1/03
A/equine/Newmarket/5/2003
A/equine/California/8560/2002
A/equine/Kentucky/5/2002
A/equine/Ohio/1/2003
A/equine/Kentucky/1/1992
Segment 3
(PA)
0.009

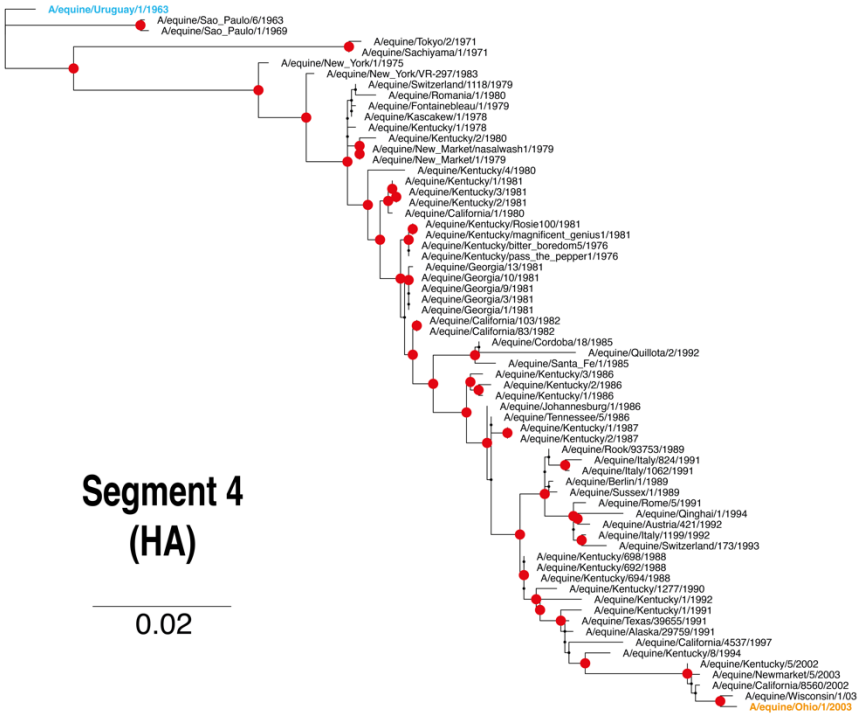
A/equine/Uruguay/1/1963
A/equine/Sao_Paulo/6/1963
A/equine/Sao_Paulo/1/1969
A/equine/Tokyo/2/1971
A/equine/Sachiyama/1/1971
A/equine/New_York/1/1975
A/equine/New_York/VR-297/1983
A/equine/Switzerland/1118/1979
A/equine/Romania/1/1980
A/equine/Fontainebleau/1/1979
A/equine/Kascakew/1/1978
A/equine/Kentucky/1/1978
A/equine/Kentucky/2/1980
A/equine/New_Market/nasalwash1/1979
A/equine/New_Market/1/1979
A/equine/Kentucky/4/1980
A/equine/Kentucky/1/1981
A/equine/Kentucky/3/1981
A/equine/Kentucky/2/1981
A/equine/California/1/1980
A/equine/Kentucky/Rosie100/1981
A/equine/Kentucky/magnificent_genius1/1981
A/equine/Kentucky/bitter_boredom5/1976
A/equine/Kentucky/pass_the_pepper1/1976
A/equine/Georgia/13/1981
A/equine/Georgia/10/1981
A/equine/Georgia/9/1981
A/equine/Georgia/3/1981
A/equine/Georgia/1/1981
A/equine/California/103/1982
A/equine/California/83/1982
A/equine/Cordoba/18/1985
A/equine/Quillota/2/1992
A/equine/Santa_Fe/1/1985
A/equine/Kentucky/3/1986
A/equine/Kentucky/2/1986
A/equine/Kentucky/1/1986
A/equine/Johannesburg/1/1986
A/equine/Tennessee/5/1986
A/equine/Kentucky/1/1987
A/equine/Kentucky/2/1987
A/equine/Rook/93753/1989
A/equine/Italy/824/1991
A/equine/Italy/1062/1991
A/equine/Berlin/1/1989
A/equine/Sussex/1/1989
A/equine/Rome/5/1991
A/equine/Qinghai/1/1994
A/equine/Austria/421/1992
A/equine/Italy/1199/1992
A/equine/Switzerland/173/1993
A/equine/Kentucky/698/1988
A/equine/Kentucky/692/1988
A/equine/Kentucky/694/1988
A/equine/Kentucky/1277/1990
A/equine/Kentucky/1/1992
A/equine/Kentucky/1/1991
A/equine/Texas/39655/1991
A/equine/Alaska/29759/1991
A/equine/California/4537/1997
A/equine/Kentucky/8/1994
A/equine/Kentucky/5/2002
A/equine/Newmarket/5/2003
A/equine/California/8560/2002
A/equine/Wisconsin/1/03
A/equine/Ohio/1/2003
Segment 4
(HA)
0.02

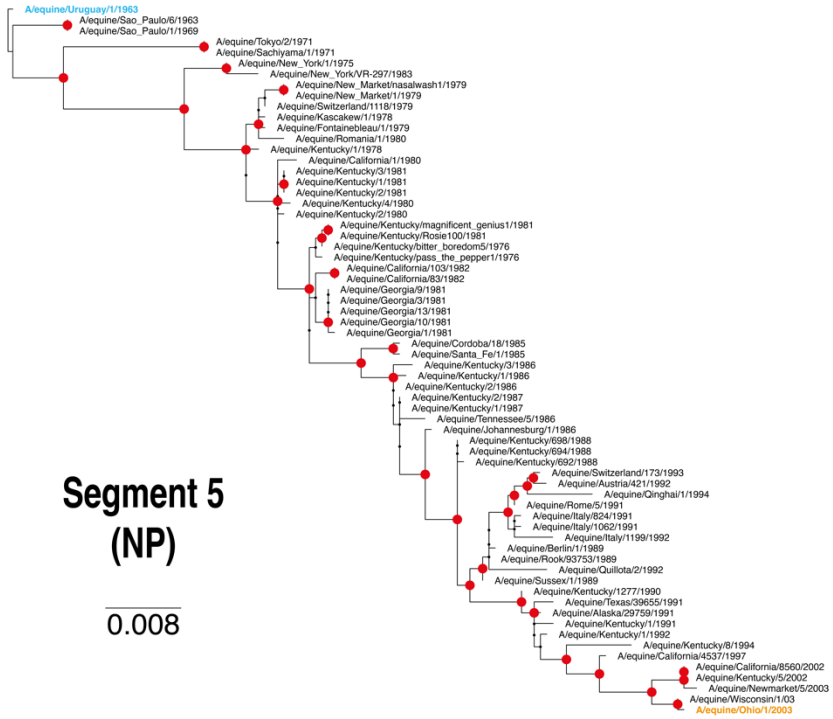
A/equine/Uruguay/1/1963
A/equine/Sao_Paulo/6/1963
A/equine/Sao_Paulo/1/1969
A/equine/Tokyo/2/1971
A/equine/Sachiyama/1/1971
A/equine/New_York/1/1975
A/equine/New_York/VR-297/1983
A/equine/New_Market/nasalwash1/1979
A/equine/New_Market/1/1979
A/equine/Switzerland/1118/1979
A/equine/Kascakew/1/1978
A/equine/Fontainebleau/1/1979
A/equine/Romania/1/1980
A/equine/Kentucky/1/1978
A/equine/California/1/1980
A/equine/Kentucky/3/1981
A/equine/Kentucky/1/1981
A/equine/Kentucky/2/1981
A/equine/Kentucky/4/1980
A/equine/Kentucky/2/1980
A/equine/Kentucky/magnificent_genius1/1981
A/equine/Kentucky/Rosie100/1981
A/equine/Kentucky/bitter_boredom5/1976
A/equine/Kentucky/pass_the_pepper1/1976
A/equine/California/103/1982
A/equine/California/83/1982
A/equine/Georgia/9/1981
A/equine/Georgia/3/1981
A/equine/Georgia/13/1981
A/equine/Georgia/10/1981
A/equine/Georgia/1/1981
A/equine/Cordoba/18/1985
A/equine/Santa_Fe/1/1985
A/equine/Kentucky/3/1986
A/equine/Kentucky/1/1986
A/equine/Kentucky/2/1986
A/equine/Kentucky/2/1987
A/equine/Kentucky/1/1987
A/equine/Tennessee/5/1986
A/equine/Johannesburg/1/1986
A/equine/Kentucky/698/1988
A/equine/Kentucky/694/1988
A/equine/Kentucky/692/1988
A/equine/Switzerland/173/1993
A/equine/Austria/421/1992
A/equine/Qinghai/1/1994
A/equine/Rome/5/1991
A/equine/Italy/824/1991
A/equine/Italy/1062/1991
A/equine/Italy/1199/1992
A/equine/Berlin/1/1989
A/equine/Rook/93753/1989
A/equine/Quillota/2/1992
A/equine/Sussex/1/1989
A/equine/Kentucky/1277/1990
A/equine/Texas/39655/1991
A/equine/Alaska/29759/1991
A/equine/Kentucky/1/1991
A/equine/Kentucky/1/1992
A/equine/Kentucky/8/1994
A/equine/California/4537/1997
A/equine/California/8560/2002
A/equine/Kentucky/5/2002
A/equine/Newmarket/5/2003
A/equine/Wisconsin/1/03
A/equine/Ohio/1/2003
Segment 5
(NP)
0.008

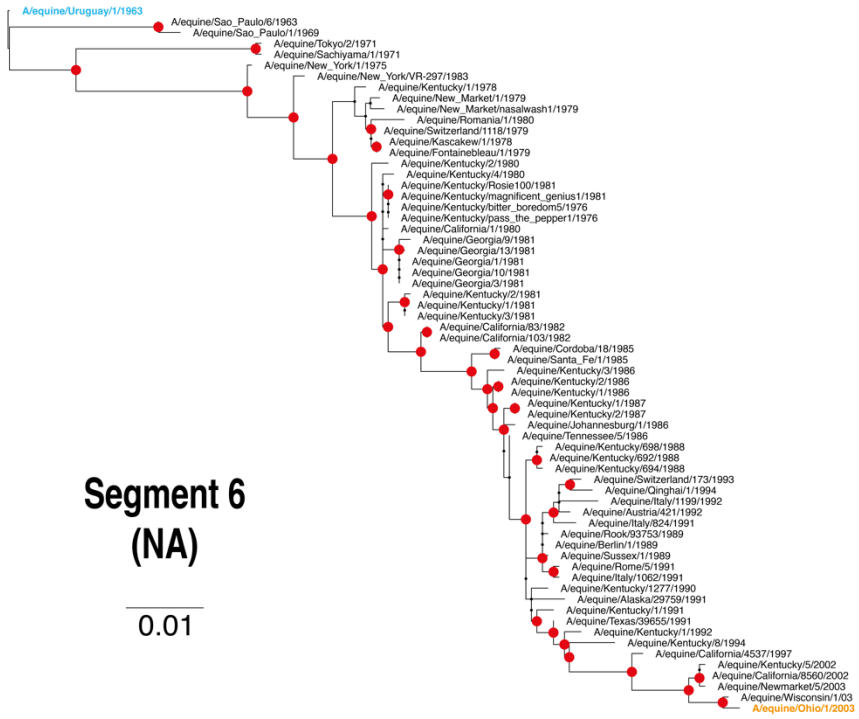
A/equine/Uruguay/1/1963
A/equine/Sao_Paulo/6/1963
A/equine/Sao_Paulo/1/1969
A/equine/Tokyo/2/1971
A/equine/Sachiyama/1/1971
A/equine/New_York/1/1975
A/equine/New_York/VR-297/1983
A/equine/Kentucky/1/1978
A/equine/New_Market/1/1979
A/equine/New_Market/nasalwash1/1979
A/equine/Romania/1/1980
A/equine/Switzerland/1118/1979
A/equine/Kascakew/1/1978
A/equine/Fontainebleau/1/1979
A/equine/Kentucky/2/1980
A/equine/Kentucky/4/1980
A/equine/Kentucky/Rosie100/1981
A/equine/Kentucky/magnificent_genius1/1981
A/equine/Kentucky/bitter_boredom5/1976
A/equine/Kentucky/pass_the_pepper1/1976
A/equine/California/1/1980
A/equine/Georgia/9/1981
A/equine/Georgia/13/1981
A/equine/Georgia/1/1981
A/equine/Georgia/10/1981
A/equine/Georgia/3/1981
A/equine/Kentucky/2/1981
A/equine/Kentucky/1/1981
A/equine/Kentucky/3/1981
A/equine/California/83/1982
A/equine/California/103/1982
A/equine/Cordoba/18/1985
A/equine/Santa_Fe/1/1985
A/equine/Kentucky/3/1986
A/equine/Kentucky/2/1986
A/equine/Kentucky/1/1986
A/equine/Kentucky/1/1987
A/equine/Kentucky/2/1987
A/equine/Johannesburg/1/1986
A/equine/Tennessee/5/1986
A/equine/Kentucky/698/1988
A/equine/Kentucky/692/1988
A/equine/Kentucky/694/1988
A/equine/Switzerland/173/1993
A/equine/Qinghai/1/1994
A/equine/Italy/1199/1992
A/equine/Austria/421/1992
A/equine/Italy/824/1991
A/equine/Rook/93753/1989
A/equine/Berlin/1/1989
A/equine/Sussex/1/1989
A/equine/Rome/5/1991
A/equine/Italy/1062/1991
A/equine/Kentucky/1277/1990
A/equine/Alaska/29759/1991
A/equine/Kentucky/1/1991
A/equine/Texas/39655/1991
A/equine/Kentucky/1/1992
A/equine/Kentucky/8/1994
A/equine/California/4537/1997
A/equine/Kentucky/5/2002
A/equine/California/8560/2002
A/equine/Newmarket/5/2003
A/equine/Wisconsin/1/03
A/equine/Ohio/1/2003
Segment 6
(NA)
0.01

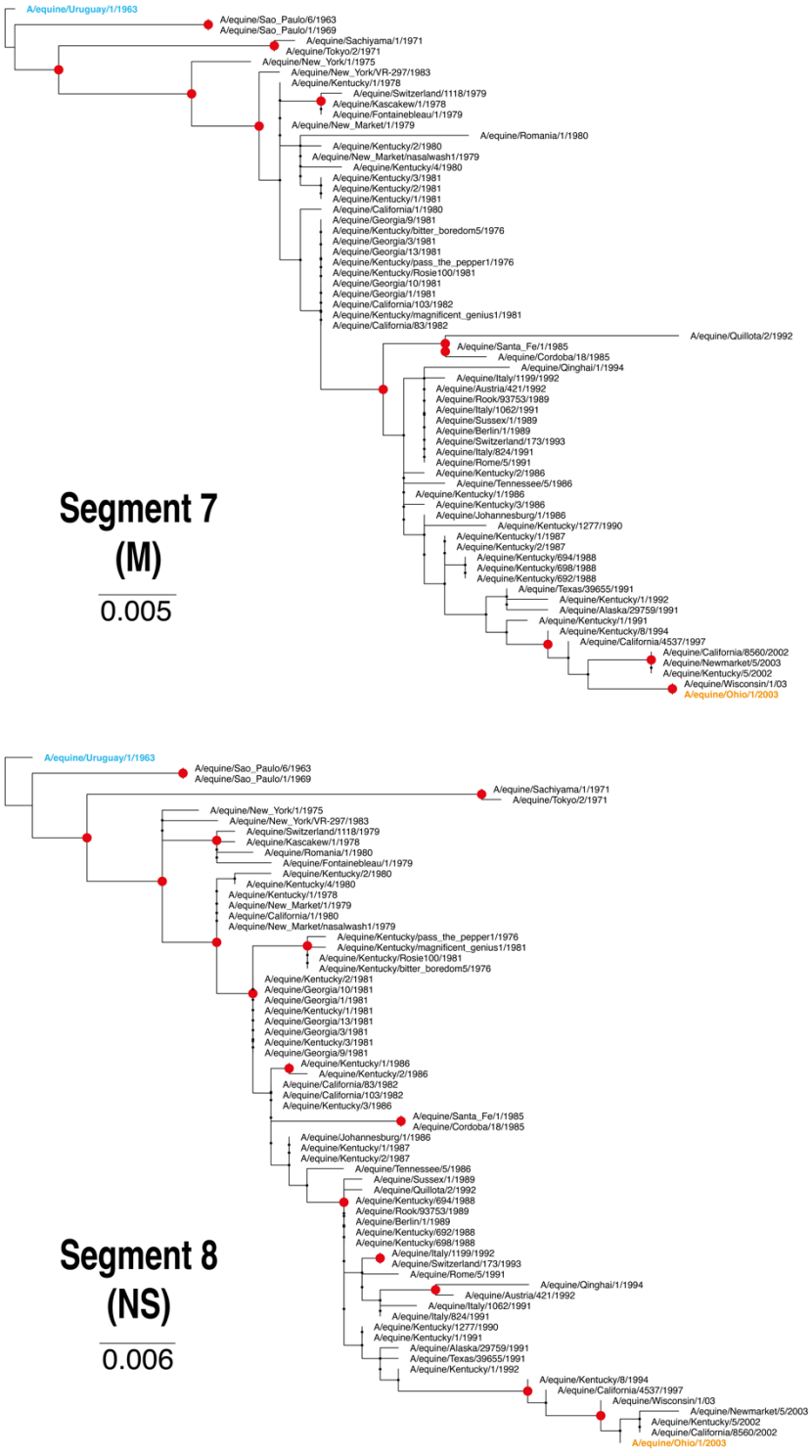

Figure 4-1: Phylogenetic relationship of H3N8 EIVs nucleotide sequences isolated between 1963 and 2003. Maximum likelihood trees using 66 complete H3N8 EIV genomes. Each tree represents the phylogenetic relationship inferred for each of the eight viral nucleotide segments. The name of each segment is indicated as follows: PB2 (polymerase basic 2); PB1 (polymerase basic 1); PA (polymerase acidic); HA (haemagglutinin); NP (nucleoprotein); NA (neuraminidase); M (matrix); and NS (non-structural). EIV/63 is indicated in cyan and EIV/2003 in orange. Horizontal branches are drawn to a scale of nucleotide substitutions per site, and all trees are rooted on the EIV Uruguay isolate from 1963. Nodes supported by a bootstrap value ≥ 75 are shown in red.

Although EIV/2003 is undoubtedly a monophyletic descendant of EIV/63, the 40 years of continuous circulation in horses led to the accumulation of numerous synonymous and nonsynonymous mutations throughout the viral genome. The observed nonsynonymous mutations (

Figure 4-2) highlight the accumulation of amino acid changes in the main EIV encoded proteins, which in turn are likely to affect their three-dimensional conformations and might alter their functions. I quantified nonsynonymous mutations ranging from 2 in M CDS to 43 affecting HA CDS. The observation (

Figure 4-2) that the maximum number of nonsynonymous mutations reached in segment 4 (HA; 43) and segment 6 (NA; 41) are in line with a HA and NA increased antigenic drift susceptibility (see section 1.7.1.1). As mentioned before, these two glycoproteins are found decorating the surface of viral particles and are essential to initiate cellular infection (see section 1.3.3). These glycoproteins are the preferred targets of host neutralising antibodies, and HA, NA increased mutational rates are the result of the succession of measures/countermeasures between the host immune system and viral evasion. Additionally, I observe specific mutations that have been already characterised and known to promote evasion of the innate immunity such as PB1-F2:S66N, NS1:E186K, as well as NS1 C-terminus truncation, which were linked to cytokine reduction, and JAK/STAT pathway interreference, respectively (Conenello et al. 2007; Chauché et al. 2018).

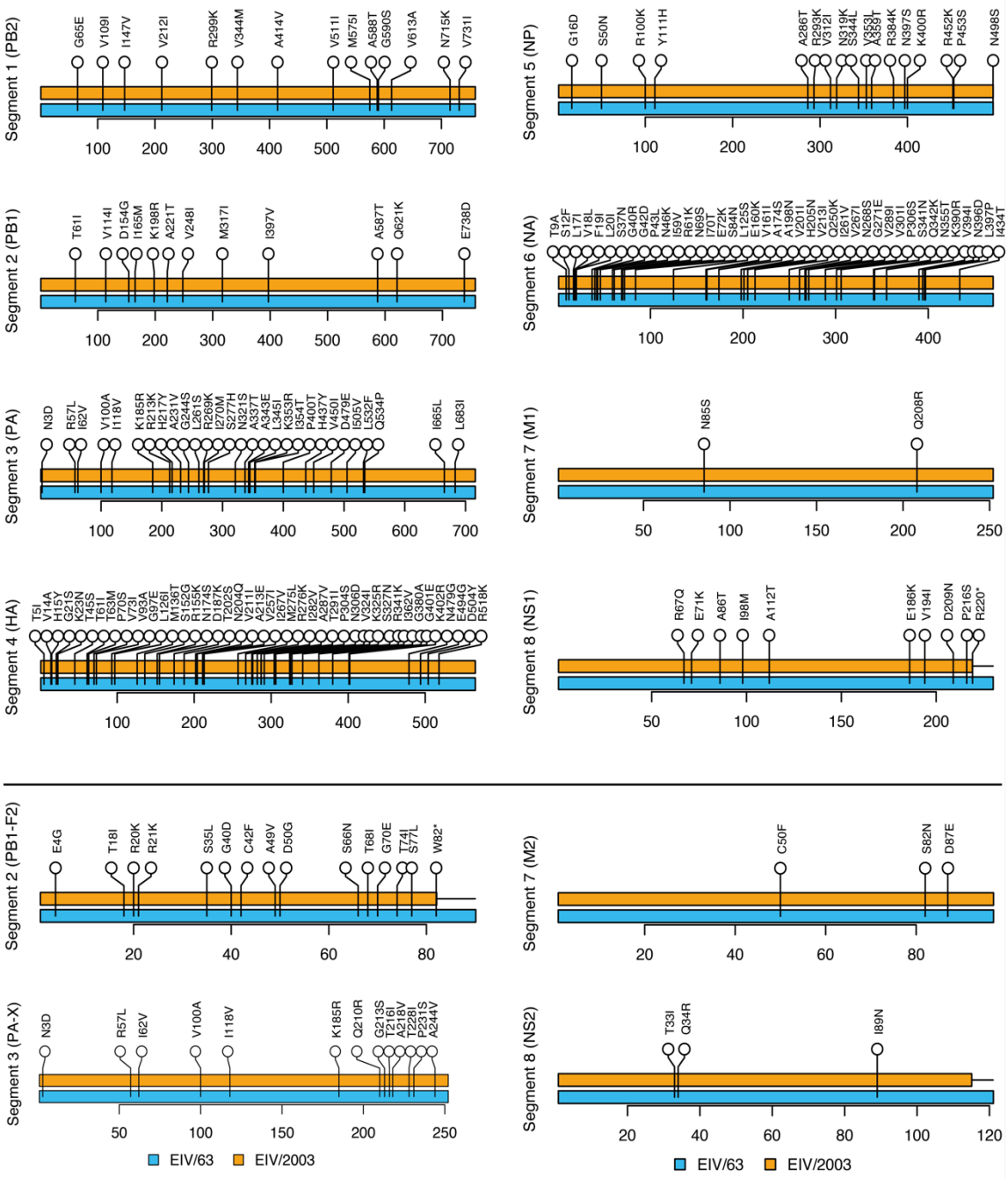

Figure 4-2: EIV/63 and EIV/2003 nonsynonymous mutations cartography. Lollipop plots showing the location and nature of amino acid mutations between EIV/63 (cyan) and EIV/2003 (orange) in each of EIV genomic segments. Individual CDS were investigated and labelled as Segment (corresponding CDS). The first amino acid in the nomenclature corresponds to EIV/63, while the last corresponds to EIV/2003, and the number in between corresponds to amino acid position starting from the initiating methionine. Additionally, the length of each segment represents the CDS from the initiating methionine to stop codon. Such feature highlights the early stop codon introduction in Segment 2 (PB1-F2), and Segment 8 (NS1 and NS2) truncations. Scales underneath each of the lollipop plots show amino acid positions.

In addition to these amino acid changes, a myriad of synonymous mutations is impacting nucleotide sequences and should not be ignored. As already demonstrated, viral genomic composition is optimised to enhance viral replication. As shown in a previous study using human IAVs, viruses with deoptimized genomes exhibited a lower pathogenicity, shown by a reduction of virus replication kinetics, cell-to-cell spread *in vitro*, and viral load in a mouse model (Gaunt et al. 2016). To assess if EIV viral sequences evolved toward a genome content optimisation during its circulation in horses, I investigated the changes in GC content and CpG observed/expected (O:E) ratio in each codon positions of H3N8 EIV sequences isolated from 1963 to 2003. As observed in Figure 4-3, I highlighted a significant reduction of both GC content (Figure 4-3 A; $r^2 = 0.901$; p-value < $2x10^{-16}$) and CpG O:E ratio (Figure 4-3 B; $r^2 = 0.395$; p-value = $1.58x10^{-8}$). These results showed that during circulation in horses, EIV genomic sequences evolved toward an overall optimised genomic composition that could, in addition to the amino acid changes observed previously, participate in phenotypic changes. Furthermore, the GC and CpG content, do not appear to be related to amino acid changes as they were mainly driven by nucleotides found in the third codon position (also known as the wobble position) (Figure 4-4 A), or the second dinucleotide (Figure 4-3 B), respectively.

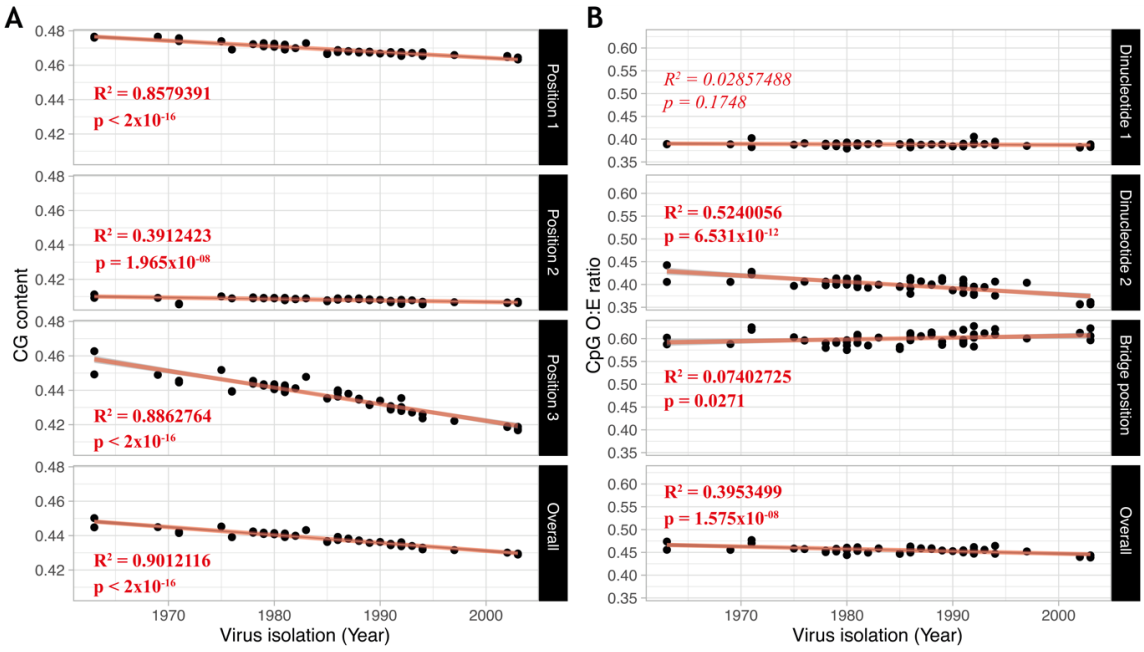

Figure 4-3: Changes in viral genome composition along the evolutionary history of H3N8 EIV from 1963 to 2003. Scatter plots showing the evolution of CG content **(A)**, and CpG O:E Ratio **(B)**, for each codon positions and calculated from 66 H3N8 EIV complete genomes isolated between 1963 and 2003. An additional panel showing the overall trends was added. Linear regressions between virus isolation date and either CG content or CpG O:E ratio are shown in red, while 95% CI are shown in grey. P-values and R^2 values are shown in red for each scatter plot, and significant results displayed as bold text.

4.2.2 EIV/2003 exhibits enhanced replication kinetics and cell-to-cell spread in MDCK cells

To investigate the consequences of viral genome composition on infection phenotypes, I infected MDCK cells with two evolutionarily distinct EIV and measured viral replication in the first 96 hpi. In

Figure 4-4 A, I back titrated inocula used in my experimental infections and did not observe significant difference between EIV/63 and EIV/2003 (p-value = 0.8137 and p-value = 0.0636 for MOI 0.001 and 0.1, respectively), indicating that infections were comparable. In

Figure 4-4 B I observed that EIV/63 and EIV/2003 viruses replicate to similar titres (10^5, and 10^6 $TCID_{50}$/mL for MOI 0.1, and MOI 0.001, respectively), and both viruses reached their replication peak at 24 and 48 hpi depending on the MOI used (MOI 0.1, or MOI 0.001, respectively). Furthermore, I did not observe a significant difference in the viral replication kinetics between EIV/63 and EIV/2003 infections (p-value = 0.5958 and p-value = 0.9738 for MOI 0.1 and MOI 0.001, respectively). However, it appears that EIV/63 and EIV/2003 maintained their viral titre at 10^5 $TCID_{50}$/mL over time in MOI 0.001 infections, while EIV/63 titre decreased from 10^5 to 10^3 $TCID_{50}$/mL between 24 and 96 hpi in MOI 0.1 infection. MDCK cells were also used to characterise the ability of both EIV/63 and EIV/2003 viruses to spread from an infected cell to surrounding cells. MDCK cells monolayers were infected and incubated with a semi solid culture overlay, restricting viral spread exclusively to short distance. As observed in

Figure 4-4 C, EIV/2003 produced significantly larger plaques ($\overline{diameter}$ = 0.19 cm (range = 0.0998—0.2865 cm)) than EIV/63 ($\overline{diameter}$ = 0.13 cm (range = 0.0588—0.2890 cm); p-value = 3.65×10^{-7}). Taken together, these results suggest that even if viruses displayed similar replication kinetics in MDCK cells, EIV/2003 can spread more efficiently than EIV/63 in an infected cell monolayer. However, MDCK cells, although routinely used in influenza research, are canine-derived cells, lack anti-influenza activity, and therefore not represent the most appropriate system to study equine virus-host interaction (Seitz et al. 2010).

4.2.3 EIV/2003 exhibits enhanced replication kinetics in E.Derm cells

To confirm the result from the previous section, in a more relevant cellular model, I decided to perform infections in E.Derm cells, which were the only commercially available equine-derived cell line at the time. Additionally, E.Derm cells are IFN-competent and encodes a Mx1 protein associated to anti-influenza property. In

Figure 4-4 D, I compared the viral titre of the inocula used in the experimental infections and did not observe a significance difference (p-value =0.1157), which allowed me to compare virus replication kinetics. Surprisingly, in E.Derm cells, only EIV/2003 virus was able to infect and replicate while EIV/63-infected supernatants never reached a titre above the limit of detection (5.62 $TCID_{50}$/mL). This result suggests that EIV/63 infection is restricted in E.Derm cells by either: i) a different cell tropism compared to EIV/2003, induced by a different targeting of cellular receptors which might be missing from E.Derm plasma membrane, or ii) an enhanced sensitivity to intracellular countermeasures developed by the host to contain the infection, such as type I IFN response. However, I know from work previously done by PhD student Caroline Chauché that pre-treating E.Derm with a Jak1/2 inhibitor that specifically blocks host cellular response to IFN (ruxotilinib) is sufficient to restore EIV/63 replication kinetic to comparable level than EIV/2003 (Chauché 2017). These results suggest that EIV/63 is more sensitive to host innate immune response in comparison to EIV/2003.

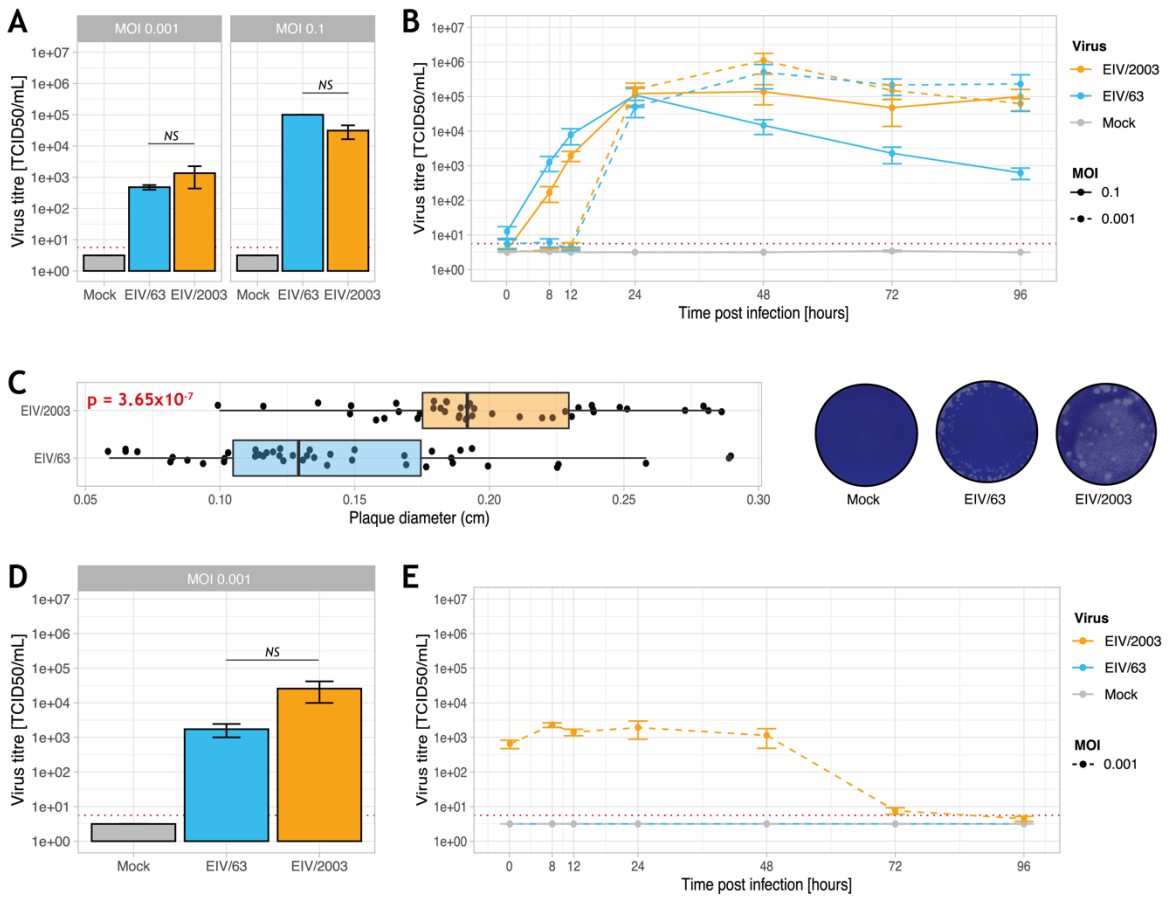

Figure 4-4: In vitro characterisation of H3N8 EIVs. (A) Viral titre of inocula used in the experimental infections of MDCK cells. **(B)** Growth kinetics of EIV/63 and EIV/2003 in MDCK cells. **(C)** Plaque phenotype of EIV/63 and EIV/2003 in MDCK cells measured at 48 hpi. The mean of at least 40 plaques were measured for each condition. **(D)** Viral titre of inocula used in the experimental infections of E.Derm cells. **(E)** Growth kinetics of EIV/63 and EIV/2003 in E.Derm cells. Cyan and orange colours represent EIV/63 and EIV/2003 infected cells, respectively, while mock-infected controls are shown in grey. Viral titres are represented as the mean ± SEM. Infections were performed three times independently and each independent experiment consisted of three technical repeats. Statistical significances were assessed using a Wilcoxon rank sum test (in A,C, and D).

4.2.4 EIV-infected E.Derm show divergent transcriptomic profiles

To investigate further the role played by the host response to infection I conducted transcriptomics analysis of E.Derm cells infected with EIV/63 or EIV/2003 at two different timepoints (4 and 24 hpi) and compared gene expression to the respective mock-infected controls. However, as assessing the global transcriptome changes induced by experimental infections relies on the simultaneous interpretation of 26,991 genes expression profile

(representing the total number of annotated equine genes available in EquCab2.0 genome release) and such interpretation is difficult to make, I decided to assess the global transcriptome changes induced by EIV infections by using principal component analysis. As observed in Figure 4-5 A, 83.92% of the variance observed was explained by the principal component 1 (PC1), while 7.09% of the remaining variance was explained by PC2, which suggest that EIV-infected E.Derm cells are associated with a different gene expression profile to control conditions. Additionally, I observed that the transcriptome of mock infections (grey) clustered together independently of the time post infection investigated, indicating a stable state of cells in absence of treatment. Regarding EIV-infected E.Derm cells, the conclusions were a bit more difficult to draw, especially at 4 hpi as both infected conditions (EIV/63 and EIV/2003) showed an overlap among them, highlighting tenuous changes. However, at 24 hpi EIV-infected E.Derm cells displayed distinct responses to infection as points clearly did not cluster together and were also distant from the mock-infected transcriptomes. These results suggest that in E.Derm cells system, EIV infection triggered an isolate-specific transcriptomic change that was accentuated with time.
To complement my initial analysis, I investigated the number of differently expressed genes (DEGs) as well as their regulation intensities. The regulation intensities were always compared to mock-infected condition, except if stated differently. I noted in Figure 4-5 B that at 4 hpi EIV/63 infection induced 83 DEGs of which 32 (38.55%) and 51 (61.45%) were respectively up and down regulated, while EIV/2003 affected 48 DEGs of which 42 (87.50%) and 6 (12.50%) were up and down regulated, respectively. However, at 24 hpi the number of DEGs increased in both conditions, to reach 3,438 (of which 64.92% (2,232) were upregulated) and 2,741 (of which 62.24% (1,706) were upregulated) for EIV/63 and EIV/2003 infection, respectively. Interestingly, I observed that at both timepoints EIV/63 induced more DEGs (83 and 3,438 at 4 and 24 hpi) than EIV/2003 (48 and 2,741), but that EIV/2003-induced DEGs were associated with an increased regulation intensity (5.9 $\log_2$ fold change (FC), and 13.66 $\log_2$ FC at 4 and 24 hpi, respectively), while EIV/63-induced DEGs reached 4.6 $\log_2$ FC and 12.17 $\log_2$ FC at 4 and 24 hpi, respectively.
Additionally, I investigated DEGs distribution among infection conditions (*i.e.* EIV/63 and EIV/2003). I observed at 4 hpi (Figure 4-5 C) a total of 103 DEGs of which 55 (53.40%) were regulated only during EIV/63 infection, and 20 (19.42%) by EIV/2003, while 28 (27.18%) were found dysregulated in both conditions. At 24 hpi I observed a total of 4,590 DEGs of which 1,849 DEGs (40.28%) were affected by EIV/63 and 1,152 (25.10%) during EIV/2003 infection, while 1,589 (34.62%) were found in both infected conditions. I expect

the transcriptomic changes highlighted previously to be driven by DEGs exclusive to either EIV/63 or EIV/2003, but also by the EIV-shared DEGs in which regulation intensities significantly differ. Therefore, I decided to determine if EIV-shared DEGs were associated with significantly different regulation intensities. To assess such differences, I directly compared the gene expressions of EIV/63-infected cells to EIV/2003-infected cells (the direct comparison did not involve mock-infected gene expression level), and selected genes with a significant difference ($p \leq 0.05$ and $|\log_2 FC| \geq 1$). The list of DEGs given from such comparison was filtered using the list of DEGs previously established (EIV/63-mock and EIV/2003-mock), which resulted in the identification of 103 and 4,590 DEGs between EIV/63 and EIV/2003 at 4 and 24 hpi, respectively. As observed in Figure 4-5 D, from the 28 shared DEGs highlighted at 4 hpi, 7 were differentially regulated among EIV infections and were: *irf9*, *tll2*, *popdc2*, *grm2*, *fcer1g*, *s100a5*, and *ifit3*. I also observed that some well characterised antiviral proteins (*i.e. ifit1*, *ifit2*, *mx1*) showed similar gene regulation intensities following EIV/63 and EIV/2003 infections and were not responsible for the change observed earlier. I observed that some of these genes are involved in pathways related to immunity functions such as *fcer1g* (IgE constant fragment (Fc) receptor subunit gamma), linked to neutrophil degranulation, or *irf9* and *ifit3*, two well-known ISGs. To complete the results focused on the early changes (4 hpi), I conducted similar analysis in E.Derm cells at 24 hpi to account for late changes. In Figure 4-5 E I observed that from the 1,589 listed DEGs, 490 displayed significant difference in their expression intensities following EIV/63 or EIV/2003 infections. Interestingly, I noted that *trim69* which is a known viral restriction factor (K. Wang et al. 2018; Kueck et al. 2019; Rihn et al. 2019) was significantly more upregulated by EIV/63 than it was for EIV/2003 (11.54 $\log_2$ FC, and 8.82 $\log_2$ FC, respectively). Additionally, I noted an important upregulation of *trim14*, *il1rl2*, *tlr3*, and *ifnl3* genes in EIV/63-only DEGs, which are involved in pathogen sensing and defense against viruses, especially in mucosal immunity (*il1rl2, ifnl3*) (Svetlikova et al. 2010). To conclude, I observed an EIV/2003 exclusive downregulation of *trim45* gene, which is known to be associated with the IFN gamma signalling pathway (Shibata et al. 2012).

These results, coupled with previous findings, suggest that the type I IFN response, and to a lesser extent the type III IFN response (*il1rl2*, *ifnl3)* are key components of the virus-host interaction, and that viral long-term adaptation to horses leads to a better control of host response to infection. However, to confirm these findings, it is essential to investigate how biological processes were affected by such gene expression changes.

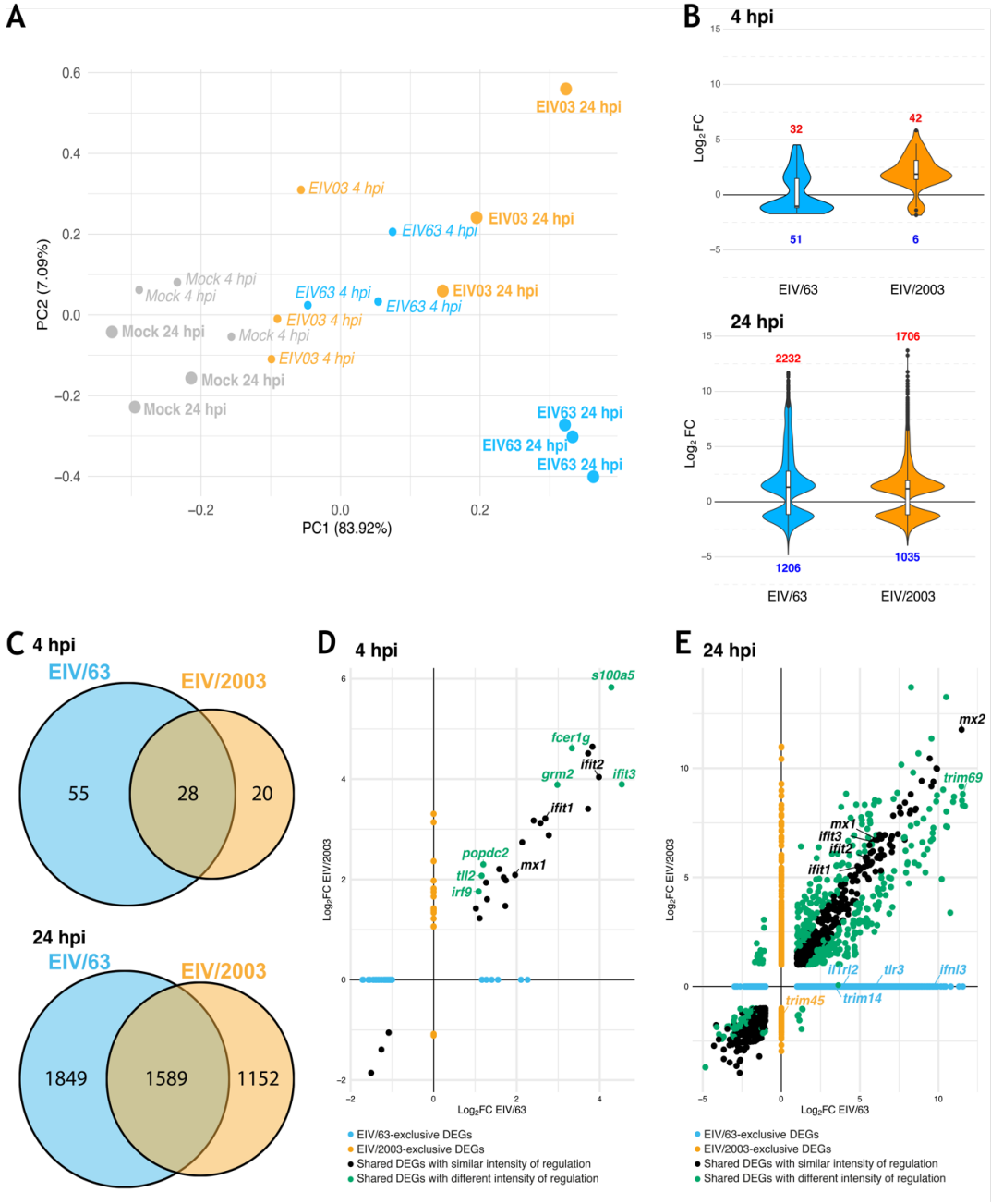

Figure 4-5: Similarities and differences of infectomes at 4 and 24 hpi. (A) Principal component analysis of infectomes in which mock treatment was displayed in grey, while EIV/63 and EIV/2003 infected conditions were displayed in cyan and orange, respectively. Different point size was used to distinguish transcriptomes obtained at 4 hpi and 24 hpi, and points were labelled for clarity. **(B)** Violin plots of DEGs ($p<0.05$, $|\log_2 FC>1|$) identified in infected E.Derm cells. EIV/63 or EIV/2003 induced DEGs at 4 hpi (top), and 24 hpi (bottom) were displayed in cyan and orange, respectively. The number of upregulated and downregulated genes in each condition was shown in red and blue, respectively. **(C)** DEGs distribution for EIV/63 (cyan) and EIV/2003 (orange) at 4 hpi (top) and 24 hpi (bottom). The number of DEGs for each subset is shown within each compartment of the Venn diagram. **(D-E)** Pairwise comparison of the intensity of regulation ($\log_2$ FC) for each DEG at 4 hpi (D), and 24 hpi (D). DEGs uniquely associated with EIV/63 or EIV/2003 are displayed in cyan, or orange, respectively, while common DEGs are coloured in black (non-significant) or emerald (significant). Data presented here represent three independent experiments.

4.2.5 EIV/63 and EIV/2003 modulate the type I IFN-mediated innate immune response differently

Based on the results obtained previously, I hypothesized that EIV/63 and EIV/2003 modulate differently the type I IFN response. To test this, I established the interferome of E.Derm cells (following IFN treatment) to highlight ISGs at 24 hpi and compared it with the corresponding infectomes (Figure 4-6). E.Derm cells treatment (universal IFN (uIFN)), as well as RNA extraction were done by Caroline Chauché, a previous PhD student in the group, while I focused on the data analysis. A list of ISGs was established by comparing gene expression between uIFN treated and control E.Derm cells. Cells treated with uIFN displayed a total of 143 DEGs and were referred as differentially expressed IFN-stimulated genes (DE-ISGs) in Figure 4-6 A. Notably, as observed in Figure 4-6, only 87 (60.84%) of the 143 total DE-ISGs were expressed in EIV-infected cells, highlighting the ability of H3N8 EIVs to limit the extent of host type I IFN response. In addition, as observed in Figure 4-6 A, 115 DE-ISGs showed a similar EIV-induced regulation (relative to mock-infected cells), while 28 DE-ISGs exhibited distinct levels of transcription between viruses (Figure 4-6 B). To investigate further the difference induced by EIV infections on DE-ISGs expression, I identified genes associated with distinct levels of expression and observed that some were involved in pathogen sensing (*i.e. tlr3*, *nod2*, *aim2*), immune response (*i.e. tnfsf13b*, *cd274*), or were known cytokines (*cxcl8). The cxcl8* gene encodes interleukin 8 (IL-8) and was reported to affect neutrophil recruitment, lung damage, as well as defence against IAV infection (Gruta et al. 2007; Peng et al. 2016). Additionally, I found that genes identified in immune activation pathways such as *tlr3* or *tnfsf13b* were exclusively upregulated in EIV/63-infected cells (6.03 $\log_2$ FC, and 4.41 $\log_2$ FC, respectively). I also observed that *cd274* (which encodes PD-L1 protein, known to prevent targeting of infected cells by $CD8^+$ T cells), was exclusively upregulated in EIV/2003-infected cells (2.51 $\log_2$ FC). Taken together, these results show that EIV/2003 i) avoids detection by innate immune sensors (*i.e. tlr3*, *nod2*, *aim2*), ii) blocks T and B cell functions (*i.e. cd274*, *tnfsf13b*) that are essential for controlling IAV infection, and iii) prevents upregulation of some well-characterised ISGs (such as *gbp1*). In contrast, EIV/63 does not appear to avoid detection by innate immune sensors (*i.e. tlr3*, *nod2*), and does not control expression of important genes involved in the adaptive immune response (*i.e. cd274*, *tnfsf13b*). However, EIV/63 can specifically prevent upregulation of well-characterised ISGs (*i.e. irf9*, *rsad2*), but not *gbp1*.

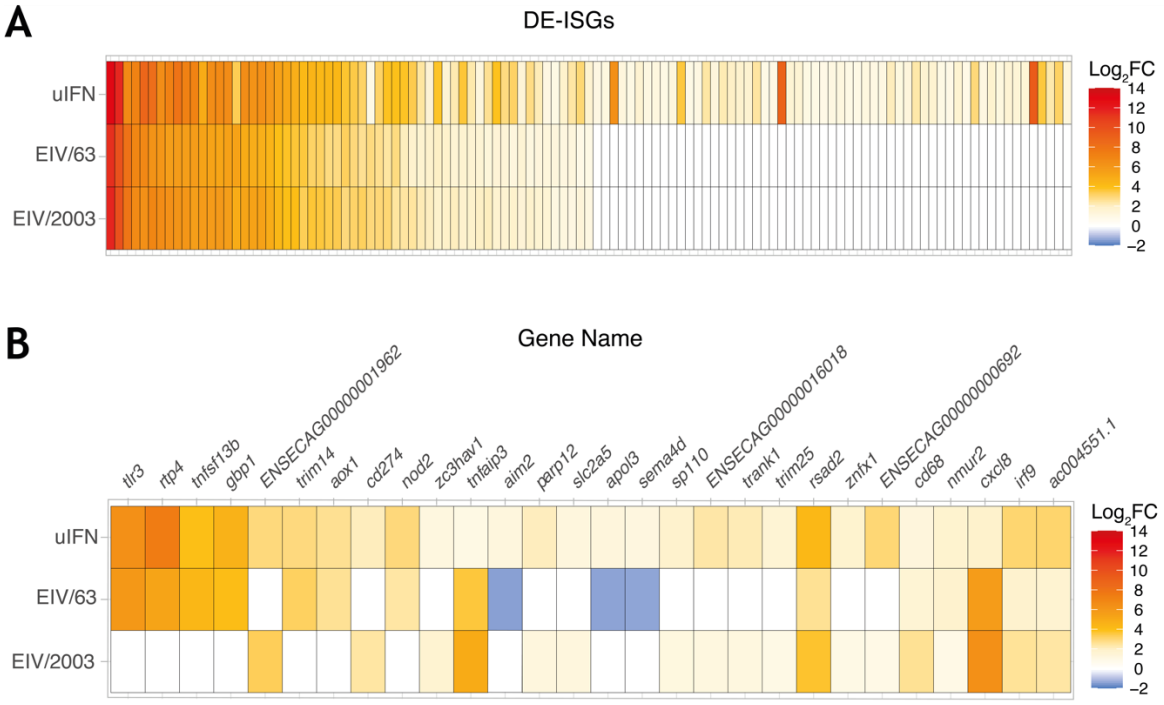

Figure 4-6: Characterisation of E.Derm ISGs at 24 hpi, and their EIV-induced regulation. (A) EIV-induced DE-ISGs associated with similar EIV-induced regulation intensity. **(B)** EIV-induced DE-ISGs associated with a significant change of their regulation between EIV/63 and EIV/2003. Gene expression levels are shown using a blue-white-red colour scale where blue indicates downregulation and white to red indicates upregulation. Data represents three independent experiments.

4.2.6 GO enrichment reveals that EIVs differentially affect biological processes

To confirm the involvement of type I IFN in the host response to infection I focused on the impact of EIV-induced gene regulation on underpinning biological processes. Therefore, I analysed the gene expression profile of infected E.Derm cells at 24 hpi and performed GO enrichment analysis. Briefly, DEGs were first divided into four subsets according to the viruses that induced them (EIV/63 or EIV/2003) and by their regulatory effect (down/up regulation). I observed at 24 hpi (Appendix 7), 103 and 98 GO terms were significantly enriched by EIV/63 and EIV/2003, respectively, of which 31 were common to both viruses. However, as my focus was to investigate the effect of infection on biological processes in relation to the host type I IFN response, I decided to specifically highlight a subset of GO terms as described in section 3.8.2.

I observed a total of 8 and 9 significantly enriched GO terms in relation to either immunity and host antiviral response induced in EIV/63 and EIV/2003 infections, respectively. In addition, I noted that 5 GO terms were significantly enriched by both viruses (Figure 4-7 A)

and included GO:0051607~Defense response to virus; GO:0060337~Type I Interferon signalling pathway; GO:0009615~Response to virus; GO:0045071~Negative regulation of viral genome replication; and GO:0019083~Viral transcription. The EIV-shared GO terms exhibited a similar regulatory effect (up/down regulation), number of genes involved, gene ratio, and significance (Figure 4-7 A). Furthermore, I noted that three GO terms were exclusive to EIV/63 infection (GO:0006954~Inflammatory response, GO:0000281~Mitotic cytokinesis, and GO:0034341~Response to interferon-gamma) while other four different GO terms (GO:0060333~Interferon-gamma-mediated signalling pathway, GO:0034097~Response to cytokine, GO:0032480~Negative regulation of type I interferon production, and GO:0035457~Cellular response to interferon-alpha) were unique to EIV/2003 infection (Figure 4-7 A).

This result showed that EIV infection is significantly affecting some of the host canonical pathways, and more particularly GO:0032480~Negative regulation of type I interferon production, as expected. In fact, my analysis found that only EIV/2003 virus infection induced an upregulation of the GO term that negatively regulates host type I IFN production, leading to a decrease of type I IFN production in infected cells (Figure 4-7 A). As I know, once produced, IFN operates following an autocrine and paracrine manner, hence, reduction of IFN production results in a decrease of JAK/STAT pathway activation, and in turn a diminution of host response to type I IFN. I then investigated the genes involved in GO:0032480~Negative regulation of type I interferon production and identified three genes associated with a significant variation of their regulation intensities induced by EIVs, *tnfaip3* (encodes A20 protein), a well-known negative regulator of NFκB activation and translocation (Maelfait et al. 2012), *uba52* (encodes ubiquitin-60S ribosomal protein L40), which decreases A/mallard/Huadong/S/2005 viral titre and proinflammatory cytokine production in chicken embryonic fibroblasts (DF1) (Wang et al. 2018), and *trim25* (encodes E3 ubiquitin ligase), which inhibits RNA synthesis (Figure 4-7 B) (Meyerson et al. 2017).

Additionally, I noticed that of the 7 differentially regulated GO terms, one stood out from the others due to the large number of genes involved (57 in EIV/63 infection) and large gene ratio (3.07%), GO:0006954~Inflammatory response (Figure 4.7 A). As virus-induced pathology could be triggered by an exacerbated host immune response (immunopathology), I decided to examine further the GO:0006954~Inflammatory response GO term and found that out of 69 DEGs involved (by either EIV/63 or EIV/2003), 82.61% (57/69) were found significantly regulated by EIV/63, while only 55.07% (38/69) were regulated in EIV/2003 infection. All EIV/2003-induced DEGs were upregulated, while of the 57 DEGs identified

in EIV/63 infected cells, 55 were upregulated and 2 downregulated (*apol3*, *aim2*; Figure 4-7 C). Differently expressed genes associated with the inflammatory response GO term and their respective transcription levels are shown in Figure 4-7 D. Similarly to Figure 4-5 D and Figure 4-5 E, I directly compared the gene expressions of EIV/63-infected cells to EIV/2003-infected cells (the direct comparison did not involve mock-infected gene expression level), and selected genes with a significant difference ($p \leq 0.05$ and $|\log_2 FC| \geq 1$). Interestingly, 11 of the common DEGs showed significant differences of their regulation intensities induced by EIV (green circles shown in Figure 4-7 D), and included *tnfaip3* (described previously), in addition to *ptgs2* (COX2), and *ptger3* (PGE2-R), two genes involved in the transformation of arachidonic acid into prostaglandin, a well-known proinflammatory molecule (Simmons et al. 2004; Ricciotti and Fitzgerald 2011). Additionally, I observed the overexpression of *cxcl8*, *cxcl5*, and *ccl2* genes whose protein products are all chemoattractant cytokines responsible for leucocyte recruitment, as well as *itgb2*, a gene encoding LFA1 integrin, a protein playing an important role in the process of vascular extravasation of circulating leucocytes.

Taken together, these results suggest that both viruses trigger qualitatively similar local inflammatory responses, albeit of different magnitude (*i.e.* EIV/63 infection triggering an exacerbated inflammatory response).

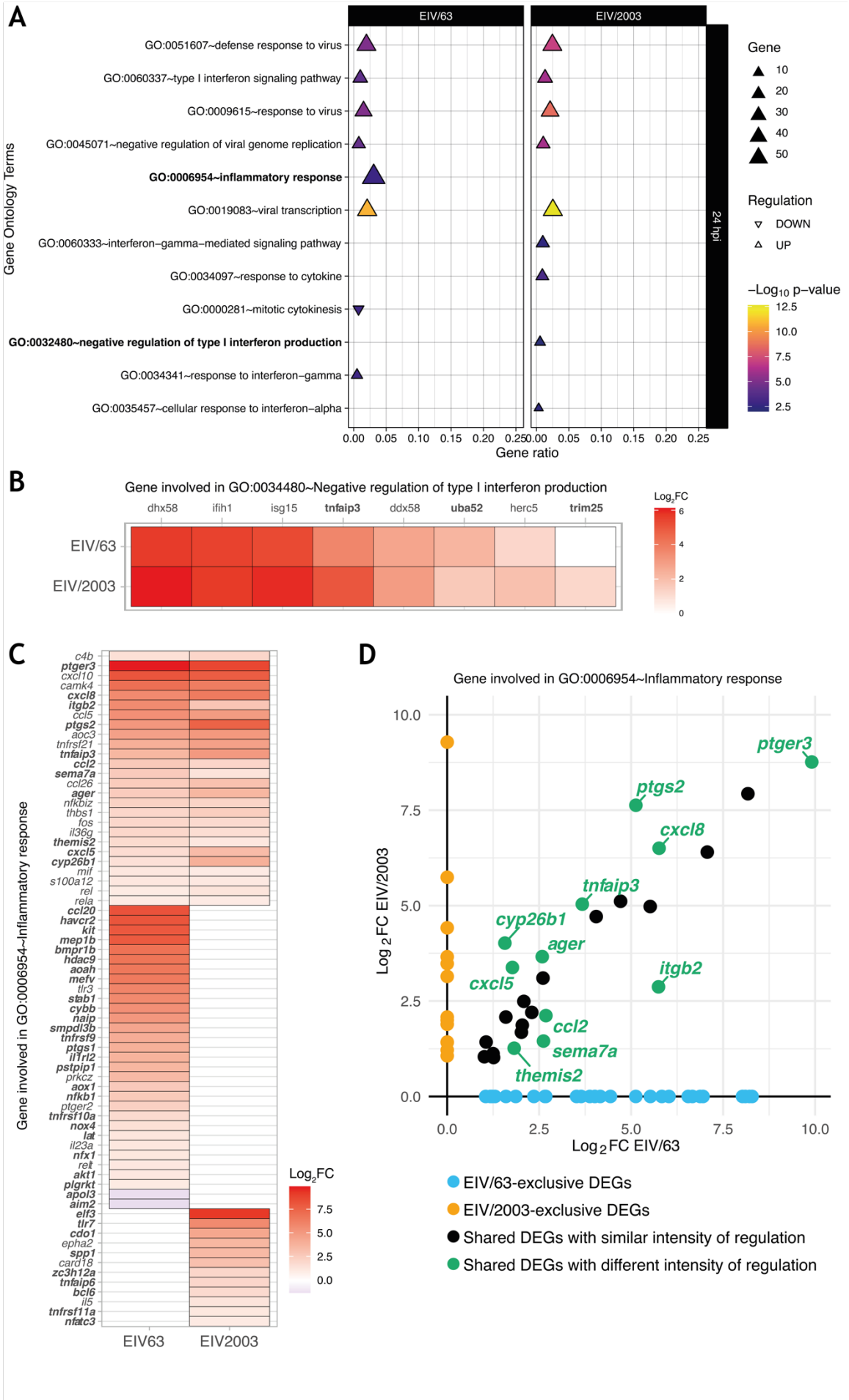
A
EIV/63
EIV/2003
GO:0051607~defense response to virus
GO:0060337~type I interferon signaling pathway
GO:0009615~response to virus
GO:0045071~negative regulation of viral genome replication
GO:0006954~inflammatory response
GO:0019083~viral transcription
GO:0060333~interferon−gamma−mediated signaling pathway
GO:0034097~response to cytokine
GO:0000281~mitotic cytokinesis
GO:0032480~negative regulation of type I interferon production
GO:0034341~response to interferon−gamma
GO:0035457~cellular response to interferon−alpha
Gene Ontology Terms
24 hpi
Gene ratio
Gene
10
20
30
40
50
Regulation
DOWN
UP
−Log10 p−value
12.5
10.0
7.5
5.0
2.5
B
Gene involved in GO:0034480~Negative regulation of type I interferon production
dhx58
ifih1
isg15
tnfaip3
ddx58
uba52
herc5
trim25
EIV/63
EIV/2003
Log2FC
C
Gene involved in GO:0006954~Inflammatory response
EIV63
EIV2003
Log2FC
D
Gene involved in GO:0006954~Inflammatory response
Log2FC EIV/2003
Log2FC EIV/63
ptger3
ptgs2
cxcl8
tnfaip3
cyp26b1
ager
itgb2
cxcl5
ccl2
sema7a
themis2
EIV/63-exclusive DEGs
EIV/2003-exclusive DEGs
Shared DEGs with similar intensity of regulation
Shared DEGs with different intensity of regulation

Figure 4-7: Comparison of GO terms associated with host response to infection in EIV/63 or EIV/2003 infected cells. (A) GO terms associated with host response to infection. Significantly upregulated GO terms are shown as triangles, while downregulated GO terms are shown as inverted triangles. The size of each triangle represents the number of DEGs fitting each GO term, while the ratio of total genes involved in each category is displayed on the x-axis. Enrichment significance is displayed according to a blue-magenta-yellow gradient ($-\log_{10}$ p-value). GO term 006954 and 0032480 are shown in bold. Regulation intensity of DEGs involved in GO: 0032480 **(B)** and GO:006954 **(C)** are shown following a blue-white-red colour scale. Downregulation is highlighted by blue shades, while upregulation uses red shades. Significant DEGs among infectomes are shown with bold names. **(D)** Pairwise comparison of intensity of regulation ($\log_2$ FC) and distribution of DEGs involved in GO:0006954 Inflammatory response. DEGs exclusively associated with EIV/63 or EIV/2003 are displayed in cyan, or orange, respectively, while common DEGs are coloured in black (non-significant) or emerald (significant). Data presented here summarise three independent experiments.

4.2.7 EIV/2003 shows enhanced viral replication and dissemination in the equine respiratory tract but exhibits milder tissue pathogenicity than EIV/63

My results converged toward the identification of host type I IFN response as an important measure raised by the host to limit EIV infection. Additionally, results highlight that during the 40 years of viral adaptation, EIVs became more effective at evading host response to infection, leading to the different infection phenotype observed *in vitro*. To determine if such differences would also be present at the natural site of EIV infection, I infected *ex vivo* equine tracheal explants with EIV/63 and EIV/2003. This experimental system allowed measurement of viral replication kinetics, intra-epithelial viral dissemination, but also virus-induced histopathological changes.

To do so, I titrated virus collected from the apical surface of infected equine tracheal explants at various times post infection (Figure 4-8 B) and observed that EIV/63 viral titres reached 10^6—10^7 $TCID_{50}$/mL, while EIV/2003 titres peaked at 10^9 $TCID_{50}$/mL at 2 day post infection (dpi) and remained stable until the end of the experiment. Overall, EIV/2003 exhibited significantly increased viral replication kinetics compared to EIV/63 (p-value = 0.0288, Figure 4-8 B) consistent with *in vitro* results. As the system was validated, I investigated virus intra-epithelial dissemination and histopathological changes by using image analyses of histological sections of formalin-fixed, paraffin-embedded equine tracheal explants collected at different times post-infection. With help from Daniel Goldfarb, a PhD

student in the group, we developed an ImageJ (Fiji) macro to automatise and accurately quantify the extent of immunostaining signal in histological sections. The steps involved in the macro are available in section 3.8.3, and a schematic representation of the process is available in Figure 4-8 A. The accuracy of the data generated by the macro was assessed and validated by Veronica Patton, an accredited veterinary pathologist (Patton 2021).

To quantify virus-induced tissue injury, I measured the number of cells (Figure 4-8 C) and the area of the epithelium (Figure 4-8 D). The number of cells in EIV-infected tracheal epithelium decreased steadily from 1 to 4 dpi, and at a higher rate than in mock-infected explants. The reduction of epithelial cell number was significantly more marked in EIV/63-infected explants than in EIV/2003 (p-value = 3.15×10^{-3}, Figure 4-8 C). Furthermore, I observed that the tracheal epithelium of EIV/63-infected explants was thinner when compared to EIV/2003-infected explants (p-value = 1.24×10^{-3}, Figure 4-8 D), indicating that EIV/2003 caused less epithelial damage compared to EIV/63. These results are in line with the previously observed reduction of inflammatory response signals that could potentially result in reduced immunopathology attributed to EIV/2003 infection.

I then performed immunohistochemistry using EIV NP antibody to quantify the intra-epithelial viral dissemination (Figure 4-8 E). I observed that both viruses reached a NP intra-epithelial dissemination peak at 2 dpi which were ~ 180 squared micrometre (μm^2) and ~ 415 μm^2 for EIV/63 and EIV/2003 infected tracheal explants, respectively. Additionally, I found that EIV/2003-infected explants showed significantly larger areas of NP staining than EIV/63 (p-value = 0.026), indicating increased virus dissemination in tracheal tissue (Figure 4-8 E). The full panel of NP immunostained histological sections is available in Appendix 8.

To compare the extent and kinetics of the innate immune response triggered by each virus, I quantified the expression of an ISG product Mx1 used as a proxy of host innate immunity raised in response to infection (Figure 4-8 F; Haller and Kochs 2020). Explants infected with EIV/63 displayed two peaks of Mx1 stained area (at 2 and 5 dpi, reaching 3,750 μm^2 and 6,050 μm^2, respectively) whereas explants infected with EIV/2003 exhibited only one peak at 4 dpi (5,440 μm^2), suggesting that the latter might delay the expression of ISGs within the respiratory tract. However, the overall differences in Mx1 expression over the five days post-infection were not statistically different (p-value = 0.12). The full panel of Mx1 immunostained histological sections is available in Appendix 9.

An additional biological process interesting to investigate is virus-induced apoptosis. To do so, I quantified the expression of CC3, an effector caspase, which triggers the most extreme

host response to infection, the apoptotic process (Figure 4-8 G; Gown and Willingham 2002). I observed that in both infected condition CC3 stained area peaked at 2 dpi reaching 365 μm^2 and 390 μm^2 in EIV/63 and EIV/2003 infection, respectively. Therefore, the overall kinetic of CC3 stained area remained similar between EIV/63 and EIV/2003 infections (p-value = 0.51), but based on the shape of the curve, it appeared that EIV/2003 infection delayed CC3 protein expression by approximatively 1 day when compared to EIV/63. The full panel of CC3 immunostained histological sections is available in Appendix 10.

Finally, I compared the level of epithelial regeneration (to compensate for cell death) by performing immunohistochemical staining of Ki67, a nuclear marker expressed in all active phases of the cell cycle (Scholzen and Gerdes 2000). I observed that in both infected condition, the percentage of Ki67 positive nuclei peaked at 3 dpi (6.8% and 1.4% in EIV/63 and EIV/2003 infection, respectively), while in mock-infected explants Ki67 never exceeded 0.44% positive nuclei (Figure 4-8 H). Statistical analysis found that EIV/63-infected explants exhibited a significantly higher number of dividing cells than EIV/2003 (p-value = 6.65×10^{-5}). This result is consistent with a stronger regenerative process in response to the higher levels of EIV/63-induced cell death previously highlighted. As expected, EIV/2003-infected explants displayed a similar number of dividing cells when compared to control. The full panel of Ki67 immunostained histological sections is available in Appendix 11.

Taken together, these results showed that EIV/2003 replicates to higher levels and disseminates over larger areas within the equine tracheal epithelium, and while both viruses induce similar pathological changes and virus-induced responses, the extent and kinetics of such changes are markedly different.

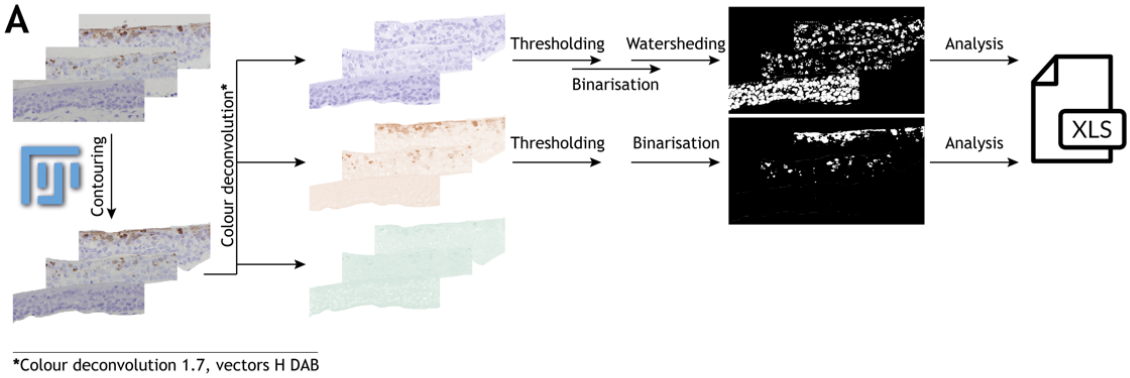

*Colour deconvolution 1.7, vectors H DAB

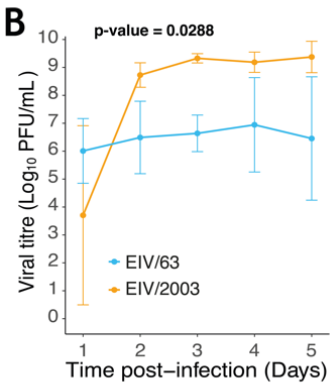

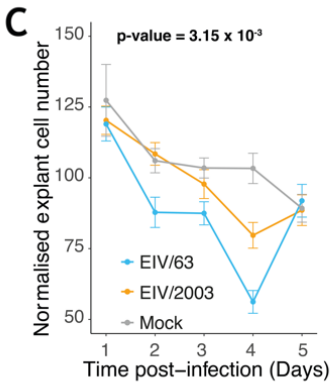

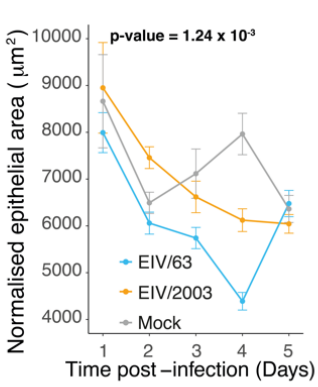

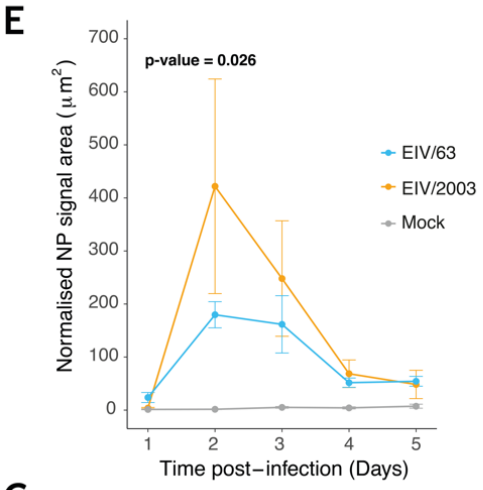

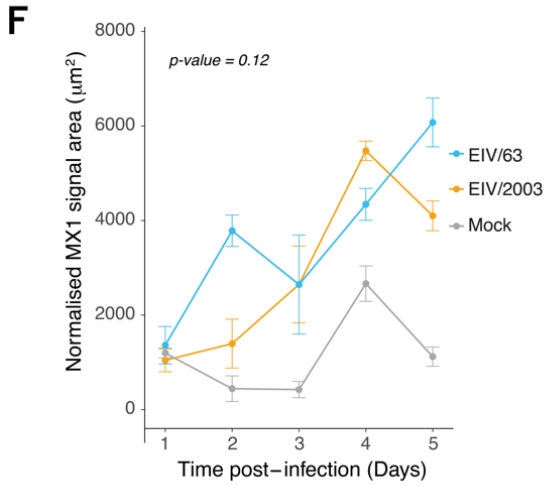

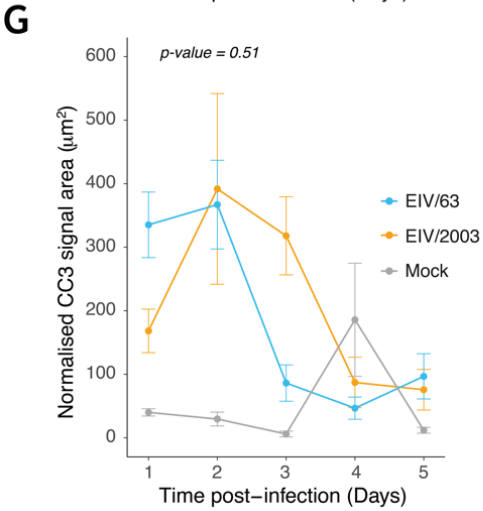

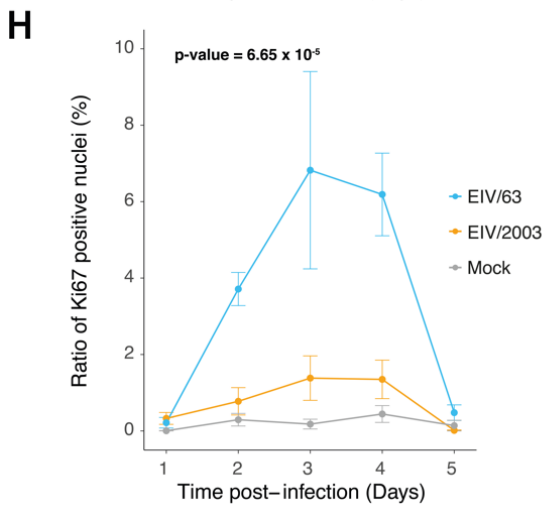

Figure 4-8 Analyses of morphological changes and cellular processes in equine tracheal explants infected. (A) Schematic representation of the Fiji macro permitting the accurate quantification of IHC signal from microphotography. **(B-H)** Plots showing measurements of the viral titre **(B)**, number of nuclei **(C)**, epithelial area **(D)**, EIV NP staining **(E)**, MX1 staining **(F)**, cleaved-caspase 3 staining **(G)**, and Ki67 staining **(H)**. Cyan, orange, and grey lines represent explants infected with EIV/63, EIV/2003 and mock-infected, respectively. Antigen quantifications are summarised as the mean ± SEM of three images per section per timepoint on three independent sections. P-values are shown in bold when significant and were calculated using GLM models.

4.3 Discussion

In this chapter, I studied the phenotypic changes induced by two viruses separated by 40 years of continuous adaptation to the horse. As theorised by Van Valen in 1973, such alterations are necessary to improve the overall viral fitness, which allowed not only EIV to establish, but also to maintain a position in the equine viriome landscape as an EIV endemic lineage. H3N8 EIV was first isolated in 1963 and since then it has been continuously circulating among horses. Interestingly, H3N8 EIV origins has been linked to a single introduction event leading to the formation of a monophyletic group, offering a rare setting to study viral evolution. As most of the published work focuses on the effect of single genomic mutations on viral traits (*i.e.* replication kinetics, cellular entry, antigenicity, polymerase activity), potential epistatic effects remain usually understudied. I scrutinised several viral traits affecting within-host fitness (*i.e.* viral spread, viral replication kinetics, viral-induced tissue damage) induced by the earliest (EIV/63) or a contemporary (EIV/2003) isolate, separated by 40 years of constant selection pressure exerted by the host. Murcia et al. (2011) demonstrated that EIV adaption to equine population was influenced by purifying segment selection (mean d_N/d_S ratio < 0.3), most likely the consequence of functionally important and conserved domains. However, the authors also found 16 sites positively selected and located in segment 1 (codon 377); segment 2 (584); segment 3 (57, 277, 337, 348, 354, 400); segment 4 (10, 23, 152, 206, 345); segment 5 (452); segment 6 (43); and segment 8 (67), which most likely directed EIV adaptation.

I initially examined the effects of viral genotype on replicative fitness (a key component of viral fitness (Wargo and Kurath 2012) by comparing viral replication kinetics of EIV/63 and EIV/2003 in MDCK and E.Derm cells. While it is clear that *in vitro* cell system did not recapitulate the process of natural infection, it allowed quantification of viral replication kinetics in a highly-controlled system. I found that EIV/2003 exhibited a significantly higher

replicative fitness than EIV/63 in E.Derm cells, but not in MDCK cells, suggesting that viral evolution led to EIV adaptation to an equine-specific IFN-competent, cellular context. These results were consistent with those observed by Stucker et al. (2012) who showed the effect of multiple concerted mutations on the replicative fitness of canine parvovirus *in vitro*. While I cannot explain this effect mechanistically, I found in transcriptomic analysis a reduction of transcriptional changes induced by EIV/2003 when compared to EIV/63 consistent with a previous study showing that human H3N2 IAV virus dysregulated a lower number of genes than H5N1 and H7N7 AIVs in human bronchial epithelial cells (Josset et al. 2014). This result suggests that adapted viruses evolve towards higher transcriptional efficiency and disrupt a lower number of genes while modifying a higher number of cellular pathways. Interestingly, I found a significant downregulation (*i.e.* upregulation of the negative regulation of the type I IFN production) of type I IFN response induced exclusively by EIV/2003, which could explain the more effective replication kinetics observed. Additionally, I identified three genes: *tnfaip3* (upregulation), *uba52* (downregulation), and *trim25* (upregulation) as key factors impacting the ability of the virus to overcome the host type I IFN response.

To examine the evolution of H3N8 EIV adaptation in a more relevant biological context I used *ex vivo*-cultured equine tracheal explants which represent the natural site of EIVs infection. Explants have been broadly used to study the infection biology of IAVs as they recapitulate the *in vivo* pathology associated with influenza infection (Fu et al. 2019). However, it is important to highlight that the explant system lacked any component of the host adaptive immunity and does not perfectly mimic experiments carried out *in vivo*. Virus titrations and image analysis of infected explants showed that EIV/2003 replicated to higher levels and spread over larger areas of the respiratory epithelium than EIV/63. These results suggest that changes of genotype acquired during H3N8 EIV evolution resulted in an enhanced pathogen load.

An extra component of the overall viral fitness resides in the cost of infection on the host organism (from lesions to pathogen-induced death) and the host response to infection (*i.e.* apoptosis or inflammatory processes), often associated with virulence. However, whether virulence is adaptative or not has been debated (Alizon and Michalakis 2015). Interestingly, severe, and lethal infections are often associated with out-of-control exacerbation of host immune responses and categorised as immunopathology (Short et al. 2017), a biological process enhanced in EIV/63-infected E.Derm cells. To determine further if EIV evolution was associated with changes in tissue damage I quantified EIV-induced lesions in respiratory

explants using image analyses. EIV/63-infected explants exhibited fewer epithelial cells than EIV/2003-infected explants, leading to a greater decrease of the respiratory epithelium area suggesting exacerbation of lesions. Overall, these results suggest that H3N8 EIV evolved towards lower virulence and are in line with a previous report that compared the *in vivo* virulence of two H3N8 EIV isolates separated by 5 years of evolution (Sussex/89 and Newmarket/93) (Wattrang et al. 2003). I noted that evolution of tissue damage is not necessarily a shift towards avirulence, but most likely an intermediate level as observed by other viruses such as myxoma virus in rabbits (Kerr 2012) or Newcastle disease virus in wild birds (reviewed by Afonso 2021).

Overall, the results of this chapter showed evidence that long-term evolution following host shift of an avian-origin H3N8 influenza virus to horses resulted in the selection of multiple traits including enhanced replication kinetics, and intra-host dissemination, as well as reduced tissue damage.

Chapter 5: Comparison of A/equine/Jilin/1/1989 and A/ruddy shelduck/Mongolia/963v/2009 *in vitro* phenotypes

5.1 Introduction

In the previous chapter, the consequences of long-term viral evolution following influenza virus host shift were investigated *in vitro* and *ex vivo*. I found that viral adaptation affected viral replication kinetics, viral spreading, host gene expression, and tissue damage. Avian-origin influenza virus crossed the species barriers and established in horses on multiple occasions. In 1989, an additional interspecies transmission event (caused by a H3N8 avian-origin influenza virus phylogenetically different to the virus that emerged in 1963) was reported in Northeast China (Guo et al. 1992). However, this virus did not establish as an equine endemic lineage as it circulated exclusively in the Jilin and Heilongjiang provinces and was not sampled after 1992 (Webster and Thomas 1993). In a more recent study, serological evidence of AIV interspecies transmission in Mongolian horses was found, and highlighted that those AIVs were phylogenetically related to the H3N8 AIV that emerged in China in 1989 (Zhu et al. 2019). Results from that study suggested that influenza interspecies transmission events are more frequent than initially thought and should therefore be considered as an important threat to equine populations.

Understanding the rules that underpin viral emergence is essential to anticipate and prevent such events from happening. The risk of viral emergence is the product of multiple intrinsic and extrinsic factors across different scales: from molecular interactions within an infected cell to species interactions within an ecosystem. At the most basic level, host susceptibility is determined by the compatibility between virus and host proteins.

In this chapter I investigated various fitness components of the EIV isolate that initiated the Northeast Chinese EI outbreak (EIV/89), and a circulating AIV/2009 sampled in 2009 in Mongolia and phylogenetically related to EIV/89 (Zhu et al. 2019). Therefore, to confirm the phylogenetic relationship between AIV/2009 and EIV/89, I compared the viral sequences of these viruses (Appendix 12). Unsurprisingly, the number of non-synonymous mutations did not exceed 34 and was found in HA CDS, a similar result to the previous chapter. As there is no evidence that AIV/2009 established in horses, the virus will be used as a representative of a circulating AIV capable of infecting horses without onward transmission, while EIV/89 will exemplify a virus of the same lineage that was able to infect and spread in an equine population. I hypothesis that these two viruses would exhibit clear differences in infection phenotype, with EIV/89 associated to a higher *in vitro* fitness. To test this, I performed a series of *in vitro* experimental infections and combined classical virology techniques with transcriptomic analyses.

5.2 Results

5.2.1 EIV/89 exhibits an enhanced replication kinetics and cell-to-cell spread.

To compare virus replication kinetics and cell-to-cell spread *in vitro* I first infected MDCK cells with AIV/2009 and EIV/89 and quantified their replication kinetics up to 96 hpi. Titrations of the inocula (Figure 5-1 A) showed no significant differences between EIV/89 and AIV/2009 (p-value = 0.7671), indicating that infections were similar. As shown in Figure 5-1 B EIV/89 and AIV/2009 replicated to similar titres (10^6—10^7 $TCID_{50}$/mL) and both viruses reached their replication peak at 48 hpi. Statistical analyses using general linear models showed that there were no significant differences in the viral replication kinetics between the two viruses (p-value = 0.239), even though EIV/89 displayed higher titres in the first 24 hpi. To measure cell-to-cell spread, I performed experimental infections under plaque-forming conditions and measured plaque sizes. As observed in Figure 5-1 C, the size of the plaques induced by EIV/89 was significantly larger ($\overline{diameter}$ = 0.2469 cm (range = 0.1023—0.4338 cm)) than AIV/2009 ($\overline{diameter}$ = 0.1616 cm (range = 0.1009—0.2460 cm); p-value = 1.159×10^{-4}). Taken together, these results indicate that EIV/89 and AIV/2009 exhibit similar replication kinetics in MDCK cells, but EIV/89 spreads more efficiently than AIV/2009.

To compare the replication kinetics of EIV/89 and AIV/2009 in an equine cellular context, I performed experimental infections in E.Derm cells. Again, the inocula were titrated, and Figure 5-1 D shows no significance differences (p-value = 0.2683), which allowed me to compare virus replication kinetics. Notably, the overall pattern of virus kinetics was different to what was observed in MDCKs: as observed in Figure 5-1 E, AIV/2009 and EIV/89 were able to infect and replicate in E.Derm cells as demonstrated by the viral titre increase in the first 12 hpi. However, at 24 hpi, AIV/2009 titres were undetectable, indicating that viral replication has been inhibited and the infection most likely resolved. In contrast, EIV/89 titres peaked at around 10^3—10^4 $TCID_{50}$/mL but declined from 48 hpi to 72 hpi, when virus became undetectable. These results suggest that while both AIV/2009 and EIV/89 could infect E.Derm cells, the former is more sensitive to equine cellular responses than EIV/89.

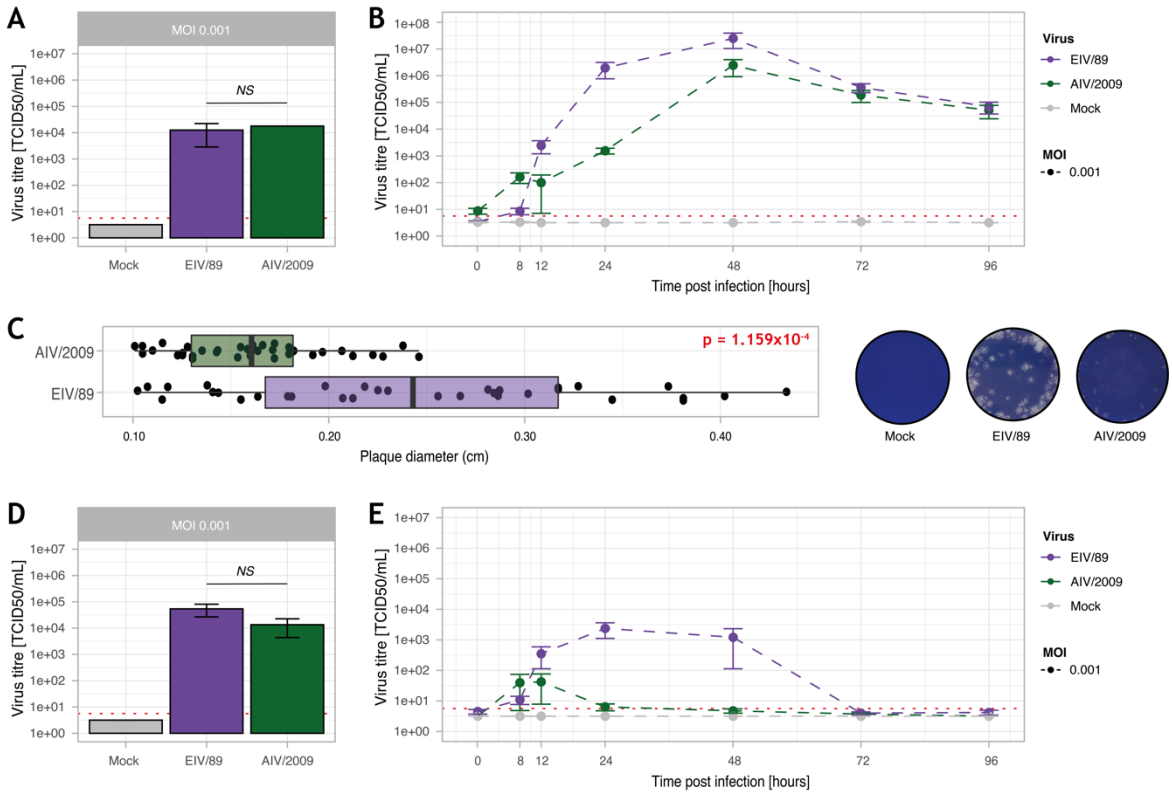

Figure 5-1: In vitro characterisation of H3N8 IAVs. (A) Viral titre of inocula used in the experimental infections of MDCK cells. **(B)** Growth kinetics of EIV/89 and AIV/2009 in MDCK cells. **(C)** Plaque phenotype of EIV/89 and AIV/2009 in MDCK cells at 48 hpi. At least 40 plaques per condition were measured. **(D)** Viral titre of inocula used in the experimental infections of E.Derm cells. **(E)** Growth kinetics of EIV/89 and AIV/2009 in E.Derm cells. Purple and green colours represent EIV/89 and AIV/2009 viruses, respectively, while non-infected controls are shown in grey. Viral titres are represented as the mean ± SEM. Infections were performed three times independently and each independent experiment consisted of three technical repeats. Statistical significances were assessed using a Wilcoxon rank sum test (in A, C, and D).

5.2.2 AIV/2009 and EIV/89 induce distinct gene expression profiles

To explore the differences in infection phenotype between EIV/89 and AIV/2009 in E.Derm cells in more detail, I used transcriptomics. Before performing analyses, I compared the infection levels of E.Derm cells over time as mentioned in section 3.6.1. Figure 5-2 A, shows that experimental infections reached the targeted proportion of infected E.Derm cells (50 ± 5%), allowing downstream analyses. However, at 24 hpi the percentage of AIV/2009-infected cells exhibited a dramatic drop (from 48.88 ± 3.01% to 17.75 ± 1.94%). In contrast, EIV/89-infected cells number increased over time (from 50.73 ± 1.08% to 91.70 ± 4.53%). This result was consistent with the viral replication kinetics observed in the

previous section, suggesting that in addition to an AIV/2009 viral replication inhibition, infected cells are eliminated from the system during the first 24 hpi.

Transcriptomic analyses (Figure 5-2 B) showed that 70.99% of the variance observed was explained by PC1, while 10.27% of the remaining variance was explained by PC2. Additionally, (Figure 5-2 C) showed that 70.41% of the variance observed in EIV/89-infected E.Derm cells was explained by PC1, and 14.22% of the remaining variance was explained by PC2. In contrast, AIV/2009-infected E.Derm cells displayed PC1 and PC2 values of 77.74 and 13.24%, respectively. These results suggest that when compared to their respective controls, AIV/2009 infection induces a greater change of the transcriptional profile than EIV/89. Additionally, a careful analysis of the dynamics of transcriptional changes induced by each infection (Figure 5-2 C inserts), indicates that EIV/89-induced transcriptional modifications tend to increase over time, while AIV/2009 transcriptional changes decrease. Such results associated with the viral replication kinetics and the decrease of infected cells over time strongly suggest that AIV/2009 infection is controlled at 24 hpi.

I further investigated the number of DEGs as well as their regulation intensities. It was noted in Figure 5-2 D that at 4 hpi AIV/2009 induced 474 DEGs of which 134 (28.27%) and 340 (71.73%) were respectively up and down regulated, while EIV/89 affected 10 DEGs which were all upregulated. These results contrasted with the number of DEGs found at 24 hpi in which EIV/89-induced genes reached 819 (representing an increase of 8,190%), of which only 80 (9.77%) were upregulated. Additionally, the number of AIV/2009-induced DEGs decreased to 363 (representing a decrease of 23.42%), of which 56.20% (204/363) were upregulated. Interestingly, it was observed that the magnitude of gene upregulation induced by EIV/89 significantly increased over time (from 5.06 to 11.88 $\log_2$ FC), while in AIV/2009 infection it did not (from 3.53 to 5.79 $\log_2$ FC).

Finally, I examined the distribution of DEGs between infections and observed no overlap at 4 hpi, while at 24 hpi, 7.87% (93/1,182) of the DEGs overlapped (Figure 5-2 E). These results provide evidence that EIV/89 and AIV/2009 triggered distinct host responses to infection at 4 hpi, which most likely reflect the biological processes underpinning the differences observed in replication kinetics.

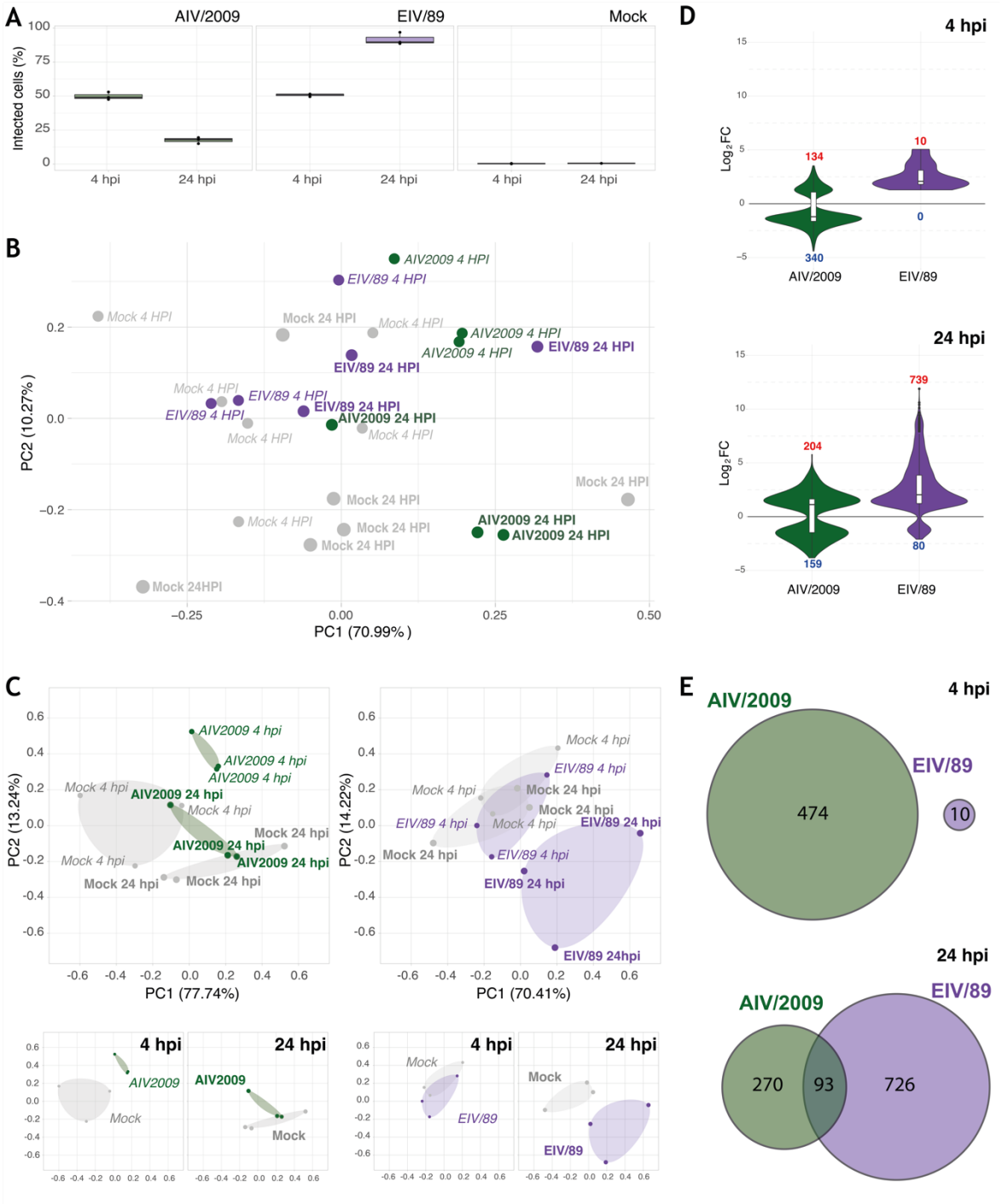

Figure 5-2: Similarities and differences of EIV/89 AND AIV/2009 infectomes at 4 and 24 hpi. (A) Paired percentage of experimentally infected E.Derm cells at 4 and 24 hpi analysed by flow cytometry. AIV/2009, EIV/89, and Mock infected cells are displayed in green, purple, and grey, respectively. **(B)** Principal component analysis of infectomes in which mock treatment was displayed in grey, while AIV/2009 and EIV/89-infected conditions were displayed in green and purple, respectively. Different point size was used to distinguish transcriptomes obtained at 4 hpi and 24 hpi, and points were labelled for clarity. **(C—D)** Principal component analysis of infectomes in which AIV/2009 and EIV/89, as well as 4 and 24 hpi time point (inserts) were separated to facilitate reading. These inserts are representing the same data as the PCA in (C). **(D)** Violin plots of DEGs ($p < 0.05$, $|\log_2 FC > 1|$)

identified in E.Derm infected cells. AIV/2009 or EIV/89 induced DEGs at 4 hpi (left), and 24 hpi (right) were displayed in green and purple, respectively. The number of upregulated and downregulated genes in each condition was shown in red and blue, respectively. **(E)** DEGs distribution for AIV/2009 (green) and EIV/89 (purple) at 4 hpi (left) and 24 hpi (right). The number of DEGs for each subset is shown within each compartment of the Venn diagram. Data presented here represent three independent experiments.

5.2.3 AIV/2009 do not triggers a significant innate immune response

The previous results combined suggest that AIV/2009 virus replication in E.Derm cells might be impaired by the host response. Based on my previous experiments using EIV/63 and EIV/2003, and the replication kinetics observed in MDCK cells, I hypothesized that the type I IFN response was involved in such differences, and this would result in different canonical pathway expression profiles. To test this hypothesis, I focused on the effect of gene regulation induced by EIV/89 or AIV/2009 and their impact on biological processes. To this end, I analysed gene expression profiles at 4 and 24 hpi of EIV/89 and AIV/2009-infected E.Derm cells and performed GO enrichment analysis similarly to chapter 4.

Figure 5-3 A highlights the lack of DEGs overlap at 4 hpi between EIV/89 and AIV/2009-induced DEGs. These gene expression profiles led to the regulation at 4 hpi of 4 GO terms, of which 3 were exclusive to EIV/89 infection and one to AIV/2009 (Figure 5-3 C). Unsurprisingly, all the EIV/89-enriched GO terms were upregulated and related to immune functions (*i.e.* GO:0051607~defense response to virus, GO:0009615~response to virus, and GO:0060337~type I interferon signalling pathway), while the only AIV/2009-enriched GO term (GO:0006695~cholesterol biosynthetic process) was negatively regulated. When focusing on DEGs involved in the immune-related GO terms (GO:0051607, GO:0009615 and GO:0060337), I found (Figure 5-3 E) that all the genes involved were upregulated by EIV/89 infection, while none of them were dysregulated by AIV/2009. Additionally, I noticed that the extent of immune-related genes upregulation in EIV/89-infected cells was limited and did not reach the levels of IFN-induced response. This result suggests that early during infection (4 hpi) EIV/89 triggers a limited host immune response in comparison to IFN-treated E.Derm cells, while there was no detectable cellular response in AIV/2009-infected cells.

This result, together with the observed decline of infected cells (Figure 5-2 A) and the limited viral replication (Figure 5-1 E), suggests that AIV/2009 might triggers a very limited cellular response (not quantifiable in these experiments) and/or is highly sensitive to alternative cellular response to infection.

5.2.4 EIV/89, but not AIV/2009, triggers an inflammatory response

Analyses of GO terms induced at 24 hpi showed the following results: in addition to the previously suggested AIV/2009 sensitivity to cell responses, I noticed in Figure 5-3 C two GO terms (GO:0006954~inflammatory response and GO:0050729~positive regulation of inflammatory response) were significantly but contrastingly enriched at 24 hpi. The GO:0006954~inflammatory response was upregulated by EIV/89 but not by AIV/2009, and suggest that EIV/89 infection induces a more potent inflammatory response than AIV/2009. Furthermore, the absence of inflammatory response in AIV/2009-infected cells is reinforced by the downregulation of the GO term GO:0050729~positive regulation of inflammatory response observed in infected E.Derm cells. Such result suggests that in *in vitro* infections, AIV/2009 does not trigger inflammatory signals, which is in line with the absence of tissue pathology observed in *ex vivo* equine tracheal explant infection (Zhu et al. 2019).

To understand better the mechanism behind the observed signalling profiles, I decided to focus on the DEGs involved in both GO terms previously highlighted (GO:0006954 and GO:0050729). In Figure 5-3 D, I found an important upregulation of *ptger3* (PGE2-R) and *ptgs2* (COX2) genes in EIV/89-infected cells, while they were either not affected or even downregulated by AIV/2009, respectively. Both genes are involved in the prostaglandin synthesis pathway which is a well-known pro-inflammatory protein. Additionally, I found several cytokines and chemokines upregulated by EIV/89 but not by AIV/2009 infection such as *il6*, *cxcl8*, *cxcl10*, *ccl2*, *ccl5*, *ccl20*. Interestingly, I also noticed in EIV/89-infected cells the overexpression of *aim2* (coding for Absent in melanoma 2 protein; also upregulated by AIV/2009), *gsdmd* and *gbp5* (coding for Guanylate binding protein 5) genes, which are all involved in NLRP3 inflammasome assembly and pyroptosis process (an inflammatory form of lytic programmed cell death different to apoptosis or necroptosis). Additionally, the exploration of GO:0050729~positive regulation of inflammatory response GO term (Figure 5-3 D) highlighted an AIV/2009-induced downregulation of interleukin and their receptor genes (*il1rl1*, *il18*, *il17rb*, *il15*) which could explain the absence of lesions observed by Zhu et al. 2019.

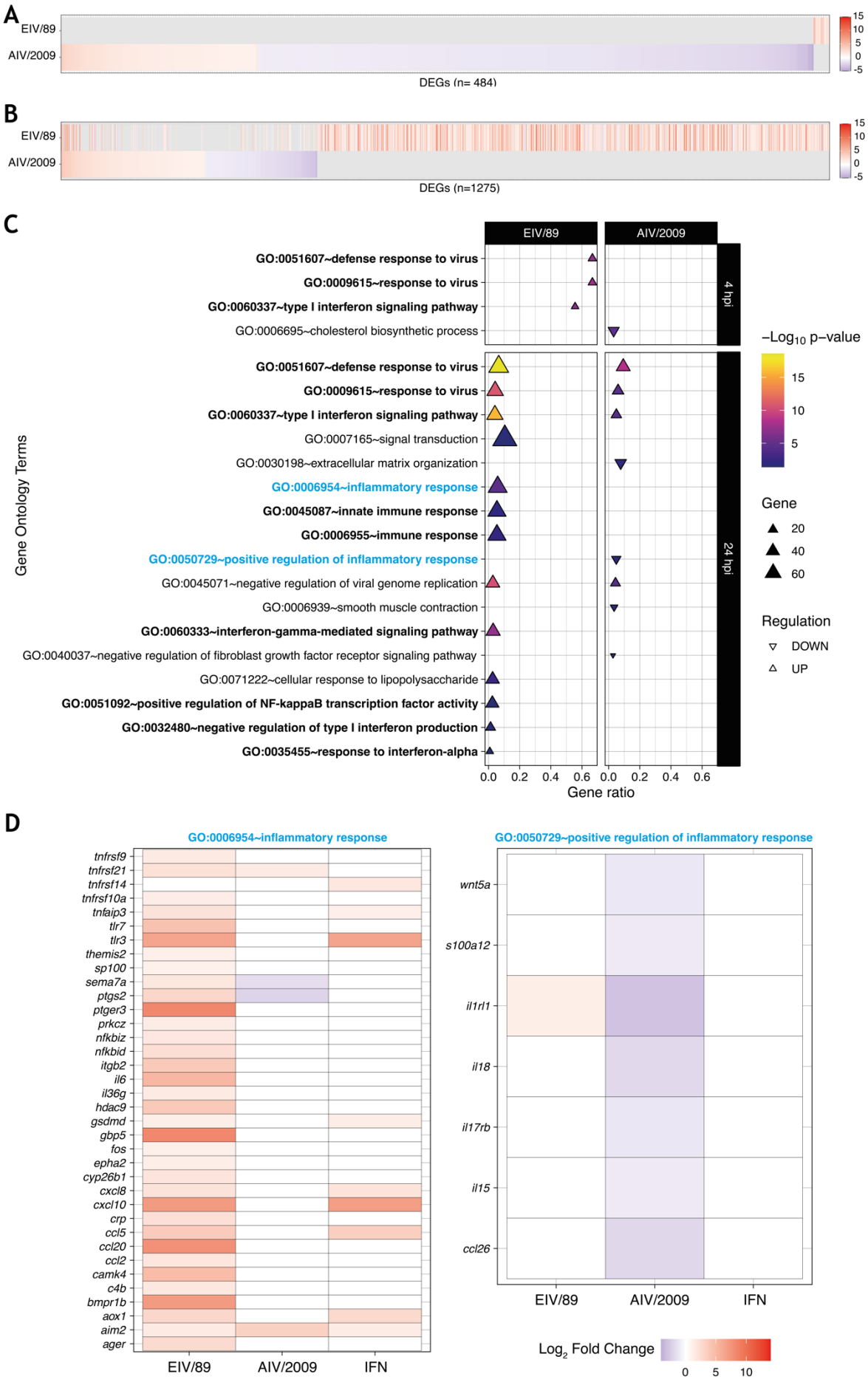
A
EIV/89
AIV/2009
DEGs (n= 484)
15
10
5
0
-5
B
EIV/89
AIV/2009
DEGs (n=1275)
15
10
5
0
-5
C
EIV/89
AIV/2009
4 hpi
24 hpi
GO:0051607~defense response to virus
GO:0009615~response to virus
GO:0060337~type I interferon signaling pathway
GO:0006695~cholesterol biosynthetic process
GO:0007165~signal transduction
GO:0030198~extracellular matrix organization
GO:0006954~inflammatory response
GO:0045087~innate immune response
GO:0006955~immune response
GO:0050729~positive regulation of inflammatory response
GO:0045071~negative regulation of viral genome replication
GO:0006939~smooth muscle contraction
GO:0060333~interferon-gamma-mediated signaling pathway
GO:0040037~negative regulation of fibroblast growth factor receptor signaling pathway
GO:0071222~cellular response to lipopolysaccharide
GO:0051092~positive regulation of NF-kappaB transcription factor activity
GO:0032480~negative regulation of type I interferon production
GO:0035455~response to interferon-alpha
Gene Ontology Terms
0.0 0.2 0.4 0.6 0.0 0.2 0.4 0.6
Gene ratio
−Log10 p−value
15
10
5
Gene
20
40
60
Regulation
DOWN
UP
D
GO:0006954~inflammatory response
tnfrsf9
tnfrsf21
tnfrsf14
tnfrsf10a
tnfaip3
tlr7
tlr3
themis2
sp100
sema7a
ptgs2
ptger3
prkcz
nfkbiz
nfkbid
itgb2
il6
il36g
hdac9
gsdmd
gbp5
fos
epha2
cyp26b1
cxcl8
cxcl10
crp
ccl5
ccl20
ccl2
camk4
c4b
bmpr1b
aox1
aim2
ager
EIV/89
AIV/2009
IFN
GO:0050729~positive regulation of inflammatory response
wnt5a
s100a12
il1rl1
il18
il17rb
il15
ccl26
EIV/89
AIV/2009
IFN
Log2 Fold Change
0
5
10

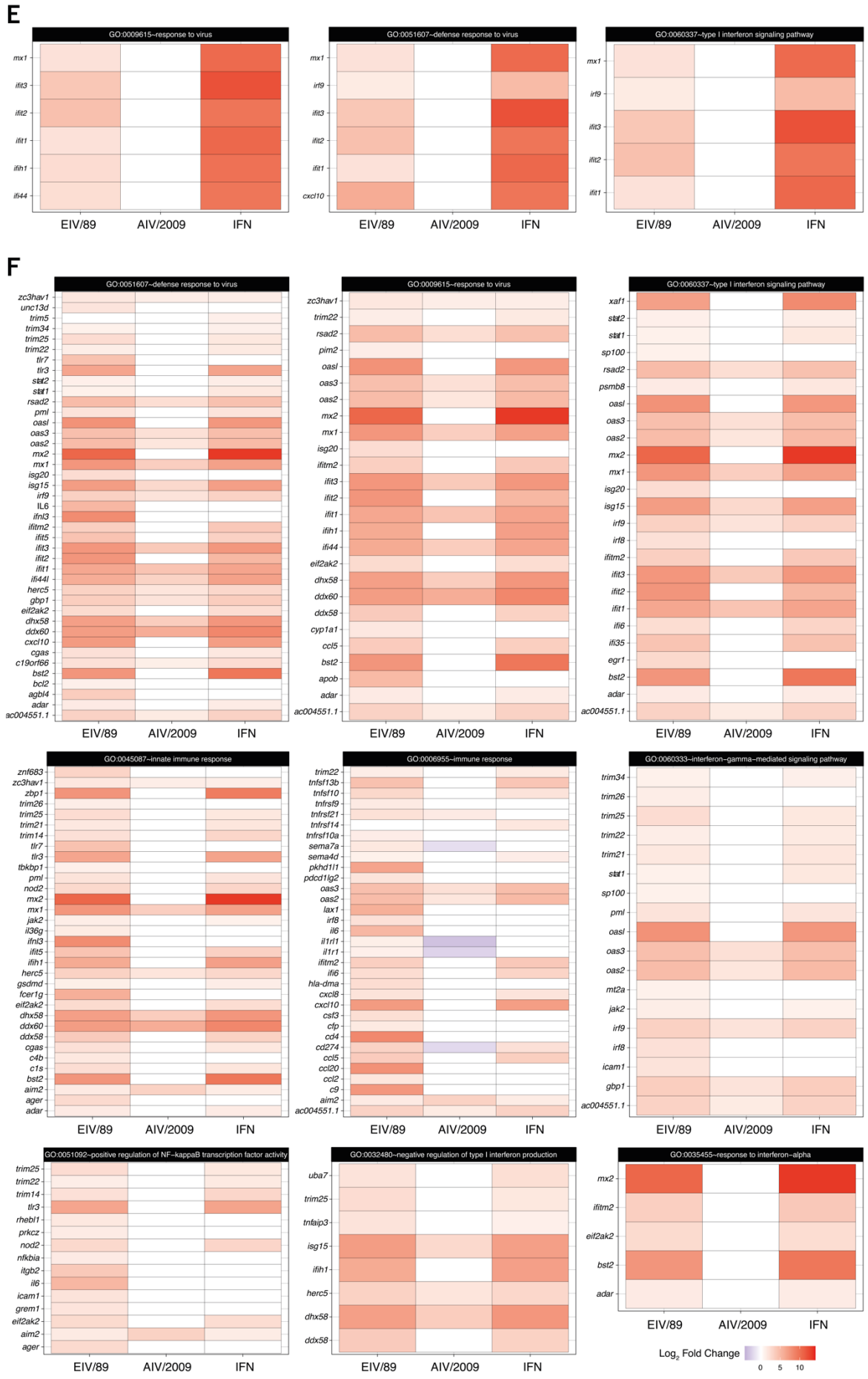
E
GO:0009615~response to virus
mx1
ifit3
ifit2
ifit1
ifih1
ifi44
EIV/89
AIV/2009
IFN
GO:0051607~defense response to virus
mx1
irf9
ifit3
ifit2
ifit1
cxcl10
EIV/89
AIV/2009
IFN
GO:0060337~type I interferon signaling pathway
mx1
irf9
ifit3
ifit2
ifit1
EIV/89
AIV/2009
IFN
F
GO:0051607~defense response to virus
zc3hav1
unc13d
trim5
trim34
trim25
trim22
tlr7
tlr3
stat2
stat1
rsad2
pml
oasl
oas3
oas2
mx2
mx1
isg20
isg15
irf9
IL6
ifnl3
ifitm2
ifit5
ifit3
ifit2
ifit1
ifi44l
herc5
gbp1
eif2ak2
dhx58
ddx60
cxcl10
cgas
c19orf66
bst2
bcl2
agbl4
adar
ac004551.1
EIV/89
AIV/2009
IFN
GO:0009615~response to virus
zc3hav1
trim22
rsad2
pim2
oasl
oas3
oas2
mx2
mx1
isg20
ifitm2
ifit3
ifit2
ifit1
ifih1
ifi44
eif2ak2
dhx58
ddx60
ddx58
cyp1a1
ccl5
bst2
apob
adar
ac004551.1
EIV/89
AIV/2009
IFN
GO:0060337~type I interferon signaling pathway
xaf1
stat2
stat1
sp100
rsad2
psmb8
oasl
oas3
oas2
mx2
mx1
isg20
isg15
irf9
irf8
ifitm2
ifit3
ifit2
ifit1
ifi6
ifi35
egr1
bst2
adar
ac004551.1
EIV/89
AIV/2009
IFN
GO:0045087~innate immune response
znf683
zc3hav1
zbp1
trim26
trim25
trim21
trim14
tlr7
tlr3
tbkbp1
pml
nod2
mx2
mx1
jak2
il36g
ifnl3
ifit5
ifih1
herc5
gsdmd
fcer1g
eif2ak2
dhx58
ddx60
ddx58
cgas
c4b
c1s
bst2
aim2
ager
adar
EIV/89
AIV/2009
IFN
GO:0006955~immune response
trim22
tnfsf13b
tnfsf10
tnfrsf9
tnfrsf21
tnfrsf14
tnfrsf10a
sema7a
sema4d
pkhd1l1
pdcd1lg2
oas3
oas2
lax1
irf8
il6
il1rl1
il1r1
ifitm2
ifi6
hla-dma
cxcl8
cxcl10
cst3
cfp
cd4
cd274
ccl5
ccl20
ccl2
c9
aim2
ac004551.1
EIV/89
AIV/2009
IFN
GO:0060333~interferon-gamma-mediated signaling pathway
trim34
trim26
trim25
trim22
trim21
stat1
sp100
pml
oasl
oas3
oas2
mt2a
jak2
irf9
irf8
icam1
gbp1
ac004551.1
EIV/89
AIV/2009
IFN
GO:0051092~positive regulation of NF-kappaB transcription factor activity
trim25
trim22
trim14
tlr3
rhebl1
prkcz
nod2
nfkbia
itgb2
il6
icam1
grem1
eif2ak2
aim2
ager
EIV/89
AIV/2009
IFN
GO:0032480~negative regulation of type I interferon production
uba7
trim25
tnfaip3
isg15
ifih1
herc5
dhx58
ddx58
EIV/89
AIV/2009
IFN
GO:0035455~response to interferon-alpha
mx2
ifitm2
eif2ak2
bst2
adar
EIV/89
AIV/2009
IFN
Log2 Fold Change
0
5
10

Figure 5-3: GO terms associated with host response to infection in EIV/89 or AIV/2009 infected cells. (A-B) Heatmap of DEGs induced by EIV/89 or AIV/2009 infections at 4 hpi **(A)**, and 24 hpi **(B)**. Gene expression is displayed in log2 FC and shown following a blue-white-red colour scale, while grey shown unaffected genes. **(C)** GO terms triggered by IAV infections. Significantly upregulated GO terms are shown as triangles, while downregulated GO terms are shown as inverted triangles. The size of each triangle represents the number of DEGs fitting each GO term, while the ratio of total genes involved in each category is displayed on the x-axis. Enrichment significance is displays according to a blue-magenta-yellow gradient ($-\log_{10}$ p-value). GO term shown in bold are associated with immune related function, while cyan GO terms were involved in inflammatory response. **(D)** Regulation intensity of DEGs involved in GO: 0006954 (left) and GO:0050729 (right). **(E-F)** Regulation intensity of DEGs involved in immune related GO terms significantly enriched at 4 hpi **(E)**, or 24 hpi **(F)**. All the heatmap shown gene expression as $\log_2$ FC following a blue-white-red colour scale, where downregulation is highlighted by blue shades, and upregulation uses red shades

5.2.5 EIV/89 triggers a strong IFN response

By focusing on DEGs involved in immune functions and their regulation at 24 hpi (Figure 5-3 F) I observed a stark contrast in gene expression profiles between viruses. Similarly to what I observed at 4 hpi, I found at 24 hpi in EIV/89-infected cells an overexpression of *mx1*, *ifit1*, *ifit2*, *ifit3* genes involved in several distinct GO terms. However, at this timepoint *mx1*, *ifit1*, and *ifit3* gene were also significantly upregulated by AIV/2009 infection, which they were not at 4 hpi. Overall, I found that the levels of immune-related gene upregulation were constantly reduced in AIV/2009-infected cells when compared to EIV/89, and in fact EIV/89 immune-related gene regulation was close to expression levels observed in IFN-induced immune-related gene. These results coupled to viral replication kinetics show that EIV/89, despite triggering an extended host immune response, can replicate to high levels, which in turn suggests that EIV/89 can tolerate a strong host response to infection, contrasting with the extreme sensitivity displayed by AIV/2009 in which a weak host response to infection (not even detectable at 4 hpi) was sufficient to abolish viral replication. However, at 24 hpi immune response induced by both infections were accentuated, although the magnitude of AIV/2009-induced response remains moderated.

However, the multitude of DEGs, and GO terms involved in the current analysis makes the data exploration difficult, therefore I decided to focus exclusively on DEGs involved in more than 3 GO terms. Figure 5-4 A shows the number of GO terms associated with each of the DEGs as well as their significance and expression levels at both timepoints. It can be observed that DEGs involved in only a few GO terms were most often associated with low

statistical significance (< 5 $-\log_{10}$ p-value) or modest expression values (< 2 $\log_2$ FC). When I applied this new filter, I observed a reduction to 28 DEGs number involved in immune-related pathways (Figure 5-4 B). Once again, I found these DEGs upregulated by EIV/89, close to IFN-induced levels, and only a handful of them were also regulated by AIV/2009. AIV/2009 upregulated genes include *mx1*, *isg15*, *ifit1*, *rsad2*, *oas2*, *oas3*, *gbp1*, *ac004551.1*, *zchav1*, *aim2*, and are all involved in host antiviral response, except for *aim2* and *ac004551.1* involved in NLRP3 inflammasome assembly and pyroptosis, and long noncoding RNA responses, respectively. Interestingly, I found 5 DEGs upregulated in EIV/89 infection but not following IFN treatment (*e.g. ccl20*, *il6*, *isg20*, *irf8*, and *ccl2*). The *ccl20*, *ccl2*, *il6* genes encodes for proteins known to be pro-inflammatory, while *irf8* is important to ISG production such as ISG20. This result suggests that the inflammatory response induced by EIV/89 is partially due to the overexpression of three genes (*ccl20*, *ccl2*, *il6*) which are not involved in the usual host antiviral response.

Finally, I normalised the virus-induced to the IFN-induced expression levels of theses DEGs (Figure 5-4 C) to identify exacerbated gene expression. In this analysis, the totality of DEGs displayed a viral-induced gene expression between 50 and 150% of the IFN-induced expression level, apart from *aim2*. This gene showed an AIV/2009-induced level of expression more than twice the IFN-induced expression. Such result, coupled with the decrease of infected cells observed previously (Figure 5-2 A) suggests that death of infected cells might be at least partially attributed to pyroptosis.

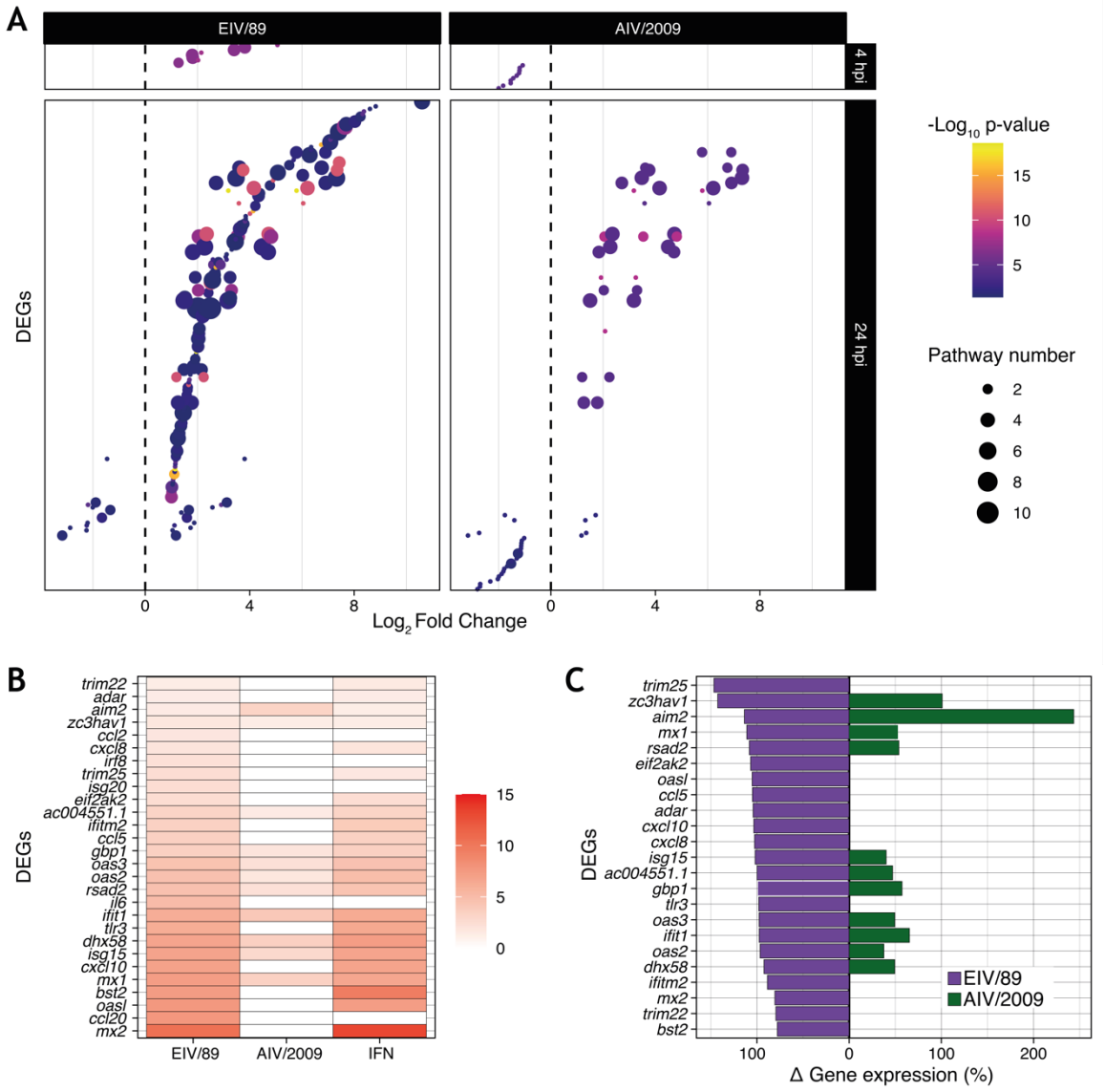

Figure 5-4: Principal genes involved GO terms and their regulation intensities. (A) Scatterplot displaying the number of GO terms associated with each DEGs at 4 and 24 hpi. Regulation intensities are shown as log_2 FC on the x-axis, while point size displayed number of GO terms in which DEG significance was displayed according to a blue-magenta-yellow gradient ($-log_{10}$ p-value). **(B)** DEGs expressions are displayed in log_2 FC following a white-red colour scale. **(C)** Viral-induced DEGs expression normalised to IFN-induced expression showed as percentage of IFN induction. Purple and green colours were used to highlight EIV/89 and AIV/2009 gene expression, respectively.

5.3 Discussion

In this chapter, I investigated the virus-induced changes of two closely-related H3N8 influenza viruses for which there is evidence of equine infection. Moreover, it has been shown that Mongolian horses are frequently exposed to circulating AIVs, and these viruses can infect the equine respiratory tract *ex vivo* (Zhu et al. 2019). However, it is unknown

whether AIV-infected animals shed viruses and if they do, for how long. Such parameters are crucial for infection outcomes, spanning from isolated infections without onward transmission to efficient, onward-transmitting infections, which could under certain circumstances (generally summarised under the term viral fitness) lead to the establishment of new lineages. To assess and measure the viral replicative fitness (a key component of viral fitness), I determined the replication kinetics, cell-to-cell spread, and gene regulation of two IAVs: i) the EIV that caused the 1989 Chinese EI outbreak (EIV/89), and ii) a phylogenetically-related avian virus isolated in Mongolia in 2009 (AIV/2009).

Results presented in this chapter show that both viruses infected and replicated in two mammalian cell lines (MDCK and E.Derm). The apparent reduction of AIV/2009 replication observed in MDCK at 24 hpi, associated with the faster viral cycle completion (highlighted by the detection of only AIV/2009 infectious particles in supernatant of infected-MDCK at 8 hpi) suggests that EIV/89 produced an increased number of virions per replication cycle than AIV/2009. If true, this feature will result in an enhanced viral spread, an infection phenotype observed in infected MDCK monolayers and might constitute a replicative fitness advantage for EIV/89 within a mammalian cell context. However, such statement will require further characterisations such as reverse-transcription qPCR to monitor the dynamics of viral genome production. Additionally, I found a lack of sustainable AIV/2009 viral replication in E.Derm cells, known to be IFN-competent (in contrast to MDCK cells, which do not possess an anti-influenza activity due to inefficient Mx protein (Seitz et al. 2010)), which highlights a potential exacerbation of virus sensitivity to the immune response to infection. Pre-treating cells with a Jak-STAT inhibitor such as ruxotilinib should enhance AIV/2009 replication in these cells and confirm this initial result, while poly(I:C) or uIFN pre-treatment should completely prevent AIV/2009 replication.

Altogether, results from this chapter show evidence that AIV/2009 triggered a different response to infection compared to EIV/89, which generates more viral progeny, but at a reduced pace, and exhibits a reduced IFN sensitivity. These results highlight the different mechanisms viruses acquired to complete their replication cycle and maximise their overall fitness. Biological parameters like the ones described in this chapter should be considered when mathematical models of viral fitness are generated. Yan et al. (2020), for example, highlighted the importance of such viral parameters in influencing potential immune evasion.

Additionally, I investigated the ability of the viruses to trigger an inflammatory response and found that mainly type I (IFN-α and IFN-β) and type II (IFN-γ) IFN responses were exacerbated by EIV/89 but not AIV/2009 at 24 hpi. This result appears to be in line with the report of Guo et al. (1992), in which the authors estimated an unusually high mortality in infected animals, reaching up to 20%, during the EIV/89 outbreak in China. This result is also in line with results from the previous chapter in which I showed that "early" circulating viruses (such as EIV/63) are associated with more potent pathological changes than "adapted" virus (EIV/2003) most likely the consequence of an enhanced inflammatory response. Furthermore, I suggested that the exaggerated EIV/89-induced inflammation is partially due to the upregulation of non-ISGs (including *ccl20*, *ccl2*, *il6*) known to encode pro-inflammatory proteins.

Further experiments are required to validate these results, including transient overexpression and/or gene knockout experiments targeting, for example, the three potential gene candidates mentioned above. Additionally, genomic segments associated with equine cellular fitness could be identified by generating reassortant viruses using reverse genetics system.

Chapter 6: *in vitro* characterisation of A/equine/Lexington/66 (H7N7)

6.1 Introduction

In the previous chapters I focused on avian-origin H3N8 IAVs. However, as described in the introduction (see section 1.3.1.1), the first EIV to be discovered was of the H7N7 subtype. The virus was first isolated in 1956, seven years earlier than H3N8 EIV lineage (Sovinova et al. 1958) and spread to multiple countries, including Czechoslovakia, Kyrgyzstan and USA. However, H7N7 EIV circulation suddenly decreased, and is now considered extinct (Sovinova et al. 1958; Sherman et al. 1977; Karamendin et al. 2016). The reasons for the extinction of H7N7 EIV are unknown.

Understanding mechanisms that underpin EIV circulation in susceptible host populations is important to control endemic equine influenza viruses, as well as the emergence of novel strains. Virus transmission dynamics relies on multiple factors, including ecological factors such as population structure, density of susceptible hosts, population spatial distribution, and contact rates. In addition, it also depends on intrinsic factors that are usually defined as virus-host interactions. Taken all together, these parameters are likely to determine the outcome of viral interspecies transmission as well as the long-term virus circulation in a new host.
The aim of this chapter is to characterise the *in vitro* phenotype of an H7N7 EIV. To this end, I designed and established a reverse genetics system to generate A/equine/Lexington/1/1966 H7N7 (EIV/66) infectious viral particles.
My hypothesis was that EIV/66 virus would exhibit clear differences in infection phenotype (*i.e.* viral replication kinetics, cell-to-cell spread, host response to infection) when compared to H3N8 EIVs. These differences might inform us on the potential reasons leading to H7N7 viral extinction and its replacement by H3N8 EIV. To test my hypothesis, I performed a series of experimental infections in mammalian cell lines (MDCKs and E.Derm cells) and combined classical virology techniques with transcriptomic analyses to determine H7N7 overall fitness. Finally, I compared the results obtained in this chapter to the ones obtained with H3N8 EIVs.

6.2 Results

6.2.1 EIV/66 replicates at slower pace than H3N8 EIVs

The first challenge working with H7N7 EIV is the scarcity of H7N7 virus isolates. While in the laboratory I have access to A/equine/Prague/56 (EIV/56, kindly provided by John McCauley), but it is known that EIV/56 has been extensively passaged in eggs and cells and thus it is unlikely to represent a *bona fide* equine-adapted virus. Therefore, my first task was to establish a reverse genetics system to rescue a representative H7N7 EIV. To this end, I adapted the protocols the group had in place to generate H3N8 EIVs (Figure 6-1 A). Briefly, the DNA expression plasmid is made by the cytomegalovirus (CMV) promoter, the antisense murine polymerase terminator, and the *BsmBI* restriction enzyme recognition sequence ($\begin{matrix} 5' - \cdots \mathrm{CGTCTC(N)_1}^{\downarrow} \ldots - 3' \\ 3' - \cdots GCAGAG(N)_{5}{}^{\uparrow} \ldots - 5' \end{matrix}$) upstream of 5′-UTR and CDS sequences. Similarly, downstream of CDS and 3′-UTR sequences are found another *BsmBI* restriction site, the antisense human polymerase promoter, and the Bgh PA (bovine growth hormone polyadenylation) terminal sequences. The CMV promoter and the Bgh PA terminal sequence are responsible for the expression of the positive stranded mRNA, which in turn is used as a template for viral protein translation, while the antisense strand associated with the human polymerase promoter and the murine polymerase terminator sequence generate the negative vRNA and is used as a template for viral cDNA formation. Newly generated cDNA is encapsidated into progeny viral particles. In addition, the *BsmBI* restriction sites were used to clone the viral sequence into the DNA expression plasmid (pDP-2002) containing an ampicillin resistance gene used for bacterial selection during plasmid stock generation. Finally, the UTR sequences are critical for viral polymerase recognition and for the transcription of the viral RNA and the translation of mRNA.

Therefore, I started by gathering sequence data of H7N7 EIVs from the public influenza research database (Bao et al. 2008) and found that only nine H7N7 isolates have been completely sequenced (summarised in Table 6-1).

Table 6-1: List of fully sequenced H7N7 EIVs publicly available

Virus	NCBI Taxonomy ID
A/equine/Prague/1956	387228
A/equine/Prague/1/1956	380337
A/equine/Prague/2/1956	506420
A/equine/Detroit/3/1964	387216
A/equine/Lexington/1/1966	475494
A/equine/Kentucky/1a/1975	475495
A/equine/Uruguay/1063/1976	500688
A/equine/Sao Paulo/4/1976	500687
A/equine/Argentine/1/1977	500685

Importantly, some of those H7N7 EIVs possessed genomic segments derived from H3N8 EIV that had been obtained by reassortment (Ito et al. 1999). As I wanted to characterise a virus with the entire genome constellation of the H7N7 EIV lineage, I selected and adapted the RG system to A/equine/Lexington/1/1966 (EIV/66), an H7N7 EIV that was not associated with H3N8 reassortment events. The accession number of the eight genomic sequences used are available in Table 0-2. Unfortunately, the genome available did not contain full length UTR sequences and I had to reconstruct them. As described in Figure 6-1 A, I performed multiple sequence alignments for each of the 8 segments and used the consensus sequences to predict the most likely EIV/66 UTR sequences. For some nucleotides, the consensus sequence was ambiguous, and an informed choice was made based on the nucleotides displayed by the closest viral sequence to EIV/66 (based on phylogenetic trees inferred by Neighbor-Joining). Once the sequences were designed *in silico*, plasmids were ordered (Genewiz) and used in transfections to rescue infectious virus as described in 3.5.2. After virus rescue, I noticed that virus-induced CPE, which usually took 48 hours to appear in H3N8 EIVs infection, seemed to be delayed in EIV/66 infection (Figure 6-1 B) and were not apparent before 84 hpi. However, the virus collected from supernatant of infected MDCK at 84 hpi did not show difference in titres when compared to the H3N8 EIVs titres obtained.

To characterised further EIV/66, I performed plaque assay experiments, and found surprisingly that the virus did not form plaques in these specific experimental conditions (Figure 6-1 C). This result contrasted with the result obtained with H3N8 viruses, however,

it is in line with the observation made during the viral stock generation as I did not observe obvious cell death compared to control cells at 48 hpi. The lack of plaque formation could be attributed to a decreased viral replication, or a delayed viral-induced cell death. Based on these results, I quantified viral titres using $TCID_{50}$ in all subsequent experiments.

To investigate the potential reduced viral replication of EIV/66, I performed experimental infections in both MDCK and E.Derm cells and determined the virus replication kinetics. As observed in Figure 6-1 D, EIV/66 can infect and replicate in MDCK cells and reached a peak titre of 10^6 $TCID_{50}$/mL at 72 hpi. E.Derm cells are also susceptible to EIV/66 infection, and Figure 6-1 E shows that the virus exhibits a maximum titre of 5.10^3 $TCID_{50}$/mL from 48 hpi and up to the end of the experiment (96 hpi).

Taken together, these results indicate that the EIV/66 RG system is functional as it allowed the generation of EIV/66 infectious virus. Additionally, EIV/66 replicates efficiently in both MDCK and E.Derm cells and does induce delayed CPE.

To understand better the host response to EIV/66 infection, I performed experimental infections and transcriptomics analyses in E.Derm cells with the aim of comparing the host response to EIV/66 infection to that observed using H3N8 IAVs and discussed in previous chapters.

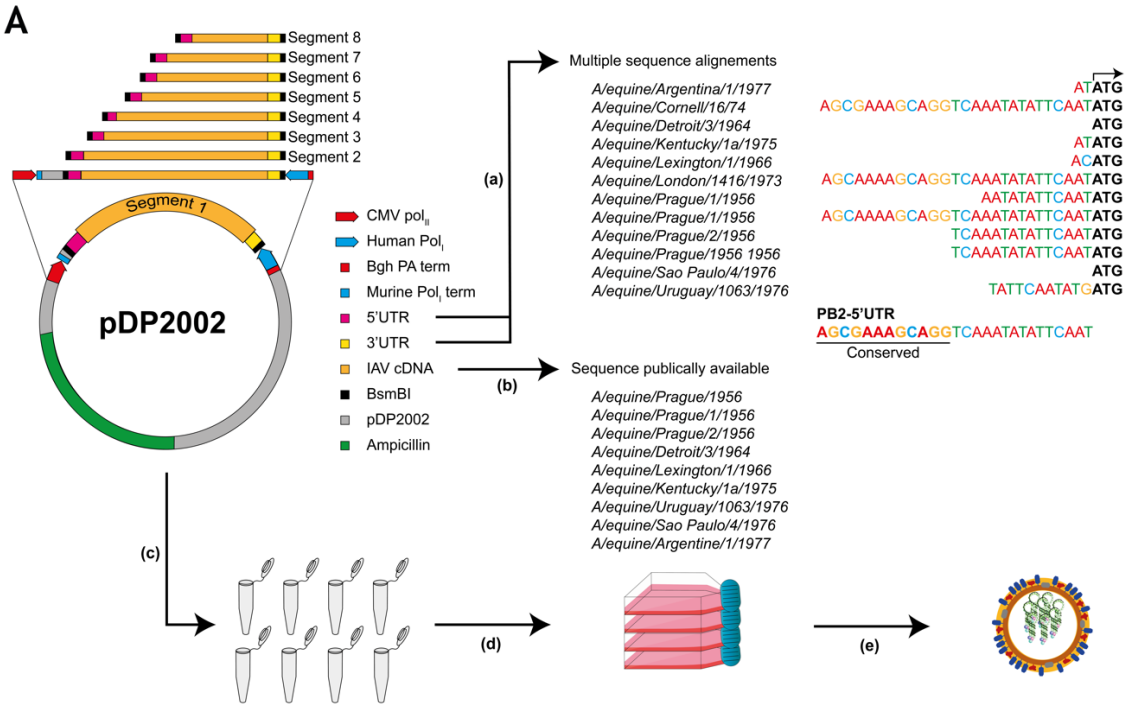
A
Segment 8
Segment 7
Segment 6
Segment 5
Segment 4
Segment 3
Segment 2
Segment 1
pDP2002
CMV pol II
Human Pol I
Bgh PA term
Murine Pol I term
5'UTR
3'UTR
IAV cDNA
BsmBI
pDP2002
Ampicillin
(a)
(b)
(c)
(d)
(e)
Multiple sequence alignements
A/equine/Argentina/1/1977
A/equine/Cornell/16/74
A/equine/Detroit/3/1964
A/equine/Kentucky/1a/1975
A/equine/Lexington/1/1966
A/equine/London/1416/1973
A/equine/Prague/1/1956
A/equine/Prague/1/1956
A/equine/Prague/2/1956
A/equine/Prague/1956 1956
A/equine/Sao Paulo/4/1976
A/equine/Uruguay/1063/1976
Sequence publically available
A/equine/Prague/1956
A/equine/Prague/1/1956
A/equine/Prague/2/1956
A/equine/Detroit/3/1964
A/equine/Lexington/1/1966
A/equine/Kentucky/1a/1975
A/equine/Uruguay/1063/1976
A/equine/Sao Paulo/4/1976
A/equine/Argentina/1/1977
PB2-5'UTR
AGCGAAAGCAGGTCAAATATATTCAAT
Conserved

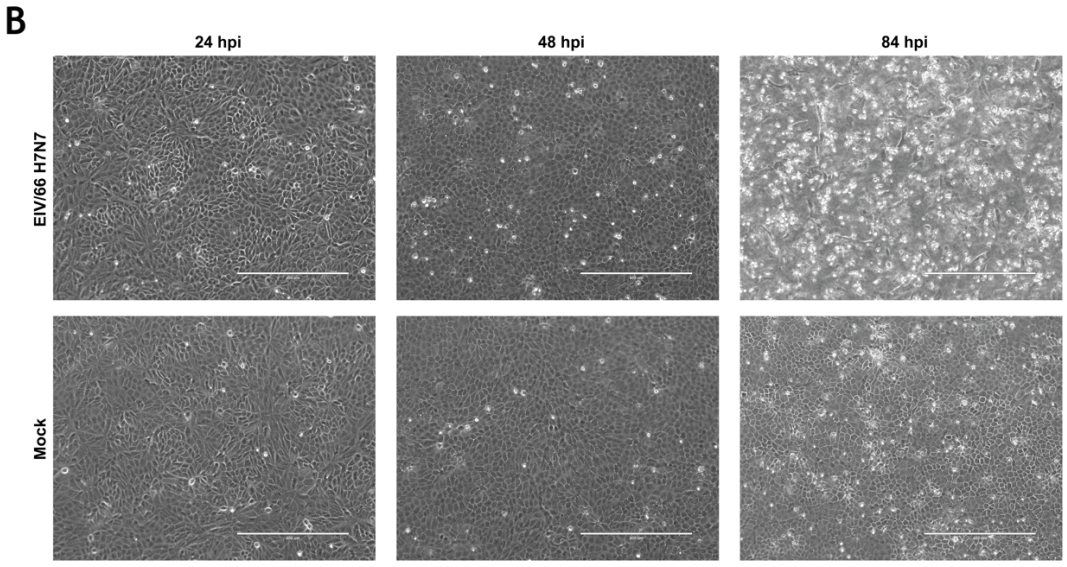
B
24 hpi
48 hpi
84 hpi
EIV/66 H7N7
Mock

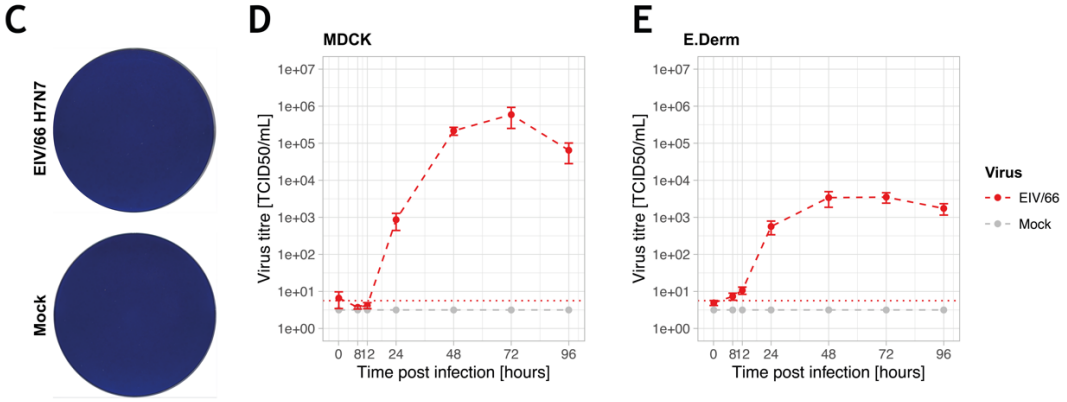
C
EIV/66 H7N7
Mock
D
MDCK
Virus titre [TCID50/mL]
Time post infection [hours]
E
E.Derm
Virus titre [TCID50/mL]
Time post infection [hours]
Virus
EIV/66
Mock

Figure 6-1: Generation and characterisation of H7N7 EIV/66 infectious viral particles. (A) Schematic representation of steps involved in the design of H7N7 EIV reverse genetics plasmid set, from *in silico* to plasmid sequences. Step (a) represents the elaboration of 5' and 3' UTRs from the sequences available. Step (b) indicates the list of all fully sequenced H7N7 EIV available. Step (c) depicts the plasmid generation (by Genewiz). Step (d) depicts the plasmid transfection of EIV/66 plasmids, while step (e) represents the harvest of released viral particles in culture supernatant. **(B)** Microphotographs of EIV/66 or mock-infected MDCK cells used during virus stock generation. The time post infection in hours (hpi) is mentioned above each time points, and scale represents 400 µm. **(C)** Photographs of EIV/66 or mock-infected MDCK monolayers obtained following a 48 hour incubation in a semisolid overlay media. **(D)** Growth kinetics of EIV/66 in MDCK cells. **(E)** Growth kinetics of EIV/66 in E.Derm cells. Red colour represents EIV/66, while non-infected controls are shown in grey. Viral titres are represented as the mean ± SEM. Infections were performed at least three times independently and each independent experiment consisted of three technical repeats.

6.2.2 EIV/66 induces significant changes of host gene expression

To explore the EIV/66 infection phenotype in E.Derm cells in more detail, I used a transcriptomics approach. First, I determined E.Derm infection levels as mentioned in section 3.6.1. Figure 6-2 A, shows that EIV/66-infected cells did not reach the target infection level (50%) as only ~4% of cells were infected at 4 hpi. However, at 24 hpi EIV/66-infected cells reached 65%. As detection of infected cells relies on NP immunostaining, this result suggests that the level of NP expression in infected cells is not sufficient for flow cytometry detection within the first 4 hpi.

To assess better the potential lack or delay of NP production, I quantified the number of sequencing reads mapping to EIV/66 genome as a proxy of viral infection and compared it to data obtained in previous experiments using EIV/63 (where 48% of cells were infected at 4 hpi). Figure 6-2 B shows that both EIV/63 and EIV/66 exhibited a similar normalised number of reads mapped to viral genome (~10^4—10^5) at 4 and 24 hpi (~10^5—10^6). These levels of reads mapped to viral genomes contrasted well with control infections were such levels never reached more than 10^1. This result suggests that the observed lack of infected cells in flow cytometry as highlighted in Figure 6-2 A is mainly a consequence of a delay in NP translation, as I found similar levels of viral mRNA in cells infected with either EIV/63 or EIV/66 at both time points. After this initial analysis, I performed transcriptomics analyses of cellular genes in cells infected with EIV/66 at 4 and 24 hpi as well as in mock-infected controls. I identified (Figure 6-2 C) 2,836 and 4,890 DEGs in EIV/66-infected E.Derm at 4

and 24 hpi, respectively, which corresponds to a 72.43% increase of DEGs number over time. I also found that from these DEGs, 48.38% and 78.53% were upregulated at 4 and 24 hpi, respectively (Figure 6-2 D). However, I also noticed a change in gene expression from an overall downregulation of approximatively 1.25 log_2 FC at 4 hpi, to an overall upregulation of nearly 3.75 log_2 FC at 24 hpi.

Overall, the transcriptomic analyses (Figure 6-2 E) showed that 79.27% of the variance observed in EIV/66-infected E.Derm cells was explained by PC1, and 14.27% of the remaining variance was explained by PC2. Such numbers indicate that EIV/66-infected cells seem to exhibit a different gene expression profile compared to the transcriptome of mock-infected cells. Additionally, in Figure 6-2 E, I highlighted a small distance separating EIV/66-infected cells at 4 and 24 hpi, which might suggest a minimal change in response to infection over time. However, after careful analysis of the 4 and 24 hpi controls, which did not show clear overlap, I was able to determine that the distance between EIV/66-infected cells and their respective controls did increase over time (Figure 6-2 E inserts). This observation was reinforced by Figure 6-2 F, which shows that only 9.93% (160/1611) of the DEGs are associated with a change in regulation direction over time (*e.g.* from upregulated to downregulated or vice versa), while the remaining DEGs were either new or more intensely dysregulated.

Taken all together, these data indicate that EIV/66 infection causes dynamic changes in gene regulation that tend to diverge over time. and are mainly the consequence of an exacerbated host response induced by either an increased number of dysregulated genes and/or an increased regulation intensity

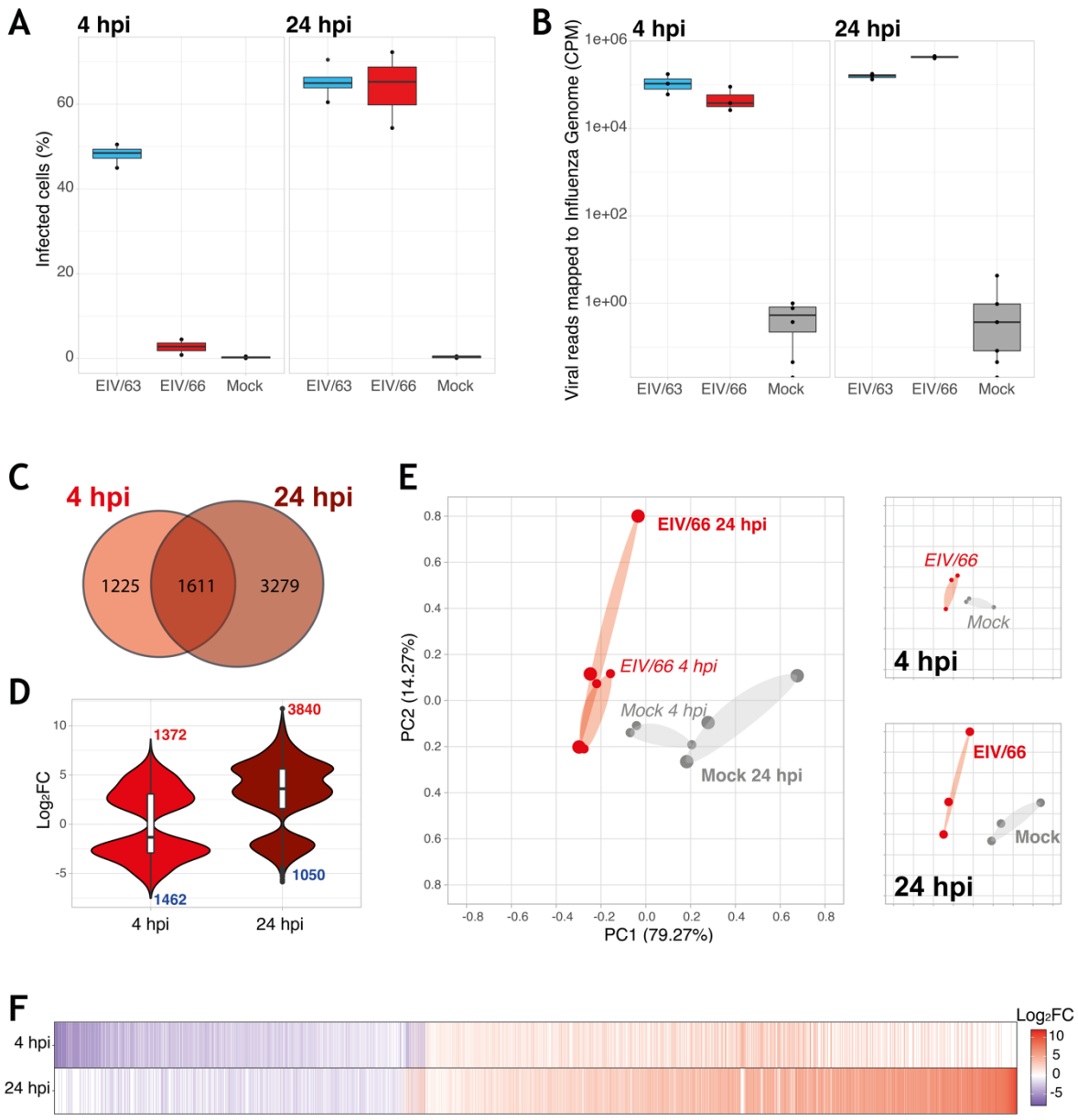

Figure 6-2: *In vitro* characterisation of the host response to EIV/66 infection. (A) Percentage of EIV/63, EIV/66, and mock-infected cells obtained from flow cytometry analysis of E.Derm cells immunostained with anti-NP. Mock is represented in grey, while EIV/63 and EIV/66 are displayed in cyan and red, respectively. **(B)** Viral segments (8) were concatenated, and sequencing reads mapped to them (*i.e.* EIV/63, EIV/66). Mapped viral read numbers were normalised to the total number of reads in each sample and expressed as counts per million (CPM). Mock is represented in grey, while EIV/63 and EIV/66 are displayed in cyan and red, respectively. **(C)** DEGs distribution between EIV/66-infected cells at 4 hpi (red) and 24 hpi (dark red). The number of DEGs for each subset is shown within each compartment of the Venn diagram. **(D)** Violin plots of DEGs identified in E.Derm-infected cells at 4 hpi (red), and 24 hpi (dark red). The number of upregulated and downregulated genes in each condition was shown in red and blue, respectively. **(E)** Principal component analysis of EIV/66 infectomes in which mock treatment was displayed in grey, while 4 hpi

and 24 hpi timepoints were displayed in red and dark red, respectively. Additionally, different point size was used to distinguish transcriptomes obtained at 4 hpi and 24 hpi, and points were labelled for clarity. Additional inserts distinguishing 4 to 24 hpi are shown underneath to facilitate reading. These inserts represent the same data as the main scatterplot. **(F)** Heatmap of DEGs induced by EIV/66 at 4 hpi and 24 hpi. Gene expression is displayed in log_2 FC and shown following a blue-white-red colour scale. Data presented here represent three independent experiments.

6.2.3 EIV/66 induces significant transcriptomic changes in pathways associated with mRNA processing

To identify potential canonical pathways affected by EIV/66 infection, I used gene expression changes to carry out a GO enrichment analysis at 4 and 24 hpi. The analyses (Figure 6-3) showed that the 2,836, and 4,890 DEGs found at 4 and 24 hpi, respectively, are responsible for dysregulating 140 and 11 GO terms, of which I noticed only 2 (1.43%) and 3 (27.27%) were upregulated by EIV/66 infection at 4 and 24 hpi, respectively. These five GO terms were GO:0030196~extracellular matrix organization and GO:0030199~collagen fibril organization (at both time points), as well as GO:0002576~platelet degranulation at 24 hpi only. Additionally, I noticed that the most significantly dysregulated GO terms ($-log_{10}$ p-value > 20) at 4 hpi were in majority (6/8; 75%) in relation with mRNA processing (GO:0000398~mRNA splicing, via spliceosome, GO:0006412~translation, GO:0006364~rRNA processing, GO:0006413~translational initiation, GO:0000184~nuclear-transcribed mRNA catabolic process, nonsense-mediated decay, and GO0002181~cytoplasmic translation). However, this effect on mRNA processing appears to decrease over time as at 24 hpi only 45.45% (5/11) of found GO terms were closely related to protein production and maturation.

This result, together with the delay of NP production observed in Figure 6-2 A, might suggest that EIV/66 triggers a non-specific host protein synthesis shutdown, negatively impacting the viral gene expression, but also cellular processes. However, the current results are not sufficient to conclude if the observed phenotype in E.Derm cells is a cause or a consequence of EIV/66 infection.

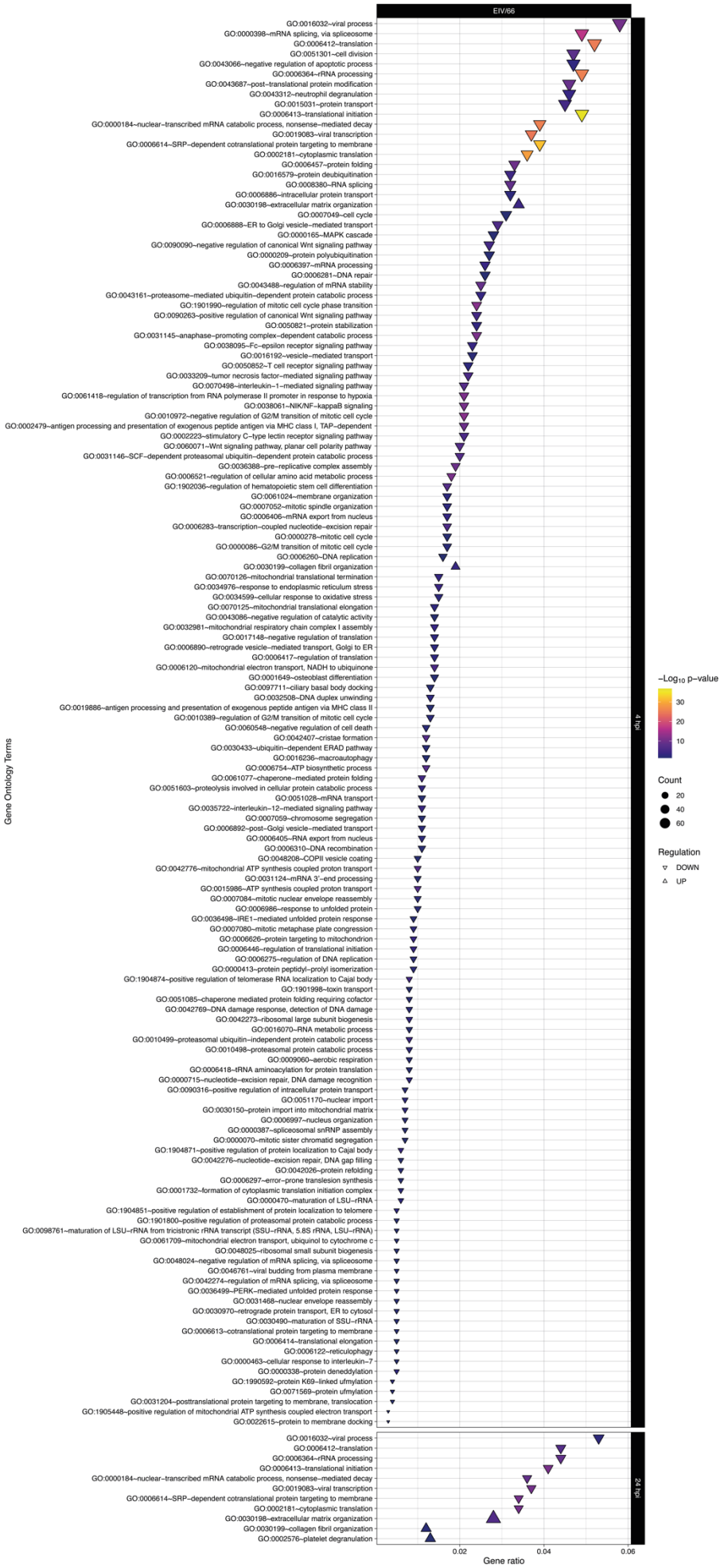
EIV/66
GO:0016032~viral process
GO:0000398~mRNA splicing, via spliceosome
GO:0006412~translation
GO:0051301~cell division
GO:0043066~negative regulation of apoptotic process
GO:0006364~rRNA processing
GO:0043687~post~translational protein modification
GO:0043312~neutrophil degranulation
GO:0015031~protein transport
GO:0006413~translational initiation
GO:0000184~nuclear~transcribed mRNA catabolic process, nonsense~mediated decay
GO:0019083~viral transcription
GO:0006614~SRP~dependent cotranslational protein targeting to membrane
GO:0002181~cytoplasmic translation
GO:0006457~protein folding
GO:0016579~protein deubiquitination
GO:0008380~RNA splicing
GO:0006886~intracellular protein transport
GO:0030198~extracellular matrix organization
GO:0007049~cell cycle
GO:0006888~ER to Golgi vesicle~mediated transport
GO:0000165~MAPK cascade
GO:0090090~negative regulation of canonical Wnt signaling pathway
GO:0000209~protein polyubiquitination
GO:0006397~mRNA processing
GO:0006281~DNA repair
GO:0043488~regulation of mRNA stability
GO:0043161~proteasome~mediated ubiquitin~dependent protein catabolic process
GO:1901990~regulation of mitotic cell cycle phase transition
GO:0090263~positive regulation of canonical Wnt signaling pathway
GO:0050821~protein stabilization
GO:0031145~anaphase~promoting complex~dependent catabolic process
GO:0038095~Fc~epsilon receptor signaling pathway
GO:0016192~vesicle~mediated transport
GO:0050852~T cell receptor signaling pathway
GO:0033209~tumor necrosis factor~mediated signaling pathway
GO:0070498~interleukin~1~mediated signaling pathway
GO:0061418~regulation of transcription from RNA polymerase II promoter in response to hypoxia
GO:0038061~NIK/NF~kappaB signaling
GO:0010972~negative regulation of G2/M transition of mitotic cell cycle
GO:0002479~antigen processing and presentation of exogenous peptide antigen via MHC class I, TAP~dependent
GO:0002223~stimulatory C~type lectin receptor signaling pathway
GO:0060071~Wnt signaling pathway, planar cell polarity pathway
GO:0031146~SCF~dependent proteasomal ubiquitin~dependent protein catabolic process
GO:0036388~pre~replicative complex assembly
GO:0006521~regulation of cellular amino acid metabolic process
GO:1902036~regulation of hematopoietic stem cell differentiation
GO:0061024~membrane organization
GO:0007052~mitotic spindle organization
GO:0006406~mRNA export from nucleus
GO:0006283~transcription~coupled nucleotide~excision repair
GO:0000278~mitotic cell cycle
GO:0000086~G2/M transition of mitotic cell cycle
GO:0006260~DNA replication
GO:0030199~collagen fibril organization
GO:0070126~mitochondrial translational termination
GO:0034976~response to endoplasmic reticulum stress
GO:0034599~cellular response to oxidative stress
GO:0070125~mitochondrial translational elongation
GO:0043086~negative regulation of catalytic activity
GO:0032981~mitochondrial respiratory chain complex I assembly
GO:0017148~negative regulation of translation
GO:0006890~retrograde vesicle~mediated transport, Golgi to ER
GO:0006417~regulation of translation
GO:0006120~mitochondrial electron transport, NADH to ubiquinone
GO:0001649~osteoblast differentiation
GO:0097711~ciliary basal body docking
GO:0032508~DNA duplex unwinding
GO:0019886~antigen processing and presentation of exogenous peptide antigen via MHC class II
GO:0010389~regulation of G2/M transition of mitotic cell cycle
GO:0060548~negative regulation of cell death
GO:0042407~cristae formation
GO:0030433~ubiquitin~dependent ERAD pathway
GO:0016236~macroautophagy
GO:0006754~ATP biosynthetic process
GO:0061077~chaperone~mediated protein folding
GO:0051603~proteolysis involved in cellular protein catabolic process
GO:0051028~mRNA transport
GO:0035722~interleukin~12~mediated signaling pathway
GO:0007059~chromosome segregation
GO:0006892~post~Golgi vesicle~mediated transport
GO:0006405~RNA export from nucleus
GO:0006310~DNA recombination
GO:0048208~COPII vesicle coating
GO:0042776~mitochondrial ATP synthesis coupled proton transport
GO:0031124~mRNA 3'~end processing
GO:0015986~ATP synthesis coupled proton transport
GO:0007084~mitotic nuclear envelope reassembly
GO:0006986~response to unfolded protein
GO:0036498~IRE1~mediated unfolded protein response
GO:0007080~mitotic metaphase plate congression
GO:0006626~protein targeting to mitochondrion
GO:0006446~regulation of translational initiation
GO:0006275~regulation of DNA replication
GO:0000413~protein peptidyl~prolyl isomerization
GO:1904874~positive regulation of telomerase RNA localization to Cajal body
GO:1901998~toxin transport
GO:0051085~chaperone mediated protein folding requiring cofactor
GO:0042769~DNA damage response, detection of DNA damage
GO:0042273~ribosomal large subunit biogenesis
GO:0016070~RNA metabolic process
GO:0010499~proteasomal ubiquitin~independent protein catabolic process
GO:0010498~proteasomal protein catabolic process
GO:0009060~aerobic respiration
GO:0006418~tRNA aminoacylation for protein translation
GO:0000715~nucleotide~excision repair, DNA damage recognition
GO:0090316~positive regulation of intracellular protein transport
GO:0051170~nuclear import
GO:0030150~protein import into mitochondrial matrix
GO:0006997~nucleus organization
GO:0000387~spliceosomal snRNP assembly
GO:0000070~mitotic sister chromatid segregation
GO:1904871~positive regulation of protein localization to Cajal body
GO:0042276~nucleotide~excision repair, DNA gap filling
GO:0042026~protein refolding
GO:0006297~error~prone translesion synthesis
GO:0001732~formation of cytoplasmic translation initiation complex
GO:0000470~maturation of LSU~rRNA
GO:1904851~positive regulation of establishment of protein localization to telomere
GO:1901800~positive regulation of proteasomal protein catabolic process
GO:0098761~maturation of LSU~rRNA from tricistronic rRNA transcript (SSU~rRNA, 5.8S rRNA, LSU~rRNA)
GO:0061709~mitochondrial electron transport, ubiquinol to cytochrome c
GO:0048025~ribosomal small subunit biogenesis
GO:0048024~negative regulation of mRNA splicing, via spliceosome
GO:0046761~viral budding from plasma membrane
GO:0042274~regulation of mRNA splicing, via spliceosome
GO:0036499~PERK~mediated unfolded protein response
GO:0031468~nuclear envelope reassembly
GO:0030970~retrograde protein transport, ER to cytosol
GO:0030490~maturation of SSU~rRNA
GO:0006613~cotranslational protein targeting to membrane
GO:0006414~translational elongation
GO:0006122~reticulophagy
GO:0000463~cellular response to interleukin~7
GO:0000338~protein deneddylation
GO:1990592~protein K69~linked ufmylation
GO:0071569~protein ufmylation
GO:0031204~posttranslational protein targeting to membrane, translocation
GO:1905448~positive regulation of mitochondrial ATP synthesis coupled electron transport
GO:0022615~protein to membrane docking
4 hpi
GO:0016032~viral process
GO:0006412~translation
GO:0006364~rRNA processing
GO:0006413~translational initiation
GO:0000184~nuclear~transcribed mRNA catabolic process, nonsense~mediated decay
GO:0019083~viral transcription
GO:0006614~SRP~dependent cotranslational protein targeting to membrane
GO:0002181~cytoplasmic translation
GO:0030198~extracellular matrix organization
GO:0030199~collagen fibril organization
GO:0002576~platelet degranulation
24 hpi
0.02
0.04
0.06
Gene ratio
Gene Ontology Terms
−Log10 p−value
30
20
10
Count
20
40
60
Regulation
DOWN
UP

Figure 6-3: Gene ontology (GO) terms associated with host response to infection in EIV/66-infected cells. GO terms triggered by IAV infections. Significantly upregulated GO terms are shown as triangles, while downregulated GO terms are shown as inverted triangles. The size of each triangle represents the number of DEGs fitting each GO term, while the ratio of total genes involved in each category is displayed on the x-axis. Enrichment significance is displays according to a blue-magenta-yellow gradient ($-\log_{10}$ p-value).

6.3 Discussion

In this chapter, I designed and established a reverse genetics system to investigate the infection phenotype of EIV/66, an H7N7 equine influenza virus. H7N7 EIV was first isolated in 1956 in Prague (Sovinova et al. 1958) and circulated over wide geographical regions as illustrated by the H7N7 EIV sequences from Europe and Americas available between 1956 and 1977 in influenza research database. The absence of H7N7 detection and isolation in equine populations since 1977 suggests that this virus might have became extinct. Very little is known about the causes underpinning H7N7 disappearance, although it is likely the result of intrinsic and extrinsic unfavourable factors. By rescuing A/equine/Lexington/1/1966 (EIV/66), I was able to assess basic but important within-host fitness parameters of H7N7 EIV such as replication kinetics, cell-to-cell spread, and transcriptomics responses to viral infection.

As expected, EIV/66 was able to infect canine (MDCK) and equine (E.Derm) cells. However, its replication kinetics were different to those observed for H3N8 EIVs such as EIV/2003 or EIV/89. Interestingly, I established that the reduced EIV/66 fitness in MDCK and E.Derm is not due to poor viral replication as EIV/66 viral titres reached similar values to H3N8 EIVs, but most likely to a replicative slowdown. However, it will be necessary to expand the study to other H7N7 EIVs to investigate if the findings could be generalised, and if the recorded reassortment events between H7N7 and H3N8 equine viruses (Ito et al. 1999) affected the observed replicative slowdown.

Additionally, I found from gene expression and gene ontology enrichment analysis that H7N7 EIV is likely to induce a transient general shutdown of host mRNA processing. This could affect the cell metabolism by affecting both cellular and viral protein synthesis. The hypothesis of a delayed protein synthesis will explain the poor NP staining observed in

infected E.Derm cells at 4 hpi. However, confirmation using immunostaining for other viral proteins such as HA are necessary, as the transcriptome analysis performed (by mapping mRNAs to the EIV genome) is an indirect quantification of viral load, similar to qPCR. I also highlighted that the lack of mRNA processing is likely to affect EIV/66 viral replication as viral protein translation will be impaired. Additional experiments such as puromycin assays, already used in another study to show host protein synthesis shutdown (Chauché et al. 2018), would shed light on this issue.

In sum, in this chapter I showed that an H7N7 EIV displays a different phenotype of infection to that observed with H3N8 EIV. While *in vitro* differences will not explain why the former became extinct and the latter still circulates in horses, they do provide some clues about differences in within-host viral fitness. It has been suggested that H7N7 EIVs became extinct because it was outcompeted by H3N8 EIVs (Murcia et al. 2011). Differences in the pace of within-host replication are likely to affect generation time (the time from infection to transmission) as well as evolutionary rates as they will lead to a slower evolution. Consequently, slow replication might contribute to a reduction in overall viral fitness. For example, in a context of H7N7 and H3N8 EIVs co-circulation, which was happening from 1963 to 1977, such host response to infection might confer a replicative advantage to H3N8 EIVs which could potentially outcompete H7N7 EIVs. Competition assays between EIV/63 (or other H3N8) and EIV/66 will be useful to test this hypothesis. However, such experiments would require careful design to avoid confounding factors such as reassortment in coinfected cells. They would also require strict risk assessments to avoid the generation and release of a novel EIV with epizootic potential.

Chapter 7: Final reflection and potential for future research

Virus-host co-evolution has shaped the pathogen landscape of humans and animals for millions of years. Respiratory viruses (including influenza viruses) constitute a constant threat to society as they have caused several epidemics and pandemics, as well as multiple epizooties and panzooties that affected animal health and caused significant economic burden. IAVs exhibit a complex ecology as they infect various avian and mammalian species. The most studied IAVs are those infecting humans and, in comparison, much less is known about animal IAVs. Comparative approaches are important to understand why IAVs infect some species and not others, which is key to elucidate the mechanisms underlying interspecies infections and virus adaptation. The aim of this thesis was to characterise the infection phenotypes of different IAVs including three H3N8 equine viruses (EIV/63; EIV/89; EIV/2003), one H7N7 equine virus (EIV/66) and an avian H3N8 virus (AIV/2009). The choice of viruses was based on direct and indirect evidence of large-scale infection in horse populations: all EIVs used in this study have been isolated from horses during outbreaks of disease, while serological studies have shown that AIV/2009 (or antigenically related viruses) routinely infect horses over broad geographical regions in Asia (Zhu et al. 2019). Notably, while H7N7 and H3N8 EIVs became endemic, their epidemiological trajectories are very different as H7N7 EIVs have not been detected since the 1970s (and are considered to be extinct), while H3N8 EIVs are still circulating. To gain insight on the virus-host interactions that lead to virus adaptation, I performed a series of experiments that combined classical virology techniques with high-throughput sequencing technologies in *in vitro* and *ex vivo* model systems.

Experimental approaches involving the quantification of within host fitness components (such as viral replication and cell-to-cell spread) have provided important information to understand the complex relationship between virus evolution and adaptation to adverse environments such as new hosts. The replication kinetics of the selected viruses in MDCK cells, a commonly used *in vitro* system to study influenza viruses, showed that all IAVs were able to establish a productive infection (Appendix 13 B for easier comparison). The ability of AIV/2009 to infect MDCK cells is consistent with previous findings by Zhu et al. (2019), who showed that this virus was able to replicate in equine tracheas. All tested viruses showed a peak viral titre of approximatively 10^6—10^7 $TCID_{50}$/mL, but interestingly, all viruses peaked within the first 48 hours, with the exception of EIV/66, whose replication peak was delayed to 72 hpi. Despite this observation, the viral replicative fitness (*i.e.* the ability of a virus to replicate to high level, and associated kinetics) of all the viruses tested in MDCKs

did not differ significantly. This is somehow expected as this cell line is broadly susceptible to infection by IAVs, most probably the consequence of the lack of an efficient anti-influenza activity (Seitz et al. 2010). However, MDCK cells are amenable for plaque assays and allow the study of cell-to-cell spread, another component of the within host viral fitness. Plaque size measurements showed that EIV/89 and EIV/2003 were associated with significantly larger plaque formation than AIV/2009 and EIV/63. However, plaques were of similar size between EIV/89 and EIV/2003, and AIV/2009 and EIV/63, respectively. Interestingly, it was noticed that EIV/66 is the only virus that did not form plaques in infected MDCK cells (Appendix 13 C). This result is most likely the consequence of the experimental design, in which infections were stopped after 48 hpi, rather than due to the lack of virus-induced cell death. Nevertheless, this result is in line with my observations during the generation of EIV/66 viral stocks, where clear CPE was not observed before 72 hpi, while with other H3N8 viruses 48 hours incubation was sufficient to induce strong CPE. Plaque assays using EIV/66 for longer incubation periods will clarify this issue.

Altogether, these results, unsurprisingly, suggest that EIV/2003 is associated with a greater *in vitro* fitness in MDCK cells than EIV/63, probably due to a longer viral circulation in horse. Interestingly, EIV/89 displayed similar replication kinetics and cell-to-cell spread to EIV/2003, while AIV/2009 and EIV/66 possessed lower replicative fitness, similar to the less adapted EIV/63. To compare the *in vitro* fitness of EIVs and AIVs within an equine cellular context, I performed similar experiments as the ones described above but using E. Derm cells, the only commercially available equine-derived cell line. Importantly, E.Derm cells are IFN-competent (Crispell 2018), while MDCK cells, although they are producing IFN, do not possess an anti-influenza activity mainly due to an inefficient Mx protein (Seitz et al. 2010).

The results from the experiments conducted in E.Derm cells highlighted stark contrasts in infection phenotypes among the selected viruses. While all viruses were able to infect E.Derm cells, only EIV/89, EIV/2003, and EIV/66 were able to replicate to high viral titre (~10^3 $TCID_{50}$/mL, Appendix 13 E). While the absence of high levels of viral replication of AIV/2009 was expected (Zhu et al. (2019) showed that AIVs exhibited lower replication compared to EIVs in equine tracheal explants), the observed lack of EIV/63 replication was puzzling. However, these results are in line with previous results that showed a decrease viral titre of 3 logs between EIV/2003 and EIV/63 (Chauché 2017). Such reduction in virus titres within my experimental setting would fall under the limit of detection. Interestingly,

EIV/2003 reached its maximum titre within the first 12 hours, EIV/89 and EIV/66 appeared to be delayed as the peak of virus titre was not observed before 24 and 48 hpi, respectively. Interestingly, EIV/66 was the only virus that exhibited sustained high levels of viral replication (up to 96 hpi, in contrast to EIV/2003 and EIV/89 whose viral titres decreased after 48 hpi (Appendix 13 E).

As known, E.Derm cells can synthesise and respond to IFN stimulation (Crispell 2018), and these results suggest that the host cellular innate immune response is an important component of the host barrier to infection, and that the selected viruses showed different levels of IFN sensitivity. In this experimental setting, EIV/63 and AIV/2009 are the most sensitive to host innate immune response and do not appear to be able to overcome it, while EIV/66, EIV/89 and EIV/2003 showed different level of susceptibility to the IFN response. Pre-treating E.Derm cells with ruxotilinib, a Jak1/2 inhibitor that specifically blocks the host cellular response to IFN, enhances EIV/63 replication (Chauché 2017) and should increase AIV/2009 titres to similar level than EIV/2003. It will be also interesting to see if EIV/66 delay is minimised by such cellular treatment.

However, it is important to highlight that those *in vitro* experimental models lack important parameters to extensively assess viral fitness (*e.g.* cellular heterogeneity, protective mucus layer, adaptive immunity), and *in vivo* infection phenotypes are likely to differ. However, the *in vitro* viral replication kinetics observed in this study were in line with EIV/63, EIV/2003 (Crispell 2018), and AIV/2009 (Zhu, et al. 2019) infection phenotypes conducted in *ex vivo*-cultured equine tracheal explants.

Altogether, these results suggest that in a well-controlled *in vitro* system that lacks adaptative immunity, has no population structure constraints, and where the tested virus is the only infecting pathogen, each of the viruses tested, showed distinct levels of within-host viral fitness.

Following the *in vitro* studies described above, bulk RNA sequencing experiments in E.Derm cells infected with EIV/63, EIV/66, EIV/2003, EIV/89, and AIV/2009 were performed. Such experimental approach enables investigation, in an unbiased fashion, of the viral-induced changes in cellular gene expression, which represent the host molecular response to infection. The use of RNAseq experiments to understand host cellular changes induced by infection has been successfully applied to characterise infection phenotypes of

emergent viruses (Josset et al. 2014), and to correlate transcriptomic changes to viral fitness (Cervera et al. 2018).

In this study, experiments were carried out at two different time points (4 and 24 hpi) to characterise the early and late cellular responses. The bulk RNA sequencing analyses showed, among the viruses under study, an important variation (from 10 to 2836) in the number and magnitude of DEGs at 4 hpi (Appendix 13 H). The sequential expansion of DEGs number (10 in EIV/89, 48 in EIV/2003 83 in EIV/63, and 2836 in EIV/66) and the enhanced gene net regulatory effect (driven by the quantity and the intensity of gene regulation) were inversely proportional with their respective viral replication fitness (*i.e.* EIVs that replicated to high levels exhibited a lower number of DEGs; Appendix 13 G). These results confirm that host responses to infection are virus-specific and quantitatively and qualitatively affect cellular gene expression. The correlation observed between the viral-induced gene regulatory effects and the viral replication kinetics, suggests that, during the initial replication cycle, a reduced but more efficient gene regulation might confer an increased viral fitness in an equine-specific intracellular context. This result is consistent with a previous study showing that in human cells, human H3N2 influenza virus dysregulated a lower number of genes while replicating to higher level than avian-origin H5N1 and H7N7 viruses (Josset et al. 2014). At later timepoints, the number of DEGs increased in all conditions, with the exception of AIV/2009. However, the lack of AIV/2009 increased DEGs at 24 hpi is in line with the reduction of infected cells found in flow cytometry, and with the lack of viral replication observed in E.Derm cells (Appendix 13 F). All together this result suggests that AIV/2009 is not fit enough to sustain a productive viral infection in an equine intracellular context. Such results are consistent with the observed lack of a sustained viral interspecies transmission, despite abundant ecological opportunities (Zhu, et al. 2019).

The RNAseq data can also be used to identify intracellular pathways affected by viral infection. Despite being optimised for human and mouse models, GO enrichment constitutes a useful tool to tackle this task, and has been applied successfully to alternative models (Ma et al. 2021; Abdelrahman et al. 2021; Zamzam et al. 2022). The GO terms enrichment analysis showed that EIV/89 induced an exacerbated host innate immune response, while EIV/63 and EIV/2003 could restrict it, and EIV/66 avoid it. Additionally, as the inflammatory response is closely related to immune activation, mainly due to cytokine production (Short et al. 2017), it is not surprising to notice that EIV/89 infection induced an

exacerbated inflammatory response in comparison to EIV/63 in which inflammation was moderate, and to EIV/2003, in which such response was absent. These results contrast with the GO terms enrichment conducted in EIV/66-infected E.Derm cells in which host innate immune, and inflammatory responses were not affected. The main GO terms enriched by EIV/66 infection were associated with mRNA processing pathways. Interestingly, the mRNA processing pathways were found to be moderately regulated in EIV/63-infected cells, while absent from EIV/2003 and EIV/89-enriched GO terms.

Taken together, these results show evidence that virus-induced gene regulation and the associated downstream biological processes are specific to each tested virus, and affect: innate immunity, inflammation, and cellular transcription. The overall regulation profile of these three pathway groups appears to influence the *in vitro* viral fitness of EIVs. Considering that exacerbation of inflammation is likely going to affect immunopathology and tissue damage *in vivo* (Chen et al. 2018), the exacerbated EIV/89-induced inflammatory response observed *in vitro*, could potentially explain the high mortality reported in EIV/89 infections (Guo et al. 1992). However the use of E.Derm, although they represent an equine-derived and IFN-competent cell line, is debatable as the cells originated from equine dermal tissue, and can only be passaged to a limited extent.

Therefore, to determine if fitness differences would also be evident at the natural site of EIV infection, *ex vivo* equine tracheal explants were infected with EIV/63 and EIV/2003. Cultures of *ex vivo* respiratory epithelium are broadly used to study the infection biology of many viruses including IAVs, severe acute respiratory syndrome coronavirus 2, and respiratory syncytial virus (Villenave et al. 2013; Zhou et al. 2013; Hui et al. 2020). Additionally, this experimental system allowed measurement of viral replication kinetics, intra-epithelial viral dissemination (key components of within-host fitness), but also virus-induced histopathological changes. It should be noted that the overall histopathological changes observed in *ex vivo* cultures were consistent with those found in horses experimentally infected with A/equine/Ibaraki/1/07 (Muranaka et al. 2012). Equine tracheal explants confirmed the enhanced within-host fitness of EIV/2003 compared to EIV/63, observed *in vitro* and showed that EIV/63-infected explants were associated with an enhanced viral-induced tissue damage. Similarly, EIV/63-infected tracheal explants were associated with an increase of Ki67 staining, a signal measuring tissue repair following injuries.

Taken together, these results suggest that H3N8 EIV evolved towards a lower virulence, without reaching complete avirulence, and such results are in line with a previous report that compared the *in vivo* virulence of A/equine/Sussex/89 and A/equine/Newmarket/2/93, two other evolutionarily related H3N8 EIVs (Wattrang et al. 2003). As viruses used in this study are genetically diverse, mapping the mutations one by one was not an option, and such approach would not have taken into consideration potential epistatic effects. However, it also appears that during H3N8 EIV adaptation, viruses were selected in favour of an optimised genomic content (reduced CG and CpG contents) to evade host PAMPs sensing as already observed by others (Greenbaum et al. 2008; Kumar et al. 2016). Optimising or deoptimizing either EIV/63 and/or EIV/2003 genome composition will be an interesting experiment to conduct as it could help to elucidate the role of genomic composition as an adaptative trait.

In summary, viral lineage establishment and viral long-term evolution to a new host are multifactorial processes that require a succession of favourable intrinsic and extrinsic conditions to happen. This project provides evidence supporting that EIV long-term adaptation to the horse led to an increased type I IFN resistance, a result in line with others showing that late H3N8 EIV NS1 (EIV/2003) is able to counteract better the host innate immune response, and so to confer an enhanced IFN resistance (Chauché et al. 2018). Furthermore, this study showed that EIV long-term adaptation to the horse was associated with an improved viral replication and viral dissemination in tissue (within-host fitness), while viral induced pathological changes were reduced, but not prevented. Additionally, this project showed that immunity, inflammation, and mRNA processing are important for viral adaptation. Moreover, this project gathered evidence suggesting that H7N7 EIVs most likely induce a strong and non-specific general protein expression shutoff, a result in line with a global host protein shutoff involving a CPSF30-dependent mechanism as already observed in early H3N8 EIV (EIV/63) infection (Chauché et al. 2018).

In sum, this work provides a more comprehensive understanding about the virus-host interactions that underpin viral emergence and long-term adaptation. Additionally, the work presented, although mainly descriptive, highlights a selection of genes that could be important to dictate the outcome of interspecies transmission events and represent an important step toward a potential description of the molecular mechanisms involved.

Table 7-1: **Summary of within-host viral fitness of H3N8 AIV and EIVs, and H7N7 EIV.**

	Parameter	EIV/63 (H3N8)	EIV/66 (H7N7)	EIV/89 (H3N8)	EIV/2003 (H3N8)	AIV/2009 (H3N8)
MDCK	Peak titre ($TCID_{50}$/mL)	5.10^5	6.10^5	5.10^7	1.10^6	4.10^6
	Peak time (hpi)	48	72	48	48	48
	Plaque formation	Yes	No	Yes	Yes	Yes
	Mean plaque diameter (cm)	0.13	*NA*	0.24	0.19	0.16
E.Derm	Peak titre ($TCID_{50}$/mL)	*NA*	5.10^3	4.10^3	4.10^3	5.10^1
	Peak time (hpi)	*NA*	48	24	12	12
	Plaque formation	*NA*	*NA*	*NA*	*NA*	*NA*
	Mean plaque diameter (cm)	*NA*	*NA*	*NA*	*NA*	*NA*
Equine tracheal explant	Peak titre (PFU/mL)	$7.10^{7\dagger}$	*NA*	*NA*	$2.10^{9\dagger}$	$8.10^{3\ddagger}$
	Peak time (hpi)	$48^{\dagger}$	*NA*	*NA*	$48^{\dagger}$	$96^{\ddagger}$
	Plaque formation	*NA*	*NA*	*NA*	*NA*	*NA*
	Mean plaque diameter (cm)	*NA*	*NA*	*NA*	*NA*	*NA*
E.Derm	Innate immune response	++	0	+++	++	-
	Inflammatory response	+	0	+++	+/-	-
	mRNA processing	+	+++	0	0	0

† Crispell, 2017

‡ Zhu et al.*, 2019*

Appendices

Appendix 1

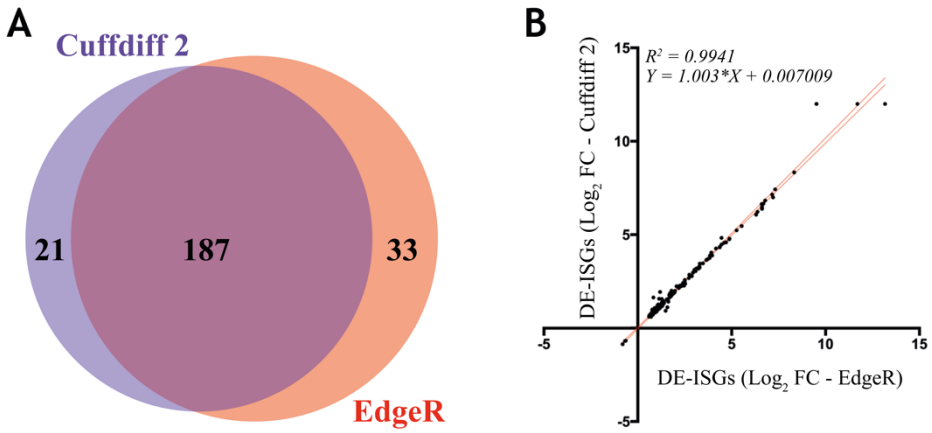

Appendix 1: IFN-treated E.Derm cells analysed with Cuffdiff2 or EdgeR. (A) DE-ISGs distribution of IFN-treated E.Derm analysed with Cuffdiff2 (purple) or EdgeR (red). The number of DEGs for each subset is shown within each compartment of the Venn diagram. **(B)** Pairwise comparison of the intensity of regulation (log2 FC) of shared DE-ISGs. Linear regression is summarised by the R2 value and curve equation.

Appendix 2

>pDP2002_Lexington_Segment1

CTAGCAGTTAACCGGAGTACTGGTCGACCTCCGAAGTTGGGGGGGATGAGACGAGCAAAAGCAGGTCAAATATATTCAAT
ATGGAGAGAATAAAAGAACTAAGGGATTTAATGTCACAATCCCGCACTCGCGAGATACTAACAACAACCACCGTGGACCA
CATGGCCATAATTAAGAGGTACACATCAGGAAGACAAGAAAAGAACCCAGCATTAAGAATGAAATGGATGATGGCAATGA
AATACCCAATTACAGCAGACAAAAGAATAATGGAGATGATCCCTGAAAGAAATGAACAAGGACAGACTCTCTGGAGCAAA
ACAAATGATGCCGGATCAGATAGAGTGATGGTTTCACCTCTAGCAGTGACATGGTGGAATAGAAATGGGCCAACAACAGC
AACAACCCATTACCCAAAGGTTTACAAAACTTATTTTGAAAAAGTTGAAAGATTAAAAAATGGGACCTTTGGCCCTGTTC
ATTTTCGAAACCAGGTTAAAATACGCCGTAGAGTAGACACAAATCCTGGTCATGCAGATCTTAGTGCCAAAGAGGCACAG
GATGTCATAATGGAAGTTGTGTTCCCTAATGAAGTGGGAGCCCGATTACTAACCTCAGAATCACAACTAAAAATAACCCA
AGAAAAAAAGGAAGAACTTCAAGACTGCAAAATAGCACCATTAATGGTAGCATACATGTTGGAAAGAGAATTAGTCCGAA
AAACCAGATTTCTCCCTGTAGCCGGTGGAACAAGCAGTGTGTATATCGAAGTCTTGCACTTGACCCAGGGAACATGTTGG
GAACAGATGTATGCCCCGGGTGGAGAAGTAAGAAATGATGATATTGATCAGAGCTTAATAATTGCTGCAAGAAACATTGT
TAGAAGAGCAACAGTATCAACAGATCCACTGGCATCGCTATTGGAGATGTGTCACAGCACACAAATTGGTGGAATAAGAA
TGGTAGACATTTTAAAGCAAAACCCAACTGAAGAACAAGCCGTGGACATATGCAAGGCAGCAATGGGTCTAAAAATAAGT
TCATCCTTCAGTTTCGGTGGATTTACCTTTAAAAGAACCAGTGGAACATCCATCAGAAAAGAAGAAGAAGTACTTACAGG
CAATCTTCAAACATTAAAAATACAAATACATGAAGGGTATGAAGAATTTACAATAGTTGGGAAGAGAGCAACAGCTATTC
TCCGAAAGGCAACCCAAAGGTTAGTCCAATTAATAATAAGTGGAAAAGATGAGCAGTCGATTGCTGAAGCAATCATTGTA
GCAATGGTATTCTCACAAGAAGACTGCATGATAAAGGCCGTGAGAGGGGATCTGAACTTTGTGAATAGAGCAAACCAACG
ATTGAACCCCATGCATCAACTCTTAAGGCATTTCCAAAAAGATGCCAAAATATTATTTCAAAATTGGGGAATTGAACCAA
TTGACAATATAATGGGAATGATTGGAGTATTACCTGATATGACCCCTAGCACAGAAATGTCATTGAGAGGAATAAGAATC
AGCAAAACAGGGGTGGATGAATATTCTAGTACAGAAAGGATAGTAGTAAGCATAGACCGTTTTTTGAGGGTTAGAGATCA
ACGTGGAAATATATTATTATCCCCCGAGGAAGTTAGTGAAACACAAGGAACAGAAAAATTGACAATAACATATTCCTCAT
CAATGATGTGGGAAATTAACGGCCCTGAATCAATACTAGTCAATACATATCAATGGATCATTAAAAATTGGGAAACAGTG
AAAATCCAATGGTCACAAGACCCCACAATACTATATAATAAAATAGAATTTGAACCCTTTCAGTCATTAATTCCAAAAGC
CGCAAGAGCCCAATATAGTGGGTTTGTGAGAACTCTGTTTCAGCAGATGCGAGATGTACTTGGAACTTTTGACACAGTTC
AGATAATAAAGCTATTACCCTTCGCAGCGGCTCCACCAGAACAAAGCCGGATACAGTTTTCTTCTCTAACAGTAAACGTG
AGGGGATCAGGAATGAGAATTCTTATAAGGGGTAATTCCCCAGTGTTTAATTATAACAAAACCACAAAACGTCTTACAGT
TCTTGGAAAAGATGCAGGTGCATTAATGAATGACCCTGATGAAGGAACAACTGGGATAGAATCTGCAGTTCTAAGAGGAT
TTCTAATTCTAGGCAAAGAAAACAAAAAATATGGACCAGCATTAAGCATCAGTGAGCTAAGCAACCTTGCAAAAGGAGAG
AAGGCAAATGTGTTAATAGGACAAGGAGATGTAGTGTTAGTAATGAAACGGAAACGGGACTCTAGCATACTTACTGACAG
CCAGACAGCGACCAAAAGAATCCGAATGGCCACCAATTAGTGTAAAACTGTTCAAAAACGACCTTGTTTCTACTCGTCTC
CAATAACCCGGCGGCCCAAAATGCCGACTCGGAGCGAAAGATATACCTCCCCCGGGGCCGGGAGGTCGCGTCACCGACCA
CGCCGCCGGCCCAGGCGACGCGCGACACGGACACCTGTCCCCAAAAACGCCACCATCGCAGCCACACACGGAGCGCCCGG
GGCCCTCTGGTCAACCCCAGGACACACGCGGGAGCAGCGCCGGGCCGGGGACGCCCTCCCGGCGGTCACCTAAATGCTAG
AGCTCGCTGATCAGCCTCGACTGTGCCTTCTAGTTGCCAGCCATCTGTTGTTTGCCCCTCCCCCGTGCCTTCCTTGACCC
TGGAAGGTGCCACTCCCACTGTCCTTTCCTAATAAAATGAGGAAATTGCATCGCATTGTCTGAGTAGGTGTCATTCTATT
CTGGGGGGGTGGGGTGGGGCAGGACAGCAAGGGGGAGGATTGGGAAGACAATAGCAGGCATGCTGGGGATGCGGTGGGCTC
TATGGCTTCTGAGGCGGAAAGAACCAGCTGCATTAATGAATCGGCCAACGCGCGGGGAGAGGCGGTTTGCGTATTGGGCG
CTCTTCCGCTTCCTCGCTCACTGACTCGCTGCGCTCGGTCGTTCGGCTGCGGCGAGCGGTATCAGCTCACTCAAAGGCGG
TAATACGGTTATCCACAGAATCAGGGGATAACGCAGGAAAGAACATGTGAGCAAAAGGCCAGCAAAAGGCCAGGAACCGT
AAAAAGGCCGCGTTGCTGGCGTTTTTCCATAGGCTCCGCCCCCCTGACGAGCATCACAAAAATCGACGCTCAAGTCAGAG
GTGGCGAAACCCGACAGGACTATAAAGATACCAGGCGTTTCCCCCTGGAAGCTCCCTCGTGCGCTCTCCTGTTCCGACCC
TGCCGCTTACCGGATACCTGTCCGCCTTTCTCCCTTCGGGAAGCGTGGCGCTTTCTCAATGCTCACGCTGTAGGTATCTC
AGTTCGGTGTAGGTCGTTCGCTCCAAGCTGGGCTGTGTGCACGAACCCCCCGTTCAGCCCGACCGCTGCGCCTTATCCGG
TAACTATCGTCTTGAGTCCAACCCGGTAAGACACGACTTATCGCCACTGGCAGCAGCCACTGGTAACAGGATTAGCAGAG
CGAGGTATGTAGGCGGTGCTACAGAGTTCTTGAAGTGGTGGCCTAACTACGGCTACACTAGAAGGACAGTATTTGGTATC
TGCGCTCTGCTGAAGCCAGTTACCTTCGGAAAAAGAGTTGGTAGCTCTTGATCCGGCAAACAAACCACCGCTGGTAGCGG
TGGTTTTTTTGTTTGCAAGCAGCAGATTACGCGCAGAAAAAAAGGATCTCAAGAAGATCCTTTGATCTTTTCTACGGGGT
CTGACGCTCAGTGGAACGAAAACTCACGTTAAGGGATTTTGGTCATGAGATTATCAAAAAGGATCTTCACCTAGATCCTT
TTAAATTAAAAATGAAGTTTTAAATCAATCTAAAGTATATATGAGTAAACTTGGTCTGACAGTTACCAATGCTTAATCAG
TGAGGCACCTATCTCAGCGATCTGTCTATTTCGTTCATCCATAGTTGCCTGACTCCCCGTCGTGTAGATAACTACGATAC
GGGAGGGCTTACCATCTGGCCCCAGTGCTGCAATGATACCGCGAGACCCACGCTCACCGGCTCCAGATTTATCAGCAATA
AACCAGCCAGCCGGAAGGGCCGAGCGCAGAAGTGGTCCTGCAACTTTATCCGCCTCCATCCAGTCTATTAATTGTTGCCG
GGAAGCTAGAGTAAGTAGTTCGCCAGTTAATAGTTTGCGCAACGTTGTTGCCATTGCTACAGGCATCGTGGTGTCACGCT
CGTCGTTTGGTATGGCTTCATTCAGCTCCGGTTCCCAACGATCAAGGCGAGTTACATGATCCCCCATGTTGTGCAAAAAA
GCGGTTAGCTCCTTCGGTCCTCCGATCGTTGTCAGAAGTAAGTTGGCCGCAGTGTTATCACTCATGGTTATGGCAGCACT
GCATAATTCTCTTACTGTCATGCCATCCGTAAGATGCTTTTCTGTGACTGGTGAGTACTCAACCAAGTCATTCTGAGAAT
AGTGTATGCGGCGACCGAGTTGCTCTTGCCCGGCGTCAATACGGGATAATACCGCGCCACATAGCAGAACTTTAAAAGTG
CTCATCATTGGAAAACGTTCTTCGGGGCGAAAACTCTCAAGGATCTTACCGCTGTTGAGATCCAGTTCGATGTAACCCAC
TCGTGCACCCAACTGATCTTCAGCATCTTTTACTTTCACCAGCGTTTCTGGGTGAGCAAAAACAGGAAGGCAAAATGCCG
CAAAAAAGGGAATAAGGGCGACACGGAAATGTTGAATACTCATACTCTTCCTTTTTCAATATTATTGAAGCATTTATCAG
GGTTATTGTCTCATGAGCGGATACATATTTGAATGTATTTAGAAAAATAAACAAATAGGGGTTCCGCGCACATTTCCCCG
AAAAGTGCCACCTGACGTCGATATGCCAAGTACGCCCCCTATTGACGTCAATGACGGTAAATGGCCCGCCTGGCATTATG
CCCAGTACATGACCTTATGGGACTTTCCTACTTGGCAGTACATCTACGTATTAGTCATCGCTATTACCATGGTGATGCGG
TTTTGGCAGTACATCAATGGGCGTGGATAGCGGTTTGACTCACGGGGATTTCCAAGTCTCCACCCCATTGACGTCAATGG
GAGTTTGTTTTGGCACCAAAATCAACGGGACTTTCCAAAATGTCGTAACAACTCCGCCCCATTGACGCAAATGGGCGGTA
GGCGTGTACGGTGGGAGGTCTATATAAGCAGAGCTCTCTGGCTAACTAGAGAACCCACTGCTTACTGGCTTATCGAAATT
AATACGACTCACTATAGGGAGACCCAAGCTGTTAACG

>pDP2002_Lexington_Segment2

CTAGCAGTTAACCGGAGTACTGGTCGACCTCCGAAGTTGGGGGGGATGAGACGAGCAAAAGCAGGCAAACCATTTGAATG
GATGTCAATCCGACTCTACTCTTATTAAAAATACCAGTGCAAAATGCCATAAGCACAACATTCCCTTACACTGGAGACCC
TCCATACAGCCATGGAACAGGAACTGGTTACACCATGGACACAGTTAATAGAACACATCAATACTCTGAAAGAGGGAAAT
GGACAACAAACACTGAAACTGGAGCATTACAACTGAACCCTATTGATGGCCCATTACCTGAAGACAACGAACCAAGTGGA
TATGCACAAACTGATTGTGTATTGGAAGCTATGGCTTTCCTTAGGGAATCCCACCCGGGGATTTTTGAGGCCTCATGTCT
TGAGACAATGGAAATTATTCAACAAACAAGAGTAGACAAGTTGACTCAAGGCCGTCAAACTTATGATTGGACTTTAAATA
AAAATCAACCTGCTGCAACTGCAATAGCCAACACAATCGAGGTTTTCAGATCAAATGATTTAAGAGCTAACGAATCAGGA
AGACTTATAGATTTCCTCAAAGATGTCACGTTATCAATGGATAAAGATGAAATAGAAATAACAACACACTTTCAGAGGAA
AAGAAGAGTAAGAGATAACATGACCAAAAAAATGGTCACACAGAGAACAATCGGGAAGAAAAAACAAAAATTAAACAAAA
AAAGTTACCTGATAAGAGCATTAACACTGAATACAATGACAAAGGATGCAGAAAGAGGTAAATTGAAGCGAAGAGCAATA
GCAACACCAGGAATGCAAATTAGAGGGTTTGTGTATTTTGTTGAAGCATTAGCTAAAAACATATGTGAAAAACTTGAGCA
ATCAGGCCTACCAGTTGGAGGGAATGAAAAAAAGGCCAAATTGGCTAATGTTGTAAGAAAAATGATGACCAATTCACAAG
ACACTGAACTCTCCTTCACTATCACTGGGGATAATACTAAATGGAATGAAAATCAAAACCCTCGCGTATTTTTGACTATG
ATAACATACATAACAAGAAACCAACCTGAATGGTTCAGAAATGTTTTGAGTATTGCACCAATAATGTTCTCAAATAAAAT
GGCAAGATTAGGGAAAGGATATATGTTTGAGAGTAAAAGTATGAAATTACGGACACAGATACCATCAGAAATGCTAGCGA
GCATTAATTTGAAATATTTCAATGAGTCAACAAGAAAAAAGATTGAGAAAATACGACCACTCTTAATAGATGGCACAGCC
TCATTAAGTCCTGGAATGATGATGGGCATGTTTAACATGCTGAGCACAGTTTTGGGAGTTTCAATTTTAAATCTAGGGCA
GAAAAAATACACAAAAACTACATATTGGTGGGATGGCCTCCAATCCTCTGATGATTTCGCTTTAATTGTGAATGCACCCA
ACCCCAATGAAATACAAGCTGGAGTCGACAAATTTTACAGAACCTGTAAGCTGGTTGGGATCAATATGAGTAAAAAGAAA
TCTTATATTAACAGGACAGGAACATTTGAATTCACAAGTTTCTTCTACCGCTATGGATTTGTTGCAAATTTCAGCATGGA
ATTGCCTAGTTTTGGAGTATCTGGGGTCAATGAATCTGCTGACATGAGTATTGGAATAACAATAATAAAAAATAACATGA
TAAACAATGATCTTGGACCAGCAACCGCTCAAATGGCTCTTCAGCTATTCATAAAGGACTACAGATACACATACCGCTGC
CATAGGGGGGACACTCAAATACAAACCAAAAGAACATTTGAACTGAAAAAACTATGGGAACAGACTCGTTCTAAGGCAGG
ACTATTAGTTTCTGATGGAGGACCAAATTTGTACAATATTAGAAACCTCCACATTCCAGAAGTCTGCCTGAAATGGGAGT
TAATGGATGAAGATTATAAAGGGAGACTGTGCAACCCATTGAATCCATTCGTCAATCATAAGGAAATTGAATCAGTGAAC
AATGCCGTGGTAATGCCCGCCCATGGTCCTGCCAAAAGCATAGAATACGATGCAGTTGCAACCACACATTCCTGGGTTCC
CAAAAGGAACCGCTCTATTTTGAATACAAGTCAAAAGGGGATTCTTGAAGATGAAAATATGTATCAGAAATGCTGCAACT
TGTTCGAGAAGTTTTTCCCTAGCAGCTCTTACAGAAGACCAGTTGGCATATCTAGCATGGTAGAGGCCATGGTTTCCAGG
GCCCGTATTGATGCACGAATTGACTTTGAGTCTGGAAAGATTAAGAAGGAAGAGTTGGCTGAGATCATGAAGACCTGTTC
CACCATTGAAGAGCTCGGACGGAAAAAATGATGAATTTAGCTTGTCCTTCATGAAAAAATGCCTTGTTTCTACTCGTCTC
CAATAACCCGGCGGCCCAAAATGCCGACTCGGAGCGAAAGATATACCTCCCCCGGGGCCGGGAGGTCGCGTCACCGACCA
CGCCGCCGGCCCAGGCGACGCGCGACACGGACACCTGTCCCCAAAAACGCCACCATCGCAGCCACACACGGAGCGCCCGG
GGCCCTCTGGTCAACCCCAGGACACACGCGGGAGCAGCGCCGGGCCGGGGACGCCCTCCCGGCGGTCACCTAAATGCTAG
AGCTCGCTGATCAGCCTCGACTGTGCCTTCTAGTTGCCAGCCATCTGTTGTTTGCCCCTCCCCCGTGCCTTCCTTGACCC
TGGAAGGTGCCACTCCCACTGTCCTTTCCTAATAAAATGAGGAAATTGCATCGCATTGTCTGAGTAGGTGTCATTCTATT
CTGGGGGGGTGGGGTGGGGCAGGACAGCAAGGGGGAGGATTGGGAAGACAATAGCAGGCATGCTGGGGATGCGGTGGGCTC
TATGGCTTCTGAGGCGGAAAGAACCAGCTGCATTAATGAATCGGCCAACGCGCGGGGAGAGGCGGTTTGCGTATTGGGCG
CTCTTCCGCTTCCTCGCTCACTGACTCGCTGCGCTCGGTCGTTCGGCTGCGGCGAGCGGTATCAGCTCACTCAAAGGCGG
TAATACGGTTATCCACAGAATCAGGGGATAACGCAGGAAAGAACATGTGAGCAAAAGGCCAGCAAAAGGCCAGGAACCGT
AAAAAGGCCGCGTTGCTGGCGTTTTTCCATAGGCTCCGCCCCCCTGACGAGCATCACAAAAATCGACGCTCAAGTCAGAG
GTGGCGAAACCCGACAGGACTATAAAGATACCAGGCGTTTCCCCCTGGAAGCTCCCTCGTGCGCTCTCCTGTTCCGACCC
TGCCGCTTACCGGATACCTGTCCGCCTTTCTCCCTTCGGGAAGCGTGGCGCTTTCTCAATGCTCACGCTGTAGGTATCTC
AGTTCGGTGTAGGTCGTTCGCTCCAAGCTGGGCTGTGTGCACGAACCCCCCGTTCAGCCCGACCGCTGCGCCTTATCCGG
TAACTATCGTCTTGAGTCCAACCCGGTAAGACACGACTTATCGCCACTGGCAGCAGCCACTGGTAACAGGATTAGCAGAG
CGAGGTATGTAGGCGGTGCTACAGAGTTCTTGAAGTGGTGGCCTAACTACGGCTACACTAGAAGGACAGTATTTGGTATC
TGCGCTCTGCTGAAGCCAGTTACCTTCGGAAAAAGAGTTGGTAGCTCTTGATCCGGCAAACAAACCACCGCTGGTAGCGG
TGGTTTTTTTGTTTGCAAGCAGCAGATTACGCGCAGAAAAAAAGGATCTCAAGAAGATCCTTTGATCTTTTCTACGGGGT
CTGACGCTCAGTGGAACGAAAACTCACGTTAAGGGATTTTGGTCATGAGATTATCAAAAAGGATCTTCACCTAGATCCTT
TTAAATTAAAAATGAAGTTTTAAATCAATCTAAAGTATATATGAGTAAACTTGGTCTGACAGTTACCAATGCTTAATCAG
TGAGGCACCTATCTCAGCGATCTGTCTATTTCGTTCATCCATAGTTGCCTGACTCCCCGTCGTGTAGATAACTACGATAC
GGGAGGGCTTACCATCTGGCCCCAGTGCTGCAATGATACCGCGAGACCCACGCTCACCGGCTCCAGATTTATCAGCAATA
AACCAGCCAGCCGGAAGGGCCGAGCGCAGAAGTGGTCCTGCAACTTTATCCGCCTCCATCCAGTCTATTAATTGTTGCCG
GGAAGCTAGAGTAAGTAGTTCGCCAGTTAATAGTTTGCGCAACGTTGTTGCCATTGCTACAGGCATCGTGGTGTCACGCT
CGTCGTTTGGTATGGCTTCATTCAGCTCCGGTTCCCAACGATCAAGGCGAGTTACATGATCCCCCATGTTGTGCAAAAAA
GCGGTTAGCTCCTTCGGTCCTCCGATCGTTGTCAGAAGTAAGTTGGCCGCAGTGTTATCACTCATGGTTATGGCAGCACT
GCATAATTCTCTTACTGTCATGCCATCCGTAAGATGCTTTTCTGTGACTGGTGAGTACTCAACCAAGTCATTCTGAGAAT
AGTGTATGCGGCGACCGAGTTGCTCTTGCCCGGCGTCAATACGGGATAATACCGCGCCACATAGCAGAACTTTAAAAGTG
CTCATCATTGGAAAACGTTCTTCGGGGCGAAAACTCTCAAGGATCTTACCGCTGTTGAGATCCAGTTCGATGTAACCCAC
TCGTGCACCCAACTGATCTTCAGCATCTTTTACTTTCACCAGCGTTTCTGGGTGAGCAAAAACAGGAAGGCAAAATGCCG
CAAAAAAGGGAATAAGGGCGACACGGAAATGTTGAATACTCATACTCTTCCTTTTTCAATATTATTGAAGCATTTATCAG
GGTTATTGTCTCATGAGCGGATACATATTTGAATGTATTTAGAAAAATAAACAAATAGGGGTTCCGCGCACATTTCCCCG
AAAAGTGCCACCTGACGTCGATATGCCAAGTACGCCCCCTATTGACGTCAATGACGGTAAATGGCCCGCCTGGCATTATG
CCCAGTACATGACCTTATGGGACTTTCCTACTTGGCAGTACATCTACGTATTAGTCATCGCTATTACCATGGTGATGCGG
TTTTGGCAGTACATCAATGGGCGTGGATAGCGGTTTGACTCACGGGGATTTCCAAGTCTCCACCCCATTGACGTCAATGG
GAGTTTGTTTTGGCACCAAAATCAACGGGACTTTCCAAAATGTCGTAACAACTCCGCCCCATTGACGCAAATGGGCGGTA
GGCGTGTACGGTGGGAGGTCTATATAAGCAGAGCTCTCTGGCTAACTAGAGAACCCACTGCTTACTGGCTTATCGAAATT
AATACGACTCACTATAGGGAGACCCAAGCTGTTAACG

>pDP2002_Lexington_Segment3

CTAGCAGTTAACCGGAGTACTGGTCGACCTCCGAAGTTGGGGGGGATGAGACGAGCAAAAGCAGGTACTAATTCAAAATG
GAAGATTTCGTTCGACAATGTTTCAACCCAATGATTGTTGAACTTGCAGAAAAAGCAATGAAAGAATATGGAGAGAATCC
AAAAATTGAGACAAACAAATTTGCCGCAATATGCACTCACTTAGAAGTGTGCTTCATGTACTCAGACTTCCATTTTATTG
ATGATAGAGGTGAATCAATAATCGTGGAGTCAGGTGATCCAAATGTTCTATTAAAACATAGATTTGAAATAATTGAAGGA
AGAGATCGAACAATAGCTTGGACAATAGTTAATAGTATTTGCAATACTACAAAAATTGAGAAACCTAGATTCCTTCCTGA
TTTATATGATTATAAAGAAAACAGATTTATAGAAATTGGGGTAACACGAAGAGAAGTCCATATCTATTATTTAGAAAAAG
CCAATAAGATAAAATCTGAAAAAACTCACATCCACATCTTCTCATTTATGGGAGAGGAAATGGCCACTAAAGCTGACTAC
ACATTAGACGAAGAAAGCCGAGCAAGAATAAAAACCAGATTATTCACAATAAGACAAGAAATGGCCAGTAGAGGCCTCTG
GGATTCCTTTCGCCAGTCCGAAAAAGGTGAGGAAACAATTGAAGAAAGATTTGAAATTACGGGGACAATACGCAAGCTTG
CTGATCAAAGCCTCCCACCAAACTTCTCCAATCTTGAACACTTTAGAGCCTATGTTGATGGGTTTGAACCAAATGGCTTC
ATAGAAGGAAAACTTTCCCAAATGTCCAAAGCAGTAAATGCAAAAATTGAGCCATTTCTAAAAACAACACCTCGCCCACT
CAAATTACCTAAGGGCCCACCCTGTTCCCAACGATCCAAATTTTTATTAATGGATGCTCTAAAATTAAGTATTGAAGATC
CAAGCCATGAGGGTGAAGGAATACCACTATACGATGCAATAAAATGCATGAAAACATTCTTTGGATGGAAAGAACCCAAG
ATCATCAAACCACATGAGAAGGGCATAAACCCGAACTATCTACTAGCTTGGAAACAAACACTATCAGAAATACAGGACAT
TGAGAATGAGGGGAAAATTCCCAAAATTAAAAACATGAAAAAAACAAGTCAATTAAAGTGGGCACTTGGTGAAAATATGG
CACCAGAAAAAGTTGATTTTGAGGACTGCAAAGACATCAATGATTTAAAACAATACAGTAGTGATGAACCAGAGCAAAGA
TCGTTTGCAAGCTGGATCCAAAATGAATTTAATAAAGCCTGCGAATTAACTGACTCAACCTGGATAGAACTCGATGAAAT
TGGGGAAGACATTGCCCCAATTGAACATATTGCAAGTATGAGAAGAAACTATTTCACAGCAGAAATATCTCATTGTAGAG
CAACTGAATATATAATGAAAGGAGTTTATATAAACACTGCTCTGTTAAACGCATCTTGTGCAGCTATGGATGATTTCCAA
CTAATCCCAATGATAAGCAAATCCAGGACTAAAGAAGGAAGACGAAAAACAAATCTGTATGGGTTCATTATAAAAGGAAG
GTCCCATTTAAGAAATGACACTGATGTAGTAAATTTTGTGAGCATGGAATTCTCTTTAACAGATCCAAGACTTGAACCAC
ACAAATGGGAAAAATATTGCGTTCTTGAAATAGGAGACATGCTTTTAAGAACTGCCATAGGCCAGGTGTCAAGGCCAATG
TTTTTATACATAAGAACAAATGGGACCTCAAAGGTAAAAATGAAATGGGGAATGGAAATGAGGCGCTGTCTTCTTCAATC
ACTTCAACAAATCGAAAGCATGATTGAAGCTGAATCATCTGTCAAAGAGAAAGACATGACAAAGGAATTCTTCGAGAACA
AAACAGAGACATGGCCTATTGGAGAATCACCCAGAGGGGTAGAAGAAGGCTCTATTGGGAAAGTCTGCAGAACTCTGTTA
GCCAAATCAGTATTTAATAGTTTATATGCATCTCCACAATTAGAAGGGTTCTCCGCTGAGTCCAGGAAACTACTCCTTAT
TGTCCAAGCTCTAAGAGATAATCTAGAACCTGGGACCTTTGATCTTGGAGGGCTATATGAAGCAATTGAGGAGTGCCTGA
TTAATGATCCCTGGGTTTTGCTTAATGCATCTTGGTTCAACTCCTTCCTTAAACATGCACTGGAGTAATTTTGGCAATGC
TACAATTTGCTGTCCATACTGTCCAAAAAAGTACCTTGTTTCTACTCGTCTCCAATAACCCGGCGGCCCAAAATGCCGAC
TCGGAGCGAAAGATATACCTCCCCCGGGGCCGGGAGGTCGCGTCACCGACCACGCCGCCGGCCCAGGCGACGCGCGACAC
GGACACCTGTCCCCAAAAACGCCACCATCGCAGCCACACACGGAGCGCCCGGGGCCCTCTGGTCAACCCCAGGACACACG
CGGGAGCAGCGCCGGGCCGGGGACGCCCTCCCGGCGGTCACCTAAATGCTAGAGCTCGCTGATCAGCCTCGACTGTGCCT
TCTAGTTGCCAGCCATCTGTTGTTTGCCCCTCCCCCGTGCCTTCCTTGACCCTGGAAGGTGCCACTCCCACTGTCCTTTC
CTAATAAAATGAGGAAATTGCATCGCATTGTCTGAGTAGGTGTCATTCTATTCTGGGGGGTGGGGTGGGGCAGGACAGCA
AGGGGGAGGATTGGGAAGACAATAGCAGGCATGCTGGGGATGCGGTGGGCTCTATGGCTTCTGAGGCGGAAAGAACCAGC
TGCATTAATGAATCGGCCAACGCGCGGGGAGAGGCGGTTTGCGTATTGGGCGCTCTTCCGCTTCCTCGCTCACTGACTCG
CTGCGCTCGGTCGTTCGGCTGCGGCGAGCGGTATCAGCTCACTCAAAGGCGGTAATACGGTTATCCACAGAATCAGGGGA
TAACGCAGGAAAGAACATGTGAGCAAAAGGCCAGCAAAAGGCCAGGAACCGTAAAAAGGCCGCGTTGCTGGCGTTTTTCC
ATAGGCTCCGCCCCCCTGACGAGCATCACAAAAATCGACGCTCAAGTCAGAGGTGGCGAAACCCGACAGGACTATAAAGA
TACCAGGCGTTTCCCCCTGGAAGCTCCCTCGTGCGCTCTCCTGTTCCGACCCTGCCGCTTACCGGATACCTGTCCGCCTT
TCTCCCTTCGGGAAGCGTGGCGCTTTCTCAATGCTCACGCTGTAGGTATCTCAGTTCGGTGTAGGTCGTTCGCTCCAAGC
TGGGCTGTGTGCACGAACCCCCCGTTCAGCCCGACCGCTGCGCCTTATCCGGTAACTATCGTCTTGAGTCCAACCCGGTA
AGACACGACTTATCGCCACTGGCAGCAGCCACTGGTAACAGGATTAGCAGAGCGAGGTATGTAGGCGGTGCTACAGAGTT
CTTGAAGTGGTGGCCTAACTACGGCTACACTAGAAGGACAGTATTTGGTATCTGCGCTCTGCTGAAGCCAGTTACCTTCG
GAAAAAGAGTTGGTAGCTCTTGATCCGGCAAACAAACCACCGCTGGTAGCGGTGGTTTTTTTGTTTGCAAGCAGCAGATT
ACGCGCAGAAAAAAAGGATCTCAAGAAGATCCTTTGATCTTTTCTACGGGGTCTGACGCTCAGTGGAACGAAAACTCACG
TTAAGGGATTTTGGTCATGAGATTATCAAAAAGGATCTTCACCTAGATCCTTTTAAATTAAAAATGAAGTTTTAAATCAA
TCTAAAGTATATATGAGTAAACTTGGTCTGACAGTTACCAATGCTTAATCAGTGAGGCACCTATCTCAGCGATCTGTCTA
TTTCGTTCATCCATAGTTGCCTGACTCCCCGTCGTGTAGATAACTACGATACGGGAGGGCTTACCATCTGGCCCCAGTGC
TGCAATGATACCGCGAGACCCACGCTCACCGGCTCCAGATTTATCAGCAATAAACCAGCCAGCCGGAAGGGCCGAGCGCA
GAAGTGGTCCTGCAACTTTATCCGCCTCCATCCAGTCTATTAATTGTTGCCGGGAAGCTAGAGTAAGTAGTTCGCCAGTT
AATAGTTTGCGCAACGTTGTTGCCATTGCTACAGGCATCGTGGTGTCACGCTCGTCGTTTGGTATGGCTTCATTCAGCTC
CGGTTCCCAACGATCAAGGCGAGTTACATGATCCCCCATGTTGTGCAAAAAAGCGGTTAGCTCCTTCGGTCCTCCGATCG
TTGTCAGAAGTAAGTTGGCCGCAGTGTTATCACTCATGGTTATGGCAGCACTGCATAATTCTCTTACTGTCATGCCATCC
GTAAGATGCTTTTCTGTGACTGGTGAGTACTCAACCAAGTCATTCTGAGAATAGTGTATGCGGCGACCGAGTTGCTCTTG
CCCGGCGTCAATACGGGATAATACCGCGCCACATAGCAGAACTTTAAAAGTGCTCATCATTGGAAAACGTTCTTCGGGGC
GAAAACTCTCAAGGATCTTACCGCTGTTGAGATCCAGTTCGATGTAACCCACTCGTGCACCCAACTGATCTTCAGCATCT
TTTACTTTCACCAGCGTTTCTGGGTGAGCAAAAACAGGAAGGCAAAATGCCGCAAAAAAGGGAATAAGGGCGACACGGAA
ATGTTGAATACTCATACTCTTCCTTTTTCAATATTATTGAAGCATTTATCAGGGTTATTGTCTCATGAGCGGATACATAT
TTGAATGTATTTAGAAAAATAAACAAATAGGGGTTCCGCGCACATTTCCCCGAAAAGTGCCACCTGACGTCGATATGCCA
AGTACGCCCCCTATTGACGTCAATGACGGTAAATGGCCCGCCTGGCATTATGCCCAGTACATGACCTTATGGGACTTTCC
TACTTGGCAGTACATCTACGTATTAGTCATCGCTATTACCATGGTGATGCGGTTTTGGCAGTACATCAATGGGCGTGGAT
AGCGGTTTGACTCACGGGGATTTCCAAGTCTCCACCCCATTGACGTCAATGGGAGTTTGTTTTGGCACCAAAATCAACGG
GACTTTCCAAAATGTCGTAACAACTCCGCCCCATTGACGCAAATGGGCGGTAGGCGTGTACGGTGGGAGGTCTATATAAG
CAGAGCTCTCTGGCTAACTAGAGAACCCACTGCTTACTGGCTTATCGAAATTAATACGACTCACTATAGGGAGACCCAAG
CTGTTAACG

>pDP2002_Lexington_Segment4

CTAGCAGTTAACCGGAGTACTGGTCGACCTCCGAAGTTGGGGGGGATGAGACGAGCAAAAGCAGGGGATACATAATGAAC
ACTCAAATTCTAATATTAGCCACTTCGGCATTCCTCTGTGTACGTGCAGATAAAATCTGCCTAGGACGTCATGCTGTGTC
TAATGGAACCAAAGTGGACACCCTTACTGAAAAGGGAATAGAAGTTGTCAATGCAACAGAAACAGTTGAACAAAAAAACA
TCCCCAAGATCTGCTCAAAAGGGAAACAGACTATTGACCTTGGTCAATGTGGATTACTAGGGACCACTATTGGTCCCCCC
CAATGCGACCAATTTCTTGAATTCTCTGCTAATTTAATAATTGAGAGAAGAGAAGGTGATGACATTTGTTATCCAGGCAA
ATTTGACAATGAAGAAACATTGAGACAAATACTCAGAAAATCCGGAGGAATTAAAAAGGAGAATATGGGATTCACATATA
CCGGAGTGAGAACCAATGGAGAGACTAGCGCATGTAGAAGGTCAAGATCTTCCTTTTATGCAGAAATGAAATGGCTCCTA
TCCAACACAGACAATGGGGTATTCCCACAAATGACAAAATCCTACAAGAACACTAAGAGGGAGCCAGCTCTGATAATCTG
GGGAATCCACCACTCAGGATCAACCGCTGAACAGACTAGATTGTATGGAAGTGGAAATAAGTTGATAACAGTTTGGAGTT
CCAAATACCAACAATCTTTTGCCCCAAATCCTGGACCAAGGCCGCAAATAAATGGCCAATCAGGAAGAATTGACTTTTAC
TGGCTGATGTTAGATCCCAATGATACTGTCACTTTTAGTTTTAATGGGGCCTTTATAGCACCTGACCGCGCCAGTTTTCT
AAGAGGTAAATCTCTAGGAATTCAGAGTGATGCACAACTTGACAACAATTGTGAAGGTGAATGTTATCATATTGGAGGTA
CTATAATTAGCAACTTGCCCTTTCAAAACATTAATAGCAGGGCAATTGGGAAATGCCCCAGATACGTAAAGCAAAAAAGC
TTAATGCTAGCAACAGGAATGAAAAATGTTCCTGAAAATTCTACACACAAACAATTAACTCATCACATGCGCAAAAAAAG
AGGTTTATTTGGTGCAATAGCAGGATTCATTGAAAATGGGTGGGAAGGATTAATAGATGGATGGTATGGATACAGACATC
AGAATGCACAAGGAGAAGGAACTGCTGCAGACTACAAAAGTACACAATCTGCTATCAATCAAATAACCGGGAAATTAAAC
AGACTAATAGAAAAAACCAACCAGCAATTTGAACTAATAGATAATGAGTTCAATGAAATAGAAAAGCAAATTGGCAATGT
TATTAACTGGACTAGAGATTCTATCATCGAAGTATGGTCATATAATGCAGAATTCCTCGTGGCAGTGGAGAATCAACACA
CTATTGATTTAACTGATTCAGAGATGAACAAATTATATGAAAAGGTAAGAAGACAACTGAGAGAAAATGCTGAGGAAGAT
GGTAATGGCTGTTTTGAAATATTCCACCAATGTGACAATGATTGCATGGCCAGCATTAGAAACAATACATATGATCATAA
AAAATACAGAAAAGAGGCAATACAAAACAGAATTCAGATTGACGCAGTAAAGTTGAGCAGCGGTTACAAAGATATAATAC
TTTGGTTTAGCTTCGGGGCATCATGTTTCTTATTTCTTGCCATTGCAATGGGTCTTGCTTTCATATGCATAAAAAATGGA
AACATGCGGTGCACTATTTGTATATAAGTTTGAAAAAACACCCTTGTTTCTACTCGTCTCCAATAACCCGGCGGCCCAAA
ATGCCGACTCGGAGCGAAAGATATACCTCCCCCGGGGCCGGGAGGTCGCGTCACCGACCACGCCGCCGGCCCAGGCGACG
CGCGACACGGACACCTGTCCCCAAAAACGCCACCATCGCAGCCACACACGGAGCGCCCGGGGCCCTCTGGTCAACCCCAG
GACACACGCGGGAGCAGCGCCGGGCCGGGGACGCCCTCCCGGCGGTCACCTAAATGCTAGAGCTCGCTGATCAGCCTCGA
CTGTGCCTTCTAGTTGCCAGCCATCTGTTGTTTGCCCCTCCCCCGTGCCTTCCTTGACCCTGGAAGGTGCCACTCCCACT
GTCCTTTCCTAATAAAATGAGGAAATTGCATCGCATTGTCTGAGTAGGTGTCATTCTATTCTGGGGGGTGGGGTGGGGCA
GGACAGCAAGGGGGAGGATTGGGAAGACAATAGCAGGCATGCTGGGGATGCGGTGGGCTCTATGGCTTCTGAGGCGGAAA
GAACCAGCTGCATTAATGAATCGGCCAACGCGCGGGGAGAGGCGGTTTGCGTATTGGGCGCTCTTCCGCTTCCTCGCTCA
CTGACTCGCTGCGCTCGGTCGTTCGGCTGCGGCGAGCGGTATCAGCTCACTCAAAGGCGGTAATACGGTTATCCACAGAA
TCAGGGGATAACGCAGGAAAGAACATGTGAGCAAAAGGCCAGCAAAAGGCCAGGAACCGTAAAAAGGCCGCGTTGCTGGC
GTTTTTCCATAGGCTCCGCCCCCCTGACGAGCATCACAAAAATCGACGCTCAAGTCAGAGGTGGCGAAACCCGACAGGAC
TATAAAGATACCAGGCGTTTCCCCCTGGAAGCTCCCTCGTGCGCTCTCCTGTTCCGACCCTGCCGCTTACCGGATACCTG
TCCGCCTTTCTCCCTTCGGGAAGCGTGGCGCTTTCTCAATGCTCACGCTGTAGGTATCTCAGTTCGGTGTAGGTCGTTCG
CTCCAAGCTGGGCTGTGTGCACGAACCCCCCGTTCAGCCCGACCGCTGCGCCTTATCCGGTAACTATCGTCTTGAGTCCA
ACCCGGTAAGACACGACTTATCGCCACTGGCAGCAGCCACTGGTAACAGGATTAGCAGAGCGAGGTATGTAGGCGGTGCT
ACAGAGTTCTTGAAGTGGTGGCCTAACTACGGCTACACTAGAAGGACAGTATTTGGTATCTGCGCTCTGCTGAAGCCAGT
TACCTTCGGAAAAAGAGTTGGTAGCTCTTGATCCGGCAAACAAACCACCGCTGGTAGCGGTGGTTTTTTTGTTTGCAAGC
AGCAGATTACGCGCAGAAAAAAAGGATCTCAAGAAGATCCTTTGATCTTTTCTACGGGGTCTGACGCTCAGTGGAACGAA
AACTCACGTTAAGGGATTTTGGTCATGAGATTATCAAAAAGGATCTTCACCTAGATCCTTTTAAATTAAAAATGAAGTTT
TAAATCAATCTAAAGTATATATGAGTAAACTTGGTCTGACAGTTACCAATGCTTAATCAGTGAGGCACCTATCTCAGCGA
TCTGTCTATTTCGTTCATCCATAGTTGCCTGACTCCCCGTCGTGTAGATAACTACGATACGGGAGGGCTTACCATCTGGC
CCCAGTGCTGCAATGATACCGCGAGACCCACGCTCACCGGCTCCAGATTTATCAGCAATAAACCAGCCAGCCGGAAGGGC
CGAGCGCAGAAGTGGTCCTGCAACTTTATCCGCCTCCATCCAGTCTATTAATTGTTGCCGGGAAGCTAGAGTAAGTAGTT
CGCCAGTTAATAGTTTGCGCAACGTTGTTGCCATTGCTACAGGCATCGTGGTGTCACGCTCGTCGTTTGGTATGGCTTCA
TTCAGCTCCGGTTCCCAACGATCAAGGCGAGTTACATGATCCCCCATGTTGTGCAAAAAAGCGGTTAGCTCCTTCGGTCC
TCCGATCGTTGTCAGAAGTAAGTTGGCCGCAGTGTTATCACTCATGGTTATGGCAGCACTGCATAATTCTCTTACTGTCA
TGCCATCCGTAAGATGCTTTTCTGTGACTGGTGAGTACTCAACCAAGTCATTCTGAGAATAGTGTATGCGGCGACCGAGT
TGCTCTTGCCCGGCGTCAATACGGGATAATACCGCGCCACATAGCAGAACTTTAAAAGTGCTCATCATTGGAAAACGTTC
TTCGGGGCGAAAACTCTCAAGGATCTTACCGCTGTTGAGATCCAGTTCGATGTAACCCACTCGTGCACCCAACTGATCTT
CAGCATCTTTTACTTTCACCAGCGTTTCTGGGTGAGCAAAAACAGGAAGGCAAAATGCCGCAAAAAAGGGAATAAGGGCG
ACACGGAAATGTTGAATACTCATACTCTTCCTTTTTCAATATTATTGAAGCATTTATCAGGGTTATTGTCTCATGAGCGG
ATACATATTTGAATGTATTTAGAAAAATAAACAAATAGGGGTTCCGCGCACATTTCCCCGAAAAGTGCCACCTGACGTCG
ATATGCCAAGTACGCCCCCTATTGACGTCAATGACGGTAAATGGCCCGCCTGGCATTATGCCCAGTACATGACCTTATGG
GACTTTCCTACTTGGCAGTACATCTACGTATTAGTCATCGCTATTACCATGGTGATGCGGTTTTGGCAGTACATCAATGG
GCGTGGATAGCGGTTTGACTCACGGGGATTTCCAAGTCTCCACCCCATTGACGTCAATGGGAGTTTGTTTTGGCACCAAA
ATCAACGGGACTTTCCAAAATGTCGTAACAACTCCGCCCCATTGACGCAAATGGGCGGTAGGCGTGTACGGTGGGAGGTC
TATATAAGCAGAGCTCTCTGGCTAACTAGAGAACCCACTGCTTACTGGCTTATCGAAATTAATACGACTCACTATAGGGA
GACCCAAGCTGTTAACG

>pDP2002_Lexington_Segment5

CTAGCAGTTAACCGGAGTACTGGTCGACCTCCGAAGTTGGGGGGGATGAGACGAGCAAAAGCAGGGTAGATAATCACTCA
CTGAGTGACATCAAAATCATGGCGCCTCAAGGCACCAAACGACCTTATGAACAAATGGAAACTGGTGGAGAACGCCAGAA
CGCCACTGAGATCAGATCATCCGTTGGAAAAATGGTTGCTGGAATAGGGAAATTCTACATCCAGATGTGCACTGAACTCA
AACTCAATGACTATGAAGGAAGGCTAATCCAAAACAGCATAACAATAGAAAAAATGGTACTCTCTGCTTTTGATGAGAGA
AGGAATAAATACTTGGAAGAACACCCCAATGCCGGGAAAGACCCTAAGAAAACGGGAGGACCTATCTACAGAAAAAGAGA
AGGAAAATGGATAAGAGAATTAATCCTCTACGACAAAGAGGAAATCAGAAGAATTTGGCGCCAGGCCAACAATGGAGAAG
ATGCAACAGCTGGTCTTACACACTTGATGATTTGGCATTCTAATCTGAACGATGCCACTTATCAAAGGACAAGGGCTCTT
GTTCGAACTGGAATGGACCCCAGAATGTGCTCTCTAATGCAAGGTTCTACTCTTCCAAGGAGATCTGGAGCAGCTGGTGC
AGCAATAAAAGGAATTGGGACAATGGTAATGGAATTAATCAGAATGATAAAACGAGGAATTAATGATCGAAACTTTTGGA
GAGGGGAAAATGGAAGAAAAACAAGAATTGCCTATGAGAGAATGTGCAACATTCTTAAGGGAAAATTTCAAACAGCAGCA
CAAAGGGCAATGATGGATCAAGTGCGAGAAAGCAGAAATCCGGGCAATGCTGAAATCGAAGATCTTATTTTTTTAGCGCG
GTCTGCACTCATACTACGAGGATCAGTAGCCCACAAATCCTGTCTGCCTGCATGTGTGTATGGACTTATTGTGGCCAGTG
GATATGATTTCGAAAGAGAGGGATACTCATTGGTTGGGGTAGACCCTTTTAAACTGCTTCAAAACAGTCAAATATTCAGC
CTTATTAGGCCTAATGAAAATCCATTACATAAAAGCCAGTTGGTATGGATGGCTTGCCACTCTGCAGCATTCGAAGATCT
GAGAATATCAAGCTTCATCAGGGGAACAAAAGTAATCCCAAGAGGACAACTGTCTACCAGAGGAATCCAGATTGCATCCA
ATGAGAAACATGGAGGTCATAGACTCCAACACTCTTGAACTAAGAAGTAAATACTGGGCAATTAGAACCAAAAGTGGAGGA
AACACCAGCCAGCAGAAAGCATCTGCTGGACAAATAAGTGTACAACCAACATTCTCAGTTCAAAGAAACCTTCCTTTTGA
AAGAACAACTATAATGGCTGCATTTACTGGAAATAACGAAGGAAGAACATCTGACATGAGAACCGAAATTATAAGAATGA
TGGAAAGTGCAAAACCAGATGATGTGTCCTTTCAAGGACGGGGAGTTTTTGAGCTCTCAGACGAAAAGGCAACTAACCCT
ATAGTGCCTTCTTTTGACATGAGTAAAGAAGGGTCTTATTTCTTCGGAGACAATGCAGAGGAATTTGACAATTAAAGAAA
AATACCCTTGTTTCTACTCGTCTCCAATAACCCGGCGGCCCAAAATGCCGACTCGGAGCGAAAGATATACCTCCCCCGGG
GCCGGGAGGTCGCGTCACCGACCACGCCGCCGGCCCAGGCGACGCGCGACACGGACACCTGTCCCCAAAAACGCCACCAT
CGCAGCCACACACGGAGCGCCCGGGGCCCTCTGGTCAACCCCAGGACACACGCGGGAGCAGCGCCGGGCCGGGGACGCCC
TCCCGGCGGTCACCTAAATGCTAGAGCTCGCTGATCAGCCTCGACTGTGCCTTCTAGTTGCCAGCCATCTGTTGTTTGCC
CCTCCCCCGTGCCTTCCTTGACCCTGGAAGGTGCCACTCCCACTGTCCTTTCCTAATAAAATGAGGAAATTGCATCGCAT
TGTCTGAGTAGGTGTCATTCTATTCTGGGGGGGTGGGGTGGGGCAGGACAGCAAGGGGGAGGATTGGGAAGACAATAGCAG
GCATGCTGGGGATGCGGTGGGCTCTATGGCTTCTGAGGCGGAAAGAACCAGCTGCATTAATGAATCGGCCAACGCGCGGG
GAGAGGCGGTTTGCGTATTGGGCGCTCTTCCGCTTCCTCGCTCACTGACTCGCTGCGCTCGGTCGTTCGGCTGCGGCGAG
CGGTATCAGCTCACTCAAAGGCGGTAATACGGTTATCCACAGAATCAGGGGATAACGCAGGAAAGAACATGTGAGCAAAA
GGCCAGCAAAAGGCCAGGAACCGTAAAAAGGCCGCGTTGCTGGCGTTTTTCCATAGGCTCCGCCCCCCTGACGAGCATCA
CAAAAATCGACGCTCAAGTCAGAGGTGGCGAAACCCGACAGGACTATAAAGATACCAGGCGTTTCCCCCTGGAAGCTCCC
TCGTGCGCTCTCCTGTTCCGACCCTGCCGCTTACCGGATACCTGTCCGCCTTTCTCCCTTCGGGAAGCGTGGCGCTTTCT
CAATGCTCACGCTGTAGGTATCTCAGTTCGGTGTAGGTCGTTCGCTCCAAGCTGGGCTGTGTGCACGAACCCCCCGTTCA
GCCCGACCGCTGCGCCTTATCCGGTAACTATCGTCTTGAGTCCAACCCGGTAAGACACGACTTATCGCCACTGGCAGCAG
CCACTGGTAACAGGATTAGCAGAGCGAGGTATGTAGGCGGTGCTACAGAGTTCTTGAAGTGGTGGCCTAACTACGGCTAC
ACTAGAAGGACAGTATTTGGTATCTGCGCTCTGCTGAAGCCAGTTACCTTCGGAAAAAGAGTTGGTAGCTCTTGATCCGG
CAAACAAACCACCGCTGGTAGCGGTGGTTTTTTTGTTTGCAAGCAGCAGATTACGCGCAGAAAAAAAGGATCTCAAGAAG
ATCCTTTGATCTTTTCTACGGGGTCTGACGCTCAGTGGAACGAAAACTCACGTTAAGGGATTTTGGTCATGAGATTATCA
AAAAGGATCTTCACCTAGATCCTTTTAAATTAAAAATGAAGTTTTAAATCAATCTAAAGTATATATGAGTAAACTTGGTC
TGACAGTTACCAATGCTTAATCAGTGAGGCACCTATCTCAGCGATCTGTCTATTTCGTTCATCCATAGTTGCCTGACTCC
CCGTCGTGTAGATAACTACGATACGGGAGGGCTTACCATCTGGCCCCAGTGCTGCAATGATACCGCGAGACCCACGCTCA
CCGGCTCCAGATTTATCAGCAATAAACCAGCCAGCCGGAAGGGCCGAGCGCAGAAGTGGTCCTGCAACTTTATCCGCCTC
CATCCAGTCTATTAATTGTTGCCGGGAAGCTAGAGTAAGTAGTTCGCCAGTTAATAGTTTGCGCAACGTTGTTGCCATTG
CTACAGGCATCGTGGTGTCACGCTCGTCGTTTGGTATGGCTTCATTCAGCTCCGGTTCCCAACGATCAAGGCGAGTTACA
TGATCCCCCATGTTGTGCAAAAAAGCGGTTAGCTCCTTCGGTCCTCCGATCGTTGTCAGAAGTAAGTTGGCCGCAGTGTT
ATCACTCATGGTTATGGCAGCACTGCATAATTCTCTTACTGTCATGCCATCCGTAAGATGCTTTTCTGTGACTGGTGAGT
ACTCAACCAAGTCATTCTGAGAATAGTGTATGCGGCGACCGAGTTGCTCTTGCCCGGCGTCAATACGGGATAATACCGCG
CCACATAGCAGAACTTTAAAAGTGCTCATCATTGGAAAACGTTCTTCGGGGCGAAAACTCTCAAGGATCTTACCGCTGTT
GAGATCCAGTTCGATGTAACCCACTCGTGCACCCAACTGATCTTCAGCATCTTTTACTTTCACCAGCGTTTCTGGGTGAG
CAAAAACAGGAAGGCAAAATGCCGCAAAAAAGGGAATAAGGGCGACACGGAAATGTTGAATACTCATACTCTTCCTTTTT
CAATATTATTGAAGCATTTATCAGGGTTATTGTCTCATGAGCGGATACATATTTGAATGTATTTAGAAAAATAAACAAAT
AGGGGTTCCGCGCACATTTCCCCGAAAAGTGCCACCTGACGTCGATATGCCAAGTACGCCCCCTATTGACGTCAATGACG
GTAAATGGCCCGCCTGGCATTATGCCCAGTACATGACCTTATGGGACTTTCCTACTTGGCAGTACATCTACGTATTAGTC
ATCGCTATTACCATGGTGATGCGGTTTTGGCAGTACATCAATGGGCGTGGATAGCGGTTTGACTCACGGGGATTTCCAAG
TCTCCACCCCATTGACGTCAATGGGAGTTTGTTTTGGCACCAAAATCAACGGGACTTTCCAAAATGTCGTAACAACTCCG
CCCCATTGACGCAAATGGGCGGTAGGCGTGTACGGTGGGAGGTCTATATAAGCAGAGCTCTCTGGCTAACTAGAGAACCC
ACTGCTTACTGGCTTATCGAAATTAATACGACTCACTATAGGGAGACCCAAGCTGTTAACG

>pDP2002_Lexington_Segment6

CTAGCAGTTAACCGGAGTACTGGTCGACCTCCGAAGTTGGGGGGGATGAGACGAGCAAAAGCAGGGGGATTTTAAAATGA
ATCCTAATCAAAAACTCTTTGCATCATCCGGAATAGCAATAGTGCTAGGAATAATAAATCTTCTCATAGGAATATCCAAT
ATGAGTTTAAATATATCTCTATACTCAAAAGGAGAAAACCACAAGAATGATAATCTAACATGCACAAATATCAACCAGAA
TGATACCACCATGGTAAATACGTACATCAATAACACAACAATAATTGACAAAAGTACAAAAATAGGAAACCCTGGTTATC
TACTGCTGAATAAAAGTCTATGCAACGTTGAGGGATGGGTTGTAATAGCAAAGGACAATGCGATTAGATTTGGAGAAAGC
GAACAAATCATAGTAACTAGAGAACCTTATGTCTCATGTGATCCTCTAAGTTGCAAAATGTATGCTCTACACCAAGGTAC
CACAATCAGAAACAAGCATTCAAATAGTACCACACACGACAGAACAGCCTTCCGAGGGCTCATTTCTACTCCATTAGGTA
GCCCCCCAACAGTGAGCAATAGTGAATTCATATGTGTTGGGTGGTCAAGCACAAGCTGCCATGATGGGGTAAGCAGGATG
ACAATTTGTGTACAAGGAGACAATGAAAATGCTACTGCAACAGTGTATTACAACAAGAGGCTTACAACCACTATTAAAAC
ATGGGCTAAAAACATTTTAAGAACCCAAGAGTCTGAATGTGTTTGTCATAACAGCACTTGTGTAGTGGTAATGACTGATG
GGCCCGCAAATAACCAGGCGTTCACAAAAGTAATATACTTTCATAAAGGAATGATAATAAAAGAAGAATCACTAAAAGGT
TCAGCCAAACACATAGAAGAATGTTCTTGTTATGGTCATAATCAAAGAGTGACTTGTGTCTGCAGAGACAACTGGCAGGG
TGCAAATAGACCTATTATAGAGATTGACATGAATAATTTGGAACATACAAGTAGATATATATGCACAGGAGTATTAACAG
ACACCAGTAGACCCAAGGATAAAACAATAGGGGAATGCTTCAATCCTATTACTGGAAGTCCTGGTGCACCAGGGATAAAA
GGTTTCGGATTCCTAAATGAGGATAATACCTGGCTAGGGAGAACAATCAGCCCCAAATTGAGGAGTGGATTTGAAATGCT
GAAGATACCTAATGCTGGGACTGACCCAGAGTCCAAAATAAAAGAAAGACAAGAAATAGTTAGTAATGACAATTGGTCAG
GCTATTCCGGAAGTTTCATTGATTATTGGAATGACAACAGTGAATGCTACAATCCATGCTTCTATGTAGAATTAATTAGA
GGAAGGCCTGAAGAGGCAAAATATGTTGAATGGACCAGTAACAGCCTAATTGCACTATGTGGGAGCCCAATCTCAGTTGG
GTCTGGATCTTTCCCTGATGGGGCACAAATCAAATACTTTTCGTAAAATGAAAAAAAACCCTTGTTTCTACTCGTCTCCAA
TAACCCGGCGGCCCAAAATGCCGACTCGGAGCGAAAGATATACCTCCCCCGGGGCCGGGAGGTCGCGTCACCGACCACGC
CGCCGGCCCAGGCGACGCGCGACACGGACACCTGTCCCCAAAAACGCCACCATCGCAGCCACACACGGAGCGCCCGGGGC
CCTCTGGTCAACCCCAGGACACACGCGGGAGCAGCGCCGGGCCGGGGACGCCCTCCCGGCGGTCACCTAAATGCTAGAGC
TCGCTGATCAGCCTCGACTGTGCCTTCTAGTTGCCAGCCATCTGTTGTTTGCCCCTCCCCCGTGCCTTCCTTGACCCTGG
AAGGTGCCACTCCCACTGTCCTTTCCTAATAAAATGAGGAAATTGCATCGCATTGTCTGAGTAGGTGTCATTCTATTCTG
GGGGGTGGGGTGGGGCAGGACAGCAAGGGGGAGGATTGGGAAGACAATAGCAGGCATGCTGGGGATGCGGTGGGCTCTAT
GGCTTCTGAGGCGGAAAGAACCAGCTGCATTAATGAATCGGCCAACGCGCGGGGAGAGGCGGTTTGCGTATTGGGCGCTC
TTCCGCTTCCTCGCTCACTGACTCGCTGCGCTCGGTCGTTCGGCTGCGGCGAGCGGTATCAGCTCACTCAAAGGCGGTAA
TACGGTTATCCACAGAATCAGGGGATAACGCAGGAAAGAACATGTGAGCAAAAGGCCAGCAAAAGGCCAGGAACCGTAAA
AAGGCCGCGTTGCTGGCGTTTTTCCATAGGCTCCGCCCCCCTGACGAGCATCACAAAAATCGACGCTCAAGTCAGAGGTG
GCGAAACCCGACAGGACTATAAAGATACCAGGCGTTTCCCCCTGGAAGCTCCCTCGTGCGCTCTCCTGTTCCGACCCTGC
CGCTTACCGGATACCTGTCCGCCTTTCTCCCTTCGGGAAGCGTGGCGCTTTCTCAATGCTCACGCTGTAGGTATCTCAGT
TCGGTGTAGGTCGTTCGCTCCAAGCTGGGCTGTGTGCACGAACCCCCCGTTCAGCCCGACCGCTGCGCCTTATCCGGTAA
CTATCGTCTTGAGTCCAACCCGGTAAGACACGACTTATCGCCACTGGCAGCAGCCACTGGTAACAGGATTAGCAGAGCGA
GGTATGTAGGCGGTGCTACAGAGTTCTTGAAGTGGTGGCCTAACTACGGCTACACTAGAAGGACAGTATTTGGTATCTGC
GCTCTGCTGAAGCCAGTTACCTTCGGAAAAAGAGTTGGTAGCTCTTGATCCGGCAAACAAACCACCGCTGGTAGCGGTGG
TTTTTTTGTTTGCAAGCAGCAGATTACGCGCAGAAAAAAAGGATCTCAAGAAGATCCTTTGATCTTTTCTACGGGGTCTG
ACGCTCAGTGGAACGAAAACTCACGTTAAGGGATTTTGGTCATGAGATTATCAAAAAGGATCTTCACCTAGATCCTTTTA
AATTAAAAATGAAGTTTTAAATCAATCTAAAGTATATATGAGTAAACTTGGTCTGACAGTTACCAATGCTTAATCAGTGA
GGCACCTATCTCAGCGATCTGTCTATTTCGTTCATCCATAGTTGCCTGACTCCCCGTCGTGTAGATAACTACGATACGGG
AGGGCTTACCATCTGGCCCCAGTGCTGCAATGATACCGCGAGACCCACGCTCACCGGCTCCAGATTTATCAGCAATAAAC
CAGCCAGCCGGAAGGGCCGAGCGCAGAAGTGGTCCTGCAACTTTATCCGCCTCCATCCAGTCTATTAATTGTTGCCGGGA
AGCTAGAGTAAGTAGTTCGCCAGTTAATAGTTTGCGCAACGTTGTTGCCATTGCTACAGGCATCGTGGTGTCACGCTCGT
CGTTTGGTATGGCTTCATTCAGCTCCGGTTCCCAACGATCAAGGCGAGTTACATGATCCCCCATGTTGTGCAAAAAAGCG
GTTAGCTCCTTCGGTCCTCCGATCGTTGTCAGAAGTAAGTTGGCCGCAGTGTTATCACTCATGGTTATGGCAGCACTGCA
TAATTCTCTTACTGTCATGCCATCCGTAAGATGCTTTTCTGTGACTGGTGAGTACTCAACCAAGTCATTCTGAGAATAGT
GTATGCGGCGACCGAGTTGCTCTTGCCCGGCGTCAATACGGGATAATACCGCGCCACATAGCAGAACTTTAAAAGTGCTC
ATCATTGGAAAACGTTCTTCGGGGCGAAAACTCTCAAGGATCTTACCGCTGTTGAGATCCAGTTCGATGTAACCCACTCG
TGCACCCAACTGATCTTCAGCATCTTTTACTTTCACCAGCGTTTCTGGGTGAGCAAAAACAGGAAGGCAAAATGCCGCAA
AAAAGGGAATAAGGGCGACACGGAAATGTTGAATACTCATACTCTTCCTTTTTCAATATTATTGAAGCATTTATCAGGGT
TATTGTCTCATGAGCGGATACATATTTGAATGTATTTAGAAAAATAAACAAATAGGGGTTCCGCGCACATTTCCCCGAAA
AGTGCCACCTGACGTCGATATGCCAAGTACGCCCCCTATTGACGTCAATGACGGTAAATGGCCCGCCTGGCATTATGCCC
AGTACATGACCTTATGGGACTTTCCTACTTGGCAGTACATCTACGTATTAGTCATCGCTATTACCATGGTGATGCGGTTT
TGGCAGTACATCAATGGGCGTGGATAGCGGTTTGACTCACGGGGATTTCCAAGTCTCCACCCCATTGACGTCAATGGGAG
TTTGTTTTGGCACCAAAATCAACGGGACTTTCCAAAATGTCGTAACAACTCCGCCCCATTGACGCAAATGGGCGGTAGGC
GTGTACGGTGGGAGGTCTATATAAGCAGAGCTCTCTGGCTAACTAGAGAACCCACTGCTTACTGGCTTATCGAAATTAAT
ACGACTCACTATAGGGAGACCCAAGCTGTTAACG

>pDP2002_Lexington_Segment7

CTAGCAGTTAACCGGAGTACTGGTCGACCTCCGAAGTTGGGGGGGATGAGACGAGCAAAAGCAGGTAGATGTTGAAAGAT
GAGCCTTCTAACCGAGGTCGAAACGTATGTTCTCTCTATCATCCCATCAGGCCCCCTCAAAGCCGAAATCGCGCAGAGAC
TTGAGAATGTTTTTGCAGGGAAAAATACAGATCTTGAGGCTCTCATGGAATGGCTAAAGACAAGACCAATTTTGTCACCT
CTGACTAAAGGGATTTTAGGATTTGTGTTCACGCTCACCGTGCCCAGTGAGCGGGGACTGCAGCGTAGACGATTTGTCCA
AAATGCCCTCAATGGGAATGGAGACCCAAACAACATGGATAAGGCAATTAAACTGTATAAAAAACTAAAAAGGGACGTAA
CATTCCACGGGGCCAAAGAAGTTGCACTTGGCTATTCTACTGGTGCTCTTGCCAGCTGTATGGGCCTCATATACAACAGA
ATGGGGACTGTAACCACTGAAGTGGCATTTGGTTTGGTATGTGCAACTTGTGAACAAATTGCTGATTCACAGCATCGCGC
ATACAGGCAAATGGCAACAACAACCAATCCGCTAATAAGACATGAGAACCGAATGGTGTTAGCAAGCACCACAGCCAAAG
CTATGGAGCAAATGGCTGGATCAAATGAGCAAGCAGCGGAAGCTATGGAAATTGCAAATCAGGCCAGGCAAATGGTGCAG
GCAATGAGAACAGTTGGGACTCACCCTAATTCCAGCACTGGTCTGAAAGATGACCTTCTCGAAAATTTACAGGCCTATCA
AAAGCGGATGGGAGTGCAGATGCAACGGTTCAAGTGATCTTCTCGTTGCCATTGCAAGCATCACTGGGATATTGCACTTG
ATATTGTGGATTTTTGATCGTCTTTTCTTCAAATGTGCCTACCGCCGATTCAGACATGGGTTGAAAAAAGGACCTTCTAC
AGGGGGGATACCTGAATCTATGAGGGAAGAATATCGGCAGGAACAACAAAGCGATGTTAGTGTTGACAATAGTCATTTTG
TCAACATAGAGCTGGAGTAAAAAACTACCTTGTTTCTACTCGTCTCCAATAACCCGGCGGCCCAAAATGCCGACTCGGAG
CGAAAGATATACCTCCCCCGGGGCCGGGAGGTCGCGTCACCGACCACGCCGCCGGCCCAGGCGACGCGCGACACGGACAC
CTGTCCCCAAAAACGCCACCATCGCAGCCACACACGGAGCGCCCGGGGCCCTCTGGTCAACCCCAGGACACACGCGGGAG
CAGCGCCGGGCCGGGGACGCCCTCCCGGCGGTCACCTAAATGCTAGAGCTCGCTGATCAGCCTCGACTGTGCCTTCTAGT
TGCCAGCCATCTGTTGTTTGCCCCTCCCCCGTGCCTTCCTTGACCCTGGAAGGTGCCACTCCCACTGTCCTTTCCTAATA
AAATGAGGAAATTGCATCGCATTGTCTGAGTAGGTGTCATTCTATTCTGGGGGGGTGGGGTGGGGCAGGACAGCAAGGGGG
AGGATTGGGAAGACAATAGCAGGCATGCTGGGGATGCGGTGGGCTCTATGGCTTCTGAGGCGGAAAGAACCAGCTGCATT
AATGAATCGGCCAACGCGCGGGGAGAGGCGGTTTGCGTATTGGGCGCTCTTCCGCTTCCTCGCTCACTGACTCGCTGCGC
TCGGTCGTTCGGCTGCGGCGAGCGGTATCAGCTCACTCAAAGGCGGTAATACGGTTATCCACAGAATCAGGGGATAACGC
AGGAAAGAACATGTGAGCAAAAGGCCAGCAAAAGGCCAGGAACCGTAAAAAGGCCGCGTTGCTGGCGTTTTTCCATAGGC
TCCGCCCCCCTGACGAGCATCACAAAAATCGACGCTCAAGTCAGAGGTGGCGAAACCCGACAGGACTATAAAGATACCAG
GCGTTTCCCCCTGGAAGCTCCCTCGTGCGCTCTCCTGTTCCGACCCTGCCGCTTACCGGATACCTGTCCGCCTTTCTCCC
TTCGGGAAGCGTGGCGCTTTCTCAATGCTCACGCTGTAGGTATCTCAGTTCGGTGTAGGTCGTTCGCTCCAAGCTGGGCT
GTGTGCACGAACCCCCCGTTCAGCCCGACCGCTGCGCCTTATCCGGTAACTATCGTCTTGAGTCCAACCCGGTAAGACAC
GACTTATCGCCACTGGCAGCAGCCACTGGTAACAGGATTAGCAGAGCGAGGTATGTAGGCGGTGCTACAGAGTTCTTGAA
GTGGTGGCCTAACTACGGCTACACTAGAAGGACAGTATTTGGTATCTGCGCTCTGCTGAAGCCAGTTACCTTCGGAAAAA
GAGTTGGTAGCTCTTGATCCGGCAAACAAACCACCGCTGGTAGCGGTGGTTTTTTTGTTTGCAAGCAGCAGATTACGCGC
AGAAAAAAAGGATCTCAAGAAGATCCTTTGATCTTTTCTACGGGGTCTGACGCTCAGTGGAACGAAAACTCACGTTAAGG
GATTTTGGTCATGAGATTATCAAAAAGGATCTTCACCTAGATCCTTTTAAATTAAAAATGAAGTTTTAAATCAATCTAAA
GTATATATGAGTAAACTTGGTCTGACAGTTACCAATGCTTAATCAGTGAGGCACCTATCTCAGCGATCTGTCTATTTCGT
TCATCCATAGTTGCCTGACTCCCCGTCGTGTAGATAACTACGATACGGGAGGGCTTACCATCTGGCCCCAGTGCTGCAAT
GATACCGCGAGACCCACGCTCACCGGCTCCAGATTTATCAGCAATAAACCAGCCAGCCGGAAGGGCCGAGCGCAGAAGTG
GTCCTGCAACTTTATCCGCCTCCATCCAGTCTATTAATTGTTGCCGGGAAGCTAGAGTAAGTAGTTCGCCAGTTAATAGT
TTGCGCAACGTTGTTGCCATTGCTACAGGCATCGTGGTGTCACGCTCGTCGTTTGGTATGGCTTCATTCAGCTCCGGTTC
CCAACGATCAAGGCGAGTTACATGATCCCCCATGTTGTGCAAAAAAGCGGTTAGCTCCTTCGGTCCTCCGATCGTTGTCA
GAAGTAAGTTGGCCGCAGTGTTATCACTCATGGTTATGGCAGCACTGCATAATTCTCTTACTGTCATGCCATCCGTAAGA
TGCTTTTCTGTGACTGGTGAGTACTCAACCAAGTCATTCTGAGAATAGTGTATGCGGCGACCGAGTTGCTCTTGCCCGGC
GTCAATACGGGATAATACCGCGCCACATAGCAGAACTTTAAAAGTGCTCATCATTGGAAAACGTTCTTCGGGGCGAAAAC
TCTCAAGGATCTTACCGCTGTTGAGATCCAGTTCGATGTAACCCACTCGTGCACCCAACTGATCTTCAGCATCTTTTACT
TTCACCAGCGTTTCTGGGTGAGCAAAAACAGGAAGGCAAAATGCCGCAAAAAAGGGAATAAGGGCGACACGGAAATGTTG
AATACTCATACTCTTCCTTTTTCAATATTATTGAAGCATTTATCAGGGTTATTGTCTCATGAGCGGATACATATTTGAAT
GTATTTAGAAAAATAAACAAATAGGGGTTCCGCGCACATTTCCCCGAAAAGTGCCACCTGACGTCGATATGCCAAGTACG
CCCCCTATTGACGTCAATGACGGTAAATGGCCCGCCTGGCATTATGCCCAGTACATGACCTTATGGGACTTTCCTACTTG
GCAGTACATCTACGTATTAGTCATCGCTATTACCATGGTGATGCGGTTTTGGCAGTACATCAATGGGCGTGGATAGCGGT
TTGACTCACGGGGATTTCCAAGTCTCCACCCCATTGACGTCAATGGGAGTTTGTTTTGGCACCAAAATCAACGGGACTTT
CCAAAATGTCGTAACAACTCCGCCCCATTGACGCAAATGGGCGGTAGGCGTGTACGGTGGGAGGTCTATATAAGCAGAGC
TCTCTGGCTAACTAGAGAACCCACTGCTTACTGGCTTATCGAAATTAATACGACTCACTATAGGGAGACCCAAGCTGTTA
ACG

>pDP2002_Lexington_Segment8

CTAGCAGTTAACCGGAGTACTGGTCGACCTCCGAAGTTGGGGGGGATGAGACGAGCAAAAGCAGGGTGACAAAAACATAA
TGGATTCCAACACAGTGTCAAGCTTTCAGGTAGATTGTTTTCTTTGGCACATTCGCAAACGATTTGCAGACCAAAAAATG
GGTGATGCCCCGTTTCTTGACCGGCTTCGCAGAGATCAGAAGTCCTTAAAAGGAAGAAGCAGCACTCTTGGTTTAGACAT
TGAAAGCTCAACACGAGCAGGGAGGCAAATAGTAAAGCGGATTCTAAAGGAAGAATCCGATAGTGAACCAAAAGGGACTA
TTGCCCCAGTACCCACTTCATATTATTTAACTGATATGACTCTTGAAGAAATGTCAAGGCCCTGGTACATGCTTATACCC
AACCAAAAAAGAGTAGGATCACTCTACATCAGAATGGATCAAGCCATAATGGATAAGAAGATCACACTGAAAGCAAACTT
TAGTGTGGTCTTTAACAAACTGGAAACTCTAACACTTTTACGAGCATTCACAAAAGATGAAGCAATCATTGGAGAAATCT
TACCAATACCTTCTCTTCCAGGACATACTAATGAGGATGTCAAAAATGCAATTGAGATCCTCATCGGAGGACTTGAATGG
AATAATAACACAGTTCGAATCTCTGAGATTCTACAGAGATTCACTTGGAGAAACAGTGATGAGAATGGGGGATTTCTACT
CTCTCCAAAACAAAAACAAAAAATGGAGGGAACAACTGGGCCAGAAGTTTGAAGAAATAAGATGGCTGATTGAAGAAATA
AGGCATAAACTAAAAATAACAGAAAACAGTTTTGAACAAATAACATTCATTCAAGCATTACAACTATTGCTTGAAGTGGA
GCAAGAGATAAGAACTTTCTCGTTTCAGCTTATTTAATGATAAAAAACACCCTTGTTTCTACTCGTCTCCAATAACCCGG
CGGCCCAAAATGCCGACTCGGAGCGAAAGATATACCTCCCCCGGGGCCGGGAGGTCGCGTCACCGACCACGCCGCCGGCC
CAGGCGACGCGCGACACGGACACCTGTCCCCAAAAACGCCACCATCGCAGCCACACACGGAGCGCCCGGGGCCCTCTGGT
CAACCCCAGGACACACGCGGGAGCAGCGCCGGGCCGGGGACGCCCTCCCGGCGGTCACCTAAATGCTAGAGCTCGCTGAT
CAGCCTCGACTGTGCCTTCTAGTTGCCAGCCATCTGTTGTTTGCCCCTCCCCCGTGCCTTCCTTGACCCTGGAAGGTGCC
ACTCCCACTGTCCTTTCCTAATAAAATGAGGAAATTGCATCGCATTGTCTGAGTAGGTGTCATTCTATTCTGGGGGGTGG
GGTGGGGCAGGACAGCAAGGGGGAGGATTGGGAAGACAATAGCAGGCATGCTGGGGATGCGGTGGGCTCTATGGCTTCTG
AGGCGGAAAGAACCAGCTGCATTAATGAATCGGCCAACGCGCGGGGAGAGGCGGTTTGCGTATTGGGCGCTCTTCCGCTT
CCTCGCTCACTGACTCGCTGCGCTCGGTCGTTCGGCTGCGGCGAGCGGTATCAGCTCACTCAAAGGCGGTAATACGGTTA
TCCACAGAATCAGGGGATAACGCAGGAAAGAACATGTGAGCAAAAGGCCAGCAAAAGGCCAGGAACCGTAAAAAGGCCGC
GTTGCTGGCGTTTTTCCATAGGCTCCGCCCCCCTGACGAGCATCACAAAAATCGACGCTCAAGTCAGAGGTGGCGAAACC
CGACAGGACTATAAAGATACCAGGCGTTTCCCCCTGGAAGCTCCCTCGTGCGCTCTCCTGTTCCGACCCTGCCGCTTACC
GGATACCTGTCCGCCTTTCTCCCTTCGGGAAGCGTGGCGCTTTCTCAATGCTCACGCTGTAGGTATCTCAGTTCGGTGTA
GGTCGTTCGCTCCAAGCTGGGCTGTGTGCACGAACCCCCCGTTCAGCCCGACCGCTGCGCCTTATCCGGTAACTATCGTC
TTGAGTCCAACCCGGTAAGACACGACTTATCGCCACTGGCAGCAGCCACTGGTAACAGGATTAGCAGAGCGAGGTATGTA
GGCGGTGCTACAGAGTTCTTGAAGTGGTGGCCTAACTACGGCTACACTAGAAGGACAGTATTTGGTATCTGCGCTCTGCT
GAAGCCAGTTACCTTCGGAAAAAGAGTTGGTAGCTCTTGATCCGGCAAACAAACCACCGCTGGTAGCGGTGGTTTTTTTG
TTTGCAAGCAGCAGATTACGCGCAGAAAAAAAGGATCTCAAGAAGATCCTTTGATCTTTTCTACGGGGTCTGACGCTCAG
TGGAACGAAAACTCACGTTAAGGGATTTTGGTCATGAGATTATCAAAAAGGATCTTCACCTAGATCCTTTTAAATTAAAA
ATGAAGTTTTAAATCAATCTAAAGTATATATGAGTAAACTTGGTCTGACAGTTACCAATGCTTAATCAGTGAGGCACCTA
TCTCAGCGATCTGTCTATTTCGTTCATCCATAGTTGCCTGACTCCCCGTCGTGTAGATAACTACGATACGGGAGGGCTTA
CCATCTGGCCCCAGTGCTGCAATGATACCGCGAGACCCACGCTCACCGGCTCCAGATTTATCAGCAATAAACCAGCCAGC
CGGAAGGGCCGAGCGCAGAAGTGGTCCTGCAACTTTATCCGCCTCCATCCAGTCTATTAATTGTTGCCGGGAAGCTAGAG
TAAGTAGTTCGCCAGTTAATAGTTTGCGCAACGTTGTTGCCATTGCTACAGGCATCGTGGTGTCACGCTCGTCGTTTGGT
ATGGCTTCATTCAGCTCCGGTTCCCAACGATCAAGGCGAGTTACATGATCCCCCATGTTGTGCAAAAAAGCGGTTAGCTC
CTTCGGTCCTCCGATCGTTGTCAGAAGTAAGTTGGCCGCAGTGTTATCACTCATGGTTATGGCAGCACTGCATAATTCTC
TTACTGTCATGCCATCCGTAAGATGCTTTTCTGTGACTGGTGAGTACTCAACCAAGTCATTCTGAGAATAGTGTATGCGG
CGACCGAGTTGCTCTTGCCCGGCGTCAATACGGGATAATACCGCGCCACATAGCAGAACTTTAAAAGTGCTCATCATTGG
AAAACGTTCTTCGGGGCGAAAACTCTCAAGGATCTTACCGCTGTTGAGATCCAGTTCGATGTAACCCACTCGTGCACCCA
ACTGATCTTCAGCATCTTTTACTTTCACCAGCGTTTCTGGGTGAGCAAAAACAGGAAGGCAAAATGCCGCAAAAAAGGGA
ATAAGGGCGACACGGAAATGTTGAATACTCATACTCTTCCTTTTTCAATATTATTGAAGCATTTATCAGGGTTATTGTCT
CATGAGCGGATACATATTTGAATGTATTTAGAAAAATAAACAAATAGGGGTTCCGCGCACATTTCCCCGAAAAGTGCCAC
CTGACGTCGATATGCCAAGTACGCCCCCTATTGACGTCAATGACGGTAAATGGCCCGCCTGGCATTATGCCCAGTACATG
ACCTTATGGGACTTTCCTACTTGGCAGTACATCTACGTATTAGTCATCGCTATTACCATGGTGATGCGGTTTTGGCAGTA
CATCAATGGGCGTGGATAGCGGTTTGACTCACGGGGATTTCCAAGTCTCCACCCCATTGACGTCAATGGGAGTTTGTTTT
GGCACCAAAATCAACGGGACTTTCCAAAATGTCGTAACAACTCCGCCCCATTGACGCAAATGGGCGGTAGGCGTGTACGG
TGGGAGGTCTATATAAGCAGAGCTCTCTGGCTAACTAGAGAACCCACTGCTTACTGGCTTATCGAAATTAATACGACTCA
CTATAGGGAGACCCAAGCTGTTAACG

Appendix 3

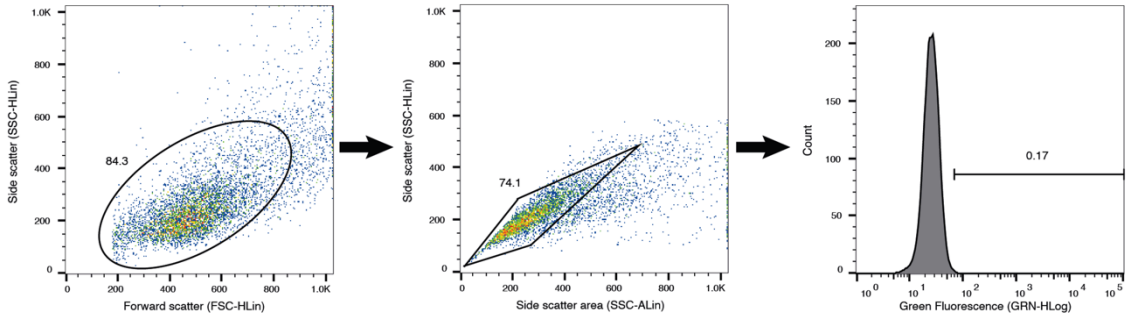

Appendix-3: Gating strategy used to analyse EIV-infected E.Derm in flow cytometry experiment. The scatter plots and density plot show from left to right the gates used to distinguish viable E.Derm (FSC-H/SSC-H), singlet (SCC-A/SSC-H), and GFP+ cells in mock-infected condition. The percentage on gated cells is given on each of the three plots.

Appendix 4

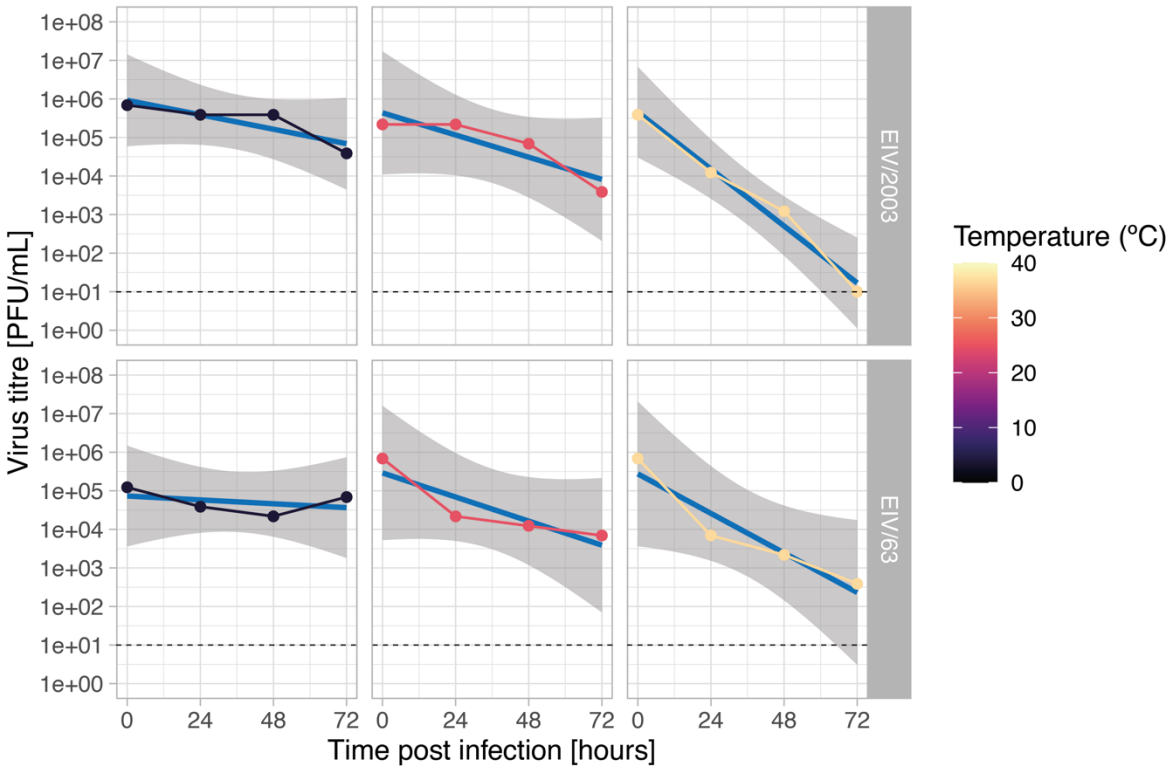

Appendix-4: Kinetics of viral decay in maintenance media. EIV/63 and EIV/2003 infectious viral particles were quantified in maintenance media following an incubation of 24, 48, and 72 hours at either 4ºC, 20ºC, or 37ºC. Incubation temperature is shown following a black-purple-yellow gradient, while linear regression is displayed as a blue line with a grey 95%CI.

Appendix 5

```
# R Code use to analyse RNAseq files obtained following: FastQC/TopHat2/Bowtie2/HTseq steps.
# First specify the packages of interest.
packages = c("readr", "edgeR","lme4","dplyr","DHARMa")

# Now load or install&load all.
package.check <- lapply(
  packages,
  FUN = function(x) {
    if (!require(x, character.only = TRUE)) {
      install.packages(x, dependencies = TRUE)
      library(x, character.only = TRUE)
    }
  }
)

# Pairwise analysis.
# This code starts by loading counts files needed for this specific comparison (Cdt1 VS Cdt2).
myfiles=c("Cdt1_A.count", "Cdt1_B.count", "Cdt1_C.count", "Cdt2_A.count", "Cdt2_B.count", "Cdt2_C.count")
myclass=c("Cdt1", "Cdt1", "Cdt1", "Cdt2", "Cdt2", "Cdt2", "Cdt2")
mylabel=c("Cdt1_A", "Cdt1_B", "Cdt1_C", "Cdt2_A", "Cdt2_B", "Cdt2_C")
cbind(myfiles, myclass, mylabel)

# /!\ header = FALSE is madatory to keep the first line in this table.
data=readDGE (files=myfiles, group=myclass, labels=mylabel, header = FALSE)

# Next step is to remove the summary lines readDGE is inserting.
# These 5 lines at the end of "data" file are all starting by "_" character.
# So here, we will call these lines by 'grep', and overwrite "data" object skipping these lines.
ToRemove=grepl ("_", rownames(data$counts), )
data=data[!ToRemove, ]

# At this step, we are exporting our table as a .csv file as following.
# FilePath will be the path leading to working directory in which output will be saved.
setwd(paste("~/FilePath/", DirLabel, sep=""))
write.csv(as.matrix(data), file="Cdt1_Cdt2_XHPI_READS.csv")
setwd("~/FilePath")

# Now, we can import the just exported file.
setwd(paste("~/FilePath/", DirLabel,sep=""))
Dataset_Cdt1_Cdt2_XHPI=read.csv("Cdt1_Cdt2_XHPI_READS.csv")
setwd("~/FilePath")

# Here, we will transform the matrix object a wee bit.
# Removing the first column (ENSEMBL_ID):
Dataset_Cdt1_Cdt2_XHPI.1=Dataset_Cdt1_Cdt2_XHPI[, -1]

# Creatign list corresponding to sample condition:
samplescondition=c(rep("Cdt1", 3), rep("Cdt2", 3))

# Naming individual replicates:
samplesshortname=c("Cdt1_A", "Cdt1_B", "Cdt1_C", "Cdt2_A", "Cdt2_B", "Cdt2_C")

# Name matrix's rows by ENSEMBL_ID, and columns by Condition$Replicate_Number.
rownames(Dataset_Cdt1_Cdt2_XHPI.1)=Dataset_Cdt1_Cdt2_XHPI[, 1]
colnames(Dataset_Cdt1_Cdt2_XHPI.1)=samplesshortname

# So far, we are working with all reads, but some could be artefactuals.
# We removed reads count < 1 Counts Per Millions (CPM).
ToKeep=rowSums(cpm(Dataset_Cdt1_Cdt2_XHPI.1)>1) >=3
Dataset_Cdt1_Cdt2_XHPI.1=Dataset_Cdt1_Cdt2_XHPI.1[ToKeep, ]

# Create a DGEList object (edgeR's container for RNA-seq count data)
DGE_List=DGEList(counts=Dataset_Cdt1_Cdt2_XHPI.1, group= factor(samplescondition))

# Estimate normalization factors
DGE_List=calcNormFactors(DGE_List)
DGE_List=estimateCommonDisp(DGE_List)
DGE_List=estimateTrendedDisp(DGE_List)
DGE_List=estimateTagwiseDisp(DGE_List)

# Create a Biological coefficient of variation (BCV) and save it as a "Cdt1_Cdt2_XHPI_BCV.tiff".
setwd(paste("~/FilePath/", DirLabel,sep=""))
tiff(filename="Cdt1_Cdt2_XHPI_BCV.tiff", width = 1200, height = 1200, units = "px", res = 300, bg = "white", compression = "lzw")
plotBCV(d, ylim=c(0,1.5), xlim=c(0,15), col.trend = "blue")
dev.off()
setwd("~/FilePath")

# Exact PValue is calculated at this step.
Exact_Pvalue=exactTest(DGE_List, pair = c("Cdt1", "Cdt2"))
# TopTags function to present a tabular summary of the differential expression statistics.
tt=topTags(Exact_Pvalue, n=nrow(DGE_List))
# Inspect the depth and adjusted reads per million.
nc=cpm(DGE_List, normalized.lib.sizes=TRUE)
rn=rownames(tt$table)

# Export results as .csv file.
setwd(paste("~/FilePath/",DirLabel,sep=""))
write.csv(tt$table, file="Cdt1_Cdt2_XHPI_ALL_DEGs.csv")
setwd("~/FilePath")
# Apply a threshold (Qvalue < 0.05) for significance.
setwd(paste("~/FilePath/",DirLabel,sep=""))
Cdt1_Cdt2_XHPI_ALL_DEGs <- read.csv("Cdt1_Cdt2_XHPI_ALL_DEGs.csv")
Cdt1_Cdt2_XHPI_SIGN_DEGs <- filter(Cdt1_Cdt2_XHPI_ALL_DEGs, FDR < 0.05)
write.csv(Cdt1_Cdt2_XHPI_SIGN_DEGs, file="Cdt1_Cdt2_XHPI_SIGN_DEGs.csv")
setwd("~/FilePath")
```

Appendix 6

serotype	country	date	name
H3N8	Argentina	1985	Influenza A virus (A/equine/Cordoba/18/1985(H3N8))
H3N8	Austria	1992	Influenza A virus (A/equine/Austria/421/1992(H3N8))
H3N8	Brazil	1963	Influenza A virus (A/equine/Sao Paulo/6/1963(H3N8))
H3N8	Brazil	1969	Influenza A virus (A/equine/Sao Paulo/1/1969(H3N8))
H3N8	Brazil	2012/04	Influenza A virus (A/equine/Sao Paulo/1.19/2012(H3N8))
H3N8	Chile	04/05/1992	Influenza A virus (A/equine/Quillota/2/1992)
H3N8	Chile	10/01/2012	Influenza A virus (A/equine/Colina/2012)
H3N8	Chile	15/02/2018	Influenza A virus (A/equine/Santiago/TT10A/2018)
H3N8	Chile	15/02/2018	Influenza A virus (A/equine/Santiago/TT11A/2018)
H3N8	Chile	15/02/2018	Influenza A virus (A/equine/Santiago/TT13A/2018)
H3N8	Chile	15/02/2018	Influenza A virus (A/equine/Santiago/TT16A/2018)
H3N8	Chile	15/02/2018	Influenza A virus (A/equine/Santiago/TT1A/2018)
H3N8	Chile	15/02/2018	Influenza A virus (A/equine/Santiago/TT3A/2018)
H3N8	Chile	15/02/2018	Influenza A virus (A/equine/Santiago/TT5A/2018)
H3N8	Chile	15/02/2018	Influenza A virus (A/equine/Santiago/TT9A/2018)
H3N8	Chile	21/02/2018	Influenza A virus (A/equine/Curico/RO3B/2018)
H3N8	Chile	21/02/2018	Influenza A virus (A/equine/Curico/RO4B/2018)
H3N8	Chile	21/02/2018	Influenza A virus (A/equine/Curico/RO7B/2018)
H3N8	Chile	25/02/2018	Influenza A virus (A/equine/Concepcion/RO1C/2018)
H3N8	Chile	25/02/2018	Influenza A virus (A/equine/Concepcion/RO3C/2018)
H3N8	Chile	25/02/2018	Influenza A virus (A/equine/Concepcion/RO4C/2018)
H3N8	Chile	25/02/2018	Influenza A virus (A/equine/Concepcion/RO6C/2018)
H3N8	Chile	25/02/2018	Influenza A virus (A/equine/Concepcion/RO7C/2018)
H3N8	China	1994	Influenza A virus (A/equine/Qinghai/1/1994(H3N8))
H3N8	China	2007	Influenza A virus (A/equine/Xinjiang/3/2007(H3N8))
H3N8	China	2007	Influenza A virus (A/equine/Xinjiang/4/2007(H3N8))
H3N8	China	2013	Influenza A virus (A/equine/Xuzhou/01/2013 (H3N8))
H3N8	China	03/12/2007	Influenza A virus (A/equine/Huabei/1/2007(H3N8))
H3N8	China	28/10/2008	Influenza A virus (A/equine/Guangxi/1/2008(H3N8))
H3N8	China	23/04/2010	Influenza A virus (A/equine/Heilongjiang/1/2010(H3N8))
H3N8	China	05/01/2015	Influenza A virus (A/equine/China/Ulumuqi/2015)
H3N8	China	27/03/2017	Influenza A virus (A/donkey/Shandong/1/2017(H3N8))
H3N8	China	2007/11	Influenza A virus (A/equine/Xinjiang/1/2007(H3N8))
H3N8	China	2007/11	Influenza A virus (A/equine/Xinjiang/2/2007(H3N8))
H3N8	China	2007/11	Influenza A virus (A/equine/Xinjiang/3/2007(H3N8))
H3N8	China	2007/12	Influenza A virus (A/donkey/Xinjiang/5/2007(H3N8))
H3N8	China	2008/01	Influenza A virus (A/equine/Gansu/7/2008(H3N8))
H3N8	China	2008/02	Influenza A virus (A/equine/Inner Mongolia/8/2008(H3N8))
H3N8	China	2008/04	Influenza A virus (A/equine/Heilongjiang/10/2008(H3N8))
H3N8	China	2008/04	Influenza A virus (A/equine/Liaoning/9/2008(H3N8))
H3N8	China	2013/02	Influenza A virus (A/equine/Heilongjiang/SS1/2013(H3N8))
H3N8	France	1979	Influenza A virus (A/equine/Fontainebleau/1/1979(H3N8))
H3N8	Germany	1989	Influenza A virus (A/equine/Berlin/1/1989(H3N8))
H3N8	Italy	1991	Influenza A virus (A/equine/Italy/1062/1991(H3N8))
H3N8	Italy	1991	Influenza A virus (A/equine/Italy/824/1991(H3N8))

H3N8	Italy	1991	Influenza A virus (A/equine/Rome/5/1991(H3N8))
H3N8	Italy	1992	Influenza A virus (A/equine/Italy/1199/1992(H3N8))
H3N8	Japan	1971	Influenza A virus (A/equine/Sachiyama/1/1971(H3N8))
H3N8	Japan	1971	Influenza A virus (A/equine/Tokyo/2/1971(H3N8))
H3N8	Japan	2007	Influenza A virus (A/equine/Tottori/1/07(H3N8))
H3N8	Malaysia	28/08/2015	Influenza A virus (A/equine/Malaysia/1/2015)
H3N8	Mongolia	2007	Influenza A virus (A/Equus caballus/Arkhangai/1/2007)
H3N8	Mongolia	2007	Influenza A virus (A/Equus caballus/Arkhangai/2/2007)
H3N8	Mongolia	2007	Influenza A virus (A/Equus caballus/Tuv/3/2007)
H3N8	Mongolia	2007	Influenza A virus (A/Equus caballus/Tuv/4/2007)
H3N8	Mongolia	05/07/2011	Influenza A virus (A/Equus caballus/Ulaanbaatar/1/2011)
H3N8	Mongolia	05/07/2011	Influenza A virus (A/Equus caballus/Ulaanbaatar/2/2011)
H3N8	Mongolia	05/07/2011	Influenza A virus (A/Equus caballus/Ulaanbaatar/3/2011)
H3N8	Mongolia	05/07/2011	Influenza A virus (A/Equus caballus/Ulaanbaatar/4/2011)
H3N8	Mongolia	05/07/2011	Influenza A virus (A/Equus caballus/Ulaanbaatar/5/2011)
H3N8	Mongolia	05/07/2011	Influenza A virus (A/Equus caballus/Ulaanbaatar/6/2011)
H3N8	Mongolia	04/07/2013	Influenza A virus (A/Equus caballus/Ulaanbaatar/1201/2013)
H3N8	Mongolia	04/07/2013	Influenza A virus (A/Equus caballus/Ulaanbaatar/1202/2013)
H3N8	Mongolia	04/07/2013	Influenza A virus (A/Equus caballus/Ulaanbaatar/1203/2013)
H3N8	Romania	1980	Influenza A virus (A/equine/Romania/1/1980(H3N8))
H3N8	South Africa	1986	Influenza A virus (A/equine/Johannesburg/1/1986(H3N8))
H3N8	South Korea	01/07/2011	Influenza A virus (A/equine/Kyonggi/SA1/2011(H3N8))
H3N8	Switzerland	1979	Influenza A virus (A/equine/Switzerland/1118/1979(H3N8))
H3N8	Switzerland	1993	Influenza A virus (A/equine/Switzerland/173/1993(H3N8))
H3N8	Turkey	17/07/2013	Influenza A virus (A/equine/Ankara/1/2013(H3N8))
H3N8	UK	1989	Influenza A virus (A/equine/Rook/93753/1989(H3N8))
H3N8	UK	1989	Influenza A virus (A/equine/Sussex/1/1989(H3N8))
H3N8	UK	2003	Influenza A virus (A/equine/Newmarket/5/2003(H3N8))
H3N8	UK	18/08/2007	Influenza A virus (A/equine/Richmond/1/2007(H3N8))
H3N8	Uruguay	1963	Influenza A virus (A/equine/Uruguay/1/1963(H3N8))
H3N8	USA	1975	Influenza A virus (A/equine/New York/1/1975(H3N8))
H3N8	USA	1976	Influenza A virus (A/equine/Kentucky/bitter_boredom5/1976(H3N8))
H3N8	USA	1976	Influenza A virus (A/equine/Kentucky/pass_the_pepper1/1976(H3N8))
H3N8	USA	1978	Influenza A virus (A/equine/Kentucky/1/1978(H3N8))
H3N8	USA	1979	Influenza A virus (A/equine/New Market/1/1979(H3N8))
H3N8	USA	1979	Influenza A virus (A/equine/New Market/nasalwash1/1979(H3N8))
H3N8	USA	1980	Influenza A virus (A/equine/California/1/1980(H3N8))
H3N8	USA	1980	Influenza A virus (A/equine/Kentucky/2/1980(H3N8))
H3N8	USA	1980	Influenza A virus (A/equine/Kentucky/4/1980(H3N8))
H3N8	USA	1981	Influenza A virus (A/equine/Georgia/1/1981(H3N8))
H3N8	USA	1981	Influenza A virus (A/equine/Georgia/10/1981(H3N8))
H3N8	USA	1981	Influenza A virus (A/equine/Georgia/13/1981(H3N8))
H3N8	USA	1981	Influenza A virus (A/equine/Georgia/3/1981(H3N8))
H3N8	USA	1981	Influenza A virus (A/equine/Georgia/9/1981(H3N8))
H3N8	USA	1981	Influenza A virus (A/equine/Kentucky/1/1981(H3N8))
H3N8	USA	1981	Influenza A virus (A/equine/Kentucky/2/1981(H3N8))
H3N8	USA	1981	Influenza A virus (A/equine/Kentucky/3/1981(H3N8))
H3N8	USA	1981	Influenza A virus (A/equine/Kentucky/Rosie100/1981(H3N8))
H3N8	USA	1981	Influenza A virus (A/equine/Kentucky/magnificent_genius1/1981(H3N8))
H3N8	USA	1982	Influenza A virus (A/equine/California/103/1982(H3N8))

H3N8	USA	1982	Influenza A virus (A/equine/California/83/1982(H3N8))
H3N8	USA	1983	Influenza A virus (A/equine/New York/VR-297/1983(H3N8))
H3N8	USA	1985	Influenza A virus (A/equine/Santa Fe/1/1985(H3N8))
H3N8	USA	1986	Influenza A virus (A/equine/Kentucky/1/1986(H3N8))
H3N8	USA	1986	Influenza A virus (A/equine/Kentucky/2/1986(H3N8))
H3N8	USA	1986	Influenza A virus (A/equine/Kentucky/3/1986(H3N8))
H3N8	USA	1986	Influenza A virus (A/equine/Tennessee/5/1986(H3N8))
H3N8	USA	1987	Influenza A virus (A/equine/Kentucky/1/1987(H3N8))
H3N8	USA	1987	Influenza A virus (A/equine/Kentucky/2/1987(H3N8))
H3N8	USA	1988	Influenza A virus (A/equine/Kentucky/692/1988(H3N8))
H3N8	USA	1988	Influenza A virus (A/equine/Kentucky/694/1988(H3N8))
H3N8	USA	1988	Influenza A virus (A/equine/Kentucky/698/1988(H3N8))
H3N8	USA	1990	Influenza A virus (A/equine/Kentucky/1277/1990(H3N8))
H3N8	USA	1991	Influenza A virus (A/equine/Alaska/29759/1991(H3N8))
H3N8	USA	1991	Influenza A virus (A/equine/Kentucky/1/1991(H3N8))
H3N8	USA	1991	Influenza A virus (A/equine/Texas/39655/1991(H3N8))
H3N8	USA	1992	Influenza A virus (A/equine/Kentucky/1/1992(H3N8))
H3N8	USA	1994	Influenza A virus (A/equine/Kentucky/8/1994(H3N8))
H3N8	USA	1997	Influenza A virus (A/equine/California/4537/1997(H3N8))
H3N8	USA	2002	Influenza A virus (A/equine/California/8560/2002(H3N8))
H3N8	USA	2002	Influenza A virus (A/equine/Kentucky/5/2002(H3N8))
H3N8	USA	2003	Influenza A virus (A/equine/Wisconsin/1/03(H3N8))
H3N8	USA	2011	Influenza A virus (A/equine/Florida/146609/2011(H3N8))
H3N8	USA	2012	Influenza A virus (A/equine/Oregon/78356/2012(H3N8))
H3N8	USA	2016	Influenza A virus (A/equine/Georgia/121362-16/2016(H3N8))
H3N8	USA	2016	Influenza A virus (A/equine/New York/135857/2016(H3N8))
H3N8	USA	2018	Influenza A virus (A/Equus caballus/USA/149632/2018)
H3N8	USA	2018	Influenza A virus (A/Equus caballus/USA/154390/2018)
H3N8	USA	21/10/2014	Influenza A virus (A/equine/Tennessee/27A/2014(H3N8))
H3N8	USA	21/10/2014	Influenza A virus (A/equine/Tennessee/28A/2014(H3N8))
H3N8	USA	21/10/2014	Influenza A virus (A/equine/Tennessee/28B/2014(H3N8))
H3N8	USA	21/10/2014	Influenza A virus (A/equine/Tennessee/29A/2014(H3N8))
H3N8	USA	21/10/2014	Influenza A virus (A/equine/Tennessee/4A/2014(H3N8))
H3N8	USA	28/08/2018	Influenza A virus (A/Equus caballus/USA/154390/2018)
H3N8	USA	11/12/2018	Influenza A virus (A/Equus ferus caballus/USA/218776/2018)
H3N8	USA	27/03/2019	Influenza A virus (A/Equus ferus caballus/USA/48519/2019)
H3N8	USA	30/03/2019	Influenza A virus (A/Equus ferus caballus/USA/51053/2019)
H3N8	USA	03/04/2019	Influenza A virus (A/Equus ferus caballus/USA/53954/2019)
H3N8	USA	25/04/2019	Influenza A virus (A/Equus ferus caballus/USA/72778/2019)
H3N8	USA	08/05/2019	Influenza A virus (A/Equus ferus caballus/USA/82889/2019)
H3N8	USA	25/09/2019	Influenza A virus (A/Equus ferus caballus/USA/176576/2019)

Appendix 7

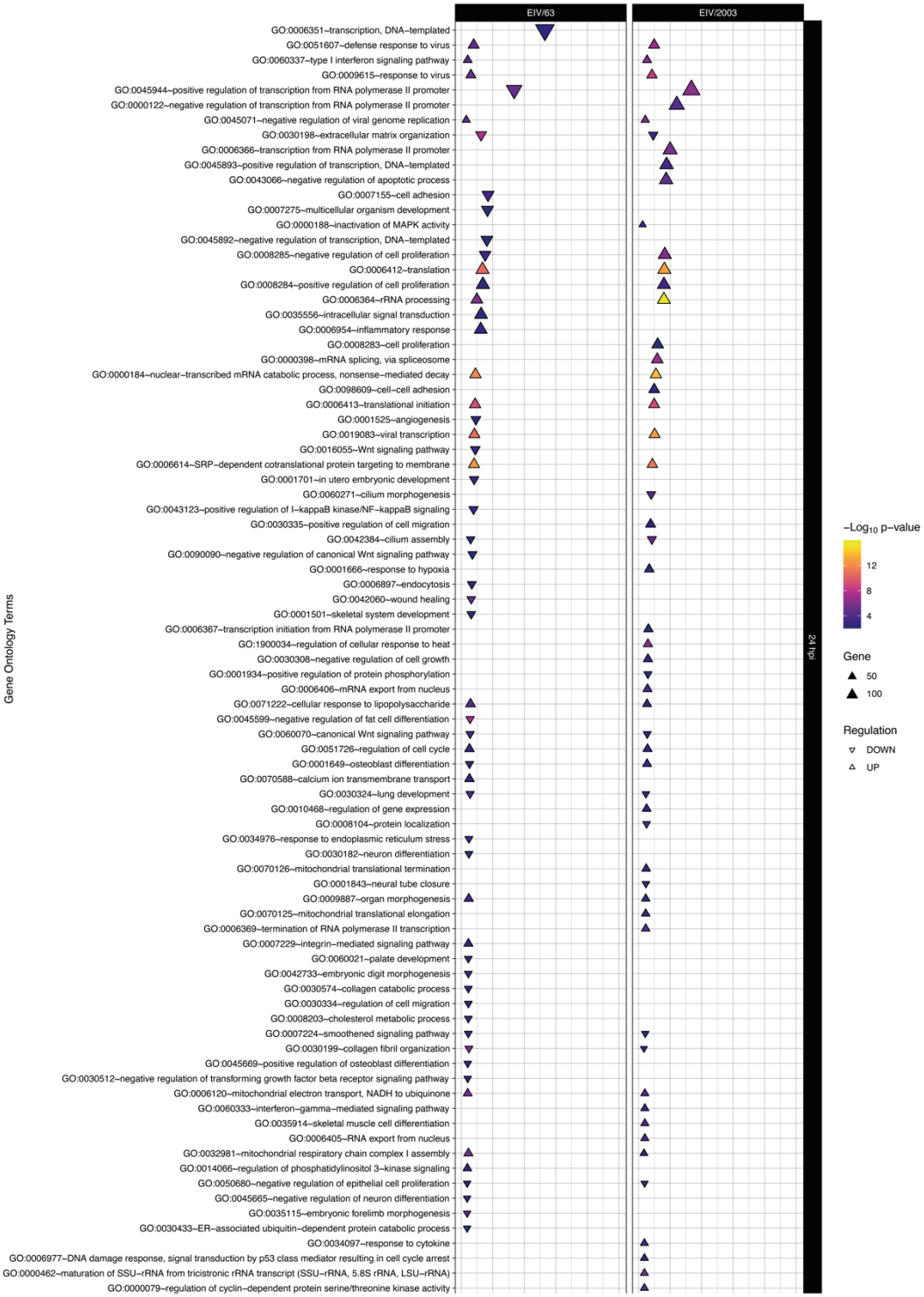
EIV/63
EIV/2003
24 hpi
Gene Ontology Terms
GO:0006351~transcription, DNA~templated
GO:0051607~defense response to virus
GO:0060337~type I interferon signaling pathway
GO:0009615~response to virus
GO:0045944~positive regulation of transcription from RNA polymerase II promoter
GO:0000122~negative regulation of transcription from RNA polymerase II promoter
GO:0045071~negative regulation of viral genome replication
GO:0030198~extracellular matrix organization
GO:0006366~transcription from RNA polymerase II promoter
GO:0045893~positive regulation of transcription, DNA~templated
GO:0043066~negative regulation of apoptotic process
GO:0007155~cell adhesion
GO:0007275~multicellular organism development
GO:0000188~inactivation of MAPK activity
GO:0045892~negative regulation of transcription, DNA~templated
GO:0008285~negative regulation of cell proliferation
GO:0006412~translation
GO:0008284~positive regulation of cell proliferation
GO:0006364~rRNA processing
GO:0035556~intracellular signal transduction
GO:0006954~inflammatory response
GO:0008283~cell proliferation
GO:0000398~mRNA splicing, via spliceosome
GO:0000184~nuclear~transcribed mRNA catabolic process, nonsense~mediated decay
GO:0098609~cell~cell adhesion
GO:0006413~translational initiation
GO:0001525~angiogenesis
GO:0019083~viral transcription
GO:0016055~Wnt signaling pathway
GO:0006614~SRP~dependent cotranslational protein targeting to membrane
GO:0001701~in utero embryonic development
GO:0060271~cilium morphogenesis
GO:0043123~positive regulation of I~kappaB kinase/NF~kappaB signaling
GO:0030335~positive regulation of cell migration
GO:0042384~cilium assembly
GO:0090090~negative regulation of canonical Wnt signaling pathway
GO:0001666~response to hypoxia
GO:0006897~endocytosis
GO:0042060~wound healing
GO:0001501~skeletal system development
GO:0006367~transcription initiation from RNA polymerase II promoter
GO:1900034~regulation of cellular response to heat
GO:0030308~negative regulation of cell growth
GO:0001934~positive regulation of protein phosphorylation
GO:0006406~mRNA export from nucleus
GO:0071222~cellular response to lipopolysaccharide
GO:0045599~negative regulation of fat cell differentiation
GO:0060070~canonical Wnt signaling pathway
GO:0051726~regulation of cell cycle
GO:0001649~osteoblast differentiation
GO:0070588~calcium ion transmembrane transport
GO:0030324~lung development
GO:0010468~regulation of gene expression
GO:0008104~protein localization
GO:0034976~response to endoplasmic reticulum stress
GO:0030182~neuron differentiation
GO:0070126~mitochondrial translational termination
GO:0001843~neural tube closure
GO:0009887~organ morphogenesis
GO:0070125~mitochondrial translational elongation
GO:0006369~termination of RNA polymerase II transcription
GO:0007229~integrin~mediated signaling pathway
GO:0060021~palate development
GO:0042733~embryonic digit morphogenesis
GO:0030574~collagen catabolic process
GO:0030334~regulation of cell migration
GO:0008203~cholesterol metabolic process
GO:0007224~smoothened signaling pathway
GO:0030199~collagen fibril organization
GO:0045669~positive regulation of osteoblast differentiation
GO:0030512~negative regulation of transforming growth factor beta receptor signaling pathway
GO:0006120~mitochondrial electron transport, NADH to ubiquinone
GO:0060333~interferon~gamma~mediated signaling pathway
GO:0035914~skeletal muscle cell differentiation
GO:0006405~RNA export from nucleus
GO:0032981~mitochondrial respiratory chain complex I assembly
GO:0014066~regulation of phosphatidylinositol 3~kinase signaling
GO:0050680~negative regulation of epithelial cell proliferation
GO:0045665~negative regulation of neuron differentiation
GO:0035115~embryonic forelimb morphogenesis
GO:0030433~ER~associated ubiquitin~dependent protein catabolic process
GO:0034097~response to cytokine
GO:0006977~DNA damage response, signal transduction by p53 class mediator resulting in cell cycle arrest
GO:0000462~maturation of SSU~rRNA from tricistronic rRNA transcript (SSU~rRNA, 5.8S rRNA, LSU~rRNA)
GO:0000079~regulation of cyclin~dependent protein serine/threonine kinase activity
−Log10 p−value
12
8
4
Gene
50
100
Regulation
DOWN
UP

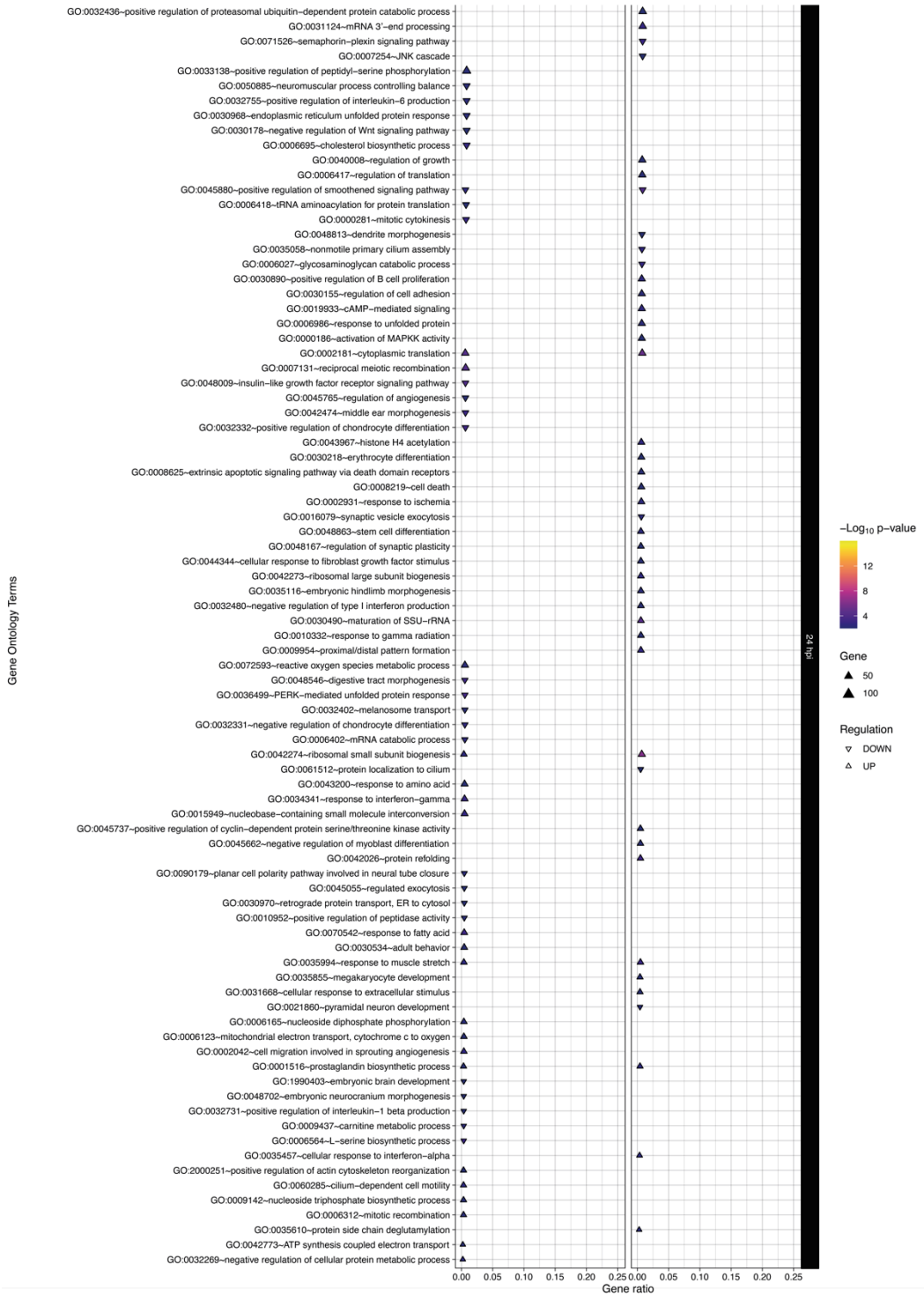

Appendix-7: Gene ontology (GO) terms in cells infected with EIV/63 or EIV/2003. Significantly upregulated and downregulated GO terms are displayed as triangles or inverted triangles, respectively. The size of each triangle represents the number of DEGs fitting the specified GO term, while the ratio of total genes involved in each category is displayed on the x-axis. Triangles are coloured according to a blue-red-yellow gradient representing the enrichment significance (-Log_{10} p-value).

Appendix 8

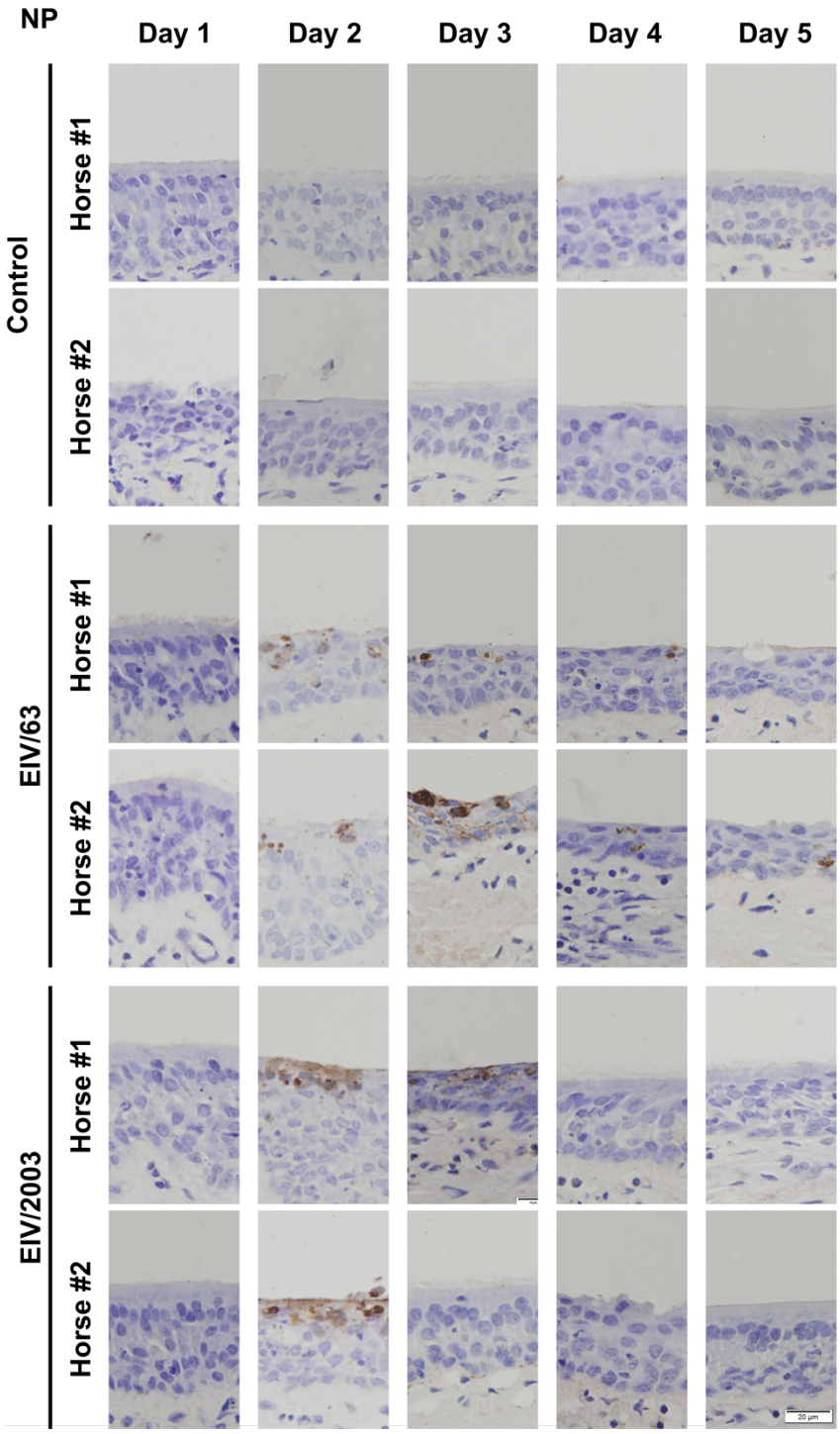

Appendix-8: Tissue distribution and kinetics of EIV/63 and EIV/2003 infected cells in equine tracheal explants. Representative images of histological sections of equine tracheal explants infected with EIV/63, EIV/2003, or mock-infected at day 1—5 pi were immunostained with an anti-NP antibody. Equine tracheal explants from two distinct individuals were used for each infection.

Appendix 9

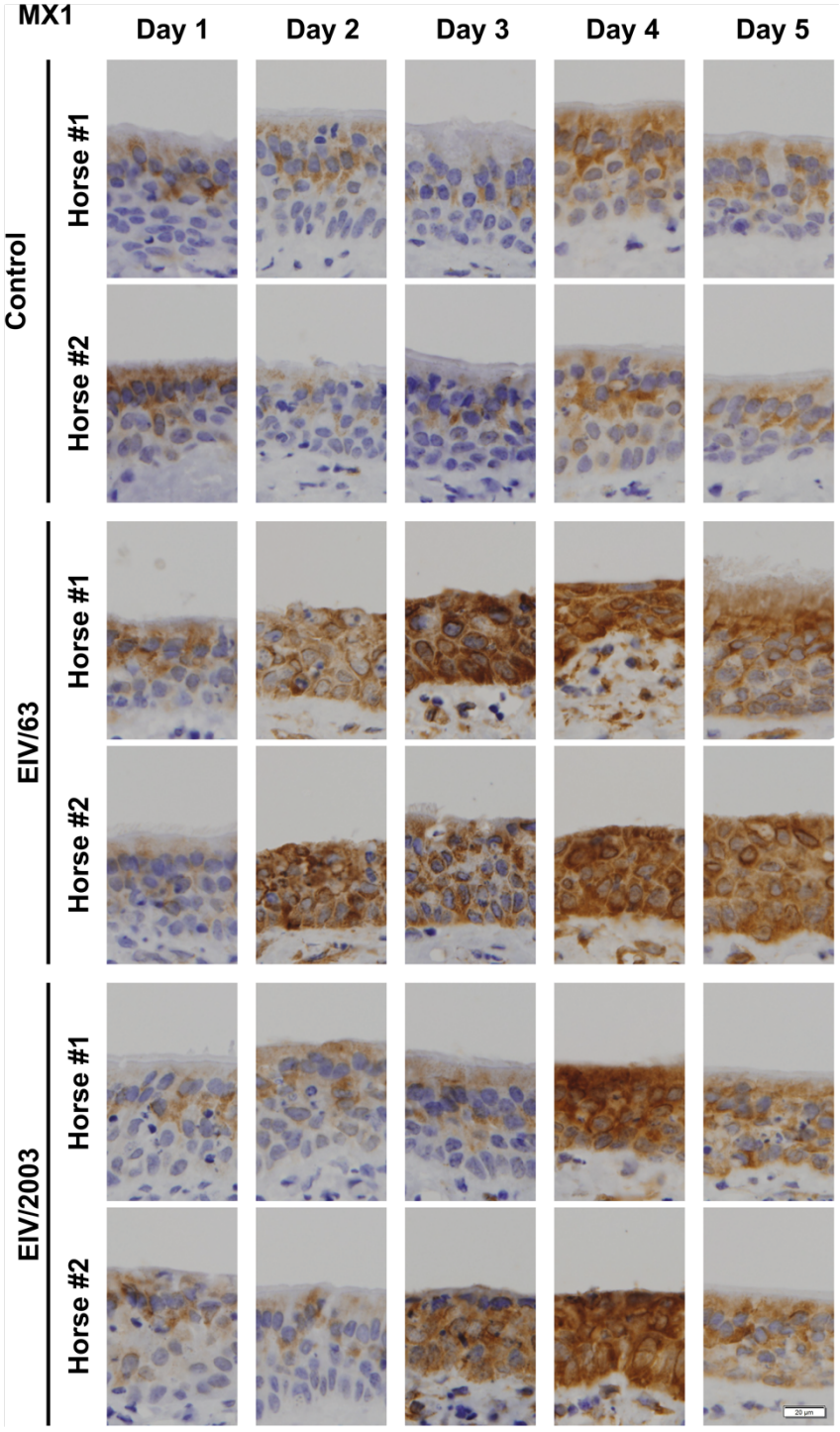

Appendix-9: Kinetics of EIV/63 and EIV/2003-induced cellular response to infection. Representative images of histological sections of equine tracheal explants infected with EIV/63, EIV/2003, or mock-infected at day 1—5 pi were immunostained using an anti-MX antibody. Equine tracheal explants from two distinct individuals were used for each infection.

Appendix 10

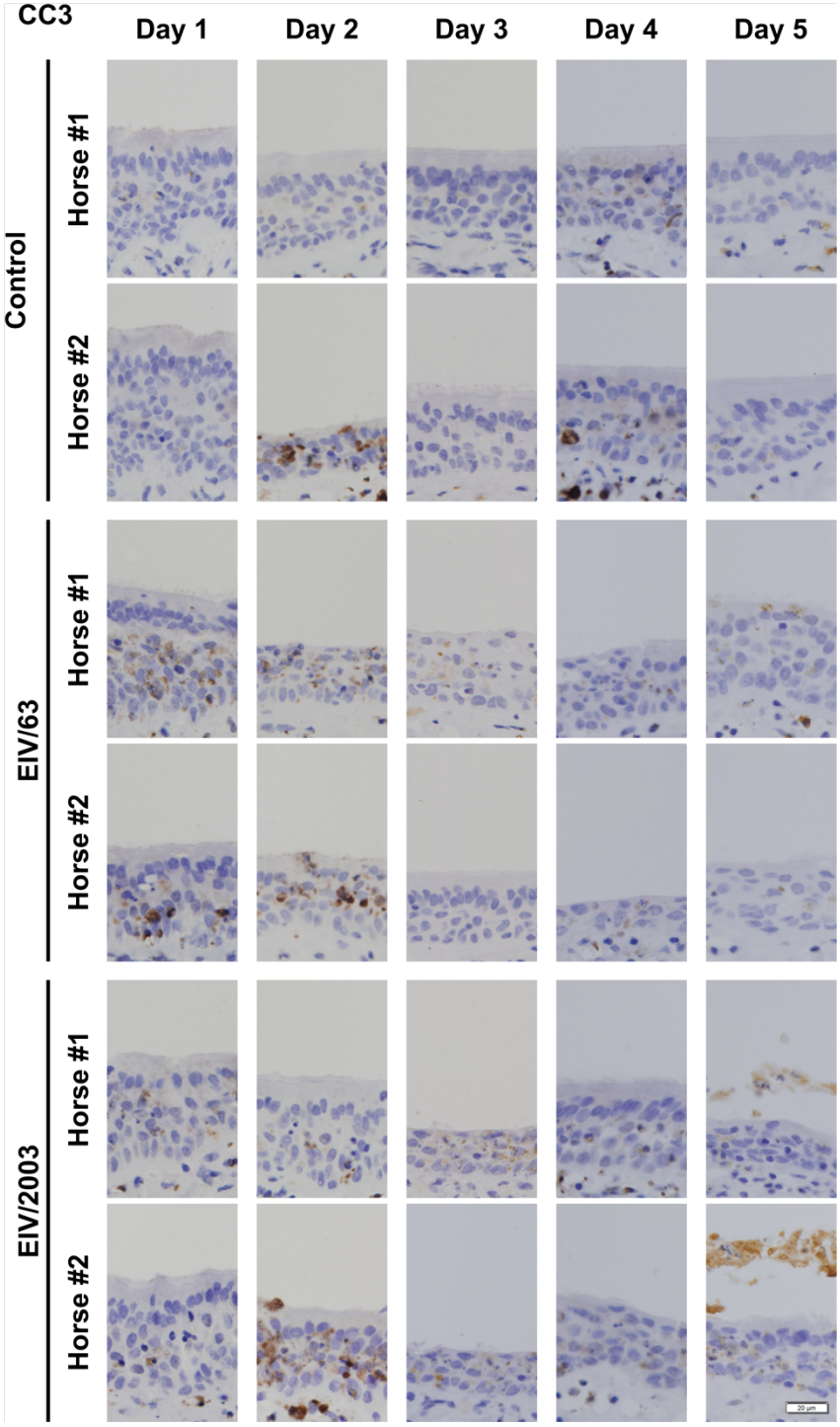

Appendix-10: Kinetics of EIV/63 and EIV/2003-induced programmed cell death. Representative images of histological sections of equine tracheal explants infected with EIV/63, EIV/2003, or mock-infected at day 1—5 pi were immunostained using an anti-CC3 antibody, a marker of cellular apoptosis. Equine tracheal explants from two distinct individuals were used for each infection.

Appendix 11

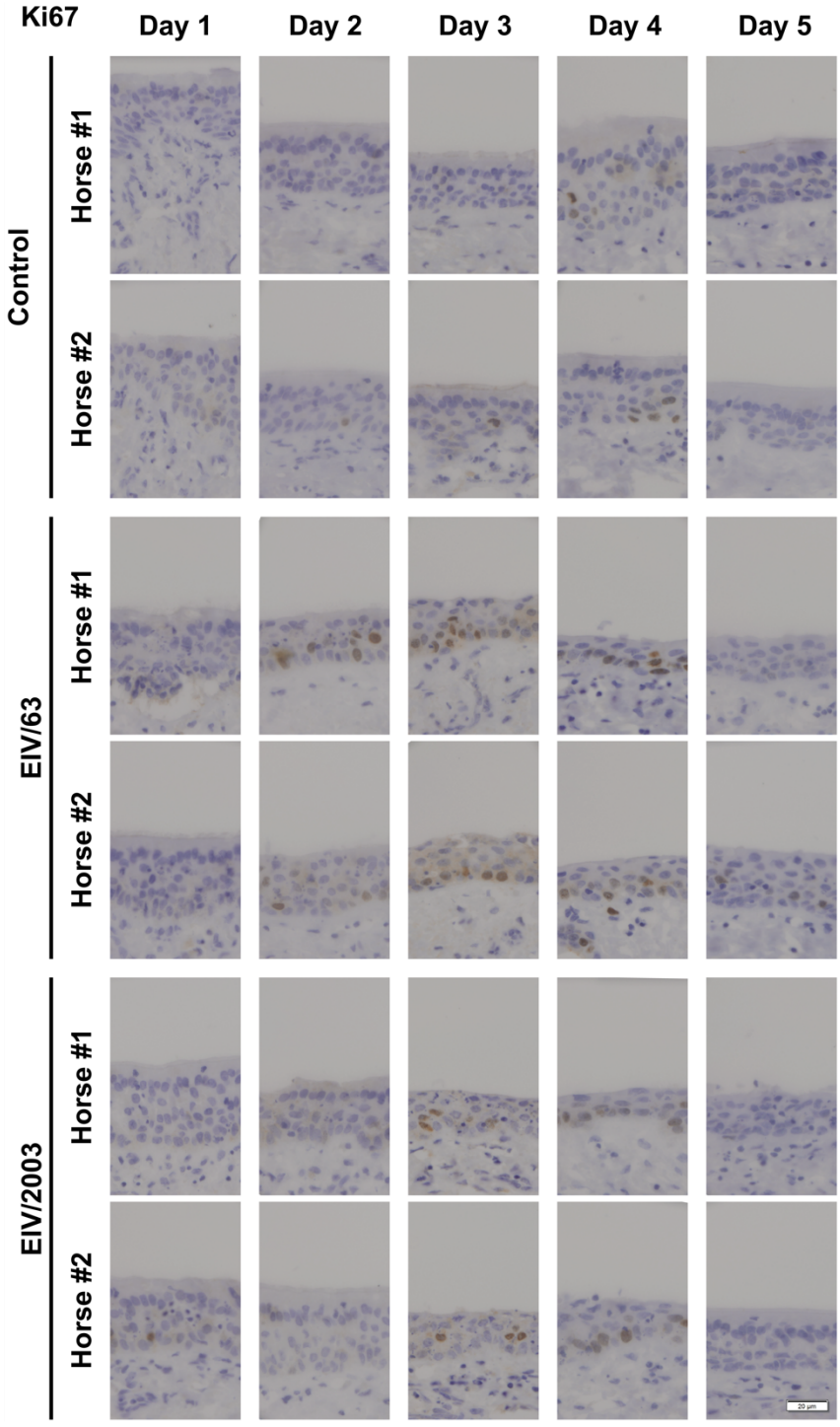

Appendix-11: Kinetics tissue regeneration following EIV/63 or EIV/2003 infection. Representative images of histological sections of equine tracheal explants infected with EIV/63, EIV/2003, or mock-infected at day 1—5 pi were immunostained using an anti-Ki67 antibody, used as a marker of active cell proliferation. Equine tracheal explants from two distinct individuals were used for each infection.

Appendix 12

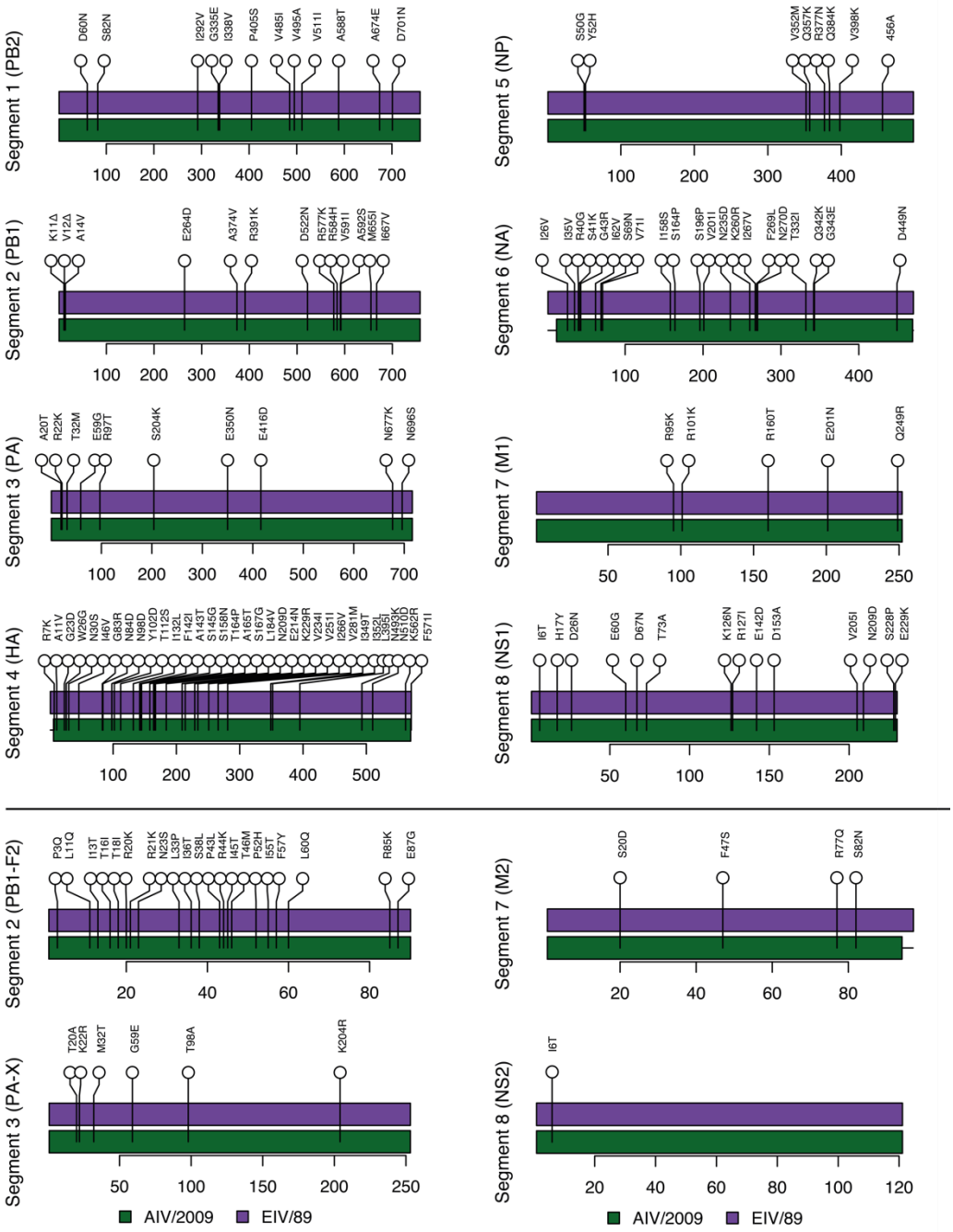

Appendix 12: AIV/2009 and EIV/89 nonsynonymous mutations cartography. Lollipop plots showing the location and nature of amino acid mutations between AIV/2009 (green) and EIV/89 (purple) in each of EIV genomic segments. Individual CDS were investigated and labelled as Segment (corresponding CDS). The first amino acid in the nomenclature corresponds to AIV/2009, while the last corresponds to EIV/89, and the number in between corresponds to amino acid position starting from the initiating methionine. Additionally, the length of each segment represents the CDS from the initiating methionine to stop codon. Scales underneath each of the lollipop plots reflect amino acid positions.

Appendix 13

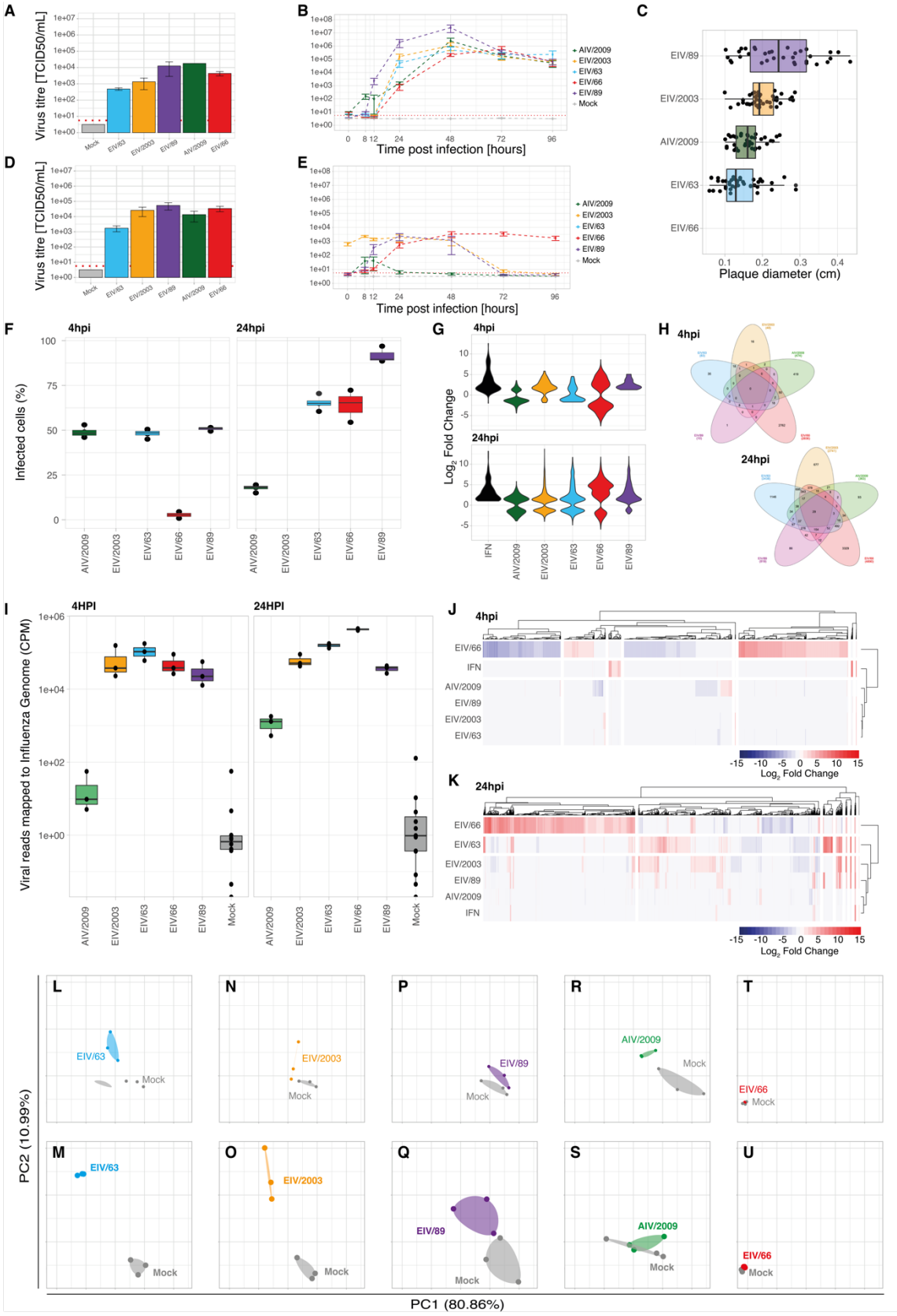
A
Virus titre [TCID50/mL]
Mock
EIV/63
EIV/2003
EIV/89
AIV/2009
EIV/66
B
Time post infection [hours]
AIV/2009
EIV/2003
EIV/63
EIV/66
EIV/89
Mock
C
EIV/89
EIV/2003
AIV/2009
EIV/63
EIV/66
Plaque diameter (cm)
D
Virus titre [TCID50/mL]
E
Time post infection [hours]
F
4hpi
24hpi
Infected cells (%)
G
4hpi
24hpi
Log2 Fold Change
IFN
H
4hpi
24hpi
I
4HPI
24HPI
Viral reads mapped to Influenza Genome (CPM)
J
4hpi
K
24hpi
Log2 Fold Change
L
N
P
R
T
M
O
Q
S
U
PC2 (10.99%)
PC1 (80.86%)

Appendix 12: Summary of data presented in this thesis. (A) Viral titre of inocula used in the experimental infections of MDCK cells. **(B)** Growth kinetics of EIV/63, EIV/66, EIV/89, EIV/2003 and AIV/2009 in MDCK cells. Viral titres are represented as the mean ± SEM. **(C)** Plaque phenotype of EIV/63, EIV/66, EIV/89, EIV/2003 and AIV/2009 in MDCK cells measured at 48 hpi. The mean of at least 40 plaques were measured for each condition. **(D)** Viral titre of inocula used in the experimental infections of E.Derm cells. **(E)** Growth kinetics of EIV/63, EIV/66, EIV/89, EIV/2003 and AIV/2009 in E.Derm cells. Viral titres are represented as the mean ± SEM. **(F)** Percentage of EIV/63, EIV/66, EIV/89, EIV/2003, AIV/2009, and mock-infected cells obtained from flow cytometry analysis of E.Derm cells immunostained with anti-NP. **(G)** Violin plots of DEGs identified in E.Derm cells infected with EIV/63, EIV/66, EIV/89, EIV/2003 or AIV/2009 at 4 hpi (top), and 24 hpi (bottom). **(H)** DEGs distribution between EIV/63, EIV/66, EIV/89, EIV/2003 or AIV/2009-infected cells at 4 hpi (top) and 24 hpi (bottom). The number of DEGs for each subset is shown within each compartment of the Venn diagram. **(I)** Viral segments (8) were concatenated, and sequencing reads mapped to them (*i.e.* EIV/63, EIV/66, EIV/89, EIV/2003 or AIV/2009). Mapped viral read numbers were normalised to the total number of reads in each sample and expressed as counts per million (CPM) at 4 hpi (left), and 24 hpi (right). **(J—K)** Heatmap of DEGs induced by EIV/63, EIV/66, EIV/89, EIV/2003 or AIV/2009 at 4 hpi (J) and 24 hpi (K). Gene expression is displayed in $\log_2$ FC and shown following a blue-white-red colour scale, while dendrograms displayed in black showed either row (right) or column (top) relationship based on gene expression profile. **(L—U)** Principal component analysis of EIV/63, EIV/66, EIV/89, EIV/2003 and AIV/2009 infectomes in which conditions and timepoints investigated were plotted individually for readability. In all the plots EIV/63, EIV/66, EIV/89, EIV/2003 or AIV/2009 infections are shown in cyan, red, purple, orange, and green, respectively, while non-infected controls are shown in grey. All the experiments presented here were performed three times independently.

References

Abdelrahman, Z., Chen, Z., Lyu, H. and Wang, X. (2021). Comparisons of the immunological landscape between COVID-19, influenza, and respiratory syncytial virus patients by clustering analysis. *Computational and Structural Biotechnology Journal*, 19.

Afonso, C.L. (2021). Virulence during newcastle disease viruses cross species adaptation. *Viruses*, 13(1).

Ali, A., Avalos, R.T., Ponimaskin, E. and Nayak, D.P. (2000). Influenza Virus Assembly: Effect of Influenza Virus Glycoproteins on the Membrane Association of M1 Protein. *Journal of Virology*, 74(18).

Alizon, S. and Michalakis, Y. (2015). Adaptive virulence evolution: The good old fitness-based approach. *Trends in Ecology and Evolution*, 30(5).

Allen, I.C., Scull, M.A., Moore, C.B., Holl, E.K., Mcelvania-TeKippe, E., Taxman, D.J., Guthrie, E.H., Pickles, R.J. and Ting, Jenny, P. (2009). The NLRP3 Inflammasome Mediates in vivo Innate Immunity to Influenza A Virus through Recognition of Viral RNA. *Immunity*, 30(4), pp.556–565.

Anders, S., Pyl, P.T. and Huber, W. (2015). HTSeq-A Python framework to work with high-throughput sequencing data. *Bioinformatics*, 31(2), pp.166–169.

Andrews, S. (2010). FastQC - A quality control tool for high throughput sequence data. http://www.bioinformatics.babraham.ac.uk/projects/fastqc/. *Babraham Bioinformatics*, 2010.

Antonny, B. et al. (2016). Membrane fission by dynamin: what we know and what we need to know. *The EMBO Journal*, 35(21).

Bao, Y., Bolotov, P., Dernovoy, D., Kiryutin, B., Zaslavsky, L., Tatusova, T., Ostell, J. and Lipman, D. (2008). The Influenza Virus Resource at the National Center for Biotechnology Information. *Journal of Virology*, 82(2).

Barber, M.R.W., Aldridge, J.R., Webster, R.G. and Magor, K.E. (2010). Association of RIG-I with innate immunity of ducks to influenza. *Proceedings of the National Academy of Sciences of the United States of America*, 107(13).

Barman, S. and Nayak, D.P. (2007). Lipid Raft Disruption by Cholesterol Depletion Enhances Influenza A Virus Budding from MDCK Cells. *Journal of Virology*, 81(22).

Barone, R. (1984). *Anatomie comparée des mammifères domestiques . 3 1, Splanchnologie Appareil digestif, appareil respiratoire / Robert Barone*. 2e éd. Paris: Vigot.

Barr, T.A., Brown, S., Ryan, G., Zhao, J. and Gray, D. (2007). TLR-mediated stimulation of APC: Distinct cytokine responses of B cells and dendritic cells. *European Journal of Immunology*, 37(11).

Bates, D., Mächler, M., Bolker, B.M. and Walker, S.C. (2015). Fitting linear mixed-effects models using lme4. *Journal of Statistical Software*, 67(1).

Beijerinck, M. (1898). Ueber ein Contagium vivurn fluidum als Ursaehe der Fleekenkrankheit der Tabaksblätter. *Verhandelingen der Koninklijke Akademie van*

Wetenschappen te Amsterdam, 6(5), pp.3–21.

Binns, M.M., Daly, J.M., Chirnside, E.D., Mumford, J.A., Wood, J.M., Richards, C.M. and Daniels, R.S. (1993). Genetic and antigenic analysis of an equine influenza H 3 isolate from the 1989 epidemic. *Archives of Virology*, 130(1–2).

Biswas, S.K. and Nayak, D.P. (1994). Mutational analysis of the conserved motifs of influenza A virus polymerase basic protein 1. *Journal of Virology*, 68(3).

Bitsikas, V., Corrêa, I.R. and Nichols, B.J. (2014). Clathrin-independent pathways do not contribute significantly to endocytic flux. *eLife*, 2014(3).

Blass, D., Patzelt, E. and Kuechler, E. (1982). Identification of the cap binding protein of influenza virus. *Nucleic Acids Research*, 10(15).

Bogunovic, D. et al. (2012). Mycobacterial disease and impaired IFN-γ immunity in humans with inherited ISG15 deficiency. *Science*, 337(6102).

Bogunovic, D., Boisson-Dupuis, S. and Casanova, J.L. (2013). ISG15: Leading a double life as a secreted molecule. *Experimental and Molecular Medicine*, 45(4).

Bolte, H., Rosu, M.E., Hagelauer, E., García-Sastre, A. and Schwemmle, M. (2019). Packaging of the Influenza Virus Genome Is Governed by a Plastic Network of RNA- and Nucleoprotein-Mediated Interactions. *Journal of Virology*, 93(4).

Botos, I., Liu, L., Wang, Y., Segal, D.M. and Davies, D.R. (2009). The Toll-like receptor 3:dsRNA signaling complex. *Biochimica et Biophysica Acta - Gene Regulatory Mechanisms*, 1789(9–10).

Botos, I., Segal, D.M. and Davies, D.R. (2011). The structural biology of Toll-like receptors. *Structure*, 19(4).

Bouwstra, R., Gonzales, J.L., de Wit, S., Stahl, J., Fouchier, R.A.M. and Elbers, A.R.W. (2017). Risk for low pathogenicity avian influenza virus on poultry farms, The Netherlands, 2007–2013. *Emerging Infectious Diseases*, 23(9).

Brach, T., Godlee, C., Moeller-Hansen, I., Boeke, D. and Kaksonen, M. (2014). The initiation of clathrin-mediated endocytosis is mechanistically highly flexible. *Current Biology*, 24(5).

Brass, A.L., Huang, I.C., Benita, Y., John, S.P., Krishnan, M.N., Feeley, E.M., Ryan, B.J., Weyer, J.L., van der Weyden, L., Fikrig, E., Adams, D.J., Xavier, R.J., Farzan, M. and Elledge, S.J. (2009). The IFITM Proteins Mediate Cellular Resistance to Influenza A H1N1 Virus, West Nile Virus, and Dengue Virus. *Cell*, 139(7).

Brisse, M. and Ly, H. (2019). Comparative structure and function analysis of the RIG-I-like receptors: RIG-I and MDA5. *Frontiers in Immunology*, 10.

British Horse Association. (2022). *Equine influenza in British racing, all you need to know*. Available from: https://www.britishhorseracing.com/regulation/equine-influenza-update/.

Broggi, A., Tan, Y., Granucci, F. and Zanoni, I. (2017). IFN-λ suppresses intestinal inflammation by non-translational regulation of neutrophil function. *Nature Immunology*, 18(10).

Bruce, E.A., Digard, P. and Stuart, A.D. (2010). The Rab11 Pathway Is Required for Influenza A Virus Budding and Filament Formation. *Journal of Virology*, 84(12).

Budras, K.D., Sack, W.O., Rock, S., Horowitz, A. and Berg, R. (2012). *Anatomy of the Horse*. 6th ed. Schluetershe.

Bugge, M., Bergstrom, B., Eide, O.K., Solli, H., Kjønstad, I.F., Stenvik, J., Espevik, T. and Nilsen, N.J. (2017). Surface toll-like receptor 3 expression in metastatic intestinal epithelial cells induces inflammatory cytokine production and promotes invasiveness. *Journal of Biological Chemistry*, 292(37).

Calder, L.J., Wasilewski, S., Berriman, J.A. and Rosenthal, P.B. (2010). Structural organization of a filamentous influenza A virus. *Proceedings of the National Academy of Sciences of the United States of America*, 107(23).

Carstens, A., Kirberger, R.M., Grimbeek, R.J., Donnellan, C.M.B. and Saulez, M.N. (2009). Radiographic quantification of tracheal dimensions of the normal thoroughbred horse. *Veterinary Radiology and Ultrasound*, 50(5).

Castro, E.R., Perez, R., Rodriguez, S., Bassetti, L., Negro, R. and Vidal, R. (2019). Epidemiological and virological findings during an outbreak of equine influenza in Uruguay in 2018. *Revue scientifique et technique (International Office of Epizootics)*, 38(3).

Cavailler, P., Chu, S., Ly, Sowath, Garcia, J.M., Ha, D.Q., Bergeri, I., Som, L., Ly, Sovann, Sok, T., Vong, S. and Buchy, P. (2010). Seroprevalence of anti-H5 antibody in rural Cambodia, 2007. *Journal of Clinical Virology*, 48(2).

Centers for Disease Control and prevention. (2022). *Influenza Type A Viruses* [online]. Available from: https://www.cdc.gov/flu/avianflu/influenza-a-virus-subtypes.htm#Subtypes [accessed 1 May 2022].

Cercone, M., Olsen, E., Perkins, J.D., Cheetham, J., Mitchell, L.M. and Ducharme, N.G. (2019). Investigation into pathophysiology of naturally occurring palatal instability and intermittent dorsal displacement of the soft palate (DDSP) in racehorses: Thyro-hyoid muscles fatigue during exercise. *PLoS ONE*, 14(10).

Cervera, H., Ambros, S., Bernet, G.P., Rodrigo, G. and Elena, S.F. (2018). Viral fitness correlates with the magnitude and direction of the perturbation induced in the host's transcriptome: The tobacco etch potyvirus'tobacco case study. *Molecular Biology and Evolution*, 35(7).

Chakrabarti, A., Jha, B.K. and Silverman, R.H. (2011). New insights into the role of RNase L in innate immunity. *Journal of Interferon and Cytokine Research*, 31(1).

Chan, P.K.S. (2002). Outbreak of avian influenza A(H5N1) virus infection in Hong Kong in 1997. *Clinical Infectious Diseases*, 34(SUPPL. 2).

Chauché, C., Nogales, A., Zhu, H., Goldfarb, D., Ahmad Shanizza, A.I., Gu, Q., Parrish, C.R., Martínez-Sobrido, L., Marshall, J.F. and Murcia, P.R. (2018). Mammalian Adaptation of an Avian Influenza A Virus Involves Stepwise Changes in NS1. Schultz-Cherry, S., ed. *Journal of Virology*, 92(5), pp.e01875-17.

Chauché, C.M. (2017). *Molecular Evolution of Equine Influenza Virus Non-Structural Protein 1* [unpublished].

Cheetham, J. (2019). Chapter 42 - Overview of Upper Airway Function. In: Auer, J. A. et al., eds. *Equine Surgery (Fifth Edition)*. Fifth Edit. W.B. Saunders, pp.678–682.

Chen, B.J., Leser, G.P., Morita, E. and Lamb, R.A. (2007). Influenza Virus Hemagglutinin and Neuraminidase, but Not the Matrix Protein, Are Required for Assembly and Budding of Plasmid-Derived Virus-Like Particles. *Journal of Virology*, 81(13).

Chen, H. and Boutros, P.C. (2011). VennDiagram: A package for the generation of highly-customizable Venn and Euler diagrams in R. *BMC Bioinformatics*, 12.

Chen, L., Deng, H., Cui, H., Fang, J., Zuo, Z., Deng, J., Li, Y., Wang, X. and Zhao, L. (2018).

Inflammatory responses and inflammation-associated diseases in organs. *Oncotarget*, 9(6).

Chen, W., Calvo, P.A., Malide, D., Gibbs, J., Schubert, U., Bacik, I., Basta, S., O'Neill, R., Schickli, J., Palese, P., Henklein, P., Bennink, J.R. and Yewdell, J.W. (2001). A novel influenza A virus mitochondrial protein that induces cell death. *Nature Medicine*, 7(12).

Chen, Y., Lin, J., Zhao, Y., Ma, X. and Yi, H. (2021). Toll-like receptor 3 (TLR3) regulation mechanisms and roles in antiviral innate immune responses. *Journal of Zhejiang University: Science B*, 22(8).

Chlanda, P., Schraidt, O., Kummer, S., Riches, J., Oberwinkler, H., Prinz, S., Kräusslich, H.-G. and Briggs, J.A.G. (2015). Structural Analysis of the Roles of Influenza A Virus Membrane-Associated Proteins in Assembly and Morphology. *Journal of Virology*, 89(17).

Christley, R.M., Hodgson, D.R., Rose, R.J., Wood, J.L.N., Reid, S.W.J., Whitear, K.G. and Hodgson, J.L. (2001). A case-control study of respiratory disease in Thoroughbred racehorses in Sydney, Australia. *Equine Veterinary Journal*, 33(3).

Chu, C.M., Dawson, I.M. and Elford, W.J. (1949). Filamentous forms associated with newly isolated influenza virus. *The Lancet*, 253(6554).

Clifford, M., Twigg, J. and Upton, C. (2009). Evidence for a novel gene associated with human influenza A viruses. *Virology Journal*, 6.

Cocucci, E., Aguet, F., Boulant, S. and Kirchhausen, T. (2012). The first five seconds in the life of a clathrin-coated pit. *Cell*, 150(3).

Cohen, M., Zhang, X.Q., Senaati, H.P., Chen, H.W., Varki, N.M., Schooley, R.T. and Gagneux, P. (2013). Influenza A penetrates host mucus by cleaving sialic acids with neuraminidase. *Virology Journal*, 10.

Collins, A., Warrington, A., Taylor, K.A. and Svitkina, T. (2011). Structural organization of the actin cytoskeleton at sites of clathrin-mediated endocytosis. *Current Biology*, 21(14).

Conenello, G.M., Zamarin, D., Perrone, L.A., Tumpey, T. and Palese, P. (2007). A single mutation in the PB1-F2 of H5N1 (HK/97) and 1918 influenza A viruses contributes to increased virulence. *PLoS Pathogens*, 3(10).

Cowled, B., Ward, M.P., Hamilton, S. and Garner, G. (2009). The equine influenza epidemic in Australia: Spatial and temporal descriptive analyses of a large propagating epidemic. *Preventive Veterinary Medicine*, 92(1–2).

Crispell, J.L. (2018). *Investigating equine host barriers to infection with influenza A viruses* [unpublished].

Crotta, S., Davidson, S., Mahlakoiv, T., Desmet, C.J., Buckwalter, M.R., Albert, M.L., Staeheli, P. and Wack, A. (2013). Type I and Type III Interferons Drive Redundant Amplification Loops to Induce a Transcriptional Signature in Influenza-Infected Airway Epithelia. *PLoS Pathogens*, 9(11).

Cullinane, A. and Newton, J.R. (2013). Equine influenza-A global perspective. *Veterinary Microbiology*, 167(1–2).

Daffis, S., Samuel, M.A., Keller, B.C., Gale, M. and Diamond, M.S. (2007). Cell-specific IRF-3 responses protect against West Nile virus infection by interferon-dependent and -independent mechanisms. *PLoS Pathogens*, 3(7).

Davis, M.S., Lockard, A.J., Marlin, D.J. and Freed, A.N. (2002). Airway cooling and mucosal injury during cold weather exercise. *Equine veterinary journal. Supplement*, 2002.

Davis, M.S., Royer, C.M., Mckenzie, E.C., Williamson, K.K., Payton, M. and Marlin, D.

(2006). Cold air-induced late-phase bronchoconstriction in horses. *Equine Veterinary Journal*, 38.

Decker, T., Kovarik, P. and Meinke, A. (1997). GAS elements: A few nucleotides with a major impact on cytokine-induced gene expression. *Journal of Interferon and Cytokine Research*, 17(3).

Department of the Environment, W. and Arts, T. (2004). Feral horse (Equus caballus) and feral donkey (Equus asinus) - invasive species fact sheet. , 2004, pp.1–2.

Diebold, S.S., Kaisho, T., Hemmi, H., Akira, S. and Sousa, C.R.E. (2004). Innate Antiviral Responses by Means of TLR7-Mediated Recognition of Single-Stranded RNA. *Science*, 303(5663).

Dochez, A.R., Mills, K.C. and Kneeland, Y. (1933). Studies of the Etiology of Influenza. *Proceedings of the Society for Experimental Biology and Medicine*, 30(8).

Drake, J.W. (1993). Rates of spontaneous mutation among RNA viruses. *Proceedings of the National Academy of Sciences of the United States of America*, 90(9), pp.4171–4175.

Dubois, J., Terrier, O. and Rosa-Calatrava, M. (2014). Influenza viruses and mRNA splicing: Doing more with less. *mBio*, 5(3).

Duffy, S., Shackelton, L.A. and Holmes, E.C. (2008). Rates of evolutionary change in viruses: Patterns and determinants. *Nature Reviews Genetics*, 9(4), pp.267–276.

Easterday, B.C., Trainer, D.O., Tůmová, B. and Pereira, H.G. (1968). Evidence of infection with influenza viruses in migratory waterfowl. *Nature*, 219(5153).

Edgar, R.C. (2004). MUSCLE: Multiple sequence alignment with high accuracy and high throughput. *Nucleic Acids Research*, 32(5).

Egorov, A., Brandt, S., Sereinig, S., Romanova, J., Ferko, B., Katinger, D., Grassauer, A., Alexandrova, G., Katinger, H. and Muster, T. (1998). Transfectant Influenza A Viruses with Long Deletions in the NS1 Protein Grow Efficiently in Vero Cells. *Journal of Virology*, 72(8).

Eisfeld, A.J., Neumann, G. and Kawaoka, Y. (2015). At the centre: Influenza A virus ribonucleoproteins. *Nature Reviews Microbiology*, 13(1).

Elton, D. and Bryant, N. (2011). Facing the threat of equine influenza. *Equine Veterinary Journal*, 43(3).

Enami, M., Sharma, G., Benham, C. and Palese, P. (1991). An influenza virus containing nine different RNA segments. *Virology*, 185(1).

Van Epps, H.L. (2006). Influenza: Exposing the true killer. *Journal of Experimental Medicine*, 203(4), p.803.

Espmark, A., Heller, L. and Viriden, P. (1956). Immunological relationship between infectious cough in horses and human influenza A. *Archiv fur die gesamte Virusforschung*, 7(1), pp.120–124.

Farrell, P.J., Broeze, R.J. and Lengyel, P. (1979). Accumulation of an mRNA and protein in interferon-treated Ehrlich ascites tumour cells [11]. *Nature*, 279(5713).

Favaro, P.F., Fernandes, W.R., Reischak, D., Brandão, P.E., de Souza Silva, S.O. and Richtzenhain, L.J. (2018). Evolution of equine influenza viruses (H3N8) during a Brazilian outbreak, 2015. *Brazilian Journal of Microbiology*, 49(2).

Fédération Equestre Internationale. (2022). *Vaccinations*. Available from:

https://inside.fei.org/fei/your-role/veterinarians/biosecurity-movements/vaccinations.

Feeley, E.M., Sims, J.S., John, S.P., Chin, C.R., Pertel, T., Chen, L.M., Gaiha, G.D., Ryan, B.J., Donis, R.O., Elledge, S.J. and Brass, A.L. (2011). IFITM3 inhibits influenza a virus infection by preventing cytosolic entry. *PLoS Pathogens*, 7(10).

Feng, K.H., Sun, M., Iketani, S., Holmes, E.C. and Parrish, C.R. (2016). Comparing the functions of equine and canine influenza H3N8 virus PA-X proteins: Suppression of reporter gene expression and modulation of global host gene expression. *Virology*, 496.

Food and Agriculture Organization of the United Nations. (2022). *Food and agriculture data* [online]. Available from: https://www.fao.org/faostat/en/#data/QCL [accessed 1 May 2022].

Fouchier, R.A.M., Munster, V., Wallensten, A., Bestebroer, T.M., Herfst, S., Smith, D., Rimmelzwaan, G.F., Olsen, B. and Osterhaus, A.D.M.E. (2005). Characterization of a Novel Influenza A Virus Hemagglutinin Subtype (H16) Obtained from Black-Headed Gulls. *Journal of Virology*, 79(5).

Fournier, E., Moules, V., Essere, B., Paillart, J.C., Sirbat, J.D., Isel, C., Cavalier, A., Rolland, J.P., Thomas, D., Lina, B. and Marquet, R. (2012). A supramolecular assembly formed by influenza A virus genomic RNA segments. *Nucleic Acids Research*, 40(5).

Fu, Y., Durrwald, R., Meng, F., Tong, J., Wu, N.H., Su, A., Yin, X., Haas, L., Schmidtke, M., Zell, R., Krumbholz, A. and Herrler, G. (2019). Infection Studies in Pigs and Porcine Airway Epithelial Cells Reveal an Evolution of A(H1N1)pdm09 Influenza A Viruses Toward Lower Virulence. *Journal of Infectious Diseases*, 219(10).

Fullam, A. and Schröder, M. (2013). DExD/H-box RNA helicases as mediators of anti-viral innate immunity and essential host factors for viral replication. *Biochimica et Biophysica Acta - Gene Regulatory Mechanisms*, 1829(8).

Galloway, A. and Cowling, V.H. (2019). mRNA cap regulation in mammalian cell function and fate. *Biochimica et Biophysica Acta - Gene Regulatory Mechanisms*, 1862(3).

García-Sastre, A., Egorov, A., Matassov, D., Brandt, S., Levy, D.E., Durbin, J.E., Palese, P. and Muster, T. (1998). Influenza A virus lacking the NS1 gene replicates in interferon-deficient systems. *Virology*, 252(2).

Gaunt, E., Wise, H.M., Zhang, H., Lee, L.N., Atkinson, N.J., Nicol, M.Q., Highton, A.J., Klenerman, P., Beard, P.M., Dutia, B.M., Digard, P. and Simmonds, P. (2016). Elevation of CpG frequencies in influenza a genome attenuates pathogenicity but enhances host response to infection. *eLife*, 5.

Gorai, T., Goto, H., Noda, T., Watanabe, T., Kozuka-Hata, H., Oyama, M., Takano, R., Neumann, G., Watanabe, S. and Kawaoka, Y. (2012). F1Fo-ATPase, F-type proton-translocating ATPase, at the plasma membrane is critical for efficient influenza virus budding. *Proceedings of the National Academy of Sciences of the United States of America*, 109(12).

Gottlieb, T.A., Ivanov, I.E., Adesnik, M. and Sabatini, D.D. (1993). Actin microfilaments play a critical role in endocytosis at the apical but not the basolateral surface of polarized epithelial cells. *Journal of Cell Biology*, 120(3).

Gown, A.M. and Willingham, M.C. (2002). Improved detection of apoptotic cells in archival paraffin sections: Immunohistochemistry using antibodies to cleaved caspase 3. *Journal of Histochemistry and Cytochemistry*, 50(4).

Greenbaum, B.D., Levine, A.J., Bhanot, G. and Rabadan, R. (2008). Patterns of evolution and host gene mimicry in influenza and other RNA viruses. *PLoS Pathogens*, 4(6).

Gruta, N.L. La, Kedzierska, K., Stambas, J. and Doherty, P.C. (2007). A question of self-preservation: Immunopathology in influenza virus infection. *Immunology and Cell Biology*, 85(2).

Guo, Y., Wang, M., Kawaoka, Y., Gorman, O., Ito, T., Saito, T. and Webster, Robert G. (1992). Characterization of a new avian-like influenza A virus from horses in China. *Virology*, 188(1), pp.245–255.

Guthrie, A.J., Stevens, K.B. and Bosman, P.P. (1999). The circumstances surrounding the outbreak and spread of equine influenza in South Africa. *OIE Revue Scientifique et Technique*, 18(1).

Häcker, H. and Karin, M. (2006). Regulation and function of IKK and IKK-related kinases. *Science's STKE : signal transduction knowledge environment*, 2006(357).

Hale, B.G., Randall, R.E., Ortin, J. and Jackson, D. (2008). The multifunctional NS1 protein of influenza A viruses. *Journal of General Virology*, 89(10).

Haller, O., Arnheiter, H., Lindenmann, J. and Gresser, I. (1980). Host gene influences sensitivity to interferon action selectively for influenza virus [10]. *Nature*, 283(5748).

Haller, O. (1981). Inborn Resistance of Mice to Orthomyxoviruses. In: Haller, O., ed. *Natural Resistance to Tumors and Viruses*. Berlin, Heidelberg: Springer Berlin Heidelberg, pp.25–52.

Haller, O. and Kochs, G. (2020). Mx genes: host determinants controlling influenza virus infection and trans-species transmission. *Human Genetics*, 139(6–7).

Hatada, E. and Fukuda, R. (1992). Binding of influenza a virus NS1 protein to dsRNA in vitro. *Journal of General Virology*, 73(12).

Helenius, A. (1992). Unpacking the incoming influenza virus. *Cell*, 69(4).

Henne, W.M., Boucrot, E., Meinecke, M., Evergren, E., Vallis, Y., Mittal, R. and McMahon, H.T. (2010). FCHo proteins are nucleators of Clathrin-Mediated endocytosis. *Science*, 328(5983).

Heuser, J. and Evans, L. (1980). Three-dimensional visualization of coated vesicle formation in fibroblasts. *Journal of Cell Biology*, 84(3).

Hierholzer, J.C. and Killington, R.A. (1996). 2-Virus Isolation and Quantitation. In: Virology methods manual. In: *Virology methods manual*.

Hinshaw, V.S., Air, G.M., Gibbs, A.J., Graves, L., Prescott, B. and Karunakaran, D. (1982). Antigenic and genetic characterization of a novel hemagglutinin subtype of influenza A viruses from gulls. *Journal of Virology*, 42(3).

Hoffmann, E., Neumann, G., Kawaoka, Y., Hobom, G. and Webster, R.G. (2000). A DNA transfection system for generation of influenza A virus from eight plasmids. *Proceedings of the National Academy of Sciences of the United States of America*, 97(11).

Hoffmann, E., Stech, J., Guan, Y., Webster, R.G. and Perez, D.R. (2001). Universal primer set for the full-length amplification of all influenza A viruses. *Archives of Virology*, 146(12).

Holcombe, S.J., Derksen, F.J. and Robinson, N.E. (2007). Electromyographic activity of the palatinus and palatopharyngeus muscles in exercising horses. *Equine Veterinary Journal*, 39(5).

Hornung, V., Ellegast, J., Kim, S., Brzózka, K., Jung, A., Kato, H., Poeck, H., Akira, S., Conzelmann, K.K., Schlee, M., Endres, S. and Hartmann, G. (2006). 5′-Triphosphate RNA is the ligand for RIG-I. *Science*, 314(5801).

Huang, D.W., Sherman, B.T., Tan, Q., Kir, J., Liu, D., Bryant, D., Guo, Y., Stephens, R., Baseler, M.W., Lane, H.C. and Lempicki, R.A. (2007). DAVID Bioinformatics Resources: Expanded annotation database and novel algorithms to better extract biology from large gene lists. *Nucleic Acids Research*, 35.

Huang, I.C., Bailey, C.C., Weyer, J.L., Radoshitzky, S.R., Becker, M.M., Chiang, J.J., Brass, A.L., Ahmed, A.A., Chi, X., Dong, L., Longobardi, L.E., Boltz, D., Kuhn, J.H., Elledge, S.J., Bavari, S., Denison, M.R., Choe, H. and Farzan, M. (2011). Distinct patterns of IFITM-mediated restriction of filoviruses, SARS coronavirus, and influenza A virus. *PLoS Pathogens*, 7(1).

Hui, E.K.-W., Barman, S., Tang, D.H.-P., France, B. and Nayak, D.P. (2006). YRKL Sequence of Influenza Virus M1 Functions as the L Domain Motif and Interacts with VPS28 and Cdc42. *Journal of Virology*, 80(5).

Hui, K.P.Y., Cheung, M.C., Perera, R.A.P.M., Ng, K.C., Bui, C.H.T., Ho, J.C.W., Ng, M.M.T., Kuok, D.I.T., Shih, K.C., Tsao, S.W., Poon, L.L.M., Peiris, M., Nicholls, J.M. and Chan, M.C.W. (2020). Tropism, replication competence, and innate immune responses of the coronavirus SARS-CoV-2 in human respiratory tract and conjunctiva: an analysis in ex-vivo and in-vitro cultures. *The Lancet Respiratory Medicine*, 8(7).

Ichinohe, T., Pang, I.K. and Iwasaki, A. (2010). Influenza virus activates inflammasomes via its intracellular M2 ion channel. *Nature Immunology*, 11(5).

ICTV. (2011). *Orthomyxoviridae - Negative Sense RNA Viruses - Negative Sense RNA Viruses* [online]. Available from: https://talk.ictvonline.org/ictv-reports/ictv_9th_report/negative-sense-rna-viruses-2011/w/negrna_viruses/209/orthomyxoviridae [accessed 1 May 2022].

Isaacs, A. and Lindenmann, J. (1987). Virus interference. I. The interferon. *Journal of Interferon Research*, 7(5).

Ito, T., Kawaoka, Y., Ohira, M., Takakuwa, H., Yasuda, J., Kida, H. and Otsuki, K. (1999). Replacement of Internal Protein Genes, with the Exception of the Matrix, in Equine 1 Viruses by Equine 2 Influenza Virus Genes during Evolution in Nature. *Journal of Veterinary Medical Science*, 61(8).

Iwasaki, A. and Pillai, P.S. (2014). Innate immunity to influenza virus infection. *Nature Reviews Immunology*, 14(5).

Jagger, B.W., Wise, H.M., Kash, J.C., Walters, K.A., Wills, N.M., Xiao, Y.L., Dunfee, R.L., Schwartzman, L.M., Ozinsky, A., Bell, G.L., Dalton, R.M., Lo, A., Efstathiou, S., Atkins, J.F., Firth, A.E., Taubenberger, J.K. and Digard, P. (2012). An overlapping protein-coding region in influenza A virus segment 3 modulates the host response. *Science*, 337(6091).

Jekl, V. (2021). Respiratory Disorders in Rabbits. *Veterinary Clinics of North America - Exotic Animal Practice*, 24(2).

Johnson, L., Montgomery, J.B., Schneider, J.P., Townsend, H.G.G., Ochs, M. and Singh, B. (2014). Morphometric examination of the equine adult and foal lung. *Anatomical Record*, 297(10).

Josset, L., Zeng, H., Kelly, S.M., Tumpey, T.M. and Katze, M.G. (2014). Transcriptomic characterization of the novel avian-origin influenza A (H7N9) virus: Specific host response and responses intermediate between Avian (H5N1 and H7N7) and human (H3N2) viruses and implications for treatment options. *mBio*, 5(1).

Kaksonen, M. and Roux, A. (2018). Mechanisms of clathrin-mediated endocytosis. *Nature Reviews Molecular Cell Biology*, 19(5).

Karamendin, K., Kydyrmanov, A., Sayatov, M., Strochkov, V., Sandybayev, N. and Sultankulova, K. (2016). Retrospective analysis of the equine influenza virus a/equine/Kirgizia/26/1974 (H7N7) isolated in central Asia. *Pathogens*, 5(3), pp.5–10.

Karpala, A.J., Stewart, C., McKay, J., Lowenthal, J.W. and Bean, A.G.D. (2011). Characterization of Chicken Mda5 Activity: Regulation of IFN-β in the Absence of RIG-I Functionality. *The Journal of Immunology*, 186(9).

Kato, H., Takeuchi, O., Sato, S., Yoneyama, M., Yamamoto, M., Matsui, K., Uematsu, S., Jung, A., Kawai, T., Ishii, K.J., Yamaguchi, O., Otsu, K., Tsujimura, T., Koh, C.S., Sousa, C.R.E., Matsuura, Y., Fujita, T. and Akira, S. (2006). Differential roles of MDA5 and RIG-I helicases in the recognition of RNA viruses. *Nature*, 441(1).

Kato, H., Takeuchi, O., Mikamo-Satoh, E., Hirai, R., Kawai, T., Matsushita, K., Hiiragi, A., Dermody, T.S., Fujita, T. and Akira, S. (2008). Length-dependent recognition of double-stranded ribonucleic acids by retinoic acid–inducible gene-I and melanoma differentiation–associated gene 5. *The Journal of Experimental Medicine*, 205(7), pp.1601–1610.

Kawai, T., Takahashi, K., Sato, S., Coban, C., Kumar, H., Kato, H., Ishii, K.J., Takeuchi, O. and Akira, S. (2005). IPS-1, an adaptor triggering RIG-I- and Mda5-mediated type I interferon induction. *Nature Immunology*, 6(10).

Kawaoka, Y., Bean, W.J. and Webster, R.G. (1989). Evolution of the hemagglutinin of equine H3 influenza viruses. *Virology*, 169(2), pp.283–292.

Kerr, P.J. (2012). Myxomatosis in Australia and Europe: A model for emerging infectious diseases. *Antiviral Research*, 93(3).

Kheraj, S. (2018). The great epizootic of 1872-73: Networks of animal disease in North American urban environments. *Environmental History*, 23(3).

Killip, M.J., Smith, M., Jackson, D. and Randall, R.E. (2014). Activation of the Interferon Induction Cascade by Influenza A Viruses Requires Viral RNA Synthesis and Nuclear Export. *Journal of Virology*, 88(8).

Kim, D., Pertea, G., Trapnell, C., Pimentel, H., Kelley, R. and Salzberg, S.L. (2013). TopHat2: Accurate alignment of transcriptomes in the presence of insertions, deletions and gene fusions. *Genome Biology*, 14(4).

Koch, R. (1884). Die Aetiologie der Tuberkulose. *Mittheilungen aus dem Kaiserlichen Gesundheitsamte*, 2, pp.1–88.

Kolakofsky, D., Kowalinski, E. and Cusack, S. (2012). A structure-based model of RIG-I activation. *RNA*, 18(12).

Koliopoulos, M.G., Lethier, M., Veen, A.G. Van Der, Haubrich, K., Hennig, J., Kowalinski, E., Stevens, R. V, Martin, S.R., Sousa, C.R.E., Cusack, S. and Rittinger, K. (2018). Molecular mechanism of influenza A NS1-mediated TRIM25 recognition and inhibition. *Nature Communications*, 9(1).

Komuro, A. and Horvath, C.M. (2006). RNA- and Virus-Independent Inhibition of Antiviral Signaling by RNA Helicase LGP2. *Journal of Virology*, 80(24).

Kotenko, S. V, Gallagher, G., Baurin, V. V, Lewis-Antes, A., Shen, M., Shah, N.K., Langer, J.A., Sheikh, F., Dickensheets, H. and Donnelly, R.P. (2003). IFN-λs mediate antiviral protection through a distinct class II cytokine receptor complex. *Nature Immunology*, 4(1).

Kowalinski, E., Lunardi, T., McCarthy, A.A., Louber, J., Brunel, J., Grigorov, B., Gerlier, D. and Cusack, S. (2011). Structural basis for the activation of innate immune pattern-recognition receptor RIG-I by viral RNA. *Cell*, 147(2), pp.423–435.

Krishnan, K., Yan, H., Lim, J.T.E. and Krolewski, J.J. (1996). Dimerization of a chimeric CD4-interferon-α receptor reconstitutes the signaling events preceding STAT phosphorylation. *Oncogene*, 13(1), pp.125–133.

Krug, R.M. (2015). Functions of the influenza A virus NS1 protein in antiviral defense. *Current Opinion in Virology*, 12.

Kueck, T., Bloyet, L.-M., Cassella, E., Zang, T., Schmidt, F., Brusic, V., Tekes, G., Pornillos, O., Whelan, S.P.J. and Bieniasz, P.D. (2019). Vesicular Stomatitis Virus Transcription Is Inhibited by TRIM69 in the Interferon-Induced Antiviral State. *Journal of Virology*, 93(24).

Kumar, N., Bera, B.C., Greenbaum, B.D., Bhatia, S., Sood, R., Selvaraj, P., Anand, T., Tripathi, B.N. and Virmani, N. (2016). Revelation of influencing factors in overall codon usage bias of equine influenza viruses. *PLoS ONE*, 11(4).

Lafortuna, C.L., Saibene, F., Albertini, M. and Clement, M.G. (2003). The regulation of respiratory resistance in exercising horses. *European Journal of Applied Physiology*, 90(3–4).

Lamaze, C., Fujimoto, L.M., Yin, H.L. and Schmid, S.L. (1997). The actin cytoskeleton is required for receptor-mediated endocytosis in mammalian cells. *Journal of Biological Chemistry*, 272(33).

Lamb, R.A., Etkind, P.R. and Choppin, P.W. (1978). Evidence for a ninth influenza viral polypeptide. *Virology*, 91(1).

Landini, G., Martinelli, G. and Piccinini, F. (2021). Colour deconvolution: Stain unmixing in histological imaging. *Bioinformatics*, 37(10).

Lane, J.G., Bladon, B., Little, D.R.M., Naylor, J.R.J. and Franklin, S.H. (2006). Dynamic obstructions of the equine upper respiratory tract. Part 1: Observations during high-speed treadmill endoscopy of 600 Thoroughbred racehorses. *Equine Veterinary Journal*, 38(5).

Lang, X., Tang, T., Jin, T., Ding, C., Zhou, R. and Jiang, W. (2017). TRIM65-catalized ubiquitination is essential for MDA5-mediated antiviral innate immunity. *Journal of Experimental Medicine*, 214(2).

Langmead, B. and Salzberg, S.L. (2012). Fast gapped-read alignment with Bowtie 2. *Nature Methods*, 9(4).

Larner, A.C., Chaudhuri, A. and Darnell, J.E. (1986). Transcriptional induction by interferon. New protein(s) determine the extent and length of the induction. *Journal of Biological Chemistry*, 261(1).

Lee, J., Wu, C.C.N., Lee, K.J., Chuang, T.H., Katakura, K., Liu, Y.T., Chan, M., Tawatao, R., Chung, M., Shen, C., Cottam, H.B., Lai, M.M.C., Raz, E. and Carson, D.A. (2006). Activation of anti-hepatitis C virus responses via Toll-like receptor 7. *Proceedings of the National Academy of Sciences of the United States of America*, 103(6).

Lenoir, J.J., Parisien, J.P. and Horvath, C.M. (2021). Immune regulator LGP2 targets Ubc13/UBE2N to mediate widespread interference with K63 polyubiquitination and NF-κB activation. *Cell Reports*, 37(13).

Leonard, J.N., Ghirlando, R., Askins, J., Bell, J.K., Margulies, D.H., Davies, D.R. and Segal, D.M. (2008). The TLR3 signaling complex forms by cooperative receptor dimerization. *Proceedings of the National Academy of Sciences of the United States of America*, 105(1).

Li, X., Leung, S., Qureshi, S., Darnell, J.E. and Stark, G.R. (1996). Formation of STAT1-STAT2 heterodimers and their role in the activation of IRF-1 gene transcription by interferon-α. *Journal of Biological Chemistry*, 271(10).

Liang, Yuhong, Huang, T., Ly, H., Parslow, T.G. and Liang, Yuying. (2008). Mutational Analyses of Packaging Signals in Influenza Virus PA, PB1, and PB2 Genomic RNA Segments. *Journal of Virology*, 82(1).

Liniger, M., Summerfield, A., Zimmer, G., McCullough, K.C. and Ruggli, N. (2012). Chicken Cells Sense Influenza A Virus Infection through MDA5 and CARDIF Signaling Involving LGP2. *Journal of Virology*, 86(2), pp.705–717.

Liu, S., Chen, J., Cai, X., Wu, J., Chen, X., Wu, Y.-T., Sun, L. and Chen, Z.J. (2013). MAVS recruits multiple ubiquitin E3 ligases to activate antiviral signaling cascades. *eLife*, 2.

Liu, Y., Zhang, Y.B., Liu, T.K. and Gui, J.F. (2013). Lineage-Specific Expansion of IFIT Gene Family: An Insight into Coevolution with IFN Gene Family. *PLoS ONE*, 8(6).

Ludwig, S., Wang, X., Ehrhardt, C., Zheng, H., Donelan, N., Planz, O., Pleschka, S., García-Sastre, A., Heins, G. and Wolff, T. (2002). The Influenza A Virus NS1 Protein Inhibits Activation of Jun N-Terminal Kinase and AP-1 Transcription Factors. *Journal of Virology*, 76(21).

Lund, J.M., Alexopoulou, L., Sato, A., Karow, M., Adams, N.C., Gale, N.W., Iwasaki, A. and Flavell, R.A. (2004). Recognition of single-stranded RNA viruses by Toll-like receptor 7. *Proceedings of the National Academy of Sciences of the United States of America*, 101(15).

Lycett, S.J. et al. (2016). Role for migratory wild birds in the global spread of avian influenza H5N8. *Science*, 354(6309).

Ma, J., Rubin, B.K. and Voynow, J.A. (2018). Mucins, Mucus, and Goblet Cells. *Chest*, 154(1).

Ma, L., Umasankar, P.K., Wrobel, A.G., Lymar, A., McCoy, A.J., Holkar, S.S., Jha, A., Pradhan-Sundd, T., Watkins, S.C., Owen, D.J. and Traub, L.M. (2015). Transient Fcho1/2·Eps15/R·AP-2 Nanoclusters Prime the AP-2 Clathrin Adaptor for Cargo Binding. *Developmental Cell*, 37(5), pp.428–443.

Ma, T., Nagy, A., Xu, G., Xin, L., Bao, D., Lu, C., Niu, S., Wu, Z., Ren, C., Zhang, T., Yang, J., Teng, Q., Li, X., Li, Z. and Liu, Q. (2021). Rna-seq analysis of influenza a virus-induced transcriptional changes in mice lung and its possible implications for the virus pathogenicity in mice. *Viruses*, 13(10).

Van Maanen, C., Bruin, G., Boer-Luijtze, E. De, Smolders, G. and Boer, G.F. De. (1992). Interference of maternal antibodies with the immune response of foals after vaccination against equine influenza. *Veterinary Quarterly*, 14(1).

Madić, J., Martinović, S., Naglić, T., Hajsig, D. and Cvetnić, S. (1996). Serological evidence for the presence of A/equine- I influenza virus in unvaccinated horses in Croatia. *Veterinary Record*, 138(3), p.68.

Maelfait, J., Roose, K., Bogaert, P., Sze, M., Saelens, X., Pasparakis, M., Carpentier, I., van Loo, G. and Beyaert, R. (2012). A20 (Tnfaip3) deficiency in myeloid cells protects against influenza A virus infection. *PLoS pathogens*, 8(3).

Mair, T.S., Batten, E.H., Stokes, C.R. and Bourne, F.J. (1987). The histological features of the immune system of the equine respiratory tract. *Journal of Comparative Pathology*, 97(5).

Malathi, K., Dong, B., Gale, M. and Silverman, R.H. (2007). Small self-RNA generated by RNase L amplifies antiviral innate immunity. *Nature*, 448(7155).

Martínez-Sobrido, L. and García-Sastre, A. (2010). Generation of recombinant influenza virus from plasmid DNA. *Journal of Visualized Experiments*, 2010.

Matrosovich, M.N., Matrosovich, T.Y., Gray, T., Roberts, N.A. and Klenk, H.-D. (2004). Neuraminidase Is Important for the Initiation of Influenza Virus Infection in Human Airway Epithelium. *Journal of Virology*, 78(22).

Matsumoto, M., Funami, K., Tanabe, M., Oshiumi, H., Shingai, M., Seto, Y., Yamamoto, A. and Seya, T. (2003). Subcellular Localization of Toll-Like Receptor 3 in Human Dendritic Cells. *The Journal of Immunology*, 171(6).

Matzinger, P. (1994). Tolerance, danger, and the extended family. *Annual Review of Immunology*, 12.

Meyerson, N.R., Zhou, L., Guo, Y.R., Zhao, C., Tao, Y.J., Krug, R.M. and Sawyer, S.L. (2017). Nuclear TRIM25 Specifically Targets Influenza Virus Ribonucleoproteins to Block the Onset of RNA Chain Elongation. *Cell Host and Microbe*, 22(5).

Meylan, E., Curran, J., Hofmann, K., Moradpour, D., Binder, M., Bartenschlager, R. and Tschopp, J. (2005). Cardif is an adaptor protein in the RIG-I antiviral pathway and is targeted by hepatitis C virus. *Nature*, 437(7062).

Min, J.Y. and Krug, R.M. (2006). The primary function of RNA binding by the influenza A virus NS1 protein in infected cells: Inhibiting the 2′-5′ oligo (A) synthetase/RNase L pathway. *Proceedings of the National Academy of Sciences of the United States of America*, 103(18).

Morens, D.M. and Taubenberger, J.K. (2010). Historical thoughts on influenza viral ecosystems, or behold a pale horse, dead dogs, failing fowl, and sick swine. *Influenza and other Respiratory Viruses*, 4(6).

Morris, D.E., Cleary, D.W. and Clarke, S.C. (2017). Secondary bacterial infections associated with influenza pandemics. *Frontiers in Microbiology*, 8.

Mosley, V.M. and Wyckoff, R.W.G. (1946). Electron micrography of the virus of influenza [2]. *Nature*, 157(3983).

Mudhasani, R., Tran, J.P., Retterer, C., Radoshitzky, S.R., Kota, K.P., Altamura, L.A., Smith, J.M., Packard, B.Z., Kuhn, J.H., Costantino, J., Garrison, A.R., Schmaljohn, C.S., Huang, I.-C., Farzan, M. and Bavari, S. (2013). IFITM-2 and IFITM-3 but Not IFITM-1 Restrict Rift Valley Fever Virus. *Journal of Virology*, 87(15).

Muramoto, Y., Noda, T., Kawakami, E., Akkina, R. and Kawaoka, Y. (2013). Identification of Novel Influenza A Virus Proteins Translated from PA mRNA. *Journal of Virology*, 87(5).

Muranaka, M., Yamanaka, T., Katayama, Y., Niwa, H., Oku, K., Matsumura, T. and Oyamada, T. (2012). Time-related Pathological Changes in Horses Experimentally Inoculated with Equine Influenza A Virus. *Journal of Equine Science*, 23(2), pp.17–26.

Murcia, P.R., Wood, J.L.N. and Holmes, E.C. (2011). Genome-scale evolution and phylodynamics of equine H3N8 influenza A virus. *Journal of virology*, 85(11), pp.5312–22.

Myers, C. and Wilson, W.D. (2006). Equine Influenza Virus. *Clinical Techniques in Equine Practice*, 5(3), pp.187–196.

Navarro, M, Ruberte, J and Carretero, A. (2017). 6 - Respiratory apparatus. In: Ruberte, Jesús, Carretero, Ana, and Navarro, Marc, eds. *Morphological Mouse Phenotyping*. Academic Press, pp.147–178.

Nelson, R. and Hampe, D.W. (1983). Measurement of tracheal mucous transport rate in the horse. *American Journal of Veterinary Research*, 44(6).

Nemoto, M., Ohta, M., Yamanaka, T., Kambayashi, Y., Bannai, H., Tsujimura, K.,

Yamayoshi, S., Kawaoka, Y. and Cullinane, A. (2021). Antigenic differences between equine influenza virus vaccine strains and Florida sublineage clade 1 strains isolated in Europe in 2019. *Veterinary Journal*, 272.

Noda, T., Sagara, H., Yen, A., Takada, A., Kida, H., Cheng, R.H. and Kawaoka, Y. (2006). Architecture of ribonucleoprotein complexes in influenza A virus particles. *Nature*, 439(7075).

Noton, S.L., Medcalf, E., Fisher, D., Mullin, A.E., Elton, D. and Digard, P. (2007). Identification of the domains of the influenza A virus M1 matrix protein required for NP binding, oligomerization and incorporation into virions. *Journal of General Virology*, 88(8).

Nunes-Correia, I., Eulálio, A., Nir, S. and Lima, M.C.P. De. (2004). Caveolae as an additional route for influenza virus endocytosis in MDCK cells. *Cellular and Molecular Biology Letters*, 9(1).

Nunes, S.F., Murcia, P.R., Tiley, L.S., Brown, I.H., Tucker, A.W., Maskell, D.J. and Wood, J.L.N. (2010). An ex vivo swine tracheal organ culture for the study of influenza infection. *Influenza and other Respiratory Viruses*, 4(1).

O'Neill, R.E., Jaskunas, R., Blobel, G., Palese, P. and Moroianu, J. (1995). Nuclear import of influenza virus RNA can be mediated by viral nucleoprotein and transport factors required for protein import. *Journal of Biological Chemistry*, 270(39).

O'Neill, R.E., Talon, J. and Palese, P. (1998). The influenza virus NEP (NS2 protein) mediates the nuclear export of viral ribonucleoproteins. *EMBO Journal*, 17(1).

Oganesyan, G., Saha, S.K., Guo, B., He, J.Q., Shahangian, A., Zarnegar, B., Perry, A. and Cheng, G. (2006). Critical role of TRAF3 in the Toll-like receptor-dependent and -independent antiviral response. *Nature*, 439(7073).

Oladunni, F.S., Oseni, S.O., Martinez-Sobrido, L. and Chambers, T.M. (2021). Equine influenza virus and vaccines. *Viruses*, 13(8).

Opdenbosch, N. Van and Lamkanfi, M. (2019). Caspases in Cell Death, Inflammation, and Disease. *Immunity*, 50(6).

Österlund, P., Strengell, M., Sarin, L.P., Poranen, M.M., Fagerlund, R., Melén, K. and Julkunen, I. (2012). Incoming Influenza A Virus Evades Early Host Recognition, while Influenza B Virus Induces Interferon Expression Directly upon Entry. *Journal of Virology*, 86(20).

Paccaud, M.F., Couard, M., Bürki, F., Gerber, H. and Löhrer, J. (1966). Outbreak of influenza A/equi-2 in Switzerland. *Nature*, 211(5044).

Parente, E.J., Martin, B.B., Tulleners, E.P. and Ross, M.W. (2002). Dorsal displacement of the soft palate in 92 horses during high-speed treadmill examination (1993-1998). *Veterinary surgery : VS : the official journal of the American College of Veterinary Surgeons*, 31(6).

Parisien, J., Lenoir, J.J., Mandhana, R., Rodriguez, K.R., Qian, K., Bruns, A.M. and Horvath, C.M. (2018). RNA sensor LGP 2 inhibits TRAF ubiquitin ligase to negatively regulate innate immune signaling. *EMBO reports*, 19(6).

Pasteur, L. (1878). La théorie des germes et ses applications à la medecine et la chirurgie. *Bulletin de l'Académie nationale de médecine*, 2nd series, pp.432–453.

Patterson-Kane, J.C., Carrick, J.B., Axon, J.E., Wilkie, I. and Begg, A.P. (2008). The pathology of bronchointerstitial pneumonia in young foals associated with the first outbreak of equine influenza in Australia. *Equine Veterinary Journal*, 40(3).

Patton, V. (2021). *Development of an unbiased methodology to quantify pathological changes in the respiratory tract* [unpublished].

Peng, N., Liu, S., Xia, Z., Ren, S., Feng, J., Jing, M., Gao, X., Wiemer, E.A.C. and Zhu, Y. (2016). Inducible Major Vault Protein Plays a Pivotal Role in Double-Stranded RNA– or Virus-Induced Proinflammatory Response. *The Journal of Immunology*, 196(6).

Perng, Y.C. and Lenschow, D.J. (2018). ISG15 in antiviral immunity and beyond. *Nature Reviews Microbiology*, 16(7).

Perroncito, E. (1878). Epizoozia tifoide nei gallinacei. *Annali Accad. Agri. Torino*, 21, pp.87–126.

Pervolaraki, K., Talemi, S.R., Albrecht, D., Bormann, F., Bamford, C., Mendoza, J.L., Garcia, K.C., McLauchlan, J., Höfer, T., Stanifer, M.L. and Boulant, S. (2018). Differential induction of interferon stimulated genes between type I and type III interferons is independent of interferon receptor abundance. *PLoS Pathogens*, 14(11).

Petes, C., Odoardi, N. and Gee, K. (2017). The Toll for trafficking: Toll-like receptor 7 delivery to the endosome. *Frontiers in Immunology*, 8.

Pflug, A., Guilligay, D., Reich, S. and Cusack, S. (2014). Structure of influenza A polymerase bound to the viral RNA promoter. *Nature*, 516(7531).

Pichlmair, A., Schulz, O., Tan, C.P., Näslund, T.I., Liljeström, P., Weber, F. and Sousa, C.R.E. (2006). RIG-I-mediated antiviral responses to single-stranded RNA bearing 5′-phosphates. *Science*, 314(5801).

Pinto, L.H., Holsinger, L.J. and Lamb, R.A. (1992). Influenza virus M2 protein has ion channel activity. *Cell*, 69(3).

Pinto R. (2019). *Identification of novel accessory proteins encoded by influenza A virus segment 2 with interferon antagonist function* [unpublished].

Plotch, S.J., Bouloy, M., Ulmanen, I. and Krug, R.M. (1981). A unique cap(m7GpppXm)-dependent influenza virion endonuclease cleaves capped RNAs to generate the primers that initiate viral RNA transcription. *Cell*, 23(3).

Poon, L.L.M., Pritlove, D.C., Fodor, E. and Brownlee, G.G. (1999). Direct Evidence that the Poly(A) Tail of Influenza A Virus mRNA Is Synthesized by Reiterative Copying of a U Track in the Virion RNA Template. *Journal of Virology*, 73(4).

Poynter, S., Lisser, G., Monjo, A. and DeWitte-Orr, S. (2015). Sensors of infection: Viral nucleic acid PRRs in fish. *Biology*, 4(3).

Precious, B., Childs, K., Fitzpatrick-Swallow, V., Goodbourn, S. and Randall, R.E. (2005). Simian Virus 5 V Protein Acts as an Adaptor, Linking DDB1 to STAT2, To Facilitate the Ubiquitination of STAT1. *Journal of Virology*, 79(21).

Putri, W.C.W.S., Muscatello, D.J., Stockwell, M.S. and Newall, A.T. (2018). Economic burden of seasonal influenza in the United States. *Vaccine*, 36(27).

Quinlivan, M., Zamarin, D., García-Sastre, A., Cullinane, A., Chambers, T. and Palese, P. (2005). Attenuation of Equine Influenza Viruses through Truncations of the NS1 Protein. *Journal of Virology*, 79(13).

Rajkumar, A.P., Qvist, P., Lazarus, R., Lescai, F., Ju, J., Nyegaard, M., Mors, O., Børglum, A.D., Li, Q. and Christensen, J.H. (2011). Experimental validation of methods for differential gene expression analysis and sample pooling in RNA-seq. , 2011.

Rajsbaum, R., Albrecht, R.A., Wang, M.K., Maharaj, N.P., Versteeg, G.A., Nistal-Villán,

E., García-Sastre, A. and Gack, M.U. (2012). Species-Specific Inhibition of RIG-I Ubiquitination and IFN Induction by the Influenza A Virus NS1 Protein. *PLoS Pathogens*, 8(11).

Randall, R.E. and Goodbourn, S. (2008). Interferons and viruses: An interplay between induction, signalling, antiviral responses and virus countermeasures. *Journal of General Virology*, 89(1).

Ricciotti, E. and Fitzgerald, G.A. (2011). Prostaglandins and inflammation. *Arteriosclerosis, Thrombosis, and Vascular Biology*, 31(5).

Rihn, S.J., Aziz, M.A., Stewart, D.G., Hughes, J., Turnbull, M.L., Varela, M., Sugrue, E., Herd, C.S., Stanifer, M., Sinkins, S.P., Palmarini, M. and Wilson, S.J. (2019). TRIM69 Inhibits Vesicular Stomatitis Indiana Virus. *Journal of Virology*, 93(20).

Roberts, P.C., Lamb, R.A. and Compans, R.W. (1998). The M1 and M2 proteins of influenza a virus are important determinants in filamentous particle formation. *Virology*, 240(1).

Robinson, M.D., McCarthy, D.J. and Smyth, G.K. (2009). edgeR: A Bioconductor package for differential expression analysis of digital gene expression data. *Bioinformatics*, 26(1), pp.139–140.

Rogers, G.N. and Paulson, J.C. (1983). Receptor determinants of human and animal influenza virus isolates: Differences in receptor specificity of the H3 hemagglutinin based on species of origin. *Virology*, 127(2).

Rose, M.A. (1966). Respiratory Virus Infections of Man and Animals [Abridged]: Equine Influenza Viruses Isolated at Cambridge in 1963 and 1965. *Journal of the Royal Society of Medicine*, 59(1).

Rossman, J.S., Jing, X., Leser, G.P. and Lamb, R.A. (2010). Influenza Virus M2 Protein Mediates ESCRT-Independent Membrane Scission. *Cell*, 142(6).

Rossman, J.S. and Lamb, R.A. (2011). Influenza virus assembly and budding. *Virology*, 411(2).

Rossman, J.S., Leser, G.P. and Lamb, R.A. (2012). Filamentous Influenza Virus Enters Cells via Macropinocytosis. *Journal of Virology*, 86(20).

Rousseau, K., Kirkham, S., McKane, S., Newton, R., Clegg, P. and Thornton, D.J. (2007). Muc5b and Muc5ac are the major oligomeric mucins in equine airway mucus. *American Journal of Physiology - Lung Cellular and Molecular Physiology*, 292(6).

Sabbah, A., Chang, T.H., Harnack, R., Frohlich, V., Tominaga, K., Dube, P.H., Xiang, Y. and Bose, S. (2009). Activation of innate immune antiviral responses by Nod2. *Nature Immunology*, 10(10).

Sack, A., Cullinane, A., Daramragchaa, U., Chuluunbaatar, M., Gonchigoo, B. and Gray, G.C. (2019). Equine influenza virus- A neglected, reemergent disease threat. *Emerging Infectious Diseases*, 25(6).

van der Sandt, C.E., Kreijtz, J.H.C.M. and Rimmelzwaan, G.F. (2012). Evasion of influenza A viruses from innate and adaptive immune responses. *Viruses*, 4(9).

Sarkar, S.N. and Sen, G.C. (2004). Novel functions of proteins encoded by viral stress-inducible genes. *Pharmacology and Therapeutics*, 103(3).

Satoh, T., Kato, H., Kumagai, Y., Yoneyama, M., Sato, S., Matsushita, K., Tsujimura, T., Fujita, T., Akira, S. and Takeuchi, O. (2010). LGP2 is a positive regulator of RIG-I- and MDA5-mediated antiviral responses. *Proceedings of the National Academy of Sciences of*

the United States of America, 107(4).

Schaefer, T.M., Desouza, K., Fahey, J. V, Beagley, K.W. and Wira, C.R. (2004). Toll-like receptor (TLR) expression and TLR-mediated cytokine/chemokine production by human uterine epithelial cells. *Immunology*, 112(3).

Schäfer, W. (1955). Vergleichende sero-immunologische Untersuchungen über die Viren der Influenza und klassischen Geflügelpest. *Zeitschrift fur Naturforschung - Section B Journal of Chemical Sciences*, 10(2).

Scheiffele, P., Rietveld, A., Wilk, T. and Simons, K. (1999). Influenza viruses select ordered lipid domains during budding from the plasma membrane. *Journal of Biological Chemistry*, 274(4).

Schmitt, A.P. and Lamb, R.A. (2005). Influenza Virus Assembly and Budding at the Viral Budozone. *Advances in Virus Research*, 64.

Schneider, W.M., Chevillotte, M.D. and Rice, C.M. (2014). Interferon-stimulated genes: A complex web of host defenses. *Annual Review of Immunology*, 32.

Scholtens, R.G. and Steele, J.H. (1964). U.S. Epizootic of Equine influenza. *Public health reports*, 79(5), pp.393–402.

Scholzen, T. and Gerdes, J. (2000). The Ki-67 protein: From the known and the unknown. *Journal of Cellular Physiology*, 182(3).

Seitz, C., Frensing, T., Höper, D., Kochs, G. and Reichl, U. (2010). High yields of influenza A virus in Madin-Darby canine kidney cells are promoted by an insufficient interferon-induced antiviral state. *Journal of General Virology*, 91(7), pp.1754–1763.

Seladi-Schulman, J., Steel, J. and Lowen, A.C. (2013). Spherical Influenza Viruses Have a Fitness Advantage in Embryonated Eggs, while Filament-Producing Strains Are Selected In Vivo. *Journal of Virology*, 87(24).

Semmelweis, I. (1861). *The cause, concept and prophylaxis of childbed fever*.

Seth, R.B., Sun, L., Ea, C.K. and Chen, Z.J. (2005). Identification and characterization of MAVS, a mitochondrial antiviral signaling protein that activates NF-κB and IRF3. *Cell*, 122(5), pp.669–682.

Shaw, M.L., Stone, K.L., Colangelo, C.M., Gulcicek, E.E. and Palese, P. (2008). Cellular proteins in influenza virus particles. *PLoS Pathogens*, 4(6).

Sheppard, P. et al. (2003). IL-28, IL-29 and their class II cytokine receptor IL-28R. *Nature Immunology*, 4(1).

Sherman, J., Thorsen, J., Barnum, D.A., Mitchell, W.R. and Ingram, D.G. (1977). Infectious causes of equine respiratory disease on Ontario standardbred racetracks. *Journal of Clinical Microbiology*, 5(3).

Shi, J., Zhao, Y., Wang, K., Shi, X., Wang, Y., Huang, H., Zhuang, Y., Cai, T., Wang, F. and Shao, F. (2015). Cleavage of GSDMD by inflammatory caspases determines pyroptotic cell death. *Nature*, 526(7575).

Shi, Y., Evans, J.E. and Rock, K.L. (2003). Molecular identification of a danger signal that alerts the immune system to dying cells. *Nature*, 425(6957).

Shibata, M., Sato, T., Nukiwa, R., Ariga, T. and Hatakeyama, S. (2012). TRIM45 negatively regulates NF-κB-mediated transcription and suppresses cell proliferation. *Biochemical and Biophysical Research Communications*, 423(1).

Shope, D.E. (1931). Swine influenza, filtration experiments and etiology. *Journal of experimental medicine*, 1931.

Short, K.R., Veeris, R., Leijten, L.M., Brand, J.M. Van Den, Jong, V.L., Stittelaar, K., Osterhaus, A.D.M.E., Andeweg, A. and Riel, D. Van. (2017). Proinflammatory Cytokine Responses in Extra-Respiratory Tissues during Severe Influenza. *Journal of Infectious Diseases*, 216(7).

Sieczkarski, S.B. and Whittaker, G.R. (2002). Influenza Virus Can Enter and Infect Cells in the Absence of Clathrin-Mediated Endocytosis. *Journal of Virology*, 76(20).

Silverman, R.H. (2007). Viral Encounters with 2′,5′-Oligoadenylate Synthetase and RNase L during the Interferon Antiviral Response. *Journal of Virology*, 81(23).

Simmonds, P. (2012). SSE: A nucleotide and amino acid sequence analysis platform. *BMC Research Notes*, 5.

Simmons, D.L., Botting, R.M. and Hla, T. (2004). Cyclooxygenase isozymes: The biology of prostaglandin synthesis and inhibition. *Pharmacological Reviews*, 56(3).

Skehel, J.J. (1973). Early polypeptide synthesis in influenza virus-infected cells. *Virology*, 56(1).

Skehel, J.J. (1972). Polypeptide synthesis in influenza virus-infected cells. *Virology*, 49(1).

Smith, W., Andrewes, C.H. and Laidlaw, P.P. (1933). A virus obtained from Influenza patients. *The Lancet*, 222(5732), pp.66–68.

Smyth, G.B., Dagley, K. and Tainsh, J. (2011). Insights into the economic consequences of the 2007 equine influenza outbreak in Australia. *Australian Veterinary Journal*, 89.

Sovinova, O., Tumova, B., Pouska, F. and Nemec, J. (1958). Isolation of a virus causing respiratory disease in horses. *Acta virologica*, 2(1), pp.52–61.

Spel, L. and Martinon, F. (2021). Detection of viruses by inflammasomes. *Current Opinion in Virology*, 46.

Staeheli, P., Grob, R., Meier, E., Sutcliffe, J.G. and Haller, O. (1988). Influenza virus-susceptible mice carry Mx genes with a large deletion or a nonsense mutation. *Molecular and Cellular Biology*, 8(10).

Stamatakis, A. (2014). RAxML version 8: A tool for phylogenetic analysis and post-analysis of large phylogenies. *Bioinformatics*, 30(9), pp.1312–1313.

Stanifer, M.L., Guo, C., Doldan, P. and Boulant, S. (2020). Importance of Type I and III Interferons at Respiratory and Intestinal Barrier Surfaces. *Frontiers in Immunology*, 11.

Stanley, W.M. (1935). Isolation of a crystalline protein possessing the properties of tobacco-mosaic virus. *Science*, 81(2113).

Stegmann, T. (2000). Membrane fusion mechanisms: The influenza hemagglutinin paradigm and its implications for intracellular fusion. *Traffic*, 1(8).

Steinhauer, D.A., Domingo, E. and Holland, J.J. (1992). Lack of evidence for proofreading mechanisms associated with an RNA virus polymerase. *Gene*, 122(2), pp.281–288.

Stucker, K.M., Pagan, I., Cifuente, J.O., Kaelber, J.T., Lillie, T.D., Hafenstein, S., Holmes, E.C. and Parrish, C.R. (2012). The Role of Evolutionary Intermediates in the Host Adaptation of Canine Parvovirus. *Journal of Virology*, 86(3).

Suzuki, Y., Ito, T., Suzuki, T., Holland, R.E., Chambers, T.M., Kiso, M., Ishida, H. and Kawaoka, Y. (2000). Sialic Acid Species as a Determinant of the Host Range of Influenza

A Viruses. *Journal of Virology*, 74(24).

Svetlikova, D., Kabat, P., Ohradanova, A., Pastorek, J. and Betakova, T. (2010). Influenza A virus replication is inhibited in IFN-λ2 and IFN-λ3 transfected or stimulated cells. *Antiviral Research*, 88(3), pp.329–333.

Takagi, H., Arimura, K., Uto, T., Fukaya, T., Nakamura, T., Choijookhuu, N., Hishikawa, Y. and Sato, K. (2016). Plasmacytoid dendritic cells orchestrate TLR7-mediated innate and adaptive immunity for the initiation of autoimmune inflammation. *Scientific Reports*, 6.

Talon, J., Horvath, C.M., Polley, R., Basler, C.F., Muster, T., Palese, P. and García-Sastre, A. (2000). Activation of Interferon Regulatory Factor 3 Is Inhibited by the Influenza A Virus NS1 Protein. *Journal of Virology*, 74(17).

Tang, X., Gao, J.S., jie Guan, Y., McLane, K.E., Yuan, Z.L., Ramratnam, B. and Chin, Y.E. (2007). Acetylation-Dependent Signal Transduction for Type I Interferon Receptor. *Cell*, 131(1).

Tang, Y., Zhong, G., Zhu, L., Liu, X., Shan, Y., Feng, H., Bu, Z., Chen, H. and Wang, C. (2010). Herc5 Attenuates Influenza A Virus by Catalyzing ISGylation of Viral NS1 Protein. *The Journal of Immunology*, 184(10).

Tengroth, L., Millrud, C.R., Kvarnhammar, A.M., Georén, S.K., Latif, L. and Cardell, L.O. (2014). Functional effects of Toll-Like Receptor (TLR)3, 7, 9, RIG-I and MDA-5 stimulation in nasal epithelial cells. *PLoS ONE*, 9(6).

Thomas, P.G., Dash, P., Aldridge, J.R., Ellebedy, A.H., Reynolds, C., Funk, A.J., Martin, W.J., Lamkanfi, M., Webby, R.J., Boyd, K.L., Doherty, P.C. and Kanneganti, T.D. (2009). The Intracellular Sensor NLRP3 Mediates Key Innate and Healing Responses to Influenza A Virus via the Regulation of Caspase-1. *Immunity*, 30(4).

Tong, S. et al. (2012). A distinct lineage of influenza A virus from bats. *Proceedings of the National Academy of Sciences of the United States of America*, 109(11).

Tong, S. et al. (2013). New World Bats Harbor Diverse Influenza A Viruses. *PLoS Pathogens*, 9(10).

Turan, K., Mibayashi, M., Sugiyama, K., Saito, S., Numajiri, A. and Nagata, K. (2004). Nuclear MxA proteins form a complex with influenza virus NP and inhibit the transcription of the engineered influenza virus genome. *Nucleic Acids Research*, 32(2).

Umasankar, P.K., Sanker, S., Thieman, J.R., Chakraborty, S., Wendland, B., Tsang, M. and Traub, L.M. (2012). Distinct and separable activities of the endocytic clathrin-coat components Fcho1/2 and AP-2 in developmental patterning. *Nature Cell Biology*, 14(5).

Urooj, F., Zhenyu, Z., Haili, Z., Xue Feng, W., Ling, X., Xiaoyu, C., Shuang, J. and Xiaojun, W. (2019). Equine Mx1 restricts influenza a virus replication by targeting at distinct site of its nucleoprotein. *Viruses*, 11(12), pp.1–19.

Vahey, M.D. and Fletcher, D.A. (2019). Influenza a virus surface proteins are organized to help penetrate host mucus. *eLife*, 8.

Van Valen, L. (1973). A new evolutionary law. *Evol Theor*, 30.

Varga, Z.T., Grant, A., Manicassamy, B. and Palese, P. (2012). Influenza Virus Protein PB1-F2 Inhibits the Induction of Type I Interferon by Binding to MAVS and Decreasing Mitochondrial Membrane Potential. *Journal of Virology*, 86(16).

te Velthuis, A.J.W. and Oymans, J. (2018). Initiation, Elongation, and Realignment during Influenza Virus mRNA Synthesis. *Journal of Virology*, 92(3).

Venkataraman, T., Valdes, M., Elsby, R., Kakuta, S., Caceres, G., Saijo, S., Iwakura, Y. and Barber, G.N. (2007). Loss of DExD/H Box RNA Helicase LGP2 Manifests Disparate Antiviral Responses. *The Journal of Immunology*, 178(10).

Villenave, R., Shields, M.D. and Power, U.F. (2013). Respiratory syncytial virus interaction with human airway epithelium. *Trends in Microbiology*, 21(5).

Vlugt, C. De, Sikora, D. and Pelchat, M. (2018). Insight into influenza: A virus cap-snatching. *Viruses*, 10(11).

Voorhees, I.E.H., Dalziel, B.D., Glaser, A., Dubovi, E.J., Murcia, P.R., Newbury, S., Toohey-Kurth, K., Su, S., Kriti, D., Bakel, H. Van, Goodman, L.B., Leutenegger, C., Holmes, E.C. and Parrish, C.R. (2018). Multiple Incursions and Recurrent Epidemic Fade-Out of H3N2 Canine Influenza A Virus in the United States. *Journal of Virology*, 92(16).

de Vries, E., Tscherne, D.M., Wienholts, M.J., Cobos-Jiménez, V., Scholte, F., García-Sastre, A., Rottier, P.J.M. and de Haan, C.A.M. (2011). Dissection of the influenza a virus endocytic routes reveals macropinocytosis as an alternative entry pathway. *PLoS Pathogens*, 7(3).

Waddell, G.H., Tiegland, M.B. and Sigel, M.M. (1963). A new influenza virus associated with equine respiratory disease. *J. Am. Vet. Med. Assoc.*, 143, pp.587–590.

Waffarn, E.E. and Baumgarth, N. (2011). Protective B Cell Responses to Flu—No Fluke!. *The Journal of Immunology*, 186(7).

Wang, K., Zou, C., Wang, X., Huang, C., Feng, T., Pan, W., Wu, Q., Wang, P. and Dai, J. (2018). Interferon-stimulated TRIM69 interrupts dengue virus replication by ubiquitinating viral nonstructural protein 3. *PLoS Pathogens*, 14(8).

Wang, Q., Li, Q., Liu, T., Chang, G., Sun, Z., Gao, Z., Wang, F., Zhou, H., Liu, R., Zheng, M., Cui, H., Chen, G., Li, H., Yuan, X., Wen, J., Peng, D. and Zhao, G. (2018). Host interaction analysis of PA-N155 and PA-N182 in chicken cells reveals an essential role of UBA52 for replication of H5N1 Avian influenza virus. *Frontiers in Microbiology*, 9(MAY).

Wang, X., Li, M., Zheng, H., Muster, T., Palese, P., Beg, A.A. and García-Sastre, A. (2000). Influenza A virus NS1 protein prevents activation of NF-kappaB and induction of alpha/beta interferon. *Journal of virology*, 74(24), pp.11566–11573.

Wang, X., Hinson, E.R. and Cresswell, P. (2007). The Interferon-Inducible Protein Viperin Inhibits Influenza Virus Release by Perturbing Lipid Rafts. *Cell Host and Microbe*, 2(2).

Wargo, A.R. and Kurath, G. (2012). Viral fitness: Definitions, measurement, and current insights. *Current Opinion in Virology*, 2(5).

Wasik, B.R., Barnard, K.N., Ossiboff, R.J., Khedri, Z., Feng, K.H., Yu, H., Chen, X., Perez, D.R., Varki, A. and Parrish, C.R. (2017). Distribution of O-Acetylated Sialic Acids among Target Host Tissues for Influenza Virus. *mSphere*, 2(5).

Watanabe, K., Takizawa, N., Katoh, M., Hoshida, K., Kobayashi, N. and Nagata, K. (2001). Inhibition of nuclear export of ribonucleoprotein complexes of influenza virus by leptomycin B. In: *Virus Research*.

Watson, J., Daniels, P., Kirkland, P., Carroll, A. and Jeggo, M. (2011). The 2007 outbreak of equine influenza in Australia: Lessons learned for international trade in horses. *OIE Revue Scientifique et Technique*, 30(1).

Wattrang, E., Jessett, D.M., Yates, P., Fuxler, L. and Hannant, D. (2003). Experimental infection of ponies with equine influenza A2 (H3N8) virus strains of different pathogenicity elicits varying interferon and interleukin-6 responses. *Viral Immunology*, 16(1).

Webster, R.G., Yakhno, M., Hinshaw, V.S., Bean, W.J. and Murti, K.C. (1978). Intestinal influenza: Replication and characterization of influenza viruses in ducks. *Virology*, 84(2).

Webster, R.G. and Thomas, T.L. (1993). Efficacy of equine influenza vaccines for protection against A/Equine/Jilin/89 (H3N8) - A new equine influenza virus. *Vaccine*, 11(10).

West, J.B. and Luks, A.M. (2016). *West's respiratory physiology : the essentials Tenth edition*.

Wickham, H. (2011). Ggplot2. *Wiley Interdisciplinary Reviews: Computational Statistics*, 3(2), pp.180–185.

Widdicombe, J.H. and Pecson, I.S. (2002). Distribution and numbers of mucous glands in the horse trachea. *Equine Veterinary Journal*, 34(6).

Wilson, A., Pinchbeck, G., Dean, R. and McGowan, C. (2021). Equine influenza vaccination in the UK: Current practices may leave horses with suboptimal immunity. *Equine Veterinary Journal*, 53(5).

Wise, H.M., Foeglein, A., Sun, J., Dalton, R.M., Patel, S., Howard, W., Anderson, E.C., Barclay, W.S. and Digard, P. (2009). A Complicated Message: Identification of a Novel PB1-Related Protein Translated from Influenza A Virus Segment 2 mRNA. *Journal of Virology*, 83(16).

Wise, H.M., Hutchinson, E.C., Jagger, B.W., Stuart, A.D., Kang, Z.H., Robb, N., Schwartzman, L.M., Kash, J.C., Fodor, E., Firth, A.E., Gog, J.R., Taubenberger, J.K. and Digard, P. (2012). Identification of a Novel Splice Variant Form of the Influenza A Virus M2 Ion Channel with an Antigenically Distinct Ectodomain. *PLoS Pathogens*, 8(11).

World Health Organization. (2016). Cumulative number of confirmed human cases for avian influenza A (H5N1) reported to WHO, 2003-2015. *Epidemic and Pandemic Alert and Response (EPR) World Health Organization.*, 2016, pp.5–6.

World Organisation for Animal Health (OIE). (2019). *Equine influenza (wild equidae) Aetiology, Epidemiology, Diagnosis, Prevention and Control Potential Impacts of Disease Agent Beyond Clinical Illness References*.

Worobey, M., Han, G.Z. and Rambaut, A. (2014). A synchronized global sweep of the internal genes of modern avian influenza virus. *Nature*, 508(7495).

Xu, L.G., Wang, Y.Y., Han, K.J., Li, L.Y., Zhai, Z. and Shu, H.B. (2005). VISA is an adapter protein required for virus-triggered IFN-β signaling. *Molecular Cell*, 19(6).

Yamamoto, M., Sato, S., Hemmi, H., Hoshino, K., Kaisho, T., Sanjo, H., Takeuchi, O., Sugiyama, M., Okabe, M., Takeda, K. and Akira, S. (2003). Role of adaptor TRIF in the MyD88-independent toll-like receptor signaling pathway. *Science*, 301(5633).

Yamanaka, T., Cullinane, A., Gildea, S., Bannai, H., Nemoto, M., Tsujimura, K., Kondo, T. and Matsumura, T. (2015). The potential impact of a single amino-acid substitution on the efficacy of equine influenza vaccines. *Equine Veterinary Journal*, 47(4).

Yan, A.W.C., Zhou, J., Beauchemin, C.A.A., Russell, C.A., Barclay, W.S. and Riley, S. (2020). Quantifying mechanistic traits of influenza viral dynamics using in vitro data. *Epidemics*, 33.

Yang, X., Steukers, L., Forier, K., Xiong, R., Braeckmans, K., Reeth, K. Van and Nauwynck, H. (2014). A beneficiary role for neuraminidase in influenza virus penetration through the respiratory mucus. *PLoS ONE*, 9(10).

Yoneyama, M., Kikuchi, M., Natsukawa, T., Shinobu, N., Imaizumi, T., Miyagishi, M.,

Taira, K., Akira, S. and Fujita, T. (2004). The RNA helicase RIG-I has an essential function in double-stranded RNA-induced innate antiviral responses. *Nature Immunology*, 5(7).

York, A. and Fodor, E. (2013). Biogenesis, assembly and export of viral messenger ribonucleoproteins in the influenza A virus infected cell. *RNA Biology*, 10(8).

Zamzam, S.H., Ghalyanchilangeroudi, A. and Khosravi, A.R. (2022). Comparative trachea transcriptome analysis in SPF broiler chickens infected with avian infectious bronchitis and avian influenza viruses. *Virus Genes*, 2022.

Zhang, Z., Ohto, U., Shibata, T., Krayukhina, E., Taoka, M., Yamauchi, Y., Tanji, H., Isobe, T., Uchiyama, S., Miyake, K. and Shimizu, T. (2016). Structural Analysis Reveals that Toll-like Receptor 7 Is a Dual Receptor for Guanosine and Single-Stranded RNA. *Immunity*, 45(4).

Zheng, D., Soh, B.S., Yin, L., Hu, G., Chen, Q., Choi, H., Han, J., Chow, V.T.K. and Chen, J. (2017). Differentiation of Club Cells to Alveolar Epithelial Cells in Vitro. *Scientific Reports*, 7.

Zheng, W., Xu, Q., Zhang, Y., Xiaofei, E., Gao, W., Zhang, M., Zhai, W., Rajkumar, R.S. and Liu, Z. (2020). Toll-like receptor-mediated innate immunity against herpesviridae infection: a current perspective on viral infection signaling pathways. *Virology Journal*, 17(1).

Zhou, J. et al. (2013). Biological features of novel avian influenza A (H7N9) virus. *Nature*, 499(7459).

Zhou, Z., Hamming, O.J., Ank, N., Paludan, S.R., Nielsen, A.L. and Hartmann, R. (2007). Type III Interferon (IFN) Induces a Type I IFN-Like Response in a Restricted Subset of Cells through Signaling Pathways Involving both the Jak-STAT Pathway and the Mitogen-Activated Protein Kinases. *Journal of Virology*, 81(14).

Zhu, H., Damdinjav, B., Gonzalez, G., Patrono, L.V., Ramirez-Mendoza, H., Amat, J.A.R., Crispell, J., Parr, Y.A., Hammond, T.A., Shiilegdamba, E., Leung, Y.H.C., Peiris, M., Marshall, J.F., Hughes, J., Gilbert, M. and Murcia, P.R. (2019). Absence of adaptive evolution is the main barrier against influenza emergence in horses in Asia despite frequent virus interspecies transmission from wild birds. *PLoS Pathogens*, 15(2).

Zhu, H., Hughes, J. and Murcia, P.R. (2015). Origins and Evolutionary Dynamics of H3N2 Canine Influenza Virus. *Journal of Virology*, 89(10).